ANALYSIS OF MODEL AND OBSERVATION DATA FOR THE DEVELOPMENT

OF A PUBLIC $PM_{2.5}$ AIR-QUALITY ADVISORIES TOOL (AQuAT)

By

Huy N.Q. Tran

RECOMMENDED: _____

_____

_____

_____

_____
Advisory Committee Chair

_____
Chair, Department of Atmospheric Sciences

APPROVED: _____
Dean, College of Natural Science and Mathematics

_____
Dean of the Graduate School

_____
Date

ANALYSIS OF MODEL AND OBSERVATION DATA FOR THE DEVELOPMENT

OF A PUBLIC PM$_{2.5}$ AIR-QUALITY ADVISORIES TOOL (AQuAT)

A

DISSERTATION

Presented to the Faculty

of the University of Alaska Fairbanks

in Partial Fulfillment of the Requirements

for the Degree of

DOCTOR OF PHILOSOPHY

By

Huy Nguyen Quang Tran, B. Eng., M. Eng.

Fairbanks, Alaska

December 2012

iii

Abstract

An air-quality advisory tool (AQuAT) that combines mobile measurements of particulate matter less than or equal to 2.5μm in diameter ($PM_{2.5}$) with air-quality simulations performed with the Alaska adapted version of the Community Multiscale Air Quality (CMAQ) model was developed to interpolate $PM_{2.5}$-measurements into unmonitored neighborhoods in Fairbanks, Alaska. AQuAT was developed as traditional interpolation methods of interpolating the mobile measurements were unsuccessful. Such a spatially differentiated air-quality advisory is highly desired in Fairbanks due to health concerns of $PM_{2.5}$, and the need to improve the quality of life.

The accuracy of AQuAT depends on the accuracy of the air-quality simulations used for its database. Evaluation of these simulations showed that they captured the observed relationships between $PM_{2.5}$-concentrations and major meteorological fields (e.g., wind-speed, temperature, and surface-inversions) well. Skill scores for simulated $PM_{2.5}$-concentrations fell in the range of modern models.

The AQuAT database can include information on the nonlinear impacts of various emission sources on $PM_{2.5}$-concentrations. This benefit was illustrated by investigating the impacts of emissions from point sources, uncertified wood-burning devices, and traffic on the distribution of $PM_{2.5}$-concentrations in the neighborhoods. Sensitivity studies on the effects of wood-burning device changeouts on the $PM_{2.5}$-concentrations suggested that the emission inventory should be updated as soon as possible to capture recent changes in the emission situation in response to the changeout program.

The performance of AQuAT was evaluated with $PM_{2.5}$-measurements from mobile and stationary sites, and with simulated $PM_{2.5}$-concentrations of winter 2010/2011 which were assumed to be "grand-truth" data. These evaluations showed that AQuAT captured the magnitudes and temporal evolutions of the $PM_{2.5}$-measurements and the "grand-truth" data well. The inclusion of wind-speed, wind-direction, and temperature in AQuAT did not improve its accuracy. This result may be explained by the fact that the relationships between meteorology and $PM_{2.5}$-concentrations were already captured by the database.

AQuAT allows quick spatial interpolation after the mobile measurements were made and provides error bars. It also allows for any route within the area for which a database of simulated concentrations exists. It was shown that AQuAT can be easily transferred for applications in other regions.

Table of Contents

List of Tables

List of Figures

List of Appendices

Acknowledgement

This dissertation would not have been possible without collaborations and supports from a variety of people acknowledged here.

First and foremost, I would like to express my deep gratitude to my advisor, Prof. Nicole Mölders, for the continuous support of my Ph.D. study and research, for her patience, motivation, enthusiasm, and immense knowledge. Her guidance helped me all the time during my research and writing of this thesis. I would have been lost without her.

In addition to my advisor, I would like to thank the rest of my thesis committee: Dr. Uma Bhatt, Dr. Catherine Cahill, Dr. Georg Grell, and Dr. Gerhard Kramm, for their encouragement, insightful comments, and hard questions. My gratitude also goes to Dr. William Simpson for his valuable recommendations and encouragement.

I would like to acknowledge the many sources of funding that made this thesis possible and that have supported me in conducting research. The exact funding sources that supported each study are acknowledged in each chapter and in Appendix A.

I owe special thanks to the other current and former faculty of the Department of Atmospheric Sciences (DAS) at UAF for their great advice and fruitful conversations over the years, especially Vladimir Alexeev, David Atkinson, Richard Collins, Javier Fochesatto, Igor Polyakov, Kenneth Sassen, Glenn Shaw, and Xiangdong Zhang. Special gratitude is owed also to Barbara Day for helping me out with all of my paperwork since I came to UAF in 2009.

I also owe countless thanks to many students and alumni of DAS/UAF, especially Peter Bieniek, Ketsiri Leelasakultum, Rebecca Legatt, Debasish PaiMazumder, Stacy

Porter, and Jeanie Talbot, for their collaboration, support and friendship, as well as for plenty of enjoyable moments I have spent with them throughout the years. My special thanks go to James (Mike) Madden and Michael Pirhalla for their great help in spell checking this dissertation.

Last but not least, I would like to thank my parents, my wife, and my daughter for supporting me spiritually throughout my adventure as a graduate student. I dedicate my thesis to my father, Khanh Mai Tran, and my mother, Thai Huynh Nguyen, for their constant supports and encouragements in every step of my life.

Chapter 1 Introduction

Spatial interpolation of observed data to locations where no data is available is a common application in air-quality studies. Such an application is needed by the Fairbanks North Star Borough (FNSB) Air Quality Division to obtain a broad picture of the spatial distribution of particulate matter less than or equal to 2.5μm in diameter ($PM_{2.5}$) and to serve for public air-quality advisories.

Health studies (Kappos et al., 2004; Dominici et al., 2006; Pope and Dockery, 2006), namely, have shown strong evidence linking premature death from heart and lung diseases and exposure to $PM_{2.5}$. Adverse health effects of $PM_{2.5}$ were found to be associated with both long-term and short-term exposure (Miller et al., 2007; Delfino et al., 2009). Evidence for increased risk of hospitalizations associated with the increased $PM_{2.5}$-concentration were also found for Fairbanks, Alaska (State of Alaska Epidemiology, 2010).

Due to these health concerns, and the need to decrease the health risk, the United States Environmental Protection Agency (EPA) tightened its National Ambient Air Quality Standard (NAAQS) for $PM_{2.5}$ in 2006. The NAAQS requires that the 24h-averaged $PM_{2.5}$-concentration at the 98th percentile in a year be less than 35μg/m^3 on average over three consecutive years, and the three-year average of the annual $PM_{2.5}$ be less than 15μg/m^3. As a consequence of the tightened standard, EPA designated $PM_{2.5}$-nonattainment areas to all regions that have violated the tightened $PM_{2.5}$ NAAQS over a three-year period, or when relevant information indicated that they contributed to violations in nearby areas (EPA, 2012).

As observations indicated that $PM_{2.5}$-concentrations exceeded the NAAQS periodically in Fairbanks, Alaska, during the past years (Tran and Mölders, 2011), Fairbanks was assigned a $PM_{2.5}$-nonattainment area in December 2009. As of July 20, 2012, Fairbanks is one of the 32 $PM_{2.5}$-nonattainment areas in the United States, and Fairbanks is the only $PM_{2.5}$-nonattainment area in Alaska (EPA, 2012).

Collaborative studies have been performed by the Fairbanks North Star Borough (FNSB), EPA, Alaska Department of Environmental Conservation, the National Weather Service in Fairbanks, various contractors, and scientists of the University of Alaska Fairbanks (UAF) to understand the meteorological and emission conditions that have led to high $PM_{2.5}$-concentrations and $PM_{2.5}$ exceedances, and to develop strategies to get Fairbanks into attainment.

To obtain a broad picture of the $PM_{2.5}$-concentration distributions within the nonattainment area and for public air-quality advisories, the FNSB expanded the stationary monitoring network from one to five sites, and started measuring $PM_{2.5}$-concentrations along roads in commercial and residential areas with instrumented vehicles (referred to as sniffer hereafter; Figure 1.1) in winter 2008/2009 (FNSB, 2010).

Based on the observations at the State Office Building and in North Pole, the air-quality index was determined and published on a webpage (http://co.fairbanks.ak.us/airquality/aqual.aspx) to provide the current status of air quality to the public. Furthermore, air-quality advisories are provided as needed to the public in accordance with the observed air quality. The FNSB also found it desirable to interpolate

these mobile $PM_{2.5}$-measurements into areas without data to provide a spatially differentiated air-quality advice.

Methods for interpolating the measurements from a limited number of sites to a broad spatial extent have been widely applied in both meteorology (e.g., Jeffrey et al., 2001; Stahla et al., 2006; Garcia et al., 2008) and air-quality applications (e.g., Kinney et al., 1998; Mulholland et al., 1998; Schwartz, 2001). The interpolation methods applied in these studies used statistical techniques and were based only on measurements (called traditional interpolation methods hereafter). Many traditional interpolation methods used in air-quality applications have been reviewed, for instance, by Eberly et al. (2004), Li and Heap (2008), and Deligiorgi and Philippopoulos (2011). These traditional interpolation methods range from simple and non-geostatistical methods (e.g., nearest neighbors, triangular irregular network, inverse distance weighting) to sophisticated and geostatistical methods (e.g., kriging, artificial neural network). Wong et al. (2004) evaluated the performance of four commonly used traditional methods in air-quality applications including the spatial averaging, nearest neighbor, inverse distance weight, and ordinary kriging in interpolating ozone and particulate matter with aerodynamic diameter less than 10µm (PM_{10}) from 739 ozone sites and 768 PM_{10} sites over the US and its territories. The results showed that the performance of the four interpolation methods hardly differed in areas where the monitor density was low, but dramatically differed in high density monitoring areas. Here, the kriging method provided the least bias. The choice of the search radius importantly affects the performance of the inverse distance weight and the spatial averaging methods, while the kriging method may only be

applied in areas having a high density monitoring network (Wong et al., 2004). Deligiorgi and Philippopoulos (2011) used the leave-one-out cross-validation method similarly to the method applied by Wong et al. (2004). Herein, one site was selected as the target site and the remaining sites were employed in the interpolation processes to interpolate the value at the selected site. By applying this method, Deligiorgi and Philippopoulos (2011) evaluated the performance of thirteen traditional methods using nitrogen dioxides and ozone observations from eight sites in metropolitan Athens, Greece. The results showed that the performance of the investigated traditional interpolation methods significantly differed among sites, and no interpolation technique could be identified as the optimal technique to provide the best performance. Therefore, Deligiorgi and Philippopoulos (2011) concluded that the underlying transport mechanisms and chemical transformations, which drive the spatial distribution of the air pollutants, are important factors limiting the performance of the traditional methods.

While traditional interpolation methods are applicable in areas of sufficient data density, their use may be problematic in areas of sparse data density (Eberly et al., 2004; Wong et al., 2004; PaiMazumder and Mölders, 2009). The distribution of air pollutants namely is a function of many factors such as atmospheric conditions, land-use, sources (e.g., emissions, chemical reactions) and sinks (e.g., chemical reactions, deposition) (Kramm et al., 1994; Clarke et al., 1997; Eberly et al., 2004; Elminir, 2005; Mölders, 2011). These factors can vary substantially in space and time. Some traditional geostatistical methods, such as kriging, adopt mathematical fitting techniques to best describe the empirical behavior of the given observations; however, there is no

requirement for those fitting equations to be consistent with any underlying atmospheric or physical processes (Eberly et al., 2004). Furthermore, the accuracy of the traditional methods heavily depends on the density and the design of the monitoring network (Eberly et al., 2004; PaiMazumder and Mölders, 2009). If a monitoring network does not measure key features of a spatial region (e.g., no monitor is placed near point sources, near a road, or in high population density area), then the traditional methods cannot accurately describe those key features (Eberly et al., 2004). Thus, interpolating data from sparse monitoring networks based alone on observation statistics may provide inadequate results (PaiMazumder and Mölders, 2009).

In Fairbanks, the availability of $PM_{2.5}$-observations differs among seasons and years. However, since winter 2008/2009, $PM_{2.5}$-concentrations have been typically measured at the State Office Building (SB), Peger Road (PR), Pioneer Road (NCORE), in the community of North Pole (NP), and at the Relocatable Air Monitoring System (RAMS) trailer locations (Figure 1.1). The distances between the SB and RAMS, SB and PR, and SB and NP sites are about 6.5km, 3km and greater than 20km, respectively. The sniffer observations provided great spatial coverage over the area bounded by its route. However, in a given drive, the route just covered a part of the $PM_{2.5}$-nonattaiment area (e.g., a drive either covers Fairbanks or North Pole; Figure 1.1).

A typical variogram for $PM_{2.5}$-observations of the sniffer data indicates relatively low spatial correlation for measurement-points that are greater than 1km apart (Figure 1.2). While a kriging interpolation can be performed for the sniffer's measurements, it is only representative for a limited horizontal area around the measurements (Figure 1.3).

When the kriging method was applied to extrapolate the sniffer's measurement to the entire nonattainment area, it produced an unrealistic spatial distribution of $PM_{2.5}$ (Figure 1.3). This behavior occurred because the kriging method applied the spatial correlations it determined for the monitored area (e.g., for Fairbanks (FB)) to extrapolate those measurements to the areas without measurement (e.g., Badger Road (BG), Hill (HL); see Figure 1.1 for locations) where the determined spatial correlations may no longer be valid. In this case, the kriging method has no information on the underlying physical and chemical processes that drive the spatial distribution of $PM_{2.5}$-concentrations in the unmonitored areas.

Besides being inferred from the observations, the distribution of $PM_{2.5}$-concentrations can be simulated by air-quality models which can produce 4-dimensional distributions of the $PM_{2.5}$-concentrations and its components. However, there are uncertainties associated with the results from air-quality models due to errors in meteorological initialization, emissions, parameterizations, discretization and model resolution (Fox, 1984; Mölders et al., 1994; Dolwick et al., 2001; Pielke, 2002; Tetzlaff et al., 2002; Jacobson, 2005; Mölders and Kramm, 2010). Despite such potential errors, Fuentes and Raftery (2005) suggested that combining the outputs of an air-quality model with observations could lead to improved interpolation results.

One of the earliest attempts in combining the two approaches was performed by Taylor et al. (1985). They calibrated the outputs of the simple line-source model (Chock, 1978) with the carbon monoxide observations using the two-parameter Weibull-distribution approach to estimate the distribution of air pollutants along a roadway in

Melbourne, Australia. The evaluation of the calibrated model predictions with observations at another site revealed great agreement (Taylor et al., 1985). Recently, Fuentes and Raftery (2005) suggested combining observations from the Clean Air Status and Trends Network (CASTNET) with outputs from an air-quality model in a Bayesian way to obtain a high-resolution sulfur-dioxide distribution over the US for model evaluation. Their interpolation approach incorporated information on the emissions and underlying driving physical and chemical processes. However, until now there has been no preferred method to combine air-quality model outputs with traditional statistical approaches for interpolating the spatial distribution of air pollutants.

This dissertation aims at developing an air-quality advisory tool that spatially interpolates mobile measured $PM_{2.5}$-concentrations to locations where no measurements are available. This tool will serve to create spatially differentiated public air-quality advisories in areas where the monitoring is sparse with respect to mobile measurements, and where there are many emission sources of different kinds. Given the fact that the traditional interpolation methods exposed large uncertainty and do not perform well under such conditions, the research hypothesis of this dissertation is that (1) *the spatial interpolation of $PM_{2.5}$-concentrations can be reasonably performed by an interpolation tool that combines mobile $PM_{2.5}$-observations with outputs of an air-quality model that includes all available information on sources and sinks of $PM_{2.5}$*. This tool is referred to as AQuAT hereafter.

Obviously, the performance of AQuAT highly depends on how well the air-quality models can reproduce the features observed in nature. Therefore, this dissertation

tests the sub-hypotheses that (2) *the air-quality models can reproduce the observed features that drive the distribution of the PM$_{2.5}$-concentrations*, and that (3) *in addition to the meteorology, the emissions from various sources influence the distribution of the PM$_{2.5}$-concentrations.* If these sub-hypotheses are confirmed, using data from air-quality models can provide needed additional information to capture these influences when performing the interpolation.

To prove the above hypotheses, four specific questions will have to be answered:

1) Under which meteorological conditions were the observed PM$_{2.5}$-concentrations high and did PM$_{2.5}$-exceedances occur in the Fairbanks nonattainment area during past winters? Which meteorological quantities are the key factors that affect the PM$_{2.5}$-concentrations?

2) How well did the air-quality models used in this dissertation simulate the PM$_{2.5}$-concentrations in Fairbanks? Are the simulations able to reproduce the observed relationship between the meteorological conditions and PM$_{2.5}$-concentrations?

3) How do emissions from major sources (point sources, traffic, uncertified wood-burning devices) affect the PM$_{2.5}$-concentrations in Fairbanks?

4) How good is the performance of AQuAT, developed within the scope of this dissertation, for application in Fairbanks?

The answer to question (1) is important to assess whether or not the meteorological conditions have to be considered directly in the development of AQuAT. The answer to question (1) will also serve to validate whether the air-quality simulations used in this dissertation can capture the typically observed PM$_{2.5}$-meteorology

relationships. To answer this question, the relationships between the meteorological conditions and $PM_{2.5}$-concentrations in Fairbanks were investigated using ten years (1999-2009) of observations from meteorological surface sites and radiosonde at the Fairbanks International Airport, and the $PM_{2.5}$-site located at the Fairbank State Office Building. This study provides valuable insight into the key meteorological quantities that drive the $PM_{2.5}$-concentrations in Fairbanks during winter. The results of this investigation are discussed in chapter 3.

When using air-quality simulation results as a database for AQuAT, the accuracy of those simulations in simulating the meteorological fields and $PM_{2.5}$-concentrations is important. The answer to question (2) helps to assess how well the air-quality models can reproduce the characteristics of the observed meteorological fields and $PM_{2.5}$-concentrations, as well as the observed climatology of the $PM_{2.5}$-meteorology relationships found from the answer of question (1). In this dissertation, the simulations with the Alaska adapted (Mölders et al., 2011) version of the Weather Research and Forecasting model (WRF; Skamarock et al., 2008) inline coupled with chemistry packages (WRF/Chem; Grell et al., 2005; Peckham et al., 2009) were performed and evaluated by Mölders et al. (2011; 2012). Additional evaluation was performed by me for WRF/Chem as well as for the simulations that I performed with the Alaska adapted WRF (Gaudet and Stauffer, 2010) decoupled with the Alaska adapted (Mölders and Leelasakultum, 2011) version of Models-3 Community Multiscale Air Quality (CMAQ; Byun and Schere, 2006) modeling systems (WRF-CMAQ). The above simulations were used for investigation of the contributions of emissions from various sources to the

$PM_{2.5}$-concentrations (see question (3)) and to serve as a database for AQuAT (see question (4)). Their evaluation was performed with observations from meteorological sites and aerosol monitoring sites, and other available data. These evaluation results and their implications for the database and AQuAT development are discussed in chapter 4.

As long-range transport from other regions hardly affects the pollution in Fairbanks (Cahill, 2003; Tran et al., 2011), $PM_{2.5}$-concentrations in Fairbanks mainly originate from the many types of sources (e.g., point source, traffic, residential heating, mining, etc.) as reflected by the emission inventory. These sources emit $PM_{2.5}$ and its precursor gases at different rates and locations. $PM_{2.5}$-concentrations are not only driven by the emissions but also by physical and chemical processes (e.g., gas-to-particle conversion, wet and dry deposition, advection). Therefore, there is a nonlinear relationship between the emission strength and the resulting $PM_{2.5}$-concentrations. Consequently, locations where the emissions are strongest are not necessarily those where the $PM_{2.5}$-concentrations are highest in the nonattainment area.

The benefit of using air-quality simulations as a database for AQuAT is that doing so includes information on the nonlinear effects of emissions from different types of sources (beside the effects of the underlying physical and chemical processes) on the distribution of $PM_{2.5}$-concentrations. The answer to question (3) is important to understand how emissions from different types of sources affect the $PM_{2.5}$-concentrations, and thereby justify using air-quality simulations as a database for AQuAT. For this purpose, the influences of point sources, uncertified wood-burning devices, traffic emissions, and wood-burning device changeouts on $PM_{2.5}$-concentrations

in Fairbanks are investigated. The importance of understanding the influence of the above source-categories on $PM_{2.5}$-concentrations is discussed below.

Emissions from point sources are of great concern as the review of the National Emission Inventory (NEI) of 2005 revealed that point-source emissions contributed up to 15% of the total $PM_{2.5}$-emissions in Fairbanks. Furthermore, unlike area and line sources, point sources emit pollutants to various vertical levels depending on stack characteristics and the local mixing height. The magnitude and radius of impacts of point-source emissions on $PM_{2.5}$-concentrations, therefore, may differ among point sources depending on their characteristics and the local meteorological conditions. Such heterogeneity of the contribution of point-source emissions to the $PM_{2.5}$-concentrations cannot be captured by measurements, especially in Fairbanks where no observed vertical profiles of $PM_{2.5}$-concentrations are available. On the contrary, air-quality simulations can provide the complexity of the contribution of point-source emissions to the $PM_{2.5}$-concentrations. The use of air-quality simulations as a database for AQuAT to include such information will be needed if point-source emissions play an important role in the distribution of $PM_{2.5}$-concentrations. Therefore, understanding the influences of point-source emissions on $PM_{2.5}$-concentrations in Fairbanks would justify the use of air-quality simulations as a database for AQuAT.

The NEI2005 and NEI2008 showed that in Fairbanks and during winter, more than 50% of primary $PM_{2.5}$-emissions originated from household heating, where 85% of the emissions came from wood-burning devices. Houck and Broderick (2005) estimated that EPA-certified wood-burning devices emit up to 87% less $PM_{2.5}$ than uncertified

ones. Because of the benefit of using certified wood-burning devices, the FNSB started a wood-burning device changeouts in fall 2010 (Bohman, 2010). This changeout program was supposed to reduce the $PM_{2.5}$-emissions and hence the $PM_{2.5}$-concentrations in the Fairbanks nonattainment area.

The air-quality simulations, which serve as a database for AQuAT, used the emission inventory for Fairbanks that was developed by the Sierra Research Inc. (pers. comm., March 2011). This emission inventory is available on a 1.3km grid-increment and was developed based on the bottom-up approach, and therefore is considered to be better for fine resolution modeling than the NEI (applicable for 4km grid-increment at the finest) that is based on top-down approach. Since the emission inventory for Fairbanks was prepared for the year 2008, it does not include information on the emission change imposed by the wood-burning device changeouts. If the uncertified wood-burning devices have contributed appreciable amounts to the $PM_{2.5}$-concentrations, and the wood-burning devices changeouts would reduce the $PM_{2.5}$-concentrations strongly, it may affect the performance of AQuAT for applications in Fairbanks in winters after the implementation of the program. Therefore, it is important to investigate the contribution of the uncertified wood-burning devices to the $PM_{2.5}$-concentrations, and the effects of the wood-burning device changeouts on the $PM_{2.5}$-concentrations in Fairbanks.

As the sniffer travels along the roads collecting data, the mobile measurements include the background $PM_{2.5}$-concentrations combined with those concentrations that could originate either from traffic emissions alone, or from the combination of traffic, point-source and area-source emissions. The contribution of traffic emissions to the

PM$_{2.5}$-concentrations may decrease quickly within 400m downwind of an actively used road (e.g., Zhu et al., 2002; Reponen et al., 2003). This fact means that if traffic would contribute appreciable amounts to the PM$_{2.5}$-concentrations, the mobile measurements, which are impacted by the traffic emissions, could be substantially different from the PM$_{2.5}$-concentrations in neighborhoods far from roads. In such a situation, the use of traditional methods (e.g., kriging) to interpolate the mobile measurements into the unmonitored neighborhoods would expose a large uncertainty. Thus, the use of air-quality simulations as a database for AQuAT is necessary as it can capture the heterogeneity caused by the contributions of traffic emissions to the PM$_{2.5}$-concentrations. Therefore, an investigation of the contributions of traffic to the PM$_{2.5}$-concentrations is performed to assess the necessity of using air-quality simulation results as a database for AQuAT.

To answer question (3), I analyzed the results of simulations of the reference and experimental scenarios performed with WRF/Chem and WRF-CMAQ as described above. In general, in a reference scenario, all emissions are as in the emission inventory (i.e., no change) and then allocated in space and time. In the simulations to assess the contribution of various emission sources to the PM$_{2.5}$-concentrations, the emissions from the source-category of interest were shut off or were replaced by emissions from another source-category at the emission inventory level prior to allocation in space and time. The influences of point-source emissions, wood-burning device changeouts, emissions from uncertified wood-burning devices in general, and traffic emissions on the PM$_{2.5}$-concentration in Fairbanks are discussed in chapters 5, 6, 7, and 8, respectively.

Based on the model results and findings of the sensitivity studies on the emission impacts and the evaluation results, AQuAT can be developed to spatially interpolate those observations into the areas without measurements.

Once AQuAT is developed, its accuracy has to be tested and assessed (question (4)). Potential challenges in applying AQuAT and its transferability are also illustrated and discussed critically. Results of this study are discussed in chapter 9.

Chapter 2 describes the model setup for the simulations, methods for model evaluation, and analyses of the impacts of the various source-categories. Finally, chapter 10 provides the overall conclusions and recommendations for the implementation of AQuAT in general and in Fairbanks in particular.

References

Bohman, A., 2010. Fairbanks borough begins its wood stove trade-in program. Fairbanks Daily News-Miner, Fairbanks, AK. Retrieved October 8, 2012, from http://newsminer.com/view/full_story/8963723/article-Fairbanks-borough-begins-its-wood-stove-trade-in-program.

Byun, D.W., Schere, K.L., 2006. Review of the governing equations, computational algorithms, and other components of the Models-3 Community Multiscale Air Quality (CMAQ) Modeling System. Applied Mechanics Reviews, 59, pp. 51-77.

Cahill, C.F., 2003. Asian aerosol transport to Alaska during ACE-Asia. Journal of Geophysical Research, 108, p. 8. doi:10.1029/2002JD003271.

Chock, D.P., 1978. A simple line-source model for dispersion near roadways. Atmospheric Environment, 12, pp. 823-829.

Clarke, J.F., Edgerton, E.S., Martin, B.E., 1997. Dry deposition calculations for the Clean Air Status and Trends Network. Atmospheric Environment, 31, pp. 3667-3678.

Delfino, R.J., Brummel, S., Wu, J., Stern, H., Ostro, B., Lipsett, M., Winer, A., Street, D.H., Zhang, L., Tjoa, T., Gillen, D.L., 2009. The relationship of respiratory and cardiovascular hospital admissions to the southern California wildfires of 2003. Occupational and Environmental Medicine, 66, pp. 189-197.

Deligiorgi, D., Philippopoulos, K., 2011. Spatial interpolation methodologies in urban air pollution modeling: Application for the greater area of metropolitan Athens, Greece. Advanced Air Pollution, Farhad Nejadkoorki (Ed.), InTech pp. 341-362.

Dolwick, P.D., Jang, C., Possiel, N., Timin, B., Gipson, G., Godowitch, J., 2001. Summary of results from a series of models-3/CMAQ simulations of ozone in the Western United States. Proceeding of the 94th Annual Air & Waste Management Association Conference and Exhibition, Orlando, FL, June 24-28, Paper #957, p. 18.

Dominici, F., Peng, R.D., Bell, M.L., 2006. Fine particulate air pollution and hospital admission for cardiovascular and respiratory diseases. Journal of the American Medical Association, 295(10), pp. 1127-1134.

Eberly, S., Swall, J., Holland, D., Cox, B., Baldridge, E., 2004. Developing spatially interpolatied surfaces and estimating uncertainty. U.S. Environmental Protection Agency, Research Triangle Park, NC, EPA-454/R-04-004, p. 169.

Elminir, H.K., 2005. Dependence of urban air pollutants on meteorology. Science of the Total Environment, 350, pp. 225-237.

EPA. 2012. Particulate matter (PM-2.5) 2006 standard nonattainment areas. U.S. Environmental Protection Agency (EPA). Retrieved August 21 2012, from http://www.epa.gov/oar/oaqps/greenbk/rnc.html.

FNSB, 2010. Fairbanks air quality symposium summary. Fairbanks North Star Borough (FNSB). Retrieved July 13, 2012, from http://co.fairbanks.ak.us/airquality/Docs/Symposium_Summary.pdf, p. 17.

Fox, D.G., 1984. Uncertainty in air quality modeling. Bulletin American Meteorological Society, 65, pp. 27-36.

Fuentes, M., Raftery, A.E., 2005. Model evaluation and spatial interpolation by Bayesian combination of observations with outputs from numerical models. Biometrics, 61, pp. 36-45.

Garcia, M., Peters-Lidard, C.D., Goodrich, D.C., 2008. Spatial interpolation of precipitation in a dense gauge network for monsoon storm events in the southwestern United States. Water Resources Research, 44, p. 14.

Gaudet, B.J., Stauffer, D.R., 2010. Stable boundary layers representation in meteorological models in extremely cold wintertime conditions. Report to the Environmental Protection Agency, p. 60.

Grell, G.A., Peckham, S.E., Schmitz, R., McKeen, S.A., Frost, G., Skamarock, W.C., Eder, B., 2005. Fully coupled "online" chemistry within the WRF model. Atmospheric Environment, 39, pp. 6957-6975.

Houck, J.E., Broderick, D.R., 2005. $PM_{2.5}$ emission reduction benefits of replacing conventional uncertified cordwood stoves with certified cordwood stoves or modern pellet stoves. Technical report, Arlington, VA, USA, p. 26.

Jacobson, M.Z., 2005. Fundamentals of atmospheric modeling. 2nd Edition, Cambridge University Press, New York, USA, p. 829.

Jeffrey, S.J., Carter, J.O., Moodie, K.B., Beswick, A.R., 2001. Using spatial interpolation to construct a comprehensive archive of Australian climate data. Environmental Modeling & Software, 16, pp. 309-330.

Kappos, A.D., Bruckmann, P., Eikmann, T., Englert, N., Heinrich, U., Höppe, P., Koch, E., Krause, G.H.M., Kreyling, W.G., Rauchfuss, K., Rombout, P., Schulz-Klemp, V., Thiel, W.R., Wichmann, H.-E., 2004. Health effects of particles in the ambient air. International Journal of Hygiene and Environmental Health, 207, pp. 399-407.

Kinney, P.L., Aggarwal, M., Nikiforov, S.V., Nadas, A., 1998. Methods development for epidemiologic investigations of the health effects of prolonged ozone exposure. Part III: an approach to retrospective estimation of lifetime ozone exposure using a questionnaire and ambient monitoring data (U.S. sites). Health Effects Institute Research Report, 81, pp. 79-107.

Kramm, G., Dlugi, R., Mölders, N., Müller, H., 1994. Numerical investigations of the dry deposition of reactive trace gases. In: Baldasano, J.M., Brebbia, C.A., Power, H., Zannetti, P. (eds.), Air Pollution II Vol. 1: Computer Simulation, Computational Mechanics Publications, Southampton, Boston, pp. 285-307.

Li, J., Heap, A.D., 2008. A review of spatial interpolation methods for environmental scientists. Geoscience Autralia, p. 154.

Miller, K.A., Siscovick, D.S., Sheppard, L., Shepherd, K., Sullivan, J.H., Anderson, G.L., Kaufman, J.D., 2007. Long-term exposure to air pollution and incidence of cardiovascular events in women. New England Journal of Medicine, 356, pp. 447-458.

Mölders, N., 2011. Land-Use and Land-Cover Changes, Atmospheric and Oceanographic Sciences Library 44, Springer Science+Business Media B.V. 2012, p. 189.

Mölders, N., Kramm, G., 2010. A case study on wintertime inversions in Interior Alaska with WRF. Atmospheric Research, 95, pp. 314-332.

Mölders, N., Hass, H., Jakobs, H.J., Laube, M., Ebel, A., 1994. Some effects of different cloud parameterizations in a mesoscale model and a chemistry transport model. Journal of Applied Meteorology, 33, pp. 527-545.

Mölders, N., Leelasakultum, K., 2011. Fairbanks North Star Borough $PM_{2.5}$ non-attainment area CMAQ modeling: Final report phase I. Report, p. 62.

Mölders, N., Tran, H.N.Q., Cahill, C.F., Leelasakultum, K., Tran, T.T., 2012. Assessment of WRF/Chem $PM_{2.5}$-forecasts using mobile and fixed location data from the Fairbanks, Alaska winter 2008/09 field campaign. Atmospheric Pollution Research, 3, pp. 180-191.

Mölders, N., Tran, H.N.Q., Quinn, P., Sassen, K., Shaw, G.E., Kramm, G., 2011. Assessment of WRF/Chem to simulate sub–Arctic boundary layer characteristics during low solar irradiation using radiosonde, SODAR, and surface data. Atmospheric Pollution Research, 2, pp. 283-299.

Mulholland, J.A., Butler, A.J., Wilkinson, J.G., Russell, A.G., 1998. Temporal and spatial distributions of ozone in Atlanta: Regulatory and epidemiologic implications. Journal of the Air & Waste Management Association, 48, pp. 418-426.

PaiMazumder, D., Mölders, N., 2009. Theoretical assessment of uncertainty in regional averages due to network density and design. Journal of Applied Meteorology and Climate, 48, pp. 1643-1666.

Peckham, S.E., Fast, J.D., Schmitz, R., Grell, G.A., Gustafson, W.I., McKeen, S.A., Ghan, S.J., Zaveri, R., Easter, R.C., Barnard, J., Chapman, E., Salzmann, M., Wiedinmyer, C., Freitas, S.R.,2009. WRF/Chemversion 3.1 user's guide, p. 78.

Pielke, R.A., 2002. Mesoscale meteorological modeling. 2nd Edition, International Geophysics Series, 78, p. 693.

Pope, C.A., Dockery, D.W., 2006. Health effects of fine particulate air pollution: Lines that connect. Journal of Air & Waste Management Association, 56, pp. 709-742.

Reponen, T., Grinshpun, S.A., Trakumas, S., Martuzevicius, D., Wang, Z.-M., LeMasters, G., Lockey, J.E., Biswas, P., 2003. Concentration gradient patterns of aerosol particles near interstate highways in the greater Cincinnati airshed. Journal of Environmental Monitoring, 5, pp. 557-562.

Schwartz, J., 2001. Air pollution and blood markers of cardiovascular risk. Environmental Health Perspectives, 109, pp. 405-409.

Skamarock, W.C., Klemp, J.B., Dudhia, J., Gill, D.O., Barker, D.M., Duda, M.G., Huang, X.-Y., Wang, W., Powers, J.G., 2008. A description of the Advanced Research WRF version 3. NCAR Technical Note, NCAR/TN-475+STR, p. 125.

Stahla, K., Moorea, R.D., Floyerc, J.A., Asplina, M.G., McKendrya, I.G., 2006. Comparison of approaches for spatialinterpolation of daily air temperature in a large region with complex topography and highly variable station density. Agricultural and Forest Meteorology, 139, pp. 224-236.

State of Alaska Epidemiology. 2010. Association between air quality and hospital visits —Fairbanks, 2003–2008. Bulletin, State of Alaska Epidemiology. Retrieved August 21, 2012, from http://www.epi.alaska.gov/bulletins/docs/b2010_26.pdf, p. 1.

Taylor, J.A., Simpson, R.W., Jakeman, A.J., 1985. A hybrid model for predicting the distribution of pollutants dispersed from line sources. The Science of the Total Environment, 46, pp. 191-213.

Tetzlaff, G., Dlugi, R., Friedrich, K., Gross, G., Hinneburg, D., Pahl, U., Zelger, M., Mölders, N., 2002. On modeling dry deposition of long-lived and chemically reactive species over heterogeneous terrain. Journal of Atmospheric Chemistry, 42, pp. 123-155.

Tran, H.N.Q., Mölders, N., 2011. Investigations on meteorological conditions for elevated $PM_{2.5}$ in Fairbanks, Alaska. Atmospheric Research, 99, pp. 39-49.

Tran, T.T., Newby, G., Mölders, N., 2011. Impacts of emission changes on sulfate aerosols in Alaska. Atmospheric Environment, 45, pp. 3078-3090.

Wong, D.W., Yuan, L., Perlin, S.A., 2004. Comparison of spatial interpolation methods for the estimation of air quality data. Journal of Exposure Analysis and Environmental Epidemiology, 14, pp. 404-415.

Zhu, Y., Hinds, W.C., Kim, S., Sioutas, C., 2002. Concentration and size distribution of ultrafine particles near a major highway. Journal of the Air & Waste Management Association, 52, pp. 1032-1042.
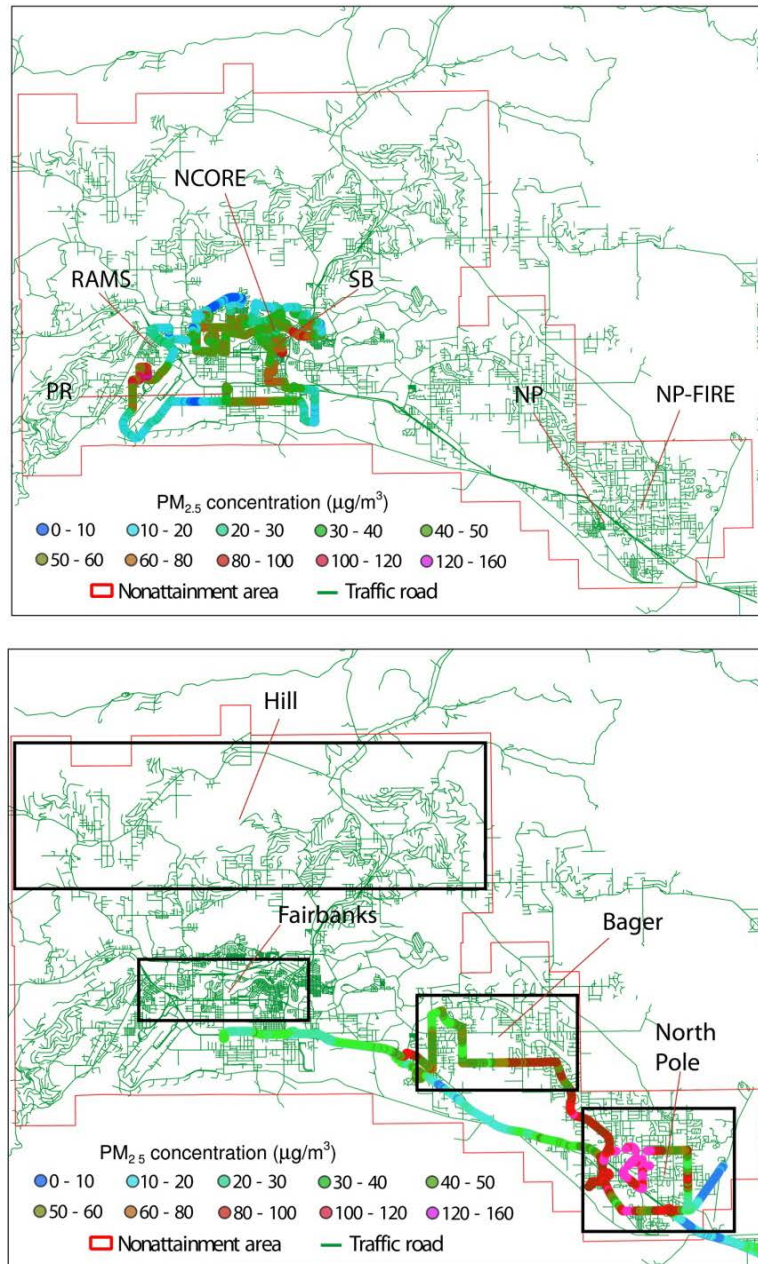
Figure 1.1 PM$_{2.5}$-concentrations as measured in Fairbanks by the sniffer (lines of dots) on (top) 01-02-2010 during the drive that started at 1404 Alaska Standard Time (AST) and (bottom) 01-08-2010 during the drive that started at 0800AST with the street network superimposed. In the top panel, SB, RAMS, PR, NP, NP-FIRE and NCORE represent the locations of stationary PM$_{2.5}$-observation sites (see section 2.4 for descriptions). In the bottom parnel, the Hill (HL), Fairbanks (FB), Badger Road (BG), North Pole (NP) areas indicated by rectangules show the geographical regions of interest in the Fairbanks nonattainment area that are discussed in subsequent chapters. Note that these regions are not the actual administrative districts in the FNSB.
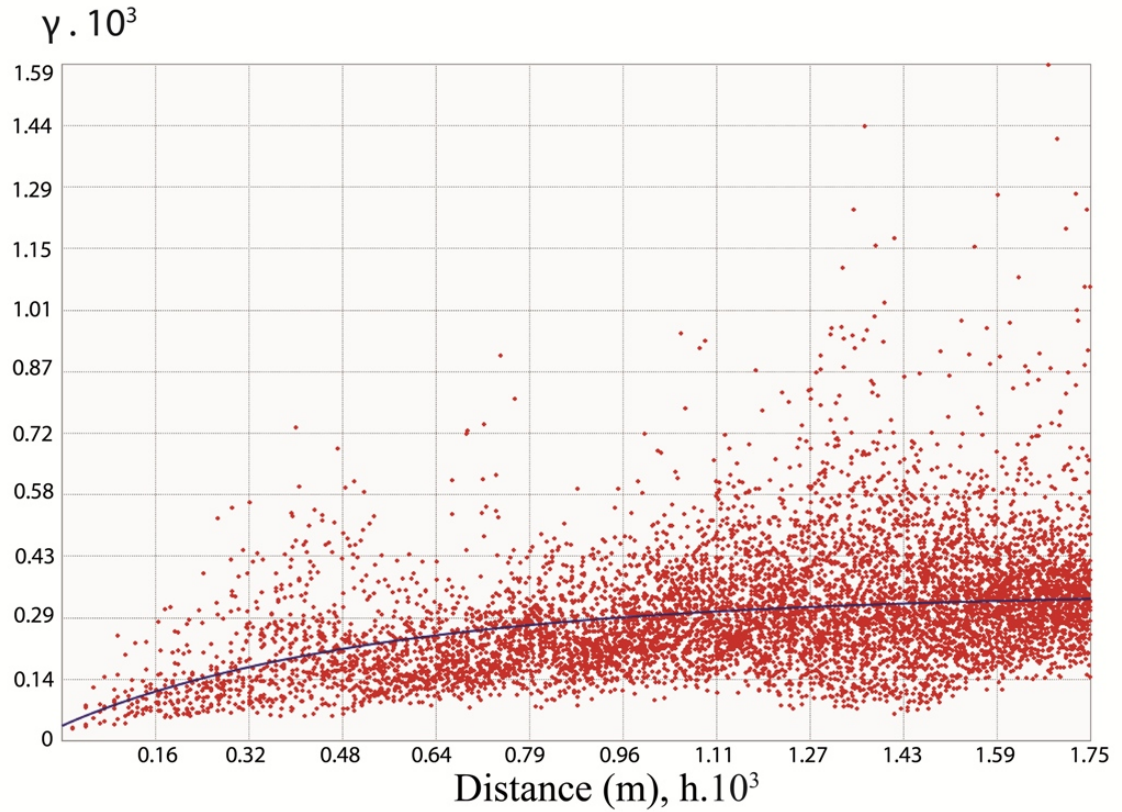
Figure 1.2 Variogram of the $PM_{2.5}$-concentrations measured by the sniffer on 01-02-2010 during the drive that started at 1404AST. Values of the $PM_{2.5}$-observations in this drive are shown in Figure 1.1. This variogram shows the empirical spatial correlation between measurement points performed in this drive. The red dots represent the differences in values (y-axis) of pairs of measurement points that are separated by a distance-lag h (x-axis). The black line represents the spherical best-fit model for the variogram. This variogram was typical for all drives performed during 12-27-2009 to 01-12-2010, and 01-01-2011 to 01-30-2011.

PM$_{2.5}$ concentration (µg/m³)

0 - 10	20 - 30	40 - 50	60 - 80	100 - 120	Nonattainment area
10 - 20	30 - 40	50 - 60	80 - 100	120 - 160	
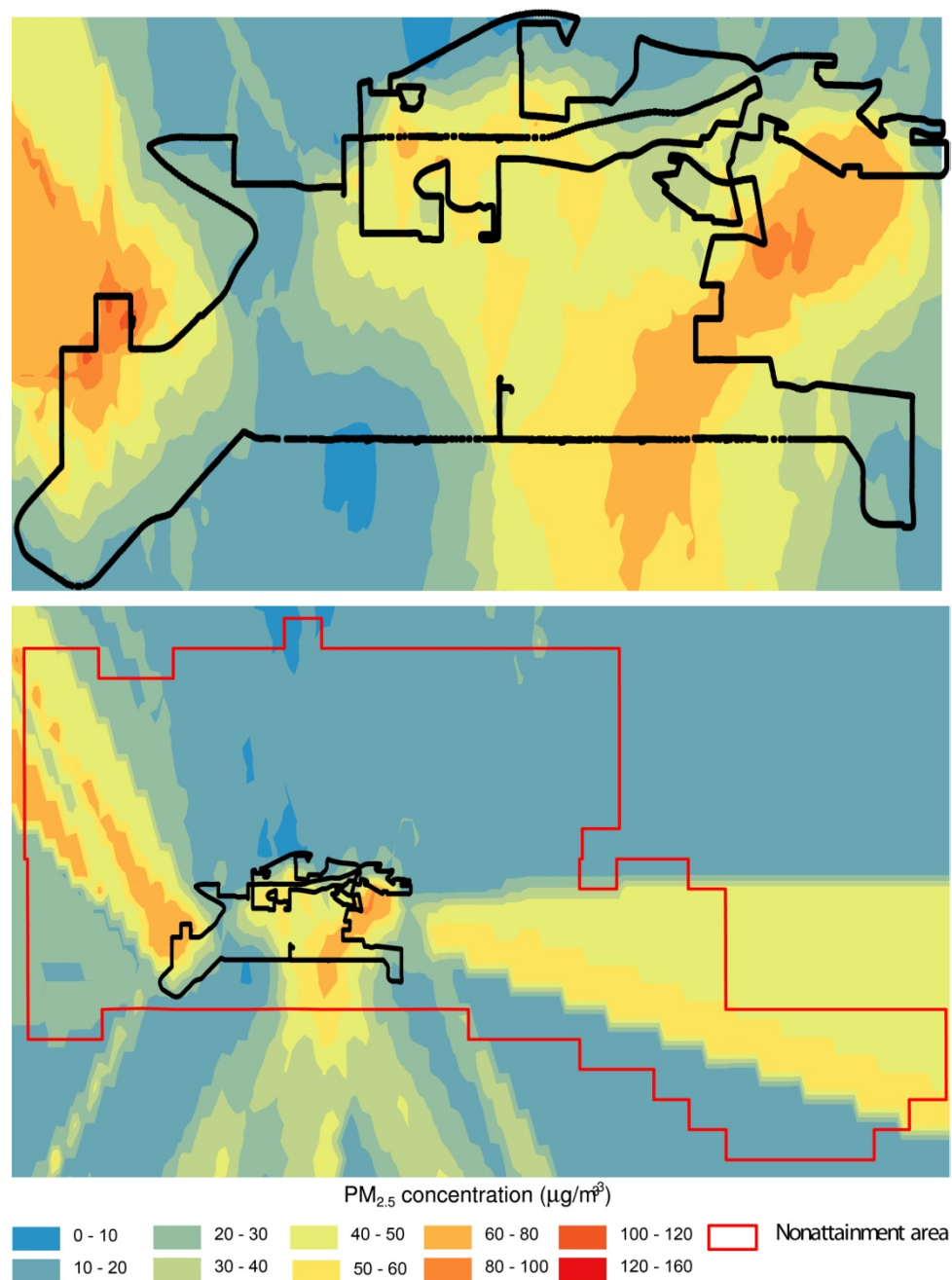
Figure 1.3 Interpolated PM$_{2.5}$-concentrations in the area covered by the sniffer measurements (top) as obtained with the universal kriging method using the ESRI ArcGIS Desktop v.10 and based on sniffer measurements during the drive on 01-02-2010, and (bottom) the extrapolated PM$_{2.5}$-concentrations in the Fairbanks nonattainment area as obtained with the same method and based on the same measurements. The red polygon indicates the PM$_{2.5}$-nonattainment area. The black lines indicate the sniffer route. Values of the PM$_{2.5}$-observations made during this drive are shown in Figure 1.1.

Chapter 2 Methodology and experimental design

2.1 Model setups

The contributions of emissions from point sources, traffic, uncertified wood-burning devices, and wood-burning device changeouts to the $PM_{2.5}$-concentrations at breathing level in the Fairbanks nonattainment area were investigated by results from simulations with all emission sources, and simulations wherein one of the aforementioned emission sources was excluded. The reference scenario considered all emissions as they were in the emission inventory (i.e., no change) and allocated in space and time by the Alaska Emission allocation Model (AkEM; Mölders, 2009; 2010) or the Sparse Matrix Operator Kernel Emissions model (SMOKE; Coast, 1996; Houyoux et al., 2000); in the experimental scenarios, the emissions from the source-category of interest were shut off or exchanged by the emissions from the replacement source-category at the emission inventory level prior to allocation in space and time.

The numerical modeling systems used in air-quality studies typically have two main components: the meteorology component that simulates the meteorological state variables and fluxes, and the chemistry component that simulates the transport, transformation and removal of chemical species. These main components of air-quality models can be operated in "decoupled" or "coupled" mode, and each of these modes has its advantages and disadvantages.

In the "decoupled" mode, the chemical quantities are driven by the simulated meteorology without feeding back to the meteorology. This mode allows for the simulation of the chemical fields under various emission-change scenarios without the

need of re-simulating the meteorology. Therefore, using such a model approach saves computational resources. For this reason, this mode is preferred in regulatory studies (EPA, 2007; Grell and Baklanov, 2011). In addition, the simulations of the chemical fields can be performed on different domain configurations from the same meteorological simulation. However, this approach may lead to inconsistencies with consequences for simulated air quality, or loss of potentially important information about atmospheric processes (Mölders et al., 1994; 1995; Grell et al., 2004; 2005). Traditionally, operational air-quality modeling systems commonly apply the "decoupled" approach (Otte et al., 2005; EPA, 2007; Grell and Baklanov, 2011).

In the "coupled" mode, the meteorological and chemical fields are simulated concurrently in each time interval. Since the various chemical and physical processes have different characteristic time scales, operator splitting is applied for each time interval (Figure 2.1). This means that the individual processes are run with their own time steps, and data is exchanged at defined time steps that are relevant for the processes. For instance, at a 4km grid-increment, a model time step of 12s is chosen to fulfill the Courant criterion for most of the physical processes while faster processes have to be simulated using shorter time steps which are typically one order of magnitude smaller than the model time step (i.e., 6s; Yamaguch and Feingold, 2012). For a 4km grid-increment and when there are few or no convective clouds and insolation is low, a time step of 4 minutes is sufficient for determining the radiative transfer (Dudhia, 2011). It is recommended that the chemistry packages be called at the same time step as the physical packages (Peckham et al., 2009). However, the chemical processes included in the

chemistry packages are determined at their individual time scale (http://ruc.noaa.gov/wrf/WG11/FAQ.htm). The data exchange made at defined time steps permits feedbacks between the meteorological and chemical processes, such as cloud-aerosols and radiation-aerosol feedbacks (Zhang, 2008; Chapman et al., 2009).

Outputs from one process are used to initialize values at the beginning of a subsequent process. Fast processes in each process category can be determined at time steps shorter than the time interval.

The feedback between the meteorological and chemical processes ensures consistency in simulating both the meteorological and chemical processes as they are performed with the same diffusion, advection, boundary layer, cloud and radiation process configurations. Note that in decoupled mode, these processes are recalculated, and sometimes even with different parameterizations (see Mölders et al., 1994), to determine the distribution of the chemical fields.

Considering feedbacks between meteorology and chemistry enhances the accuracy in simulating both the meteorological and chemical fields (Grell et al., 2005; Grell and Baklanov, 2011). However, it requires a complete recalculation of all meteorological state variables and fluxes for each emission-change scenario. Therefore, the "coupled" approach requires more computational resources and provides less flexibility in testing various scenarios than the "decoupled" approach. The "coupled" approach is favored in weather and climate research that investigates the interactions between meteorology and chemistry, such as interactions between radiation transport and aerosols (e.g., Chapman et al., 2009) or aerosols and clouds (e.g., Grell et al., 2011).

This study used simulations performed with the Alaska adapted (Mölders et al., 2011b) version of the Weather Research and Forecasting model (WRF; Skamarock et al., 2008) "coupled" with chemistry packages (WRF/Chem; Grell et al., 2005; Peckham et al., 2009) version 3.1.1 to investigate the impacts of point-source emissions and emissions from uncertified wood-burning devices on the $PM_{2.5}$-concentrations in the Fairbanks nonattainment area. The Alaska adapted WRF/Chem was chosen for this study as its performance had been evaluated frequently for Alaska conditions (e.g., Mölders et al., 2011b; 2012) and as it was the only air-quality model adapted for Fairbanks at the beginning of my thesis work.

Tran and Mölders (2011) showed that the distribution of $PM_{2.5}$-concentrations differed among months during winter (chapter 3). In addition, EPA-recommended emission allocations showed that emissions from point-sources and wood-burning devices vary over the winter cycle. These findings mean that the contributions of emissions from point-sources and wood-burning devices to the $PM_{2.5}$-concentrations should be investigated for an entire winter cycle. As WRF/Chem simulations for Fairbanks were already available for November 2005 to February 2006, and for October 2008 to March 2009 (Mölders et al., 2011b; 2012), I used these simulations for this purpose.

Note that, for the above purpose, the simulations with the Alaska adapted WRF/Chem were performed with the emission of the National Emission Inventory (NEI) of 2005 and 2008. These NEIs were the only emission inventories available at the time

when these studies were performed. For applications with these NEIs, grid-increments finer than 4km or so are not recommended (EPA, 2007).

To investigate the contribution of traffic emissions to the PM$_{2.5}$-concentration in Fairbanks, I performed simulations using the Alaska adapted WRF version by Gaudet and Staufer (2010) "decoupled" with the Alaska adapted (Mölders and Leelasakultum, 2011a) version of Model-3 Community Multiscale Air Quality (CMAQ; Byun and Schere, 2006) modeling systems – called WRF-CMAQ hereafter. The WRF-CMAQ was chosen for this part of the study as it permits utilizing the high resolution emission inventory (1.3km×1.3km) that was developed for Fairbanks by Sierra Research Inc. and prepared for simulations with WRF-CMAQ (T.R. Carlson, pers. comm., March 2011). This emission inventory used the bottom-up approach. This approach is considered to be better at fine resolution. Note that the NEI is based on a top-down approach. In addition, at the 1.3km×1.3km resolution, the emission inventory provided by Sierra Research Inc. allows the WRF-CMAQ simulations to be performed at this fine horizontal resolution. In simulations at such resolution, the scale of the traffic emissions and their impacts on the PM$_{2.5}$-concentrations are better represented than in the simulations at the lower resolution required by the use of NEI. More importantly, air-quality simulations at high resolution (1.3km×1.3km as in this study) are needed for AQuAT which is aimed for the public air-quality advisories.

At this time, CMAQ is considered to be one of the regulatory models recognized by EPA. Prior to the work of Mölders and Leelasakultum (2011a; 2012), air-quality studies for the Fairbanks area were only performed with the Alaska adapted WRF/Chem

(e.g., Mölders et al., 2011b; 2012; Leelasakultum et al., 2012; Tran and Mölders, 2012a; b). Besides being used for the investigation of the contributions of traffic emissions to the $PM_{2.5}$-concentrations, and to serve as a database for AQuAT, the WRF-CMAQ simulations used in this study also provide an opportunity to further evaluate the performance of the Alaska adapted WRF-CMAQ in simulating air quality for Fairbanks.

As the emission inventory for Fairbanks (Sierra Research Inc., pers. comm., March 2011) showed that traffic emissions marginally differ over the winter cycle, their contributions to the $PM_{2.5}$-concentrations in the Fairbanks nonattainment area were investigated for two episodes: episode 1 (December 27, 2009 to January 11, 2010), and episode 2 (January 1 to 30, 2011). During these two episodes, the observed $PM_{2.5}$-concentrations frequently exceeded the NAAQS at the official monitoring site at the State Office Building or other sites.

Note that the emission inventory for Fairbanks that was used for the WRF-CMAQ simulations in this study was not available at the time when studies with WRF/Chem simulations were performed. Nevertheless, evaluations of WRF/Chem and WRF-CMAQ simulations performed for Fairbanks show relatively similar skill scores despite the differences in the model setups (Mölders and Leelasakultum, 2011b; see also section 4.2). Therefore, the WRF/Chem and WRF-CMAQ simulations used in the studies of this dissertation still allow for the investigation of the contributions of point source, uncertified wood-burning devices, and traffic emissions to the $PM_{2.5}$-concentrations in Fairbanks.

A detailed description of the model setup of the Alaska adapted WRF/Chem is given in section 2.1.1 and Mölders et al. (2011b, 2012). The detailed description of the model setup of the Alaska adapted WRF-CMAQ is given in section 2.1.2 and Tran et al. (2012). The emission inventories used for these simulations are described in section 2.2.

2.1.1 Alaska adapted WRF/Chem

WRF/Chem is a state-of-the-art Eulerian model and is widely used in atmospheric pollution and air-quality research (Jacobson et al., 2007; Rosenfeld et al., 2007; Ying et al., 2009; Mölders et al., 2010; 2011b; 2012; Zhang et al., 2010a; b; Tran et al., 2011). WRF/Chem is fully compressible and uses the Euler non-hydrostatic equations. Its dry hydrostatic-pressure terrain-following vertical coordinate permits the stretching of the grid-layers. This stretching helps to capture the stronger gradients of meteorological and chemical fields in the atmospheric boundary layer where most of the emissions occur. WRF/Chem uses an Arakawa C[1] (Arakawa and Lamb, 1977) staggered horizontal grid (Figure 2.2).

Simulations with the Alaska adapted WRF/Chem were performed from 11/01/2005 to 2/28/2006 (Mölders et al., 2011b), and from 10/01/2008 to 3/31/2009 (Mölders et al., 2012). The simulation results were investigated for the contribution of emissions from point sources (Tran and Mölders, 2012a), wood-burning device changeouts (Tran and Mölders, 2012b), and uncertified wood-burning devices in general,

---

[1] Note that staggered grids provide more accurate results at fine resolutions than do unstaggered grids, for instance, an Arakawa A grid (Warner, 2011).

to the $PM_{2.5}$-concentrations in the Fairbanks nonattainment area. The emission inventories used for these simulations are discussed in section 2.2.

The domain of interest for the analysis encompasses the Fairbanks nonattainment area and its adjacent land with 80×70 grid-cells and a 4km increment (Figure 2.3). There are 28 stretched vertical layers from the surface to 100hPa. The first layer is 8m thick above the ground and is referred to as the breathing level, hereafter. There are 10 layers below 1km.

The $1^{o}×1^{o}$ and 6h-resolution global final analyses data obtained from the National Centers for Environmental Prediction was downscaled to provide the meteorological initial and boundary conditions. Initial soil and snow conditions were also downscaled from this data.

The meteorology was initialized every five days. As discussed by Mölders (2008) and Mölders et al. (2011b), the performance of the 120h forecast lead was only slightly different from those of the 24-, 48-, 72-, and 96-h forecast leads over Interior Alaska.

The initial conditions for the chemical fields are the distributions achieved from a simulation started with background concentration profiles 14 days prior to the beginning day of the episode of interest. Since Fairbanks is the only major emission source in the area, typical Alaska background concentrations served as the chemical boundary conditions. Note that observational studies (e.g., Cahill, 2003) and modeling studies (e.g., Tran et al., 2011; Mölders et al., 2012) showed that advected concentrations of $PM_{2.5}$ are small (an order of magnitude less) compared to the NAAQS.

The selected physical packages used in this study were based on experience from previous studies that had provided acceptable simulations of Alaska winter conditions (e.g., Chigullapalli and Mölders, 2008; Mölders, 2008; Mölders et al., 2010; Mölders and Kramm, 2010; Yarker et al., 2010). Their parameterizations and the modifications made to WRF/Chem for Alaska conditions are briefly discussed in the following sections.

2.1.1.1 Physical packages

Cloud and precipitation processes were calculated by the WRF Single-Moment 5-class (WSM5) scheme (Hong et al., 2004; Hong and Lim, 2006). This scheme considers mixed-phase cloud microphysical processes and includes five categories of hydrometers: vapor, rainwater, snow, cloud-water and cloud-ice. Super-cooled cloud-water droplets and cloud-ice are allowed to co-exist at temperatures below the freezing point.

Cloud formation through deep and shallow convection was treated using the Grell-3D scheme, which is the modified version of the ensemble scheme developed by Grell and Dévényi (2002). In this scheme, several simulations of convective clouds with different entrainment/detrainment rates of downdraft/updraft and precipitation efficiencies are performed as ensembles in each model grid-column. A statistical technique is then applied to average the outputs and provide feedback to the model. By default, equal weight averaging is applied (Skamarock et al., 2008). The Grell-3D scheme allows subsidence effects to spread into neighboring grid columns. This modified scheme is suitable for horizontal grid-increments <10km (Skamarock et al., 2008) and is therefore suitable for use in this study where the horizontal grid-increment is 4km.

The exchange of heat and moisture at the land-atmosphere interface was treated with a modified version of the Rapid Update Cycle (RUC) scheme (Smirnova et al., 2000). The RUC takes into account the phase changes of soil water. Given the fact that the Fairbanks area is underlain by permafrost or discontinuous permafrost this feature is important for this study. The RUC's multi-layer soil model expands from the Earth's surface to 300cm depth. The RUC also has a multi-layer snow model with features such as changing snow density, snow depth and temperature dependent albedo, and melting algorithms applied at both the snow-atmosphere interface and the snow-soil interface. Note that such features permit better simulation of the exchange of heat and moisture at the end and beginning of the snow season and for moderate snow layers (Fröhlich and Mölders, 2002; Mölders et al., 2008).

The turbulent transports in the Atmospheric Boundary Layer (ABL) and in the free atmosphere were determined by the Mellor-Yamada-Janjić scheme (Mellor and Yamada, 1982; Janjić, 2002). This scheme determines the flux profiles within the ABL and provides tendencies of temperature, moisture, and momentum. To determine the ABL height, the Mellor-Yamada-Janjić scheme uses a prognostic equation for the turbulence kinetic energy (TKE) as a closure. Under stable atmospheric conditions, the Mellor-Yamada-Janjić scheme determines the ABL height based on the requirement that the ratio of the variance of the vertical velocity deviation and TKE cannot be smaller than an empirical critical value (Janjić, 2002). Note that in this study, simulations were performed for Fairbanks in winter when extreme stable conditions dominated and buoyancy was marginal (Mölders and Kramm, 2010).

Atmospheric radiative transfer was determined by the Rapid Radiative Transfer Model (RRTM; Mlawer et al., 1997) for long-wave radiation and by the Goddard scheme for shortwave radiation (Chou and Suarez, 1994). These schemes have been found to provide good results for Alaska (e.g., Chigullapalli and Mölders, 2008; Mölders and Kramm, 2010; Hines et al., 2011) and allow consideration of various species, aerosols and cloud species. The RRTM is a spectral-band scheme that uses the correlated-k method. This method is based on the concept that the spectral transmittance is independent of the order of the absorption coefficient (k) for a given spectral interval and hence the wave-number domain may be converted to the k-domain in the integration. This approach determines the radiative transport with reasonable accuracy (Mlawer et al., 1997), and greatly reduces the computational time. The RRTM takes into account cloud optical depth, and the absorptions and emissions of gases including water vapor, ozone, CO_2 and trace gases (e.g., methane, nitrous oxide and the common halocarbons).

The k-distribution approach is also adopted in the Goddard shortwave scheme. This scheme considers 11 spectral bands including the visible range and surrounding wavelengths, and includes water vapor, carbon dioxide, and ozone as the main absorbers of terrestrial shortwave radiation. Shortwave radiation fluxes are calculated under consideration of the absorption, reflection and scattering effects of atmospheric gases and aerosols. The upward shortwave radiation flux by reflection from the surface is also taken into account. Surface albedo is determined depending on land-use type and the fractional snow-cover if snow exists. Note that a continuous snow cover exists most of the time for the episodes examined here.

2.1.1.2 Chemistry packages

Gas-phase chemistry is treated by the Regional Acid Deposition Model (RADM; Chang et al., 1987) upgraded gas-phase mechanism (RADM2; Stockwell et al., 1990). The RADM2 mechanism considers 21 inorganic and 42 organic species, and 156 chemical reactions. Inorganic reactions and rate constants follow DeMore et al. (1988). Reactions with hydroxyl radicals and nighttime chemistry of nitrate are also taken into account. Volatile organic compounds (VOCs) are grouped into 26 groups of stable organic compounds and 16 groups of organic short-lived intermediates (peroxy radicals). Their reaction mechanism follows Middleton et al. (1990), which is based on the species' oxidation reactivity and emission magnitudes. As is common practice in air-quality modeling, most emitted organic compounds are lumped into surrogate species of similar reactivity and molecular weight (Stockwell et al., 1990). Photolysis rates are calculated in accordance with Madronich (1987). In total, 21 photo-chemical reactions are considered.

Dry deposition of trace gases is treated following Wesely (1989) with the modifications for Alaska introduced by Mölders et al. (2011b). The dry deposition scheme includes sulfur dioxide, ozone, the nitrogen oxide group, sulfate in the gas phase, and other trace gases. The deposition velocity of the gases is determined as the function of aerodynamic resistance, the sublayer resistance and the bulk surface resistance. In this study, the bulk surface resistance is determined using the winter values as in Interior Alaska, October through March are the cold season months. The bulk-resistance is determined based on the respective land-use types with consideration of other factors such as surface temperature, stomatal resistance to environmental conditions, the wetting

of the surface by dew and rain, and the covering of the surface by snow. The modifications for dry deposition on snow that were introduced by Mölders et al. (2011b), follow Zhang et al. (2003). Further modifications introduced by Mölders et al. (2011b) take into account that the stomata of some Alaska vegetation are still open at -5°C.

Aerosols in the atmosphere may stem directly from emissions (primary aerosols) and/or from gas-to-particle conversions (secondary aerosols) that occur under the presence of precursor gases and appropriate atmospheric conditions. In this study, the Secondary Organic Aerosol Model (SORGAM; Schell et al., 2001) and Modal Aerosol Dynamics Model for Europe (MADE; Ackermann et al., 1998), known as MADE/SORGAM served to describe the aerosol dynamics, chemistry and physics including inorganic and secondary organic aerosol, and wet and dry removal processes of aerosols. In MADE, the sub-micrometer aerosols are distributed into two overlapping lognormal modes. MADE considers nucleation and emissions as sources, and coagulation, condensation, transport, and deposition as processes modifying the aerosol population in the atmosphere. The aerosol chemistry of MADE currently involves sulfate, nitrate, ammonium, and water components in the aerosol phase. In SORGAM, the gas-to-particle partitioning of reactive organic gas compounds is simulated as an absorption process into the organic mass on the aerosol particle assuming the formation of a quasi-ideal solution (Schell et al., 2001).

2.1.2 The Alaska adapted WRF-CMAQ

The selection of the physical packages (Table 9.1) for the WRF simulation in the WRF-CMAQ Alaska adapted version (Mölders and Leelasakultum, 2011a) are as those selected in the WRF/Chem simulations of which the detailed description was given in section 2.1.1 but follow the domain setup of Gaudet and Stauffer (2010).

In this study, the WRF simulations were performed on three one-way nested domains (Figure 9.1) which have 38 full vertical layers following Gaudet and Stauffer (2010). The outermost and largest domain (domain 1) is centered at 64.92749N and 147.957W and encompasses Alaska, parts of Siberia, the North Pacific, and the Arctic Ocean with 400×300 grid-cells of 12km increment. Domain 2 covers central Alaska with 201×201 grid-cells of 4km increment. The inner most domain covers the Fairbanks nonattainment area and the western part of it with 201×201 grid-cells of 1.3km increment (Figure 9.2). In this configuration, WRF simulations were performed concurrently in all three domains. The boundary conditions for the inner domain were taken from the simulation of its parent domain and no feedback to the parent domain was allowed. This setup helps to smoothly downscale the boundary conditions for domain 3. The initial and boundary conditions for domain 1 stemmed from the 1°×1°, 6h-resolution National Centers for Environmental Prediction global final analysis data. In total, 13 vertical layers were within 1km above ground level, and the thickness of the lowest layer was 4m.

Nested domain configurations are commonly applied in studies where the domains of interest require high resolution (e.g., Fierro et al., 2009; Loughner et al., 2009). Such setups proved themselves to provide better accuracy than simulations

without nested domains (e.g., Shu-Chang et al., 2006). The meteorological initial conditions for all three domains stemmed from the same global final analysis data and were re-initialized every five days similar to the procedure applied in the WRF/Chem simulations. In contrast to Gaudet and Stauffer (2010), the WRF simulations in this study were performed in retrospective forecast mode (i.e., neither analysis nor observational nudging was applied). This mode allows freedom in the simulations (i.e., not being constrained by nudged meteorological fields) and avoids potential errors due to the sparse observational network in Alaska which could happen if observational nudging was used.

The chemical and aerosol processes, transport, diffusion, and removal of species were simulated by CMAQ version 4.7 for the finest resolved domain (i.e., domain 3) and driven by the meteorological fields simulated by WRF for domain 3. The CMAQ domain is one grid-cell smaller to each side of the WRF domain 3 due to the fact that those outmost grid-cells serve as boundaries for the CMAQ domain.

The Meteorology-Chemistry Interface Processor (MCIP; Byun et al., 1999) with modifications introduced by Mölders and Leelasakultum (2011a) serves as an interface to translate and process outputs of WRF and to provide needed inputs to the CMAQ Chemical Transport Model (CCTM). MCIP provides flexibility in incorporating outputs from various meteorological models into CCTM. It takes care of issues related to data format translation, unit conversions, and if needed, performs extraction or interpolation of meteorological data on different domain configurations to the target CCTM domain (Byun et al., 1999). In this study, CCTM operated on the same domain configuration and

projection as WRF in domain 3. Parameters needed by CCTM, but not provided by WRF were diagnosed via MCIP.

Gas-phase chemistry was treated in CCTM by the Carbon Bond mechanism developed in 2005 (CB05; Yarwood et al., 2005) which is the updated version of the Carbon Bond mechanism IV (Gery et al., 1989). The CB05 considers 51 chemical species and 156 reactions. Inorganic species in CB05 include carbon monoxide, ozone, various inorganic nitrogen compounds, sulfur dioxide, sulfuric acid, hydroxyl, and nitrate radical compounds. Unlike the RADM2 mechanism, the CB05 mechanism groups the organic compounds (except those which are treated explicitly) according to their carbon bond type (e.g., single bonds, double bonds, carbonyl bonds) and treats them similarly regardless of the molecules in which they occur. Noticeable updates in CB05 from its predecessor include updated reaction rate constants and photolysis rates, extended inorganic and organic reaction sets, and more species (Yarwood et al., 2005).

Aerosol chemistry was treated in CCTM by the fifth-generation CMAQ aerosol model (Binkowski and Roselle, 2003) which is based on the modal aerosol modeling approach. The aerosol chemistry module applied in CCTM and the MADE applied in WRF/Chem share common features. As in MADE, in CCTM, particles are grouped into Aitken, accumulation and coarse modes assuming log-normal distribution. Currently, the Aitken and accumulation modes may interact with each other through coagulation but interactions with the coarse mode are not allowed (Binkowski and Roselle, 2003).

For AQuAT, the horizontal increment of the database was to be 1.3km. Therefore, aerosol processes in clouds were treated by the resolved cloud module considers

scavenging, aqueous chemistry, and wet deposition. Aqueous chemistry is treated following the approach applied in RADM (Chang et al., 1987). Secondary organic aerosols are treated in CCTM based on SORGAM (Schell et al., 2001) with modifications in gas-phase chemistry yields and saturation concentrations for aromatics, terpenes, alkanes and cresols as described in Byun et al. (1999). The aerosol module of CCTM treats secondary organic aerosols from anthropogenic and biogenic emission sources separately.

Dispersion of the chemical species is driven by transport processes which consist of advection and diffusion. Horizontal and vertical advections were treated using the global mass-conserving scheme (Yamartino, 1993) following the recommendations of Mölders and Leelasakultum (2011a). This scheme is based on the local grid-cell-centered polynomials approach to determine the flux transport through grid-cells of various thicknesses while ensuring mass-conservation. Horizontal diffusion was determined based on the diffusion coefficient derived from local wind deformation (Byun and Schere, 2006). Vertical diffusion was calculated using the K-theory approach which is suitable for simulations where the scale of turbulent motion is smaller than the scale of the mean motion. This condition commonly occurs under stable or neutral static stability conditions (Pleim and Chang, 1992).

I used the model with the modifications for Alaska conditions described in Mölders and Leelasakultum (2011a). They included slightly lower minimum and maximum thresholds of the eddy diffusivity coefficients (K_z) than the original CMAQ, and a decreased minimum mixing height from (50m to 16m) as observed in Fairbanks

(Wendler and Nicpon, 1975). Dry deposition of aerosols was treated in CCTM using the second-generation CMAQ aerosol deposition velocity routine (Byun et al., 1999). In this study, the CCTM used the dry deposition module with the modifications introduced by Mölders and Leelasakultum (2011a). These modifications, among other things, consider dry deposition on various types of tundra, modified plant specific parameters following Erisman et al. (1994), reduced thresholds for photosynthesis activity (Mölders et al.; 2011b), and modifications in the formulation of dry deposition over snow (Mölders et al.; 2011b) that is based on Zhang et al. (2003).

As previous studies (e.g., Cahill, 2003; Tran et al., 2011; Mölders et al., 2012) showed that the $PM_{2.5}$-concentrations in Fairbanks were hardly impacted by long-range transport from other regions, Alaska background concentrations (Mölders and Leelasakultum, 2011a) were used as chemical boundary and initial conditions for the CMAQ simulations. Except the first day that used the Alaska background concentrations as initial conditions, the chemical fields at the end of a simulation day served as the initial conditions for the next simulation. Outputs from simulations that served as spin up time (three days) for the chemical field were discarded from the analysis as recommended by Mölders and Leelasakultum (2012).

2.2 Emission data

2.2.1 The National Emission Inventory

The NEI is developed and maintained by the US EPA to provide estimates of annual emissions by source of air pollutants over the US

(http://capita.wustl.edu/NAMEN/EPA_NEI.htm). The NEI database is used for tracking trends of emissions over time, regional strategic development and as input for air-dispersion and air-quality modeling. It is based on a top-down approach with input from state and local agencies, tribes, and industry. Emission estimates are available for individual major point sources, and are allocated by county/borough for area, mobile and other sources. The current NEI-database has data on more than 52,000 point sources, 400 categories of highway and nonroad mobile sources, and 300 categories of area sources (EPA, 2012). Since the release of the NEI2008, EPA considers airports as point sources (EPA, 2009). Information on stationary and mobile sources that emit air pollutants is also included in the NEI-database. The NEI-database is available for critical pollutants since 1985 and for hazardous air pollutants since 1999. It is updated on a 1-in-3-year basis. The NEI-database is currently available for all 50 states, the District of Columbia, Puerto Rico, and the Virgin Islands.

2.2.2 Emission data for WRF/Chem 2005/2006 simulations

The NEI2005 provided estimates of anthropogenic emissions of PM_{10}, $PM_{2.5}$ and its precursor gases for the winter 2005/2006 simulations performed by Mölders et al. (2011a; b) with the Alaska adapted WRF/Chem. Missing stack parameters and/or coordinates of some point-sources were filled in and/or corrected by contacting the respective facilities.

The Alaska Emission allocation Model (AkEM; Mölders, 2009) was used to spatially allocate emissions from area and mobile sources based on Fairbanks population

density data of 2000 and traffic data, respectively. The temporal allocation of emissions from area and mobile sources follows EPA's recommendations with modifications for Alaska (e.g., no lawn mowing after snowfall, no motor boat traffic after freeze up). The AkEM employed data provided by some point-source facilities in Fairbanks to temporally allocate emissions from all point-sources in the domain. Plume rise was calculated based on stack height, exit velocity, ambient temperature and wind-speed. Differences in emissions between weekends and weekdays were also considered by AkEM. For all sources, the temporal allocations differ with time of the day, day of the week, and month. For 2006 an increase of 1.5% in the annual emissions was assumed (Mölders et al., 2011a; b). The AkEM split the emitted pollutants into the species required by the RADM2 and MADE/SORGAM modules used in WRF/Chem. The split of $PM_{2.5}$-emissions into sulfate, nitrate, ammonium, potassium, carbon, and other unspecified aerosols was made based on the 2005/2006 observations in Fairbanks (Mölders et al., 2011a; b). Depending on emissions-source types, the AkEM split the total anthropogenic VOC emissions into various species such as alkanes, alkenes, ketones, etc. (Mölders et al., 2011a; b).

Biogenic emissions were calculated inline by WRF/Chem as described in Simpson et al. (1995). In this approach, emissions of isoprene, monoterpenes, other biogenic volatile organic carbon, and nitrogen compounds were determined based on land-use, temperature, and radiation fluxes which are provided by WRF/Chem.

WRF/Chem simulations in the 2005/2006 study were performed in two scenarios. The reference scenario (REF) considered all emissions as they are in the NEI2005 (i.e.,

no change) and was allocated in space and time onto the domain by AkEM. In the experimental scenario (NPE), the emissions from point-sources in Fairbanks and its neighborhood were shut off to investigate the contribution of emissions from point-sources to the $PM_{2.5}$-concentrations in the Fairbanks nonattainment area.

2.2.3 Emission data for WRF/Chem 2008/2009 simulations

The anthropogenic emissions for the 2008/2009 simulations performed by Mölders et al. (2012) were based on the early version of the NEI2008, which was released in 2010. Point-source emissions were not updated in this version of the NEI2008. Therefore, emissions from some point sources were updated with data provided by the facility holders in Fairbanks. For those point sources, for which no data was provided, the emissions were assumed to increase by 1.5%/yr from those given in the NEI2005.

Some nonpoint-emission sectors were not available in this version of the NEI2008. Those sectors include industrial/commercial/institutional fuel combustion and residential wood combustion. The 2008 emissions from industrial/commercial/institutional fuel combustions were assumed to be the same as in the NEI2005 because these sectors just marginally changed over 2005-2008 in Fairbanks. The emissions from residential combustion make up a large portion of the emissions in the Fairbanks North Star Borough (FNSB) according to the NEI2005. Emissions from residential combustions were obtained from Davies et al. (2009). Their data showed a much higher emissions from residential wood combustion in 2008 as compared to the

NEI2005. The increase in woodstove emissions, however, is expected to represent the situation of emissions in the FNSB in winter 2008/2009 more accurately since the increase in oil prices resulted in many households adding woodstoves or using wood more intensively. Over the past few years, the use of wood-burning devices has further increased to reduce heating costs in response to the bad economic situation. The number of wood cutting permits in Fairbanks has increased threefold in 2009 as compared to 2007 (J. Conner, pers. comm., June 2010).

The mobile emissions as listed in the NEI2008 are less than they were in the NEI2005. This is consistent with the lower traffic activity in 2008 as compared to 2005 (DOT, 2009). Some nonpoint-emission sectors were required to be updated with the latest borough employment data. These updates were done using the data from Alaska Department of Labor and Workforce Development (*http://laborstats.alaska.gov)*.

The modified version of AkEM (Mölders, 2010) was used to allocate the anthropogenic emissions for 2008/2009 into space and time depending on population density, traffic network, sources activity and temperature. The modified AkEM aims at improving the allocation functions by using temperature dependent correction factors to account for higher (lower) cold-start emissions and emissions from heating as temperatures are below (above) the longterm monthly mean temperature based on the experiences from the 2005/2006 simulations (Mölders et al., 2011b) and other studies. Several studies (e.g., Stump et al., 1990; Laurikko, 1995) showed that emissions drastically increased under extremely cold weather conditions. Biogenic emissions for the 2008/2009 simulation were treated as in the 2005/2006 simulations.

2.2.3.1 Emissions for the woodstove scenarios

As discussed above, the emission rates from residential combustions were obtained from Davies et al. (2009) following recommendations from the FNSB as data for residential combustion was not available in the NEI2008 at the time this study was performed.

In the reference scenario for the 2008/2009 study (REF), WRF/Chem simulations considered emissions from all source-categories. The fact that some households have two heating devices, i.e., woodstoves co-exist with oil furnaces, was considered and described in detail in Mölders (2010) and Mölders et al. (2011a).

Carlson et al. (2010) reported different numbers of home-heating devices, including the number of uncertified wood-burning devices, than Davies et al. (2009). Carlson et al. (2010) estimated a total of 9240 wood-burning devices in Fairbanks of which 2930 were uncertified woodstoves and 90 were outdoor wood boilers. Meanwhile, Davies et al. (2009) estimated that there exist 13829 wood-burning devices in Fairbanks of which 5042 were uncertified woodstoves and 1500 were outdoor wood boilers, respectively.

The benefit of using air-quality simulations as a database for AQuAT is that it can include information on the effects of emissions from different kinds of sources on the distribution of $PM_{2.5}$-concentrations. As pointed out in chapter 1, understanding the contribution of uncertified wood-burning devices in general, and of the wood-burning device changeouts in particular, to the $PM_{2.5}$-concentrations in the Fairbanks

nonattainment area helps the assessment of the value of air-quality data for the development of AQuAT.

Because of the inconsistency in the reported numbers, five sensitivity studies (WSR, WSS1, WSS2, WSS3, WSS4) were performed by Mölders et al. (2011a) and Mölders (2012; pers. com). I used these simulations to investigate the contributions of uncertified wood-burning devices on the $PM_{2.5}$-concentrations in Fairbanks. In WSR, WSS1 and WSS2, the emissions from uncertified wood-burning devices were exchanged by emissions from the certified woodstoves to investigate their effects on the $PM_{2.5}$-concentrations. In WSS3 and WSS4, the emissions from uncertified woodstoves were excluded to investigate the contribution of these devices to the $PM_{2.5}$-concentrations in Fairbanks. Note that the sensitivity studies WSS1, WSS2, WSS3, and WSS4 were only performed from October 1 to October 14 to assess the importance of the number and type of wood-burning devices.

In WSR, the uncertified wood-burning devices were exchanged by certified ones based on the data of Carlson et al. (2010). In WSS1, the exchange of uncertified wood-burning devices was based on the numbers reported by Davies et al. (2009). The number of uncertified wood-burning devices exchanged in WSS2 was based on unpublished data by Carlson and collaborators (pers. comm., November 2009). That data marginally differed in the number of total wood-burning devices (9241) and uncertified woodstoves (2934) from the numbers published in Carlson et al. (2010) and used in WSR, but did not consider pellet stoves (0 versus 370 devices). In WSS3 and WSS4, the amount of

emissions from uncertified wood-burning devices excluded from the total emission was based on the report of Carlson et al. (2010) and Davies et al. (2009), respectively.

By excluding uncertified wood-burning devices at large numbers and by exchanging the uncertified with certified wood-burning devices, the emissions, of both primary $PM_{2.5}$ and its precursors as well as of other emitted species, change. The total annual emission rate from heating of the ith specie after wood-burning device replacements is given by (Mölders et al., 2011a)

$$E_{WSY}=E_{REF}+N_{exch}E_2-\sum_j N_j E_j \tag{2.1}$$

where E_{WSY} is the total annual emission rate from heating of the ith specie in the WSR, WSS1, WSS2, WSS3, WSS4, respectively; E_{REF} is the total annual emission rate from heating of the ith specie in the reference simulation (REF). Furthermore, N_{exch} and E_2 are the number of wood-burning devices replaced and emission rates per certified wood-burning device; N_j and E_j are the emission rates and numbers of uncertified wood-burning devices, and the index j stands for the category of the noncertified wood-burning devices that were excluded/exchanged, respectively. For WSS3 and WSS4, $N_{exch}E_2$ equals zero.

2.2.4 Emission data for CMAQ simulations

The anthropogenic emissions used for the CMAQ simulations stem from the first version of the Fairbanks 2008 emission inventory provided by Sierra Research Inc. (pers. comm., March 2011). To apply this emission inventory to the simulation years (winter 2009/2010 and winter 2011), I assumed an emission increase of 1.5%/yr in accord with

Mölders et al. (2011b; 2012). SMOKE served to allocate these "updated" emissions onto the CMAQ-domain in time and space based on the information on emission-source activities, land-use, and population density within each grid-cell. The spatial and temporal allocations, as well as the partitioning of emitted species, used by SMOKE in this study were those recommended for Fairbanks (Sierra Research Inc., pers. comm., March 2011).

Anthropogenic emissions include emissions from point sources, area sources, traffic and non-road traffic. Plume rise was determined by SMOKE (Houyoux, 1998) based on stack characteristics and meteorological inputs provided by the Alaska adapted MCIP (Mölders and Leelasakultum, 2011a). Emission rates of traffic for Fairbanks (Sierra Research Inc., pers. comm., March 2011) were determined by the Mobile Source Emission Factor model (MOBILE6, http://www.epa.gov/otaq/m6.htm) and allocated spatially and temporally onto the model domain by SMOKE.

I applied a temperature-adjustment factor to the temporal allocation of the anthropogenic emissions. Herein, emissions will be higher (lower) on days having daily mean temperatures below (above) the 1970-1999 monthly mean temperature following Mölders (2010) and Mölders et al. (2012).

Biogenic emissions were not considered for the WRF-CMAQ simulations as during winter, the region is snow-covered for which emissions can be assumed to be negligibly small.

2.3 Methods for model performance evaluation

The model outputs were compared with observed meteorological and aerosol data to evaluate the models' performance. The observed surface meteorological data was taken from the Western Regional Climate Center (http://www.wrcc.dri.edu/) and the National Climatic Data Center (http://www.ncdc.noaa.gov/oa/ncdc.html). Shortwave downward radiation (SW), 10m wind-speed (v), 10m wind-direction, 2m air temperature (T), 2m dew-point temperature (T_d), relative humidity (RH) and precipitation were recorded hourly. Additionally, sea-level pressure (SLP) data was available for some sites, too. Vertical temperature and wind-field profiles were available from the twice-daily radiosonde ascents at the Fairbanks International Airport, and from the Doppler SOund Detection And Ranging (SODAR) (K. Sassen, pers. comm., April 2005; J. Fochesatto, pers. comm., December 2008). Aerosol observations were available for the Fairbanks nonattainment area at the State Office Building (SB), Sadler, Peger Road (PR), Pioneer Road (NCORE), and North Pole elementary school (NP) sites, and the Relocatable Air Monitoring System (RAMS) trailer locations (Figure 1.1). Hourly observations of total $PM_{2.5}$-mass measured by Met-One Beta Attenuation Monitors were available at the SB (called SB_BAM hereafter), NP (called NP_BAM hereafter), and the RAMS (called RAMS_BAM hereafter). Filter based 24h-average $PM_{2.5}$-concentrations using the Federal Reference Method were available on a 1-in-3-days basis at the SB (called SB_FRM hereafter), RAMS (RAMS_FRM), NP (NP_FRM), PR and NCORE. The SB and NCORE sites are located in commercial-residential areas whereas the PR and NP-sites are located in mixed industrial-residential areas. The site located in Denali National Park

(DP) is the only site outside the nonattainment area and belongs to the Interagency Monitoring of Protected Visual Environments (IMPROVE) network. At this site, $PM_{2.5}$ and speciation data is available on a 1-in-3-days basis.

The mobile measurements were instantaneously collected by the sniffer traveling at 32-56km/h along planned routes. The sniffer is equipped with a data RAM4000 monitor, BGi $PM_{2.5}$ sharp cut cyclone, sample liner heaters, Garmin GPS, drycal flow calibrator, and temperature loggers. $PM_{2.5}$-concentration and temperature measurements were taken every two seconds.

Note that not all the above data was available for each simulation of this study. Sites where data was available for each study are discussed explicitly in chapter 3.

Performance skill-scores were determined following von Storch and Zwiers (1999) to evaluate the WRF and WRF/Chem performances with respect to simulating meteorological quantities. These skill-scores include the mean bias, root-mean-square error (RMSE), standard deviation of error (SDE), and the correlation coefficient (R). The mean bias indicates systematic errors resulting from model discretization and parameterizations, whereas the SDE indicates nonsystematic errors resulting from initial and boundary conditions and uncertainty of the observations. The R indicates how well the simulated and observed quantities correspond to each other.

Performance skill-scores for evaluating WRF/Chem's and CMAQ's performance with respect to simulating aerosols were determined in accord with Chang and Hanna (2004) and Boylan and Russell (2006). These skill-scores include the fractional bias $(FB = 200\% \times [\sum_{i=1}^{N}(C_{s,i} - C_{o,i})/\sum_{i}^{N}(C_{s,i} + C_{o,i})])$, fractional error $(FE = 200\% \times$

$[\sum_{i=1}^{N}|C_{s,i} - C_{o,i}|/\sum_{i}^{N}(C_{s,i} + C_{o,i})])$, normalized mean bias ($NMB = 100\% \times$

$[\sum_{i=1}^{N}(C_{s,i} - C_{o,i})/\sum_{i=1}^{N} C_{o,i}])$, normalized means error ($NME = 100\% \times [\sum_{i=1}^{N}|C_{s,i} -$

$C_{o,i}|/\sum_{i=1}^{N} C_{o,i}])$, mean fractional bias ($MFB = (200\%/N) \times \sum_{i=1}^{N}[(C_{s,i} - C_{o,i})/(C_{s,i} +$

$C_{o,i})])$, and mean fractional error ($MFE = (200\%/N) \times \sum_{i=1}^{N}[|C_{s,i} - C_{o,i}|/(C_{s,i} + C_{o,i})])$.

Here N is the number of pairs of simulated (C_s) and observed (C_o) PM$_{2.5}$-concentrations.

In addition, we determined the fraction of pairs of simulated and observed PM$_{2.5}$-concentrations that agreed within a factor of two (FAC2). The correlation R between simulated and observed quantities was tested for its statistical significance using the Student t-tests at the 95% confidence level.

Chang and Hanna (2004) suggested that air-quality model simulations that have FB within ±30% and a FAC2 ≥50% are considered as having good performance. Boylan and Russell (2006) recommends the MFB within ±60% and MFE ≤ 75% as the criteria for a model's performance to be considered as acceptable, and MFB within ±60% and MFE ≤ 50% as the goal that a best state-of-the-art model can reach. These criteria consider that it is harder to simulate low concentrations correctly than high concentrations.

2.4 Methods for examining the contributions of emission sources to the PM$_{2.5}$-concentrations

I compared the simulated PM$_{2.5}$-concentrations in the experimental simulations (EXP) with the PM$_{2.5}$-concentrations in the corresponding reference simulations (REF) to investigate the differences of PM$_{2.5}$ and its speciation. Here EXP stands for experimental

simulations without emissions from the examined sources (point sources, traffic and uncertified wood-burning devices), and the experimental simulations where the uncertified wood-burning devices were exchanged. REF stands for the reference simulations with WRF/Chem for winter 2005/2006 and 2008/2009 with WRF/Chem, and with WRF-CMAQ for winter 2009/2010 and 2010/2011. The $PM_{2.5}$-concentration differences (REF-EXP) were tested for their significance at the 95% confidence level by using the Student t-test with *the null hypothesis that $PM_{2.5}$-concentrations in REF and EXP do not differ*. The $PM_{2.5}$-concentration differences were examined in space and time to investigate the impact of the three major source categories on the $PM_{2.5}$-concentrations at breathing level.

I calculated the relative response factors (RRF) in response to the emission changes EXP by dividing the concentrations in EXP by those of corresponding REF (EXP/REF). Beside the RRFs determined at the grid-cell holding the official monitoring site at the State Office Building, I also determined the RRFs for all grid-cells in the nonattainment area to evaluate the effects of emissions changes over the nonattainment area.

References

Ackermann, I.J., Hass, H., Memmesheimer, M., Ebel, A., Binkowski, F.S., Shankar, U., 1998. Modal aerosol dynamics model for Europe: Development and first applications. Atmospheric Environment, 32, pp. 2981-2299.

Arakawa, A., Lamb, V.R., 1977. Methods of computational physics. Academic Press: New York, 17, pp. 174-265.

Binkowski, F.S., Roselle, S.J., 2003. Models-3 Community Multiscale Air Quality (CMAQ) model aerosol component, 1, Model description. Journal of Geophysical Research 108(D6), 4183, p. 18. doi:10.1029/2001JD001409.

Boylan, J.W., Russell, A.G., 2006. PM and light extinction model performance metrics, goals, and criteria for three-dimensional air quality models. Atmospheric Environment, 40, pp. 4946-4959.

Byun, D.W., Pleim, J.E., Tang, R.T., Bourgeois, A., 1999. Science algorithms of the EPA Models-3 Community Multiscale Air Quality (CMAQ) modeling system - Chapter 12: Meteorology-Chemistry Interface Processor (MCIP) for CMAQ modeling system. Technical Report to U.S. EPA, EPA/600/R-99/030, p. 91.

Byun, D.W., Schere, K.L., 2006. Review of the governing equations, computational algorithms, and other components of the Models-3 Community Multiscale Air Quality (CMAQ) Modeling System. Applied Mechanics Reviews, 59, pp. 51-77.

Cahill, C.F., 2003. Asian aerosol transport to Alaska during ACE-Asia. Journal of Geophysical Research, 108, p. 8. doi:10.1029/2002JD003271.

Carlson, T.R., Yoon, S.H., Dulla, R.G., 2010. Fairbanks home heating survey. Sacramento, CA, p. 63.

Chang, J.C., Hanna, S.R., 2004. Air quality model performance evaluation. Meteorology and Atmospheric Physics, 87, pp. 167-196.

Chang, J.S., Brost, R.A., Isaksen, I.S.A., Madronich, S., Middleton, P., Stockwell, W.R., Walcek, C.J., 1987. A three-dimensional Euledan acid deposition model: Physical concepts and formulation. Journal Geophysical Research, 92, pp. 14,681-14,700.

Chapman, E.G., Jr., W.I.G., Easter, R.C., Barnard, J.C., Ghan, S.J., Pekour, M.S., Fast, J.D., 2009. Coupling aerosol-cloud-radiative processes in the WRF-Chem model: Investigating the radiative impact of elevated point sources. Atmospheric Chemistry and Physics, 9, pp. 945-964.

Chigullapalli, S., Mölders, N., 2008. Sensitivity studies using the Weather Research and Forecasting (WRF) model. REU-report, Fairbanks, p. 15.

Chou, M.-D., Suarez, M.J., 1994. An efficient thermal infrared radiation parameterization for use in general circulation models. NASA - Technical Memorandum 104606, 3, p. 85.

Coast, C.J., Jr., 1996. High-performance algorithms in the Sparse Matrix Operator Kernel Emissions (SMOKE) modeling system. Ninth AMS Joint Conference on Applications of Air Pollution Meteorology with Air & Waste Management Association, pp. 584-588.

Davies, J., Misiuk, D., Colgan, R., Wiltse, N., 2009. Reducing $PM_{2.5}$ emissions from residential heating sources in the Fairbanks North Star Borough: Emission estimates, policy options, and recommendations. Cold Climate Housing Reseach Center, Fairbanks, AK, p. 56.

DeMore, W.B., Sander, S.P., Molina, M.J., Golden, D.M., Hampson, R.F., Kurylo, M.J., Howard, C.J., Ravishankara, A.R., 1988. Chemical kinetics and photochemical data for use in stratospheric modeling, evaluation number 8. National Aeronautics and Space Administration, Jet Propulsion Laboratory, California Institute of Technology, Pasadena, p. 278.

DOT, 2009. Northern region annual traffic volume report - Volume I 2009. Alaska Department of Transport and Public Facilities, Alaska, p. 200.

Dudhia, J., 2011. WRF physics options. Retrieved March 11, 2011, from http://www.mmm.ucar.edu/wrf/users/tutorial/201001/WRF_Physics_Dudhia.pdf, p. 106.

EPA, 2007. Guidance on the use of models and other analyses for demonstrating attainment of air quality goals for ozone, $PM_{2.5}$, and regional haze. U.S. Environmental Protection Agency, Research Triangle Park, NC, p. 262.

EPA, 2009. 2008 NEI-EIS Implementation Plan: Section 12. U.S. Environmental Protection Agency, p. 11.

EPA, 2012. Preparation of fine particulate emissions inventories - Chapter 12: The National Emissions Inventory and Emission Inventory Tools. U.S. Environmental Protection Agentcy, p. 10.

Erisman, J.W., Van, P.A., Wyers, P., 1994. Parameterization of surface resistance for the quantification of atmospheric deposition of acidifying pollutants and ozone. Atmospheric Environment , 28, pp. 2595-2607.

Fierro, A.O., Rogers, R.F., Marks, F.D., 2009. The impact of horizontal grid spacing on the microphysical and kinematic structures of strong tropical cyclones simulated with the WRF-ARW Model. Monthly Weather Review, 137, pp. 3717-3743.

Fröhlich, K., Mölders, N., 2002. Investigations on the impact of explicitly predicted snow metamorphism on the microclimate simulated by a meso-β/γ-scale non-hydrostatic model. Atmospheric Research, 62, pp. 71-109.

Gaudet, B.J., Stauffer, D.R., 2010. Stable boundary layers representation in meteorological models in extremely cold wintertime conditions. Report to the Environmental Protection Agency, p. 60.

Gery, M.W., Whitten, G.Z., Killus, J.P., Dodge, M.C., 1989. A photochemical kinetics mechanism for urban and regional scale computer modeling. Journal of Geophysical Research, 94, pp. 12925-12956.

Grell, G., Baklanov, A., 2011. Integrated modeling for forecasting weather and air quality: A call for fully coupled approaches. Atmospheric Environment, 45, pp. 6845-6851.

Grell, G.A., Dévényi, D., 2002. A generalized approach to parameterizing convection combining ensemble and data assimilation techniques. Geophysical Research Letters, 29, p. 4. doi:10.1029/2002GL015311.

Grell, G., Freitas, S.R., Stuefer, M., Fast, J., 2011. Inclusion of biomass burning in WRF-Chem: impact of wildfires on weather forecasts. Atmospheric Chemistry and Physics, 11, pp. 5289-5303.

Grell, G.A., Knoche, R., Peckham, S.E., McKeen, S.A., 2004. Online versus offline air quality modeling on cloud-resolving scales. Geophysical Research Letters, 31, p. 4. doi:10.1029/2004GL020175.

Grell, G.A., Peckham, S.E., Schmitz, R., McKeen, S.A., Frost, G., Skamarock, W.C., Eder, B., 2005. Fully coupled "online" chemistry within the WRF model. Atmospheric Environment, 39, pp. 6957-6975.

Hines, K.M., Bromwich, D.H., Bai, L.-S., Barlage, M., Slater, A.G., 2011. Development and testing of Polar WRF. Part III: Arctic Land. Journal of Climate, 24, pp. 26-48.

Hong, S.-Y., Dudhia, J., Chen, S.-H., 2004. A revised approach to ice microphysical processes for the bulk parameterization of clouds and precipitation. Monthly Weather Review, 132, pp. 103-120.

Hong, S.-Y., Lim, J.-O.J., 2006. The WRF Single-Moment 6-class microphysics scheme (WSM6). Journal Korean Meteorological Society, 42, pp. 129-151.

Houyoux, M.R., 1998. Technical report: Plume rise algorithm summary for the Sparse Matrix Operator Modeling System (SMOKE). Prepared for the North Carolina Department of Environment and Natural Resource, UNC, Chapel Hill, NC, ENV-98TR004-v1.0, p. 38.

Houyoux, M.R., Vukovich, J.M., Coats, C.J., Wheeler, N.J.M., Kasibhatla, P.S., 2000. Emission inventory development and processing for the Seasonal Model for Regional Air Quality (SMRAQ) project. Journal of Geophysical Research, 105, pp. 9079-9090.

Jacobson, M.Z., Kaufmann, Y.J., Rudich, Y., 2007. Examining feedbacks of aerosols to urban climate with a model that treats 3-D clouds with aerosol inclusions. Journal of Geophysical Research, 112, p. 18. doi:10.1029/2007JD008922.

Janjić, Z.I., 2002. Nonsingular implementation of the Mellor-Yamada level 2.5 scheme in the NCEP meso model. NCEP Office Note No. 437, p. 61.

Laurikko, J., 1995. Ambient temperature effect on automotive exhaust emissions: FTP and ECE test cycle responses. The Science of the Total Environment, 169, pp. 195-204.

Leelasakultum, K., Mölders, N., Tran, H.N.Q., Grell, G.A., 2012. Potential impacts of the introduction of low-sulfur fuel on $PM_{2.5}$ concentrations at breathing level in a subarctic city. Advances in Meteorology, 2012, p.16. doi:10.1155/2012/427078.

Loughner, C.P., Allen, D.J., Dickerson, R.R., Zhang, D.-L., Shou, Y.-X., Pickering, K.E., 2009. Investigating the use of a high resolution WRF-URBAN CANOPY model simulation with CMAQ. Extended abstract to the 8th Annual CMAS Conference, Chapel Hill, NC, 19–21 October, 2009, p. 4.

Madronich, S., 1987. Photodissociation in the atmosphere, 1, actinic flux and the effects of ground reflections and clouds. Journal of Geophysical Research, 92, pp. 9740-9752.

Mellor, G.L., Yamada, T., 1982. Development of a turbulence closure model for geophysical fluid problems. Reviews of Geophysics and Space Physics, 20, pp. 851-875.

Middleton, P., Stockwell, W.R., Carter, W.P.L., 1990. Aggregation of volatile organic compound emissions for regional modeling. Atmospheric Environment, 6, pp. 1107-1133.

Mlawer, E.J., Taubman, S.J., Brown, P.D., Iacono, M.J., Clough, S.A., 1997. Radiative transfer for inhomogeneous atmospheres: RRTM, a validated correlated-k model for the longwave. Journal of Geophysical Research, 102(D14), pp. 16663-16682.

Mölders, N., Hass, H., Jakobs, H.J., Laube, M., Ebel, A., 1994. Some effects of different cloud parameterizations in a mesoscale model and a chemistry transport model. Journal of Applied Meteorology, 33, pp. 527-545.

Mölders, N., 2008. Suitability of the Weather Research and Forecasting (WRF) model to predict the June 2005 fire weather for Interior Alaska. Weather and Forecasting, 23, pp. 953-973.

Mölders, N., 2009. Alaska Emission Model (AkEM) description. Internal Report, Fairbanks, AK, p. 10.

Mölders, N., 2010. Alaska Emission Model (AkEM) - version 1.01 description. Internal Report, Fairbanks, AK, p. 16.

Mölders, N., Hass, H., Jakobs, H.J., Laube, M., Ebel, A., 1994. Some effects of different cloud parameterizations in a mesoscale model and a chemistry transport model. Journal of Applied Meteorology, 33, pp. 527-545.

Mölders, N., Kramm, G., 2010. A case study on wintertime inversions in Interior Alaska with WRF. Atmospheric Research, 95, pp. 314-332.

Mölders, N., Laube, M., Raschke, E., 1995. Evaluation of model generated cloud cover by means of satellite data. Atmospheric Research 39, pp. 91-111.

Mölders, N., Leelasakultum, K., 2011a. Fairbanks North Star Borough $PM_{2.5}$ non-attainment area CMAQ modeling. Final report phase I, p. 62.

Mölders, N., Leelasakultum, K., 2011b. CMAQ – January/February episode: Results/challenges. Presentation at the Fairbanks $PM_{2.5}$ modeling symposium, Fairbanks, AK, June 14-16, 2011.

Mölders, N., Leelasakultum, K., 2012. Fairbanks North Star Borough $PM_{2.5}$ nonattainment area CMAQ modeling: Final report phase II. Report, p. 66.

Mölders, N., Luijting, H., Sassen, K., 2008. Use of atmospheric radiation measurement program data from Barrow, Alaska, for evaluation and development of snow-albedo parameterizations. Meteorology and Atmospheric Physic, 99, pp. 199-219.

Mölders, N., Porter, S.E., Cahill, C.F., Grell, G.A., 2010. Influence of ship emissions on air quality and input of contaminants in southern Alaska National Parks and Wilderness Areas during the 2006 tourist season. Atmospheric Environment, 44, pp. 1400-1413.

Mölders, N., Tran, H.N.Q., Cahill, C.F., Leelasakultum, K., Tran, T.T., 2012. Assessment of WRF/Chem PM$_{2.5}$-forecasts using mobile and fixed location data from the Fairbanks, Alaska winter 2008/09 field campaign. Atmospheric Pollution Research, 3, pp. 180-191.

Mölders, N., Tran, H.N.Q., Leelasakultum, K., 2011a. Investigation of means for PM$_{2.5}$ mitigation through atmospheric modeling - Final report. p. 75.

Mölders, N., Tran, H.N.Q., Quinn, P., Sassen, K., Shaw, G.E., Kramm, G., 2011b. Assessment of WRF/Chem to simulate sub-Arctic boundary layer characteristics during low solar irradiation using radiosonde, SODAR, and surface data. Atmospheric Pollution Research, 2, pp. 283-299.

Otte, T.L., Poulliot, G., Pleim, J.E., Young, J.O., Schere, K.L., Wong, D.C., Lee, P.C.S., Tsidulko, M., McQueen, J.T., Davidson, P., Mathur, R., Chuang, H.-Y., DiMego, G., Seaman, N.L., 2005. Linking the Eta Model with the Community Multiscale Air Quality (CMAQ) modeling system to build a national air quality forecasting system. Weather and Forecasting, 20, pp. 367-384.

Peckham, S.E., Fast, J.D., Schmitz, R., Grell, G.A., Gustafson, W.I., McKeen, S.A., Ghan, S.J., Zaveri, R., Easter, R.C., Barnard, J., Chapman, E., Salzmann, M., Wiedinmyer, C., Freitas, S.R., 2009. WRF/Chem version 3.1 user's guide,   p. 78.

Pleim, J.E., Chang, J.S., 1992. A non-local closure model for vertical mixing in the convective boundary layer. Atmospheric Environment, 26A, pp. 965-981.

Rosenfeld, D., Khain, A., Lynn, B., L.Woodley, W., 2007. Simulation of hurricane response to suppression of warm rain by sub-micron aerosols. Atmospheric Chemistry and Physics, 7, pp. 3411-3424.

Schell, B., Ackermann, I.J., Hass, H., Binkowski, F.S., Ebel, A., 2001. Modeling the formation of secondary organic aerosol within a comprehensive air quality model system. Journal of Geophysical Research, 106, pp. 28275-28293.

Shu-chang, W., Si-xun, H., Yi, L., 2006. Sensitive numerical simulation and analysis of rainstorm using nested WRF model. Journal of Hydrodynamics, 18, pp. 578-586.

Simpson, D., Guenther, A., Hewitt, C.N., Steinbrecher, R., 1995. Biogenic emissions in Europe 1. Estimates and uncertainties. Journal of Geophysical Research, 100(D11), pp. 22875-22890.

Skamarock, W.C., Klemp, J.B., Dudhia, J., Gill, D.O., Barker, D.M., Duda, M.G., Huang, X.-Y., Wang, W., Powers, J.G., 2008. A description of the Advanced Research WRF version 3. NCAR Technical Note, NCAR/TN–475+STR, p. 125.

Smirnova, T.G., Brown, J.M., Benjamin, S.G., Kim, D., 2000. Parameterization of cold season processes in the MAPS land-surface scheme. Journal of Geophysical Research, 105(D3), pp. 4077-4086.

Stockwell, W.R., Middleton, P., Chang, J.S., Tang, X., 1990. The second-generation regional acid deposition model chemical mechanism for regional air quality modeling. Journal of Geophysical Research, 95, pp. 16343-16367.

Stump, F., Tejada, S., Ray, W., Dropkin, D., Black, F., 1990. The influence of ambient temperature on tailpipe emissions from 1985 to 1987 model year light-duty gasoline motor vehicles. Atmospheric Environment, 24, pp. 2105-2112.

Tran, H.N.Q., Leelasakultum, K., Mölders, N., 2012. A tool for public $PM_{2.5}$-concentration advisory based on mobile measurements. Journal of Environmental Protection *(in print)*, p. 18.

Tran, H.N.Q., Mölders, N., 2011. Investigations on meteorological conditions for elevated $PM_{2.5}$ in Fairbanks, Alaska. Atmospheric Research, 99, pp. 39-49.

Tran, H.N.Q., Mölders, N., 2012a. Numerical investigations on the contribution of point source emissions to the $PM_{2.5}$-concentrations in Fairbanks, Alaska. Atmospheric Pollution Research, 3, pp. 199-210.

Tran, H.N.Q., Mölders, N., 2012b. Wood-burning device changeout: Modeling the impact on $PM_{2.5}$-concentrations in a remote subarctic urban nonattainment area. Advances in Meteorology, 2012, p. 12. doi:10.1155/2012/853405.

Tran, T.T., G. Newby, Mölders, N., 2011. Impacts of emission changes on sulfate aerosols in Alaska. Atmospheric Environment, 45, pp. 3078-3090.

von Storch, H., Zwiers, F.W., 1999. Statistical Analysis in Climate Research. Cambridge University Press, Cambridge, UK, p. 455.

Warner, T.T., 2011. Numerical Weather and Climate Prediction. Cambridge University Press, Cambridge, UK, p. 548.

Wendler, G., Nicpon, P., 1975. Low-level temperature inversion in fairbanks, central Alaska. Monthly Weather Review, 103, pp. 34-44.

Wesely, M.L., 1989. Parameterization of surface resistances to gaseous dry deposition in regional-scale numerical models. Atmospheric Environment, 23, pp. 1293-1304.

Yamaguch, T., Feingold, G., 2012. Technical note: Large-eddy simulation of cloudy boundary layer with the Advanced Research WRF model. Journal of Advances in Modeling Earth Systems, 4, p. 16. doi: 10.1029/2012MS000164.

Yamartino, R.J., 1993. Nonnegative, conserved scalar transport using grid-cell-centered, spectrally constrained blackman cubics for applications on a variable-thickness mesh. Monthly Weather Review, 121, pp. 753-763.

Yarker, M.B., PaiMazumder, D., Cahill, C.F., Dehn, J., Prakash, A., Mölders, N., 2010. Theoretical investigations on potential impacts of high-latitude volcanic emissions of heat, aerosols and water vapor and their interactions on clouds and precipitation. The Open Atmospheric Science Journal, 4, pp. 24-44.

Yarwood, G., Rao, S., Yocke, M., Whitten, G.Z., 2005. Updates to the carbon bond chemical machanism: CB05. Final report to the U.S. EPA, RT-04000675, p. 246.

Ying, Z., Tie, X., Li, G., 2009. Sensitivity of ozone concentrations to diurnal variations of surface emissions in Mexico City: A WRF/Chem modeling study. Atmospheric Environment, 43, pp. 851-859.

Zhang, L., Brook, J.R., Vet, R., 2003. A revised parameterization for gaseous dry deposition in air-quality models. Atmospheric Chemistry and Physics, 3, pp. 2067-2082.

Zhang, Y., 2008. Online-coupled meteorology and chemistry models: history, current status, and outlook. Atmospheric Chemistry and Physics, 8, pp. 2895-2932.

Zhang, Y., Olsen, S.C., Dubey, M.K., 2010a. WRF/Chem simulated springtime impact of rising Asian emissions on air quality over the U.S. Atmospheric Environment, 44, pp. 2799-2812.

Zhang, Y., Wen, X.Y., Jang, C.J., 2010b. Simulating chemistry-aerosol-cloud-radiation-climate feedbacks over the continental U.S. using the online-coupled Weather Research Forecasting Model with Chemistry (WRF/Chem). Atmospheric Environment, 44, pp. 3568-3582.
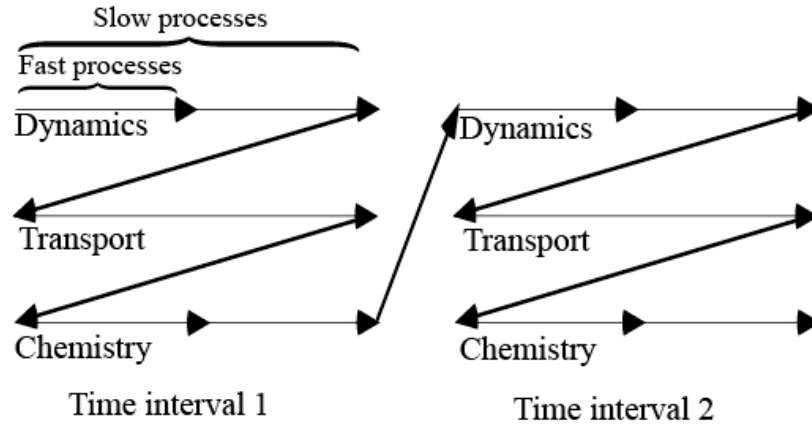
Figure 2.1 Schematic view of operator splitting (modified after Jacobson (2005)). The dynamical, transport and chemistry processes are simulated sequentially in each time interval.
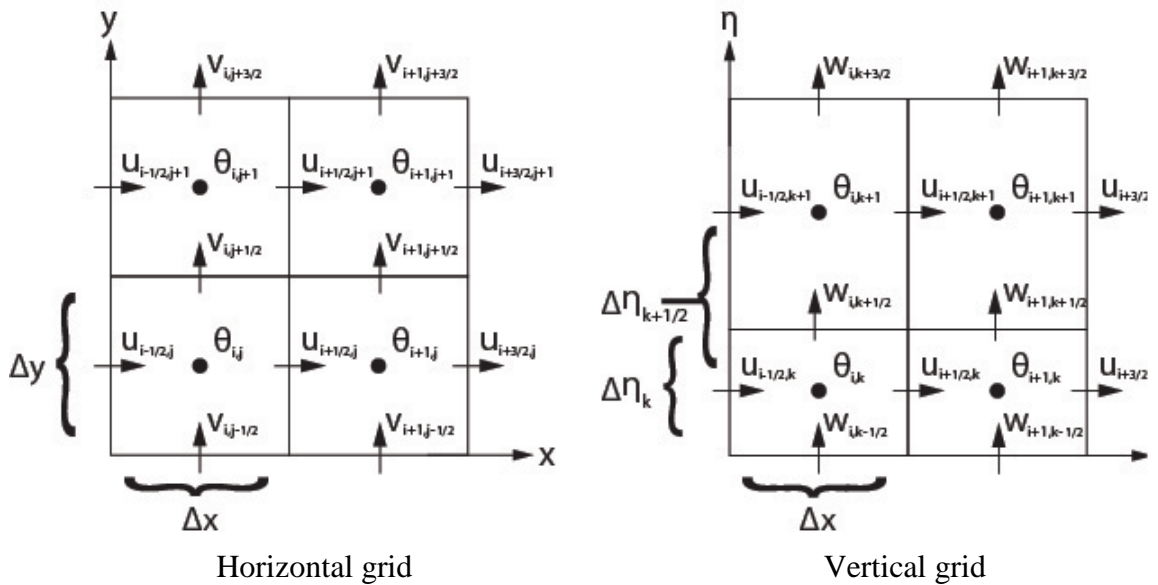
Figure 2.2 Horizontal and vertical structure of the Arakawa C staggered grid as used in WRF (Skamarock et al., 2008). Here i, j and k are variable locations in horizontal (x and y) and vertical (η) directions; u, v and w represent for velocity-related variables that be defined at the centers of grid interfaces in x, y and η; and θ represents the mass-related variables that are defined at the center of the grid, respectively.
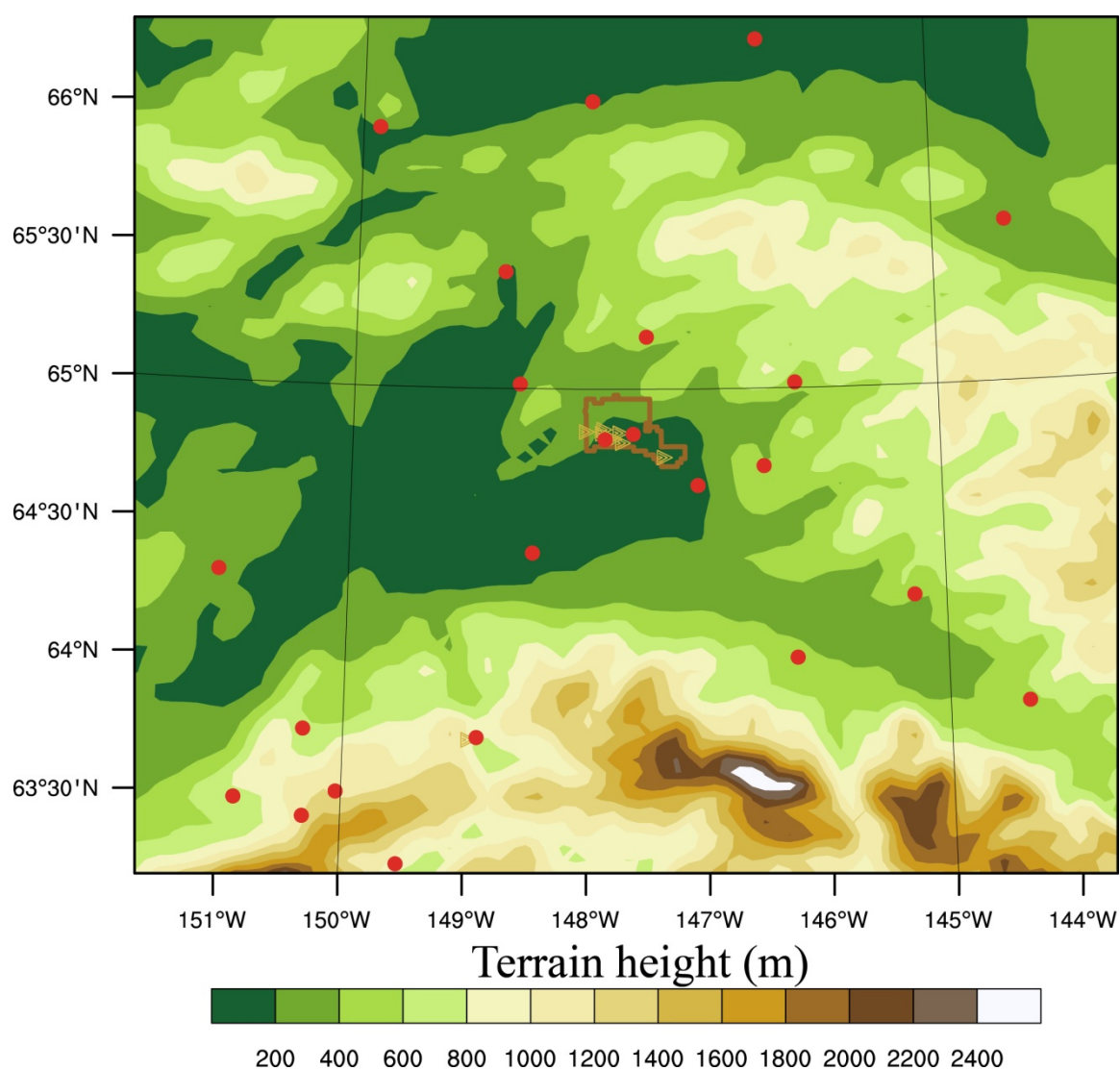
Figure 2.3 Domain of interest for the analysis of WRF/Chem results from the 2005/2006 and 2008/2009 simulations with color terrain contours overlain. The red dots indicate the locations of the 23 meteorological observational sites. Yellow triangles indicate the locations of the six $PM_{2.5}$ sites in the Fairbank North Star Borough. The brown polygon indicates the outline of the Fairbank $PM_{2.5}$-nonattainment area.

Chapter 3   Investigations on meteorological conditions for elevated PM$_{2.5}$ in Fairbanks, Alaska[1]

Abstract

The relationships between meteorological conditions (temperature, wind-speed and direction, relative humidity, surface-inversion depth and strength, stability) and PM$_{2.5}$-concentrations in Fairbanks, Alaska were investigated using ten years of observational data. The results show that during wintertime (November thru February) PM$_{2.5}$-concentrations exceeding the 24h National Air Quality Standard (35µg/m^3) occurred under calm wind, extremely low temperature ($<-20^{\circ}$C) and moisture (water-vapor pressure $<$2hPa) multiday surface-inversion conditions that trap the pollutants in the breathing level and inhibit transport of polluted air out of Fairbanks. PM$_{2.5}$-concentrations tend to be higher under stable than other conditions, but are not sensitive to the degree of stability. The presence of surface inversions and calm winds is necessary, but in combination with the low temperatures and humidity, the conditions are sufficient for high PM$_{2.5}$-concentrations. The low temperatures are required because they lead to increased emission rates from domestic heating. During multiday inversions with temperatures above -20°C, high relative humidity ($>$75%) partly caused by water-vapor emission reduces PM$_{2.5}$-concentrations.

3.1 Introduction

Concentrations of particulate matter less than or equal to 2.5µm in diameter ($PM_{2.5}$) are of concern in air-quality regulations since $PM_{2.5}$ can affect human health (e.g., Godish, 2004; Dominici et al., 2006; Miller et al., 2007; Delfino et al., 2009). Adverse health effects of PM can be associated with both long-term and short-term exposure (e.g., Schwartz et al., 1997; Bernard et al., 2001; Kappos et al., 2004). To decrease health risks, in the United States of America, the 24h National Ambient Air Quality Standard (NAAQS) for $PM_{2.5}$ was tightened to 35µg/m^3 in 2006. Communities, for which the last three years of $PM_{2.5}$-monitoring prior to 2006 showed violation of this new standard, were assigned $PM_{2.5}$-nonattainment areas. These communities have to develop strategies to get into and remain in compliance. Such planning requires understanding of the meteorological and emission situations that lead to high $PM_{2.5}$-concentrations and exceedances.

In Fairbanks, Alaska, $PM_{2.5}$-concentrations have exceeded frequently the new NAAQS in all winters (November to February) since the onset of monitoring in 1999 (Figure 3.1). During winter, Fairbanks' high latitude location (64.838N, 147.716W) leads to a negative radiation balance as the outgoing is greater than the incoming radiation. This fact and being enclosed by hills to three sides and being located about 800km land-inwards lead to frequent winter inversions that are among the strongest anywhere and persist much longer than in mid-latitudes (Wendler and Nicpon, 1975; Bourne et al., 2010). Daytime and nighttime surface inversion occur on about 82% of the days in

December and January, and on about 68% of the days for November, and February to April during the episode 1957-2008 (Bourne et al., 2010).

During winter, PM$_{2.5}$ exists in abundance from traffic and other combustion processes. The extremely cold weather and long dark nights lead to huge fuel consumption for heating and power supply. Both fuel consumption for heating and power supply increase with decreasing temperature (e.g., Hart and de Dear, 2004). The power generation of the UAF power plant, for instance, was about 5, 4 and 4% lower in November, December, and February 2008, respectively, than in January 2008 (C. Ward, pers. comm., February 2009). Cold start particle emissions from vehicles increase by an order of magnitude as temperature drops from 23°C to -20°C (e.g., Weilenmann et al., 2009). Furthermore, people are more likely to use their car or to idle their car as temperature decreases. Thus, during winter, traffic may be the cause for roughly 30% of the PM$_{2.5}$ in downtown Fairbanks (Johnson et al., 2009).

Several statistical and modeling studies examined the relationship between PM$_{2.5}$ and meteorological conditions (Triantafyllou et al., 2002; Elminir, 2005; Wise and Comrie, 2005; Liao et al., 2006; Unger et al., 2006; Dawson et al., 2007). They illustrated the difficulty in identifying causal relationships between specific meteorological parameters and measured PM$_{2.5}$-concentrations when the meteorological variables correlate strongly with one another. PM$_{2.5}$-concentrations were found to depend strongly on wind-speed, wind-direction, temperature, humidity, mixing height, precipitation and cloud cover (Elminir, 2005; Wise and Comrie, 2005; Dawson et al., 2007). Stable conditions associated with temperature inversions, strongly correlate with high pollutant

concentration since inversions hinder the upward transport of polluted near-surface air (Chow et al., 1995; Triantafyllou et al., 2002).

These studies mainly focused on low and mid-latitude regions with quite different meteorological conditions than Fairbanks. The goal of our study is to examine the relationship between Fairbanks' wintertime inversions, high $PM_{2.5}$-concentrations and meteorological conditions.

3.2 Data collection and analyses methods

$PM_{2.5}$-concentrations have been monitored in downtown Fairbanks since 1972. The monitoring site (Figure 3.2) is located on the roof of a building in the middle of the central business district. This site is equipped with two Thermo Electron Partisol 2000 samplers and a single Met-One Beta SASS Speciation Monitor running on a 1-in-3-day sampling schedule, and a single Met-One Beta Attenuation Monitor (BAM1020) running on a real-time schedule. The inlets of all samplers are approximately 6m above the ground (DEC, 2009). We used the SASS data since 1999, and the BAM 1020 available since June 2004 through 2009.

Since the NAAQS looks at the 24h-average $PM_{2.5}$-concentrations, we calculated 24h daily average concentrations using the BAM 1020 data for all days with complete datasets from June 2004 to February 2009. To examine whether the data from 1999 to 2004 provide valuable additional information for our study, we prepared three time-series from the 2004 to 2009 24h-average $PM_{2.5}$-concentrations. These time-series start on June 1, 2, and 3 2004 and only consider every third day's $PM_{2.5}$ data. Comparison of these

time-series with the full 2004-2009 time-series shows that all three 1-in-3-days time-series of this episode well represent the relationships between $PM_{2.5}$ and meteorology. Therefore, we included the 1999-2004 $PM_{2.5}$-monitoring data in our analysis.

Radiosonde data of temperature, dew-point temperature, potential temperature, wind-speed and wind-direction are available from daily soundings at the Fairbanks International Airport (FIA) at 0000 and 1200 UTC (1500 and 0300 Alaska Standard Time (AST)), respectively.

Inversion layer is defined as the layer wherein temperature increases with height and is associated with a positive temperature gradient. An algorithm was developed applying the technique first used by (Kahl, 1990) to identify the first inversions layer (if any) from the sounding data at levels below 700hPa. Surface inversions included those inversion layers starting at the ground or those starting at less than 100m above ground. Inversion layers starting 100m above the ground were accounted as elevated inversion layers.

At night (0300 AST) inversions are common phenomena due to the negative radiation balance (Wendler and Nipcon, 1975; Bourne et al., 2010). For the period considered here, 94% of the winter days had nighttime inversions with bases within 500m height above the surface. Hereof, 93% had their base within the first 100m above ground. In our study, we considered a day to be influenced by an inversion event when an inversion layer existed at 1500 AST. If several consecutive days had an inversion at 1500AST as well as at 0300 AST, we will call this event a multiday inversion. In the

analysis, we distinguished between single-day inversions lasting a day and multiday inversions lasting two or more days.

We defined the inversion depth (Δz) as the depth between the bottom and the top of the first inversion layer. Temperature gradients between the inversion base and the next 100m, 200m, 300m, 400m, 500m, 600m, 800m, and the top layer were determined to represent the inversion strength. The temperatures for these critical levels were interpolated by the values of closest lower and upper levels recorded by the radiosonde. This method of looking at the temperature gradient of the inversion is called STRXs hereafter. Here X denotes the distance over which the gradient was determined (e.g., for STR100 the gradient is determined for 100m). If an inversion ended below 200m, for example, then just STR100 would be defined and no temperature gradients would be determined for the levels 200m and above.

Potential temperature increases with height under stable conditions (positive gradient) whereas it decreases with height under unstable conditions (negative gradient). To examine the role of atmospheric stability on $PM_{2.5}$-concentrations we analyzed the vertical gradient of potential temperature. Similarly, to the method described above, the potential temperature gradient was determined from the ground to 100m, 200m, 300m, 400m, 500m, 600m and 800m. These potential temperature gradients are denoted as PGXs. Again X denotes the distance over which the gradient was determined.

Additionally, our analysis considers surface observations at FIA of 2m temperature (T) and dewpoint temperature (T_d), 10m wind-speed (v) and direction (dir), sea-level pressure (SLP), and reported fog/mist conditions. To evaluate the atmospheric

moisture, the water-vapor partial pressure (e) and relative humidity (RH) were determined by applying the Magnus-Tetens approximation (Lawrence, 2005).

Since the 24h-average $PM_{2.5}$-concentrations were determined by averaging the hourly $PM_{2.5}$ data from 0000AST to 0000AST of the next day, we calculated daily averages for all meteorological data to investigate the correlation between meteorological conditions and $PM_{2.5}$-exceedances. The relative importance of thermal and mechanical turbulence in the local near-surface atmosphere was evaluated through the gradient Richardson number (Ri) which was calculated in accord with (Rohli and Vega, 2007)

$$Ri = \frac{g}{\bar{\theta}} \frac{\Delta\theta/\Delta z}{(\Delta u/\Delta z)^2} \qquad (3.1)$$

Here Δ represents the difference of the potential temperature (θ), wind-speed (u) and geometric height (z) at the first two sounding levels with valid data, g is the gravitational acceleration (9.81m/s^2) and $\bar{\theta}$ is the mean potential temperature between these two levels. The calculation of the daily average Ri utilizes the radiosonde data of 0300 and 1500 AST.

In accord with our definition of "inversion days", we determined the correlation between 24h-average $PM_{2.5}$--concentrations and the inversion heights, inversion strengths, potential temperature gradient and Ri at 1500AST for 1999 to 2009. The correlation between 24h-average $PM_{2.5}$-concentrations and daily average meteorological quantities (e.g., RH, e, T, v, dir, SLP, Ri) was also calculated. For confidence in the correlations, we tested them for statistical significance at the 95% confidence level using

a Student's t-test. In this study, the term "significant" will be only used if the correlation according to this test is significant at the 95% or higher confidence level.

We examined the individual influence of the various meteorological parameters on the 24h-average $PM_{2.5}$-concentrations and their importance with respect to the other parameters using a multi-regression method (Storch and Zwiers, 1999). To evaluate the effect of inversion conditions on the ecxceedances, we calculated the ratio between the frequencies of inversions to the frequency of exceedances associated with inversion conditions. Analogously, we examined the effect of temperature below a certain threshold on exceedances.

3.3 Result and discussion

3.3.1 $PM_{2.5}$-concentrations

Temporal variation of 24h-average $PM_{2.5}$-concentrations in Fairbanks during the winters of 1999 to 2009 shows numerous exceedances of the NAAQS (Figure 3.1). There were 128 exceedances during the winters of 2004 to 2009, and 17 (over 160 observed days) during the winters of 1999 to 2004. The variation of 24h-average $PM_{2.5}$ - concentrations among these months is non-uniform from 2004 to 2009 (Figure 3.1). In general, the number of exceedance days is highest in January followed by December. The highest and second highest exceedances occurred on December 29 and January 30, 2008 with over $135\mu g/m^3$ and $110\mu g/m^3$, respectively. On these days, the atmosphere was remarkably stable, extremely cold, and dry with temperatures of -38^oC and -32^oC, and relative humidity of 57% and 71%, and there was no wind.

3.3.2 Inversions

In Fairbanks, a snow-cover exists continuously from mid October through early May (Shulski and Wendler, 2007). The high albedo of the snow-covered surface reflects incident shortwave radiations. The temperature-albedo feedback results in cooler temperature close to the ground than in the air layers aloft and therefore may contribute to the formation of surface inversions. The frequency of surface inversions during November, December, January and February in the years 1999–2009 was 65%, 82%, 80% and 72%, respectively. These frequencies are slightly higher than the average frequencies of 60%, 76%, 77%, and 60% reported by Bourne et al. (2010) for the winters 1957-2008. January 2009 had the highest frequency with surface inversions on 94% of the days. The variance of frequency is highest in November, and lowest in December followed by January and February. For the winters considered in this study, 96% of the surface inversions have their base at the ground surface.

In the winters of 2004–2009, all 128 exceedances were associated with surface inversions. In the winters of 1999-2004, 17 out of 18 detected exceedances were associated with surface inversions. Of the 128 exceedances in the winters of 2004-2009 18%, 25%, 35% and 22% occurred in November, December, January and February, respectively (Figure 3.3). This means January has the highest exceedance occurrence and highest frequency of surface-inversion events.

No exceedances occurred when elevated inversions existed, even with those based within 100–200m, which make up 15% of the total 153 elevated inversion events during the winters 2004-2009. Based on these findings, one has to conclude that inversion layers

having their base within the first 100m above ground play a major role for the occurrence of $PM_{2.5}$-exccedances. Therefore, in the following, all discussion focuses on surface inversions.

Among the 440 surface inversions during the winters of 2004 to 2009, 18 were single-day inversions out of which only two days had $PM_{2.5}$-exceedances. During these winters, 86% of the $PM_{2.5}$-exceedances occurred under multiday inversion conditions (Figure 3.4). For the winters 1999-2003, $PM_{2.5}$ data were only available every three days. Out of the total 473 surface inversions during these winters, 28% fall on a day with $PM_{2.5}$ data. Out of these 13% were associated with $PM_{2.5}$-exceedances that occurred under multiday inversion conditions. The results suggest that formation of a $PM_{2.5}$-exceedance is an accumulated effect of continuous pollutant trapping over several days in the inversion above Fairbanks and the poor dispersion associated with multiday inversions. However, the number of $PM_{2.5}$-exceedances is uncorrelated with the duration of multiday inversions (Figure 3.4). A large number of single and multiday inversions had no exceedance and the temporal evolution of surface-inversion events differs from that of $PM_{2.5}$-exceedance events. Therefore, one has to conclude that the presence of a surface inversion is not the only factor leading to $PM_{2.5}$-exceedance.

Surface-inversion depth varies from less than 100m up to more than 2000m. However, although the $PM_{2.5}$-exceedances occur at all scales of inversion depths, they are more likely to occur for inversion depths greater than 300 m. During the winters of 1999 to 2009, 41% of the surface inversions had depths less than 300 m, but they were just associated with 18.4% of total exceedances, resulting in a ratio of occurrence–frequency

of 0.45. Surface-inversion layers having depths greater than 300m had an occurrence–frequency ratio of 1.39 indicating that they were more likely associated with exceedances. The highest occurrence–frequency ratio (1.49) was found for inversion layers having depths in the range 300–350m. They made up 7.9% of the total surface-inversion events and were associated with 11.8% exceedances. Nevertheless, inversion depth does not strongly influence the 24 h-average $PM_{2.5}$-concentrations as indicated by the generally low (0.272), but significant correlation between these quantities. Inversion layers having depths in the range of 0 to 200m have weak and insignificant correlation with the $PM_{2.5}$-concentrations and make up 26% of the total inversion events. Correlation between inversion depth and 24h-average $PM_{2.5}$-concentrations increases and becomes significant as the depth range increases. The highest correlation (0.382, significant) was found for the depth range 0-350m that made up 49% of the total inversion events. At greater depth ranges (e.g., 0-400m, 0-500m and more), correlation decreases, but is still significant. This means that inversion layers having depths greater than 350m do not influence the $PM_{2.5}$-concentrations as effectively as those layers having depths less than this threshold.

Because of the interesting behavior of highest correlation at 350m, we included this height into the investigation of inversion strength as STR350. From a theoretical point of view, one has to expect that the 24h-average $PM_{2.5}$-concentrations will increase if the inversion strength increases. The strongest inversions usually occurred within the first 100m above ground when for STR100 the frequency of inversions with strength >8K/100m is 10.7% compared to less than 1% when strength is determined for levels 0-

200m or higher. $PM_{2.5}$-exceedances may occur at all magnitudes of inversion strength, but they are more likely to occur when inversion strength exceeds 2K/100m. Inversions with strength less than 2K/100m made up for 39% of all cases, but they were only associated with 18% of all exceedances, resulting in a ratio of occurrence frequency of 0.45. Inversions with strength greater than 2K/100m have occurrence-frequency ratios greater than 1. The ratio increases with inversion strength. The correlation behavior of inversion strength with 24h-average $PM_{2.5}$-concentrations is similar to that of inversion depth with 24h-average $PM_{2.5}$-concentrations. Correlations are 0.221, 0.293, 0.325 for STR100, STR200, STR300, respectively and reach 0.376 as the highest correlation for STR350 (all significant). Above 350m, correlations decrease to 0.373, 0.369, 0.230 for STR400, STR600 and STR800, respectively (all significant). Overall-correlation of inversion strength with 24h-average $PM_{2.5}$-concentrations is low (0.296), but significant. In general, neither inversion depth nor inversion strength correlated strongly with the 24h-average $PM_{2.5}$-concentrations. Instead, $PM_{2.5}$-exceedances occurred at different ranges of inversion strength and depth (Figure 3.5).

3.3.3 Stability

In the Fairbanks' winter surface-inversion layers, the atmosphere is extremely stable and the potential gradient is largely positive (16K/100m at the highest). We included PG350 in the analysis of potential temperature-gradient impacts, and investigated the correlation of PGX with the 24h-average $PM_{2.5}$-concentrations on inversion days and on all winter days. Here again X denotes the distance over which the

potential temperature gradient (PGX) or inversion strength (STRX) was determined (e.g., X equals 100m, 200m, etc.). PGX show different correlation behaviors with 24h-average $PM_{2.5}$-concentrations on inversion days and on all winter days (Figure 3.5). Under inversion conditions, PGX-$PM_{2.5}$-behavior is similar to STRX-$PM_{2.5}$-behavior. The highest correlation between $PM_{2.5}$ and potential temperature exists at 350m (0.379, significant) with gradual decrease towards higher and lower levels. $PM_{2.5}$-exceedances were found for PGX greater than 1K/100m which is the typical condition observed during surface-inversion events. The ratio of frequency of exceedances to PGX>3K/100m is higher than 1. These ratios indicate that more exceedances occurred when PGX exceeded this threshold. However, the highest potential temperature gradients as obtained with PG100 were not necessarily associated with the highest 24h-average $PM_{2.5}$-concentrations and exceedances. For all winter days, PGX correlate much stronger with the 24h-average $PM_{2.5}$-concentrations than for inversion days and correlations increase when the potential temperature gradient was calculated over a greater layer. Correlations were 0.418, 0.515, 0.561, 0.576, 0.586 and 0.595 for PG100, PG200, PG300, PG350, PG400, and PG500, respectively (all significant). For PG600 and beyond, correlations decreased, but remained significant. The lower correlation on inversion days suggests that the degree of stability does not effectively influence the magnitude of the 24h-average $PM_{2.5}$-concentrations during an inversion event. Obviously, like inversion strength, the degree of stability plays a role, but it does not govern the $PM_{2.5}$-exceedances alone.

3.3.4 Wind-speed and direction

Various studies showed that wind-speed plays an important role for dispersion of pollutants and thus 24h-average $PM_{2.5}$-concentrations (Elminir, 2005; Dawson et al., 2007). Wind direction may lead to $PM_{2.5}$ advection from upwind sources (Chu et al., 2009). During wintertime, calm winds (average wind-speed <0.5m/s) dominate in the Fairbanks area (Shulski and Wendler, 2007). During the winters 1999 to 2009, wind was calm on 68.4% of the days. During these winters 92.6% of the $PM_{2.5}$-exceedances occurred under inversion, calm-wind conditions. Under inversion conditions, wind-speed correlates higher with the 24h-average $PM_{2.5}$-concentrations than under non-inversion conditions (-0.347 and -0.213, respectively), while for the entire winters the correlation is -0.330. All these correlations are significant. Low 24h-average $PM_{2.5}$-concentrations may nevertheless occur on days with calm-wind conditions. Thus, one has to conclude that calm wind is a critical pre-requisite for high 24h-average $PM_{2.5}$-concentrations, but it is not the key factor.

During the 1999-2009 winters, winds from North-Northeast dominated in Fairbanks. This wind-direction also dominated during inversion events (Figure 3.6). None of the wind-directions favored accumulation of high 24h-average $PM_{2.5}$-concentrations. Most of the high 24h-average $PM_{2.5}$-concentrations occurred under calm-wind condition under which wind-direction cannot be identified clearly. Thus, we have to conclude that none of the point sources (e.g., power plants, industrial facilities that emit into higher atmospheric layers than the breathing level) is the major cause for the 24h-average $PM_{2.5}$-concentrations measured at the Fairbanks downtown site.

3.3.5 Temperature

In Fairbanks, monthly mean temperature is -16°C, -21°C, -23°C and -20°C in November, December, January and February, respectively; during these months temperatures can range from -51 to 10°C (Shulski and Wendler, 2007). The winters 1999 to 2009 fall into this typical range. In January, inter-annual variability shows frequently extreme temperature changes where temperature drops to below -40°C within 60 hours at the longest and then goes up to values above freezing. Such rapid temperature changes occurred in 2005, 2008, 2009. For the episode considered in our study, the lowest daily average temperature was -47°C in December 1999, which is 7K higher than the lowest temperature observed and is the 8th lowest temperature since onset of record in 1930.

In the winters of 1999 to 2009, PM$_{2.5}$-exceedances occurred more likely at temperatures below -15°C and were intensively associated with temperatures below -20°C (Figure 3.7). Higher 24h-average PM$_{2.5}$-concentrations were associated with lower temperatures. No obvious relationship between temperature and inversion condition exists as inversions occur at various temperatures. During these winters 4.4% of the exceedances occurred at temperature above -15°C. Such temperature conditions occurred on 30.5% of the days. Thus, we obtain a ratio of exceedance of PM$_{2.5}$ to temperature above this threshold of 0.14. The ratio for temperature in the range of -20°C to -15°C was 0.49 (10.5% vs. 21.3%) whereas the ratio for temperatures between -35°C and -20°C was 1.41 (54.4% vs. 38.5%). Temperatures <-35°C have the highest ratio with 3.20 (30.7% vs. 9.6%). Correlations between temperature and 24h-average PM$_{2.5}$-concentrations are -0.577, -0.396 and -0.568 (all significant) under inversion, non-inversion and for all

winter days, respectively. This behavior of ratios demonstrates the strong influence of temperature on the $PM_{2.5}$-concentration. The ratios explain why the greatest number of exceedance days and the highest $PM_{2.5}$-concentrations typically occur in late December and in January when temperatures reach their lowest values during wintertime. Elimir (2005) and Dawson et al. (2007) found similar correlation and behavior for Cairo, Egypt and the Eastern US, respectively.

3.3.6 Partial water-vapor pressure and relative humidity

Both vapor partial pressure (e) and relative humidity (RH) represent atmospheric moisture. In a moist atmosphere, aerosol particles take up water vapor, swell and may coagulate. This change in size and density increases their sedimentation velocity (e.g., Donateo et al., 2006). Therefore, $PM_{2.5}$-concentrations are reduced when e and RH is high. In our study, 97% of observed exccedances coincide with e less than 2hPa, out of which 84% of the exceedances occurred at e less than 1hPa (Figure 3.7). Water-vapor pressure and 24h-average $PM_{2.5}$-concentrations correlate moderately (-0.438), but significantly.

Several studies performed for the Apulia, Italy and Los Angeles, CA revealed that RH exceeding 70% would affect $PM_{2.5}$ characteristics (e.g., MIE, 1994; Shen et al., 2002; Donateo et al. 2005). In our study, a threshold of RH 75% was found to affect the $PM_{2.5}$-concentration. The ratio of the occurrence frequency of $PM_{2.5}$-exceedances over RH is greatly reduced for RH>75% (1.53 and 0.58 for RH≤75% and RH>75%, respectively). No exccedances occurred at RH>90%. The 75% threshold for RH well correlates with the

e-threshold of 1hPa that indicates atmospheric conditions as being "dry" in Fairbanks if RH≤75%. This RH-threshold also correlates well with the threshold of -20°C that temperature has to be below for PM$_{2.5}$-exceedances to be likely to occur. Around this temperature, the atmosphere is still super-saturated with respect to ice. As temperatures fall below -20^{0}C, ice crystals form efficiently and fall out. This process reduces the atmospheric moisture load that would otherwise have been favorable for high PM$_{2.5}$-concentrations and thus exceedances. At temperature above -20°C, the atmosphere may be supersaturated with respect to water. The particles swell and may achieve diameter greater than 2.5µm, for which the PM$_{2.5}$-concentrations go down. These phenomena indicate indirect effects of temperature on PM$_{2.5}$-concentrations. Note that no relationship between inversion conditions and e as well as RH was found.

3.3.7 Gradient Richard number, sea-level pressure and ice fog

No evident relationship between gradient Richardson number (Ri) and 24h-average PM$_{2.5}$-concentrations exists. Within a wide range of Ri, 78% of the Ri are larger than 2. This fact indicates that the thermal buoyancy is stronger than the wind shear. Large positive Ris were found for non-inversion days due to the close to zero wind shear and calm wind conditions that are common during winter in Fairbanks (Figure 3.8). The 24h-average PM$_{2.5}$-concentrations and Ri insignificantly correlate (0.059), i.e., no relationship between Ri and exceedances occurred at all ranges of Ri>1.

Sea-level pressure marginally (0.184, significant) correlates with the 24h-average PM$_{2.5}$-concentrations, but typically correlates slightly better on inversion days (0.222,

significant) than non-inversion days (0.0.51, insignificant). No typical range of SLP on inversion days or exceedance events exists. Therefore, we conclude that SLP has marginal impact on $PM_{2.5}$-concentration.

Theoretically, formation of ice fog weakens the strength of surface-based inversion, and hence, may help to reduce the $PM_{2.5}$-concentrations. However, in Fairbanks, normally ice fog does not achieve a sufficient thickness to destroy the inversion in the lowest 16m above ground where ice fog is formed (Wendler and Nicpon, 1975). In our study, we found that the $PM_{2.5}$-exceedances occurred on days with and without ice fog suggesting ice fog has no effect on exceedances in Fairbanks. This behavior well agrees with the finding discussed above that the inversion strength does not effectively govern the $PM_{2.5}$-concentrations.

3.3.8 Combined effects

Analysis of the correlation coefficients between the various meteorological quantities and the 24h-average concentrations suggest excluding wind-direction, Ri and SLP from the multi-linear regression analysis due to their low correlations. Both RH and e represent atmospheric moisture for which only one of them should be considered to avoid redundant information. We selected e as to avoid ambiguities related to saturation over ice and water that would require to break the multi-linear regression into two equations in corresponding to RH≤75% and RH>75%. Out of all X for PGX and STRX, we chose 350m as here the strongest correlations were found. PG350 is included in the analysis as it can represent both the inversion strength and atmospheric stable conditions.

We excluded STR350 as it provides slightly redundant information to PG350. All other parameters were included in the multi-regression analysis. We determined the multi-linear regression equations for inversion days only (denoted INV) and the entire winters (denoted ALL). For INV, we investigated the relationship of 24h-average $PM_{2.5}$-concentrations with the above-identified meteorological parameters ($\frac{\partial\theta}{\partial z}\big|_{0-350m}$, Δz, v, T, e) for surface-inversion events only. For ALL, we determined the relationships between the 24h-average $PM_{2.5}$-concentrations and these quantities except inversion depth. Note that the multi-linear regression calculation requires data availability for all quantities at the time of calculation. This requirement reduced the number of days considered in the calculation of multi-regression coefficients from 601 to 458 for ALL and INV, respectively. The regression analysis provided

$$PM_{2.5} = -0.538 + 3.009\frac{\partial\theta}{\partial z}\Big|_{0-350m} + 0.001\Delta z - 1.728v - 0.843T + 1.85232e \qquad (3.2)$$

for inversion days only (INV) and

$$PM_{2.5} = -6.181 + 4.081\frac{\partial\theta}{\partial z}\Big|_{0-350m} - 0.936v - 0.888T + 2.451e \qquad (3.3)$$

for all winters (ALL) with R^2 of 0.435 and 0.509, respectively. Reasons for the relatively low values of R^2 can be unidentified parameters that affect the 24h-average $PM_{2.5}$-concentrations, the limited data availability, measurement errors, the distance between the radiosonde and $PM_{2.5}$-measurement sites (about 8km), the impact of local $PM_{2.5}$-emission sources, or combination of those. The impact of low data availability is obvious, as adding more data increases the R^2-value (all winters vs. inversion days only).

Nevertheless, the regression coefficients of Eqs. (3.2) and (3.3) still permit for evaluating the importance of the various quantities for the $PM_{2.5}$-concentrations. The standardized coefficient (SC) indicates the role of each quantity for the 24h-average $PM_{2.5}$-concentrations. Positive (negative) SC implies a positive (negative) correlation of the quantity with the 24h-average $PM_{2.5}$-concentrations. The importance of a quantity was judged based on the magnitude of its SC that indicates the ratio of deviation of its value to the deviation of 24h-average $PM_{2.5}$-concentrations. Parameters having large SC are more important to the 24h-average $PM_{2.5}$-concentrations than those with low SC (Schroeder et al., 1986).

In further multi-linear regression tests, quantities were removed and included alternatively to examine their role and interaction effects with other quantities on $PM_{2.5}$-concentrations. For INV, inversion depth has positive and the lowest SC (Table. 3.1). This behavior well agrees with the finding that the 24h-average $PM_{2.5}$-concentrations are not very sensitive to inversion depth. One has to conclude that out of the quantities examined here inversion depth is least important for the 24h-average $PM_{2.5}$-concentrations. For both INV and ALL, wind-speed is of second least importance to the 24h-average $PM_{2.5}$-concentrations during winter. This finding may be misleading and results from the fact that on average over all winters considered, low wind-speeds dominate in Fairbanks and high as well as low 24h-average $PM_{2.5}$-concentrations occurred at any wind-speed less than 1m/s. However, investigation of individual cases shows that as wind-speed was high (>10m/s), $PM_{2.5}$-concentrations were low as the pollutants quickly leave the area. Exclusion of wind-speed from the analysis only slightly

reduces R^2 (Table. 3.1). However, the finding emphasizes that low wind-speed is a mandatory condition for $PM_{2.5}$-exceedances to occur. The third least important contributor is e. It has positive SC although it has negative correlation with the 24h-average $PM_{2.5}$-concentrations. This phenomenon is due to the strong correlation between e and temperature. Removing temperature from the analyses results in e regaining its negative SC, but a great decrease of R^2. This behavior indicates that temperature is more important than e. Considering only $\left.\frac{\partial\theta}{\partial z}\right|_{0\text{-}350m}$, Δz, v and T for inversion days only and $\left.\frac{\partial\theta}{\partial z}\right|_{0\text{-}350m}$, v and T for all winters yields

$$PM_{2.5} = 5.966 + 3.052 \left.\frac{\partial\theta}{\partial z}\right|_{0\text{-}350m} + 0.001\Delta z - 1.738v - 0.645T \tag{3.4}$$

$$PM_{2.5} = -2.566 + 4.189 \left.\frac{\partial\theta}{\partial z}\right|_{0\text{-}350m} - 1.022v - 0.616T \tag{3.5}$$

with R^2 being reduced marginally to 0.430 and 0.501, respectively as compared to the full regression equations. This means that both the potential temperature gradient and temperature are the most important meteorological quantities that affect the $PM_{2.5}$-concentrations. Interestingly, their roles in influencing the 24h-average $PM_{2.5}$-concentrations differ for inversion days as compared to all winter days. Under inversion conditions, temperature was more important than the potential temperature gradient, while for the entire winter their roles were almost equal. Thus, the findings of the multi-regression analysis further emphasize that the characteristics of surface inversions are not the key factors that determine the magnitude of $PM_{2.5}$-exceedances. Instead, temperature is the determining factor for $PM_{2.5}$-exceedances to occur, which in turn relates to the

emission strength. Hart and de Dear (2004), for instance, reported an increase in emissions from heating with decreasing temperatures. Timmer and Lamb (2007) found a strong correlation (R>0.8) between natural gas consumption for heating and heating degree-days in the northern states of the US that on average experience colder winters than do the other states except Alaska. Weilenmann et al. (2009) reported that the cold-start emissions from passenger cars rise drastically at −20°C as compared with those at −7°C. Nam et al. (2010) found that regardless of vehicle model year, the emission of particulate matter doubles for every 20°F-decrease of the ambient temperature.

Another potential reason for the relationship between temperature and $PM_{2.5}$-concentrations is the effect of temperature on the gas-to-particle conversion. As temperature decreases, the vapor pressure decreases accordingly and the gas-to-particle partitioning shifts towards the aerosol phase (Strader et al., 1999). A temperature decrease by 10K leads to an increase of 20 to 150% in the secondary organic aerosol (SOA) concentrations (Sheehan and Bowman, 2001). These studies, however, were all carried out for mid-latitudes, and knowledge of the formation mechanisms of SOAs under extremely cold temperature and low solar radiation conditions like during winters in Fairbanks are still subject to research.

3.4 Conclusions

In Fairbanks, 24h-average $PM_{2.5}$-concentrations frequently exceeded the new NAAQS during the winters (November through February) of 1999 to 2009. During winter, surface inversions existed 75% of the time. The results of our study suggest that

inversion layers with bases within the first 100m above ground enhance the likelihood for PM$_{2.5}$-exccedances. Based on the low correlations between 24h-average PM$_{2.5}$-concentrations and inversion depth (R=0.272), potential temperature gradient (R=0.379), wind-speed (R=-0.347) or inversion strength (R=0.296), we conclude that the characteristics of the surface inversion are of marginal impact for high PM$_{2.5}$-concentrations. The duration of an inversion event has no impact on the magnitude of PM$_{2.5}$-concentrations. The results also lead to the conclusion that the presence of a surface inversion and calm wind are only necessary, but not sufficient conditions for high PM$_{2.5}$-concentrations. In addition, the atmosphere must be sufficiently dry and cold. If the atmosphere becomes colder than -20°C and drier than 1hPa, PM$_{2.5}$ exceedance will occur if a surface inversion exists. For water-vapor pressure less than 2hPa, the likelihood for exceedances is already 97%. Under these cold and dry conditions, the PM$_{2.5}$-concentrations become temperature-sensitive. On the contrary, if temperatures and water-vapor pressure exceed -20°C and 2hPa, respectively, both atmospheric stability and temperature will mainly influence the 24h-average PM$_{2.5}$-concentrations. Under these conditions, the microphysical processes related to fog reduce the PM$_{2.5}$-concentrations.

The fact that temperature is a sufficient condition for elevated PM$_{2.5}$-concentrations suggests that the enhanced emissions as temperatures drop are the major cause for increased PM$_{2.5}$-concentrations. Emissions increase at low temperatures as more energy is consumed for heating and production of electrical power. Emissions from traffic (cold starts, idling of cars, increased use of cars for even short distances) also increase with decreasing temperature. Based on our study we conclude that reducing the

emissions from area sources and traffic could be an effective measure to reduce the frequency of $PM_{2.5}$-exceedances during winter in Fairbanks.

Acknowledgements

References

Bernard, S.M., Samet, J.M., Grambsch, A., Ebi, K.L., Romieu, I., 2001. The potential impacts of climate variability and change on air pollution related health effects in the United States. Environmental Health Perspectives, 109 (Suppl. 2), 199-209.

Bourne, S.M., Bhatt, U.S., Zhang, J., Thoman, R., 2010. Surface-based temperature inversions in Alaska from a climate perspective. Atmospheric Research, 95, 353-366.

Chow, J., Fairley, D., Watson, J., DeMandel, R., Fujita, E., Lowenthal, D., Lu, Z., Frazier, C., Long, G., Cordova, J., 1995. Source apportionment of wintertime PM10 at San Jose, Calif. Journal of Environmental Engineering, 121, 378-387.

Chu, N., Kadane, J.B., Davidson, C.I., 2009. Identifying likely $PM_{2.5}$ sources on days of elevated concentration: a simple statistical approach. Environmental Science & Technology, 43, 2407-2411.

Dawson, J.P., Adams, P.J., Pandis, S.N., 2007. Sensitivity of $PM_{2.5}$ to climate in the Eastern US: a modeling case study. Atmospheric Chemistry and Physics, 7, 4295-4309.

Delfino, R.J., Brummel, S., Wu, J., Stern, H., Ostro, B., Lipsett, M., Winer, A., Street, D.H., Zhang, L., Tjoa, T., Gillen, D.L., 2009. The relationship of respiratory and cardiovascular hospital admissions to the southern California wildfires of 2003. Occupational and Environmental Medicine, 66, 189-197.

Department of Environmental Conservation (DEC), 2009. Alaska's Air Monitoring 2010 Network Plan - Chapter 4 - Fairbanks. Department of Air Quality, State of Alaska Department of Environmental Conservation, p. 27.

Dominici, F., Peng, R.D., Bell, M.L., 2006. Fine particulate air pollution and hospital admission for cardiovascular and respiratory diseases. Journal of the American Medical Association, 295(10), 1127-1134.

Donateo, A., Contini, D., Belosi, F., 2006. Real time measurements of $PM_{2.5}$ concentrations and vertical turbulent fluxes using an optical detector. Atmospheric Environment, 40, 1346-1360.

Elminir, H.K., 2005. Dependence of urban air pollutants on meteorology. Science of the Total Environment 350, 225-237.

Godish, T., 2004. Air Quality. Lewis Publishers, Boca Raton, FL. p. 480.

Hart, M., de Dear, R., 2004. Weather sensitivity in household appliance energy end-use. Energy and Buildings, 36, 161-174.

Johnson, R., Marsik, T., Lee, M., Cahill, C.F., 2009. Helping Fairbanks meet new air quality requirements: developing ambient PM-2.5 management strategies. Transportation safety, security, and innovation in cold regions 3, p. 1.

Kahl, J.D., 1990. Characteristics of the low-level temperature inversion along the Alaskan Arctic coast. International Journal of Climatology, 10, 537-548.

Kappos, A.D., Bruckmann, P., Eikmann, T., Englert, N., Heinrich, U., Höppe, P., Koch, E., Krause, G.H.M., Kreyling, W.G., Rauchfuss, K., Rombout, P., Schulz-Klemp, V., Thiel, W.R., Wichmann, H.-E., 2004. Health effects of particles in the ambient air. International Journal of Hygiene and Environmental Health 207, 399-407.

Lawrence, M.G., 2005. The Relationship between Relative Humidity and the Dewpoint Temperature in Moist Air: A Simple Conversion and Applications. American Meteorological Society, 86, 225-233.

Liao, H., Chen, W.-T., Seinfeld, J.H., 2006. Role of climate change in global predictions of future tropospheric ozone and aerosols. Journal of Geophysical Research, 111, D12304, p. 18. doi:10.1029/2005JD006852.

MIE, 1994. Monitoring with data Ram in wet/high humidity environments. MIE Inc., IL Application Note 10-B.

Miller, K.A., Siscovick, D.S., Sheppard, L., Shepherd, K., Sullivan, J.H., Anderson, G.L., Kaufman, J.D., 2007. Long-term exposure to air pollution and incidence of cardiovascular events in women. New England Journal of Medicine, 356, 447-458.

Nam, E., Kishan, S., Baldauf, R.W., Fulper, C.R., Sabisch, M., Warila, J., 2010. Temperature effects on particulate matter emissions from light-duty, gasoline-powered motor vehicles. Environmental Science & Technology, 44, 4672-4677.

Rohli, R.V., Vega, A.J., 2007. Climatology. Jones and Barlett Publishers, Sudbury, MA. p. 466.

Schroeder, L.D., Sjoquist, D.L., Stephan, P.E., 1986. Understanding regression analysis: An introduction guide. Sage, Sage University Paper, Newbury Park, CA, p. 95.

Schwartz, J., Dockery, D., Neas, L., 1997. Is daily mortality associated specifically with fine particles. Journal of the Air & Waste Management Association, 46, 927-939.

Sheehan, P.E., Bowman, F.M., 2001. Estimated effects of temperature on secondary organic aerosol concentrations. Environmental Science & Technology, 35, 2129-2135.

Shen, S., Jaques, P.A., Zhu, Y., Geller, M.D., Sioutas, C., 2002. Evaluation of the SMPS-APS system as a continuous monitor for measuring $PM_{2.5}$, PM_{10}, and coarse ($PM_{2.5-10}$) concentrations. Atmospheric Environment, 36, 3939-3950.

Shulski, M., Wendler, G., 2007. Climate of Alaska. University of Alaska Press, Fairbanks, AK. p. 208.

Storch, H.V., Zwiers, F.W., 1999. Statistical analysis in climate research. Cambridge University Press, Cambridge, UK. p. 455.

Strader, R., Lurmann, F., Pandis, S.N., 1999. Evaluation of secondary organic aerosol formation in winter. Atmospheric Environment, 33, 4849-4863.

Timmer, R.P., Lamb, P.J., 2007. Relations between temperature and residential natural gas consumption in the Central and Eastern United States. American Meteorological Society, 46, 1993-2013.

Triantafyllou, A.G., Kiros, E.S., Evagelopoulos, V.G., 2002. Respirable particulate matter at an urban and nearby industrial location: Concentrations and variability and synoptic weather conditions during high pollution episodes. Journal of the Air & Waste Management Association, 52, 287-296.

Unger, N., Shindell, D.T., Koch, D.M., Amann, M., Cofala, J., Streets, D.G., 2006. Influences of man-made emissions and climate changes on tropospheric ozone, methane, and sulfate at 2030 from a broad range of possible futures. Journal of Geophysical Research, 111 (D12313), p. 15. doi:10.1029/2005JD006518.

Weilenmann, M., Favez, J.-Y., Alvarez, R., 2009. Cold-start emissions of modern passenger cars at different low ambient temperatures and their evolution over vehicle legislation categories. Atmospheric Environment, 43, 2419-2429.

Wendler, G., Nicpon, P., 1975. Low-level temperature inversion in Fairbanks, Central Alaska. Monthly Weather Review, 103, 34-44.

Wise, E.K., Comrie, A.C., 2005. Meteorologically adjusted urban air quality trends in the Southwestern United States. Atmospheric Environment, 39, 2969-2980.

Table 3.1 Standard coefficients of meteorological parameters in functional with $PM_{2.5}$-concentrations. Blank cells indicate which quantities have been excluded in the respective tests

Case of analysis	$\dfrac{\partial\theta}{\partial z}\bigg|_{0-350m}$	Δz	v	T	e_v	R^2	Valid data
INV	0.280	0.019	-0.092	-0.609	0.157	0.435	458
	0.298	0.031	-.-	-0.632	0.158	0.428	
	0.316	0.072	-0.124	-.-	-0.355	0.369	
	0.284	0.022	-0.0922	-0.466	-.-	0.430	
ALL	0.418	-.-	-0.0582	-0.599	0.199	0.508	601
	0.431	-.-	-.-	-0.620	0.207	0.506	
	0.475	-.-	-0.102	-.-	-0.315	0.444	
	0.429	-.-	-0.064	-0.416	-.-	0.501	
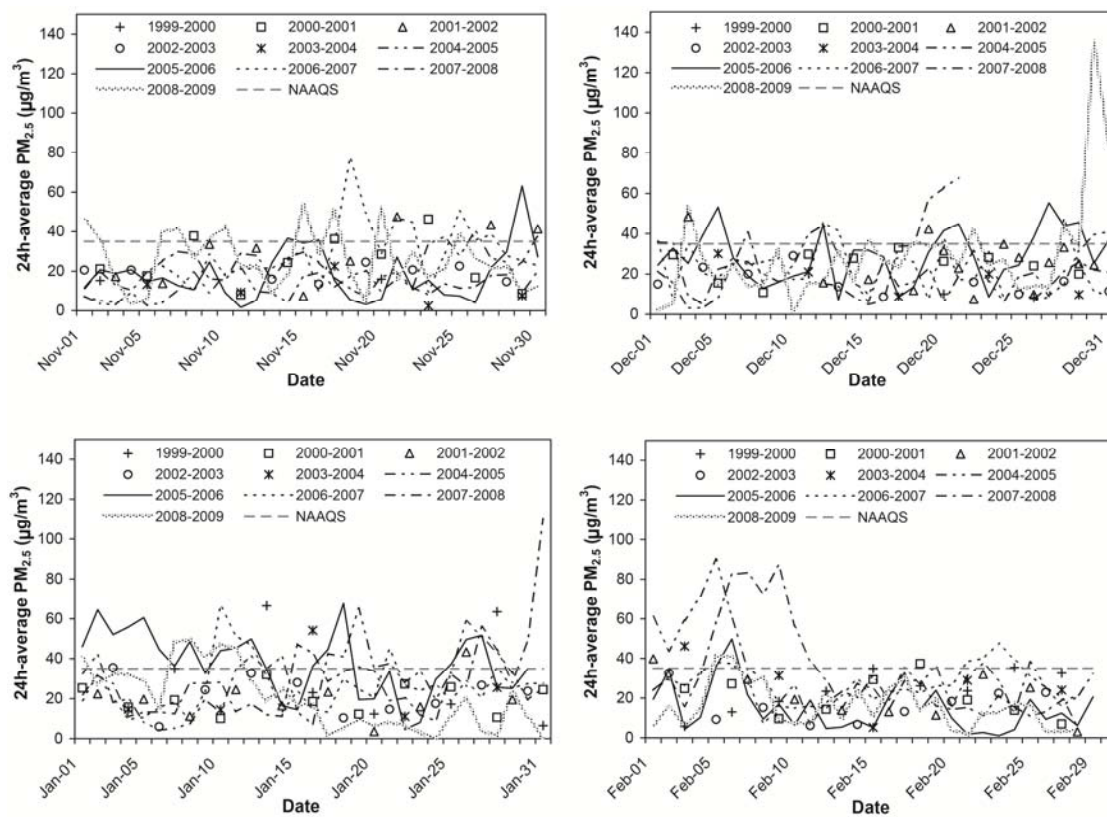
Figure 3.1 Temporal evolution of 24-hour average PM$_{2.5}$-concentrations for 1999 to 2009 for (upper left to lower right) November, December, January, and February.

Figure 3.2 View of the PM$_{2.5}$ monitoring site in downtown Fairbanks. Source: DEC (2009)
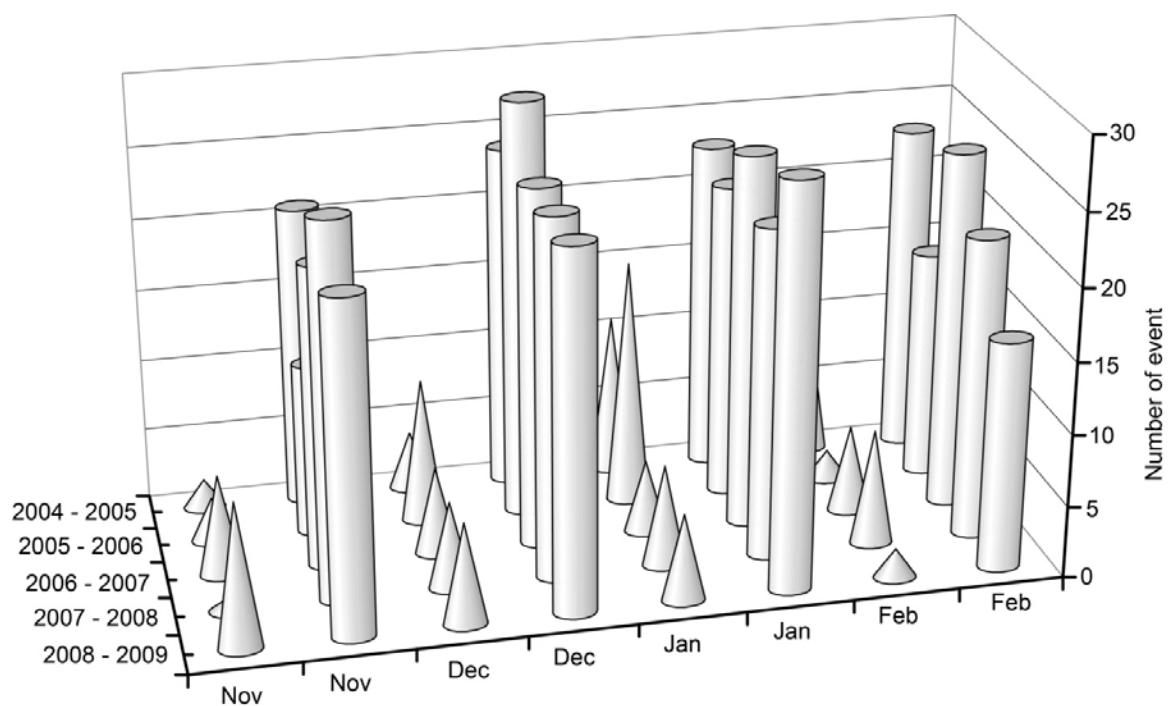
Figure 3.3 Evolution of PM$_{2.5}$ exceedance (cone) and surface-based inversion (cylinder) from November through February in 2004-2009.
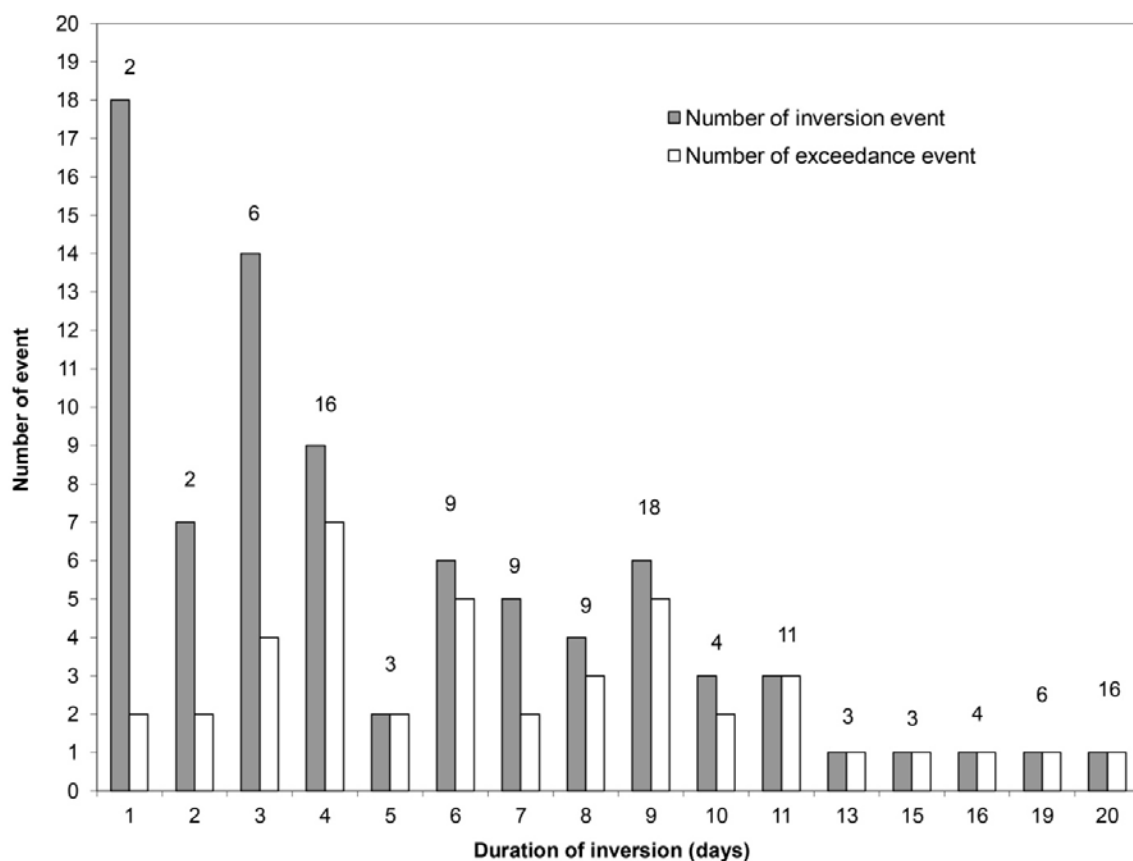
Figure 3.4 Frequency of multiday-inversion occurrence and its associated PM$_{2.5}$-exceedances. The grey shaded bar shows the occurrence frequency of inversions with a given duration; the white bar represents for the number of exceedance events that each duration is associated with; the number above each bar represents the total number of days having exceedance. For example, single day inversions occurred 18 times and two times, they coincided with exceedances.
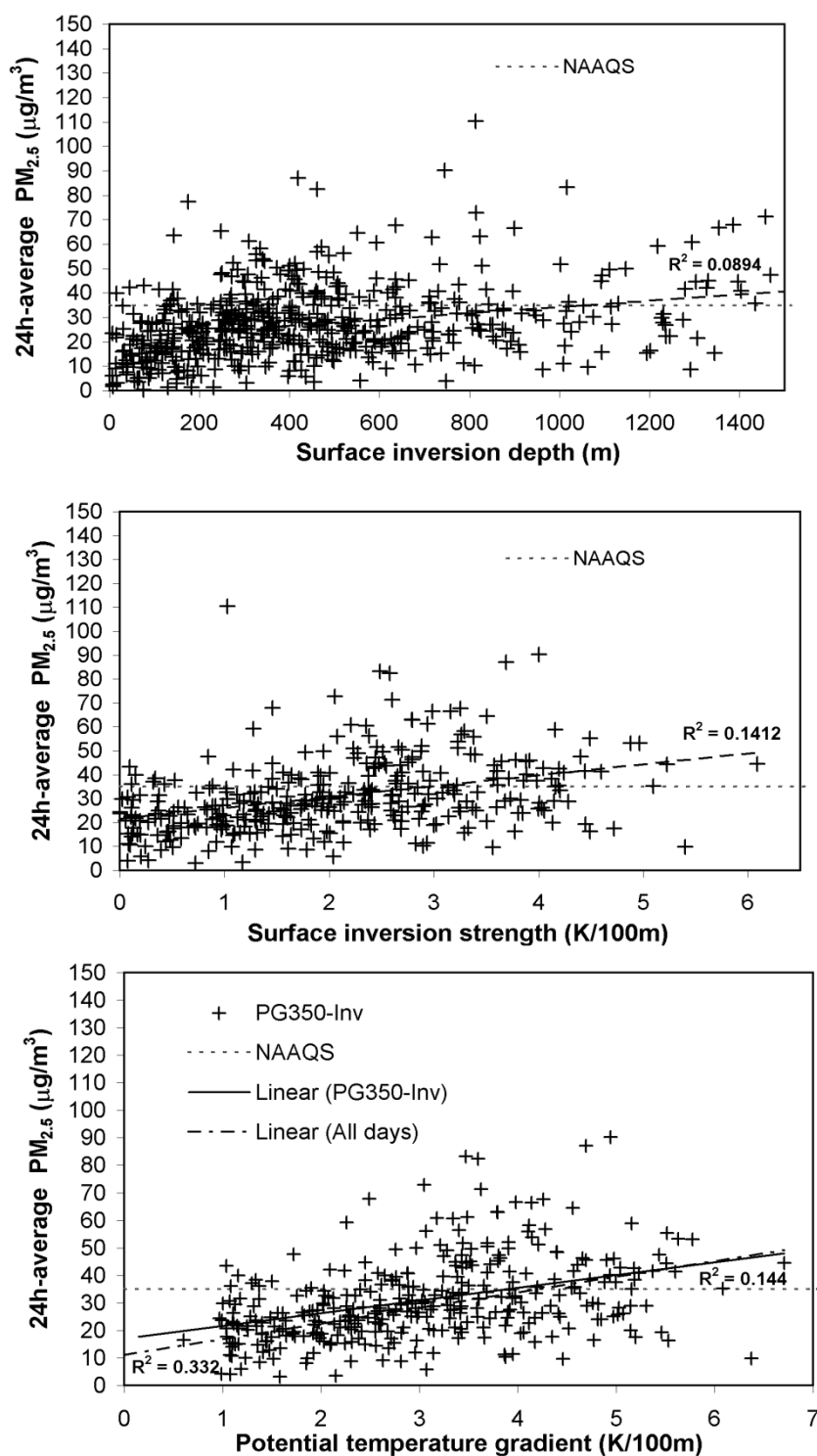
Figure 3.5 Correlation between inversion depth, inversion strength, or potential temperature (from top to bottom) and 24h-average $PM_{2.5}$-concentrations.
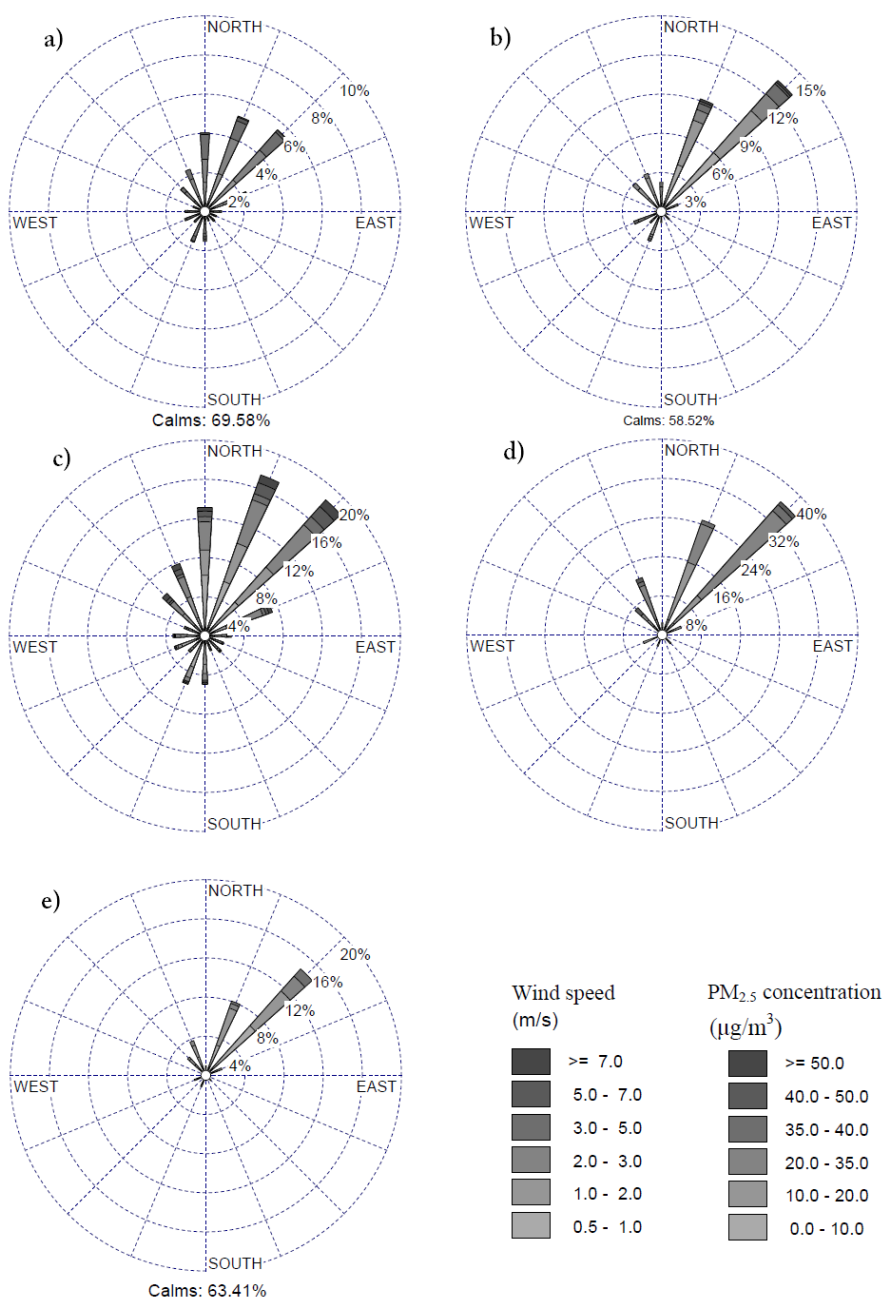
Figure 3.6 Wind-rose profile (a) on an hourly basis, (b) on daily average and (e) under inversion events during winters 2004-2009. The PM$_{2.5}$-concentration rose for (c) hourly and (d) daily averages represents the relation between PM$_{2.5}$-exceedances and wind-direction on days having wind-speeds higher than 0.5m/s, the threshold that allows the average wind-direction to become important.
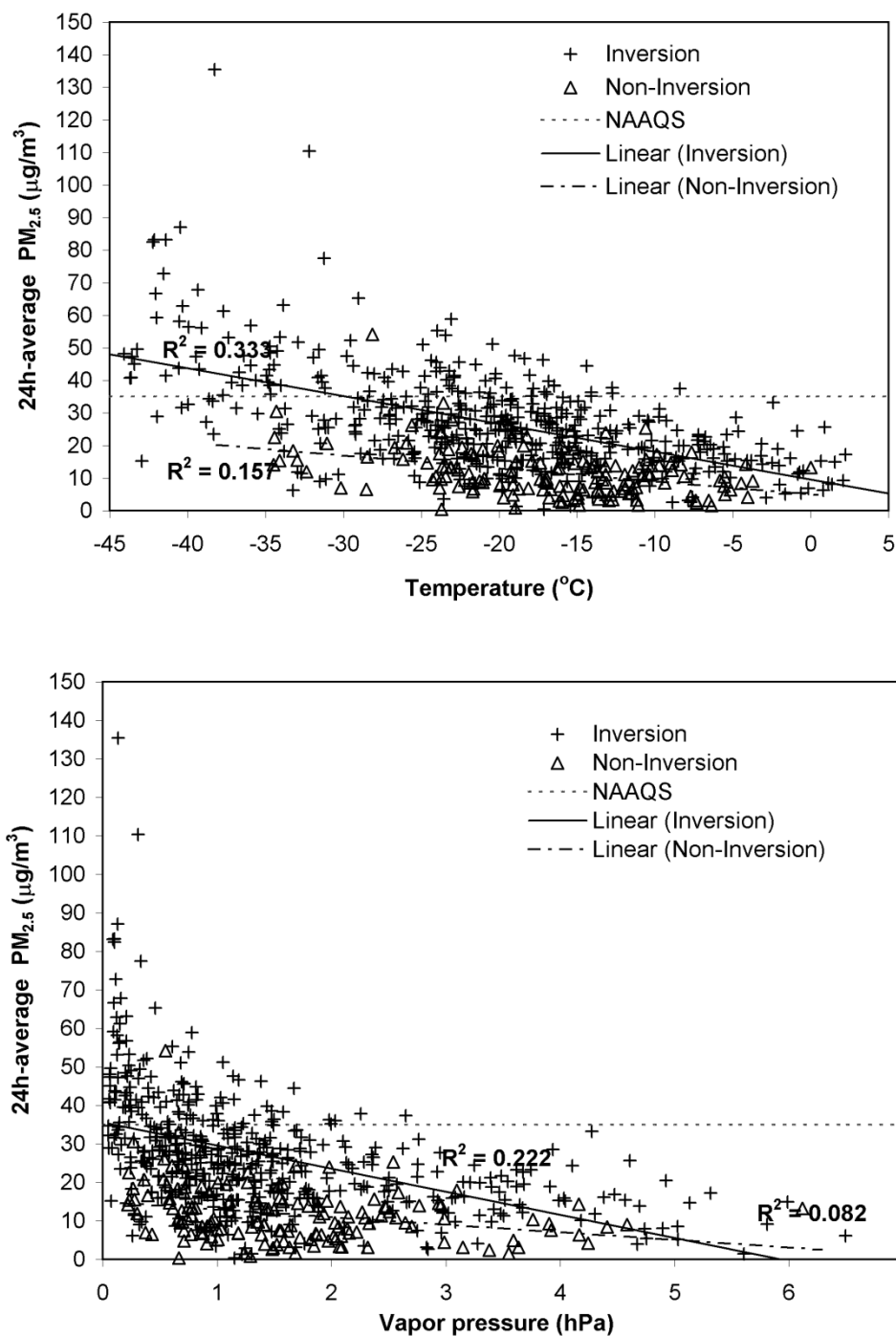
Figure 3.7 Correlation of temperature (top) and partial water-vapor pressure (bottom) with PM$_{2.5}$-concentrations with the trend line being superimposed.

Chapter 4 Evaluation of WRF, WRF/Chem and WRF-CMAQ

Numerical modeling permits assessment of the local impacts of emissions from various sources on the $PM_{2.5}$-concentrations in the Fairbanks nonattainment area. It also allows creation of a database for AQuAT. For the use of air-quality simulations for this assessment and as a database for AQuAT, accuracy in simulating meteorological and chemical fields is key.

4.1 General WRF's performance in the Arctic and subarctic

Evaluation of WRF's performance in the Arctic and subarctic has been extensively performed in various studies using different WRF configurations and for different sub-regions and seasons (e.g., Hines and Bromwich, 2008; Mölders, 2008; Bromwich et al., 2009; Mölders and Kramm, 2010; Yarker et al., 2010; Cassano et al., 2011; Hines et al., 2011; Wilson et al., 2011; PaiMazumder et al., 2012). These evaluations were performed with observations from surface measurement sites (e.g., Mölders, 2008), radiosonde observations (e.g., Mölders and Kramm, 2010), satellite data (e.g., Yarker et al., 2010; PaiMazumder et al., 2012), analysis data (e.g., PaiMazumder et al., 2012), or reanalysis data (e.g., Cassano et al., 2011). Despite the differences in model configurations, model domains, and resolutions in these studies, the results of the evaluations showed that WRF's performance in the Arctic and subarctic shares common features as documented by comparable performance skill-scores.

In these studies, the temporal evolutions of all meteorological fields were relatively well captured. The correlations between the simulated and observed quantities

are typically >0.8 for 2m temperature, 2m dew-point temperature, and sea-level pressure. The daily average 2m temperature was well captured but the amplitude of the 2m-temperature diurnal cycle was not fully captured (e.g., Mölders, 2008; PaiMazumder et al., 2012). Hines et al. (2011) and Wilson et al. (2011) found that WRF tended to have cold bias during nighttime and warm/cold bias around noon. Yarker et al. (2010) attributed difficulties of WRF in capturing the amplitude of the diurnal cycle of 2m-temperature and 2m dew-point temperature to the boundary conditions, misinterpretation of surface processes, terrain height, snow cover, and/or errors in downward radiation fluxes due to the occasional misrepresentation of cloudiness.

Many studies reported that WRF had difficulties in capturing the temporal evolution of hourly precipitation, but acceptably captured the temporal evolution of the daily-accumulated precipitation (e.g., Mölders, 2008; Yarker et al., 2010). PaiMazumder et al. (2012) found that WRF captured the temporal behavior of precipitation well with the overall correlation >0.70 in Siberia. The discrepancies in simulating the precipitation were attributed to deficiencies of the microphysics scheme, incorrect land-use type in the case of convective precipitation, and to the catch deficits and poor regional representation by available observations (e.g., Mölders, 2008; PaiMazumder and Mölders, 2009; PaiMazumder et al., 2012).

Typically, the correlation between simulated and observed 10m wind-speed is the lowest among the correlations of all surface meteorological quantities. It ranges from 0.5 to 0.7 on average (Mölders, 2008; Yarker et al., 2010; Wilson et al., 2011; PaiMazumder et al., 2012).

On average, WRF has warm biases in simulating 2m temperature and 2m dew-point temperature. Warm biases are usually found more often in simulations for winter months than summer months, and at sites located inland than those located at the coast or over the ocean. Yarker et al. (2010) reported biases of 0.9K and 2.8K in simulated 2m temperature and dew-point temperature, respectively. Warm biases (>4K) or cold biases (<1K) were found for 2m temperature and 2m dew-point temperature for WRF simulations over Interior Alaska during a 5-day winter episode depending on the selection of the physical packages (Mölders and Kramm, 2010). A bias of 1.2K for 2m temperature was reported by Hines and Bromwich (2008) for WRF simulations over Greenland for December 2002. For their simulation period from 15 November 2006 to 1 August 2007 for the western Arctic region, Hines et al. (2011) reported warm biases for 2m temperature on average at all sites, and large biases (>4K) occurred at sites in Central Alaska during winter. PaiMazumder et al. (2012) found a cold bias (-0.5K) and warm bias (1.4K) in July and December 2005, respectively, for their WRF simulations over Siberia. They also found that WRF's performance in simulating temperature typically decreased with (1) increasing atmospheric stability, (2) over regions having erroneous land-cover distribution, and (3) at times when there were frontal passages. For simulations over the Arctic Ocean, WRF had a cold bias of -1.8K in January 1998 and a warm bias of 0.4 and 0.1K in June and August 1998, respectively (Bromwich et al., 2009). Over the Arctic, a cold bias of -1.6K on average was found by Wilson et al. (2011) for their 12-months simulation with WRF. They concluded that the choice of the NOAH land-surface model beginning with WRF version 3.1 could be the cause. The choice of

the NOAH land-surface model (Chen and Dudhia, 2001) was also likely the cause for the cold bias (up to about -3K) that occurred in most WRF configurations examined by Cassano et al. (2011). Note that for the simulation in this dissertation, the NOAH land-surface scheme was not used.

Overestimation of wind-speed was commonly found in all WRF evaluation studies. For Interior Alaska, Mölders and Kramm (2010), for instance, found that 10m wind-speed was overestimated, with average biases of 1.55m/s and 0.98m/s in two WRF setups and that WRF also slightly overestimated the wind-speeds within the atmospheric boundary layer (ABL) in their January 2008 simulations. In PaiMazumder et al. (2012), the simulated 10m wind-speeds were slightly stronger than observed with an overall mean bias < 0.36m/s. An average bias of 1.1m/s of daily average 10m wind-speed was found by Yarker et al. (2010) for their January 2006 simulations over southern Alaska. Hines and Bromwich (2008) reported a bias in 10m wind-speed of 1.6m/s on average for a simulation in December 2002. Positive biases in simulating wind-speed occurred at almost all sites in the polar and mid-latitude regions (1.1m/s and 1m/s on average, respectively) throughout the 12 months of simulations in Wilson et al.'s study (2011). Overestimation of wind-speed was also commonly found in simulations with WRF over mid or low latitude regions (e.g., Zhang et al., 2009; Zhao et al., 2011). The main reasons for the positive biases in simulating 10m wind-speed are the complexity of terrain and other local effects (e.g., channeling, misinterpretation of roughness length) that cannot be resolved well by the model (e.g., Mölders, 2008; Mölders et al., 2011b; Wilson et al., 2011). However, negative bias in 10m wind-speed occurred at sites located over sea-ice

as shown in Bromwich et al. (2009) and Wilson et al. (2011). This bias is due to the larger roughness length in WRF than observed over sea-ice (Bromwich et al., 2009).

WRF simulations for the Arctic and subarctic either overestimated or underestimated the downward shortwave and long-wave radiation mainly depending on whether they underestimated or overestimated cloud coverage. Mölders (2008) found that her WRF simulations for Interior Alaska for June 2005 overestimated the daily accumulated downward shortwave radiation by 10% on average. Both WRF configurations in Mölders and Kramm (2010) overestimated the daily-accumulated downward shortwave radiation by 50W/m^2 at the very least. They concluded that the discrepancy in simulating downward shortwave radiation was also partially due to icing of the radiometer during winter as this effect could cause huge observational errors (cf. Mölders et al., 2008). In Bromwich et al.'s study (2009), the average biases in simulating monthly downward shortwave (long-wave) radiation in June and August 1998 were about -9 (18) W/m^2 and 1.1 (3.1) W/m^2, respectively, due to the overestimation of cloud cover. Errors in simulating the radiation balance also contributed to the error in simulating the near-surface air temperatures and moisture as well as stability (Bromwich et al., 2009; Mölders and Kramm, 2010; PaiMazumder et al., 2012).

The magnitude of sea-level pressure was well captured in all studies with typical bias of ±3hPa. Yarker et al. (2010) showed that their WRF simulation over southeast Alaska underestimated the daily mean sea-level pressure by 1.1hPa most of the time. Bias in simulating sea-level pressure found at inland sites for the northern polar region was -3.2hPa on average (Wilson et al., 2011). Mölders (2008) reported a positive bias of

4.3hPa for sea-level pressure for Interior Alaska for June 2005. Bromwich et al. (2009) found small biases in simulated surface-pressure (0.4-1.2hPa) for the Arctic Ocean in January, June and August 1998. The evaluations with reanalysis data over Siberia in July and December 2005 showed that WRF slightly overestimated sea-level pressure by 3.8-6.8hPa (PaiMazumder et al., 2012).

WRF's performance in capturing the vertical profiles of air temperature, dew-point temperature and wind-speed is typically weaker within the ABL, but relatively better above the ABL (e.g., Hines and Bromwich, 2008; Mölders and Kramm, 2010). As shown by Hines and Bromwich (2008), WRF well captures the vertical profiles of temperature and wind-speed in the middle and upper troposphere (above 700hPa), but was relatively weak in doing so below 700hPa. Mölders and Kramm (2010) reported that WRF captured the existence of the surface inversions, but underestimated their strength and height. The vertical profile of dew-point temperatures was not captured well on days when multiple elevated dew-point temperature inversions occurred, but was acceptably captured on the other days (Mölders and Kramm, 2010). As shown in Wilson et al. (2011), biases of air temperature and horizontal wind-speed were greatest below 800hPa and decreased toward upper levels until about 500hPa where the biases again increased.

The performance of WRF was usually weakest during frontal passages or when other large-scale forcing events intruded the simulation domains (e.g., Mölders, 2008; Hines et al., 2011; PaiMazumder et al., 2012).

The effect of the forecast length on the WRF performance was also investigated (e.g., Hines and Bromwich, 2008; Mölders, 2008). Mölders (2008) investigated WRF

24-, 48-, 72-, 96-, and 120-h forecast leads over Interior Alaska for each day of June 2005 and evaluated the performance of each forecast-lead time. The results showed that WRF's performance only slightly differed among different forecast-lead times. Similar results were also found by Hines and Bromwich (2008) for simulations over Greenland for June 2001 and December 2002.

Sensitivity studies with different configurations for WRF have been performed to find an optimized setup for central Alaska (e.g., Chigullapalli and Mölders, 2008; Hines and Bromwich, 2008; Bromwich et al., 2009; Gaudet and Stauffer, 2010; Mölders and Kramm, 2010; Hines et al., 2011; Cassano et al., 2011). The results showed that each of the examined WRF configurations has its strengths and weaknesses. Based on these sensitivity studies, Mölders and Kramm (2010) and Hines and Bromwich (2008) suggested optimized model setups for their applications. These suggested model setups share several selections of physical parameterizations. However, as discussed by Bromwich et al. (2009) who compared the WRF configuration suggested by Hines and Bromwich (2008) with several sensitivity studies, the preferred physical parameterization appears to depend upon the application. This finding confirmed Chirgularpalli and Mölders (2008) who compared and assessed 120 different WRF configurations. No parameterizations and their combinations gave the best performance for all case studies. Cassano et al. (2011) evaluated the performances of seven WRF configurations with reanalysis data and chose the configuration that was most suitable for their application (simulation of the circulations over the Pan Arctic) despite this configuration did not have the best performance in simulating 2m temperature and precipitation.

The above WRF simulations were performed on various domain configurations with different resolutions and for different episodes. Their evaluations were also performed with different types of observational datasets. Therefore, the comparisons of WRF's performances obtained in the above studies serve only to demonstrate that the performance of WRF in the Arctic and subarctic is comparable among studies, and that the performance of WRF and WRF/Chem in the simulations used in this dissertation fall in the same ballpark.

The WRF simulation setups applied in this dissertation were based on the experiences of Chigullapalli and Mölders' (2008), Mölders' (2008), Mölders et al.'s (2010), and Mölders and Kramm's (2010) studies with similar domain configurations that were used in the simulations analyzed in this thesis.

4.2 WRF/Chem and WRF-CMAQ performance for this dissertation

4.2.1 WRF/Chem performance for the 2005/2006 simulations

This section summarizes the evaluation of WRF/Chem's performance for the 2005/2006 simulations that was performed by Mölders et al. (2011a; b).

4.2.1.1 Evaluation of meteorology

Mölders et al. (2011b) evaluated WRF/Chem's performance for the 2005/2006 simulations with observations from a Doppler SOund Detection And Ranging (SODAR) device, twice-daily radiosondes, 33 surface meteorological and four aerosol sites.

WRF/Chem well captured the inversion layers observed at the two radiosonde sites during the episode. In Fairbanks, WRF/Chem simulated 103 nocturnal surface inversions and 22 elevated inversions while 97 and 19, respectively, were observed. However, WRF/Chem underestimated the inversion strength. It had difficulties in capturing the inversions that have vertical temperature gradients > 8K/100m, but captured relatively well the occurrence of the surface inversions that have vertical temperature gradients < 3K/100m. As shown in Mölders et al. (2011b), biases of the simulated vertical temperature, dew-point temperature, wind-speed and wind-direction profiles were positive and largest within the ABL below 1km height, and so were the RMSEs. This behavior is a typical characteristic of WRF's performance as discussed in section 4.1.

The evaluation of WRF/Chem with the SODAR observation also showed that WRF/Chem overestimated (underestimated) wind-speed below (above) 600m above the ground-level, and performed well in capturing the presence of low-level jets. Mölders et al. (2011b) concluded that random errors (e.g., initial and boundary conditions) rather than systematic errors (e.g., model parameterizations) were the major causes for the overall error.

The evaluation of WRF/Chem with surface observations showed average biases over the entire episode and all meteorological sites of 1.6K, 1.8K, 1.85m/s, -5°, and 1.2hPa for temperature, dew-point temperature, wind-speed, wind-direction, and sea-level pressure, respectively. WRF/Chem captured the general temporal evolution of downward shortwave radiation well, but overestimated it by 9W/m^2 on average as

WRF/Chem underestimated cloudiness. The temporal evolution of 2m air temperature, dew-point temperature, wind-speed and sea-level pressure were captured well except when there were frontal passages. The relatively weaker performance of WRF/Chem during frontal passages was also found by Mölders (2008) and PaiMazumder et al. (2012). The standard deviations of sea-level pressure, wind-speed and wind-direction over the 33 sites were well captured showing that WRF/Chem simulated the pattern variations of these quantities well. The standard deviations of 2m air temperature and dew-point temperature were acceptably captured, and those of relative humidity and daily-accumulated downward shortwave radiation were broadly captured.

4.2.1.2 Evaluation of simulated $PM_{2.5}$-concentrations

The overall FAC2 of simulated $PM_{2.5}$, particulate matters having diameters of less than 10µm (PM_{10}), nitrate aerosol (NO_3), ammonium aerosol (NH_4) and sulfate aerosol (SO_4) over the 2005/2006 simulation were 41%, 13%, 4%, 2% and 50%, respectively. The FBs of the respective aerosol species were 20%, -150%, -120%, -190% and 30% (Mölders et al., 2011b). Based on the criteria suggested by Chang and Hanna (2004), WRF/Chem has acceptable performance in simulating $PM_{2.5}$ and SO_4, but the simulations of PM_{10}, NO_3 and NH_4 aerosol were at the lower end of acceptable performance. The correlations of the 24h-average PM_{10}, NO_3, NH_4 and SO_4 were low (<0.15). The underestimation of NO_3 and NH_4 may be due to the too low emissions of ammonia (NH_3) found in the NEI2005 for Fairbanks during winter. Note that similar behavior was found for the NEI2008 (Tran and Mölders, 2012a).

WRF/Chem simulated PM$_{2.5}$ at the Fairbanks site better than at the remote sites in Denali Park and Poker Flat (Mölders et al., 2011b). The overall bias and correlation of the 24h-average PM$_{2.5}$-concentrations at the Fairbanks site were 4.0µg/m^3 and 0.59 (statistically significant). The temporal evolution of the 24h-average PM$_{2.5}$ at this site was broadly captured. WRF/Chem slightly overestimated the 24h-average PM$_{2.5}$-concentrations on weekends, but strongly underestimated the extremes and the 24h-average PM$_{2.5}$-concentrations on weekdays. Errors in the emission allocations could be the cause for this behavior. WRF/Chem's performance was better for high than low 24h-average PM$_{2.5}$-concentrations.

Mölders et al. (2011b) found that the performance in simulating PM$_{2.5}$-concentrations was strongly affected by the accuracy of the simulated meteorological conditions. Differences between the simulated and observed PM$_{2.5}$-concentrations were large when WRF/Chem overestimated the inversion strength, and/or had offset in capturing the temporal/spatial distribution of the meteorological quantities. Mölders et al. (2011b) concluded that WRF/Chem's errors in simulating air and dew-point temperature partially contributed to its underestimations of PM$_{2.5}$-concentrations. This finding agrees with Tran and Mölders' (2011) analysis of observations that air temperature is the most important factor for elevated PM$_{2.5}$-concentrations in Fairbanks in winter.

4.2.2 WRF/Chem performance for the 2008/2009 simulations

This section summarizes the evaluation of WRF/Chem for the 2008/2009 simulations that had been performed by Mölders et al. (2011a) and was discussed in

detail in Mölders et al. (2012). Additional evaluations of WRF/Chem were performed within the scope of this dissertation using observations from the radiosonde site in Fairbanks and the SODAR located on the University of Alaska Fairbanks campus (J. Fochesatto, pers. comm., December 2010).

4.2.2.1 Evaluation of simulated meteorology

Mölders et al. (2012) evaluated the performance of WRF/Chem in simulating meteorological quantities for winter 2008/2009 with observations from 23 surface sites, the meteorological tower in downtown Fairbanks, and temperature observations by an instrumented vehicle. At the meteorological tower, WRF/Chem overestimated air temperature at 3, 11 and 22m by 0.6K, 0.7K and 1.1K, respectively, and captured the temporal evolution well at all levels (R >0.881). WRF/Chem overestimated wind-speed at 11m and 22m by 1.15m/s and 2.39m/s, respectively. These results suggested that WRF/Chem overestimated the observed vertical mixing.

WRF/Chem captured the temporal evolution of the meteorological quantities observed at the 23 surface meteorological sites well (Mölders et al., 2012). The overall correlation between the simulated and observed 2m air temperature, 2m dew-point temperature and 10m wind-speed were 0.897, 0.905 and 0.573, respectively. The biases of 2m air temperature, 2m dew-point temperature, 10 wind-speed, wind-direction and sea-level pressure were 1.3K, 2.1K, 1.55m/s, -4° and -1.9hPa, respectively. The performance skill-scores varied with months. The bias of the monthly average air temperature was highest in December (6.1K) and lowest in March (0.3K). WRF/Chem

simulated wetter conditions than observed overall. Mölders et al. (2012) also reported that the discrepancies between simulated and observed meteorological quantities were mainly due to mistiming of frontal passages or occurred after sudden strong temperature changes.

My evaluation of WRF/Chem with the radiosonde observations showed that like for 2005/2006, WRF/Chem had difficulty in capturing the complex vertical profile of air temperature, dew-point temperature, wind-speed and wind-direction within the layer below 850hPa. Here, WRF/Chem typically simulated warmer (4K) and drier conditions (9% in RH) than observed, especially in October 2008. It broadly captured the elevated inversions observed below this level. WRF well (broadly) captured the vertical profiles of wind-speed and wind-direction above (below) 900hPa. It well captured the occurrence of low-level jets at about 900hPa and the jets above 900hPa throughout October 2008 to March 2009 (OTM). In October and March, WRF/Chem relatively well captured the existence and magnitude of the nocturnal surface inversions at local nighttime (1200UTC), and either underestimated/overestimated the stability at local daytime (0000UTC). WRF/Chem well captured the occurrence of surface inversions, which were dominant throughout November to February. However, like for winter 2005/2006, it failed to fully capture the strength of these inversions, especially within the first 100m above ground. The observed vertical temperature gradient was as large as 18K/100m, while the largest simulated gradient was about 6K/100m (Figure 4.1). WRF/Chem also had difficulties in capturing the multiple inversions that occurred below the 850hPa level. This difficulty can be partly attributed to the vertical resolution.

SODAR observations (J. Fochesatto, pers. comm., December 2010) were available from December 18, 2008 to February 14, 2009 at the site located at the experimental farm on the University of Alaska Fairbanks campus. Throughout this time, the SODAR observations were only available for the layer below 1km height (below 900hPa). The evaluations of WRF/Chem's performance by the SODAR observations showed that like in winter 2005/2006, WRF/Chem captured the occurrences of low-level jets well, but generally overestimated their strength (Figure 4.2). The relative biases of horizontal wind-speed (Figure 4.3) and wind-direction (not shown) were strongest in the layer between 400-1000m height. Here the relative bias was determined as ($RB = (100\%/N) \times \sum_{i=1}^{N} [(v_{s,i} - v_{o,i})/v_{o,i}]$) where N is the number of pairs of simulated (v_s) and observed (v_o) winds. Overall, WRF/Chem overestimated the SODAR-determined horizontal wind-speed by 1.41m/s. The offset between the simulated and SODAR-determined wind-direction was 11° on average. The SODAR-determined temperature-structure parameter (C_T^2) exceeded the WRF/Chem derived quantity by more than five orders of magnitude, especially in the layer below 800m (Figure 4.3). Here in accordance with Mölders et al. (2011b), C_T^2 was determined as

$$C_T^2 = \left[\left(\bar{\theta}_k - \bar{\theta}_{k-1} \right) / \left(z_k - z_{k-1} \right)^{1/3} \right]^2$$ where $\bar{\theta}$ is the mean potential temperature at height z and k is the model layer. The underestimation of C_T^2 means that WRF/Chem overestimated the vertical mixing. This confirms the findings by Mölders et al. (2012) based on the meteorological tower observations.

4.2.2.2 Evaluation of simulated PM$_{2.5}$-concentrations

WRF/Chem slightly overestimated the 24h-average PM$_{2.5}$-concentrations on exceedance days (days with 24h-averaged PM$_{2.5}$-concentrations $> 35\mu g/m^3$), but failed to capture the extremes to their full extent (Mölders et al., 2012). The FB, FE, NMB, NME and FAC of the 24h-average PM$_{2.5}$-concentrations obtained over all fixed sites from October 2008 to March 2009 were 22%, 67%, 13%, 71%, 56%. The corresponding values for the 1h-average PM$_{2.5}$-concentrations were 35%, 98%, 18%, 94%, 39% (Mölders et al., 2012). The occurrence frequency was acceptably captured for PM$_{2.5}$-concentrations between 15-50$\mu g/m^3$. Furthermore, WRF/Chem simulated 52 exceedances at the grid-cell holding the SB-site where only 26 exceedances were observed.

WRF/Chem met the performance goals recommended by Chang and Hanna (2004) and EPA (2007) at the PR and NP sites in all months and at the SB-site in all months except October and March. WRF/Chem also met the performance goals at other sites, but its performance varied with time. WRF/Chem had the weakest performance in simulating PM$_{2.5}$-concentrations during October and March (Mölders et al., 2012).

WRF/Chem had relatively good performance in simulating the SO$_4$-aerosol concentrations, acceptably captured the organic carbon (OC) and elemental carbon (EC) aerosol concentrations, but had relatively weak performance in simulating the NO$_3$ and NH$_4$-aerosol concentrations. The discrepancies in simulating NH$_4$-aerosol concentrations mainly were due to the underestimation of NH$_4$ emissions in the NEI2008 (Mölders et al., 2012).

WRF/Chem was also evaluated with $PM_{2.5}$-concentrations measured at 3m above ground level by instrumented vehicles along traffic roads in 86 days during OTM (Mölders et al., 2012). WRF/Chem slightly underestimated the mobile-observed $PM_{2.5}$-concentrations by $2.8\mu g/m^3$, on average, but its skill-scores are better than those obtained at the fixed location sites.

WRF/Chem acceptably captured the temporal evolution of $PM_{2.5}$-concentrations except when it underestimated the inversion strengths or mistimed frontal passages, or when there were sudden temperature changes. Like for winter 2005/2006, the accuracy in simulating $PM_{2.5}$-concentrations heavily depended on the accuracy in simulated temperature (Mölders et al., 2012). The overestimated relative humidity was frequently associated with underestimation of $PM_{2.5}$-concentrations. The above $PM_{2.5}$-meteorological relationships well agreed with the observed meteorological conditions that drive the $PM_{2.5}$-concentrations in Fairbanks as found by Tran and Mölders (2011).

4.2.3 Evaluation of WRF-CMAQ in the 2009/2010 and 2010/2011 simulations

CMAQ has just recently been adapted for Alaska by Mölders and Leelasakultum (2011) and Leelasakultum and Mölders (2012). Thus, except for the evaluations described by these authors, no independent evaluation of the Alaska adapted CMAQ exists so far.

I performed an evaluation of the Alaska adapted WRF-CMAQ for the 2009/2010 and 2010/2011 simulations. Some of the main findings in this section are briefly discussed in Tran et al. (2012) and in chapter 9 – sections 9.4.1 and 9.4.2. Thus, in this

section, I provide additional material not covered by the paper of chapter 9, but I refer to figures and tables displayed in chapter 9 to avoid redundancy.

In the following discussion, the Alaska adapted CMAQ is used and the term "Alaska adapted" is dropped for simplicity.

4.2.3.1 Evaluation of meteorology

The performance of WRF in simulating the meteorological quantities was relatively similar for episode 1 and 2 (Table 9.2). WRF well captured the temporal evolutions of 2m temperature and 2m dew-point temperature, 10m wind-speed, and sea-level pressure. Throughout both episodes, WRF consistently predicted warmer (3K) and drier near-surface conditions (15% in RH), and stronger 10m wind-speeds (1.4m/s) than observed (Figure 9.4). The overestimation of wind-speed under weak wind conditions (v <1.5m/s), like in these two episodes, is common to all modern meteorological models (e.g., Zhang et al., 2009; Mölders et al., 2011b; Zhao et al., 2011; Mölders et al., 2012; see also section 4.1).

Except for wind-speed and downward shortwave radiation, WRF acceptably captured the variances in the meteorological fields at all sites (Figure 9.4). WRF well captured the temporal evolution and magnitude of sea-level pressure. WRF predicted much drier (27% lower relative humidity) conditions than observed especially between January 8 and 10, 2011 (Figure 9.4). WRF simulated wind-direction with a mean bias $<30^{o}$, i.e., this performance falls within the range of other model studies for this region (e.g., Mölders, 2008, 2010; Yarker et al., 2010; see also section 4.1), but is weaker than

WRF/Chem's performance in Mölders et al. (2011b; 2012). WRF generally underestimated downward shortwave radiation throughout episode 1 by 33W/m^2. In episode 2, WRF underestimated downward shortwave radiation for January 1 to 10, 2011 by 63W/m^2, on average, while it overestimated shortwave radiation on the other days by 97W/m^2, on average. The underestimation of downward shortwave radiation for January 1 to 10, 2011 of WRF simulations in this study is similar to the finding of Mölders and Kramm (2010). Discrepancies in the simulated cloud cover could be the reason for the discrepancies in the simulated downward shortwave radiation.

The evaluation of WRF's performance by radiosonde observations in Fairbanks showed that WRF well captured the existence of surface inversions that occurred throughout the two episodes. However, as in the studies discussed above, it had difficulties in capturing the vertical temperature gradients > 15K/100m of surface inversions within the first 100m above the ground. WRF broadly captured the occurrence of the multiple inversions within the ABL below 850hPa with slight offsets in their height (200m) and thickness (300m). These offsets may have consequences for simulated PM$_{2.5}$-concentrations. A too thin (thick) an inversion layer means that more (less) PM$_{2.5}$ can be advected vertically, which consequently leads to low (high) PM$_{2.5}$-concentrations at the breathing level than otherwise. WRF captured the vertical profiles of air temperature, wind-speed and wind-direction well, but broadly captured the vertical profiles of dew-point temperature (Figure 4.4).

4.2.3.2 Evaluation of simulated PM$_{2.5}$-concentrations

The evaluation with measurements at the fixed location sites showed that CMAQ performed relatively better in simulating PM$_{2.5}$-concentrations for episode 1 than for episode 2 (Table 9.3, Figure 4.5). Over all sites and days, the mean bias, RMSE, NMB, NME, and FAC2 of 24h-average PM$_{2.5}$-concentrations for episode 1 are 4.4µg/m^3, 28.8µg/m^3, 9%, 42% and 91%, respectively. The corresponding values for episode 2 are 31.7 µg/m^3, 44.1µg/m^3, 125%, 129% and 49%. The performance skill-scores of the simulations for episode 1 (2) are better (weaker) than the skill-scores of CMAQ simulations over the contiguous U.S. for winter months (December, January and February) reported in previous studies (e.g., EPA, 2005; Eder and Yu, 2006). For episode 1, 66% and 100% of the pairs of NMB-NME obtained at all stationary sites fell within the EPA (2007) recommended goals and criteria of performance, respectively (Figure 4.6). In episode 2, only the pair of NMB-NME at the SB-site reached the performance goal, while the pairs of NMB-NME at other sites fell outside the performance criteria.

Boylan and Russell (2006) recommend MFB within ±60% and MFE ≤ 75% as the criteria for a model's performance to be considered as acceptable, and MFB within ±60% and MFE ≤ 50% as the goal that the best state-of-the-art model can reach. According to Chang and Hanna (2004), air-quality model simulations that have FB within ±30% and a FAC2 ≥50% are considered to have good performance. Based on the criteria and skill-scores, CMAQ's performance has to be considered good for episode 1 and acceptable for episode 2.

In both episodes, CMAQ underestimated the frequency of $PM_{2.5}$-concentrations $<20\mu g/m^3$, well captured the frequency of $PM_{2.5}$-concentrations between 40 and $100\mu g/m^3$, and slightly overestimated the frequency of $PM_{2.5}$-concentrations between 20 and $40\mu g/m^3$ and $>110\mu g/m^3$. In episode 2, CMAQ strongly overestimated the frequency of $PM_{2.5}$-concentrations $>30\mu g/m^3$.

For both episodes, CMAQ simulated the $PM_{2.5}$-concentrations at the SB-site better than at other sites. At the SB-site, its performance was better for episode 1 than 2 (Table 9.3). CMAQ captured all but two observed exceedances at the SB-site for each episode (Figure 4.7). However, CMAQ predicted 11 non-observed exceedances for episode 2. CMAQ captured the temporal evolution of $PM_{2.5}$-concentrations in both episodes well except for December 27 to 31, 2009 when CMAQ predicted the peak of the hourly $PM_{2.5}$-concentrations about 5h ahead (Figure 4.7). This temporal offset propagated into the simulated 24h-average $PM_{2.5}$-concentrations on these days.

My investigations showed that this offset was due to the errors in simulated meteorology rather than due to emission errors. Mölders and Leelasakultum (2012) and Leelasakultum and Mölders (2012) also reported similar errors for their WRF-CMAQ simulations. However, they reported a 24h offset. CMAQ highly overestimated the 24h-average $PM_{2.5}$-concentrations at the SB-site (by $22\mu g/m^3$ on average) between January 7 and 9, 2011. My investigations showed that discrepancies in simulated meteorology fields were not larger than the discrepancies found on other days. Therefore, these overestimations can be attributed to the uncertainty/errors in the emission allocations.

For episode 1 and 2, 24h-average observations of SO_4, NO_3, NH_4, OC and EC aerosols were available at the SB-site on a 1-in-3-days basis. Observations were available for seven days for episode 1, and four days for episode 2. The evaluation of WRF-CMAQ's performance with these observations showed that WRF-CMAQ largely underestimated SO_4, but overestimated NO_3 aerosols. WRF-CMAQ captured the magnitude of NH_4 and OC aerosols relatively well, and fairly captured the magnitude of EC aerosols. Underestimation of SO_4 aerosols was also found by Leelasakultum and Mölders (2012) for their CMAQ simulations for January, February and November 2008. Leelasakultum and Mölders (2012) concluded that the discrepancy in the partitioning of the emitted $PM_{2.5}$ was part of the reason for this behavior. Over the two episodes, the mean bias, RMSE, NMB, NME, and FAC2 of 24h-average SO_4 (NO_3) aerosols were -5.1 (4.6) $\mu g/m^3$, 5.6 (2.8) $\mu g/m^3$, -84 (139) %, 84 (147) % and 0 (67) %, respectively. The corresponding skill-scores for 24h-average OC (EC) aerosols were 4.2 (1.3) $\mu g/m^3$, 8.1 (1.6) $\mu g/m^3$, 24 (92) %, 42 (103) %, and 100 (33) %, respectively. For the 24h-average NH_4 aerosols, the corresponding skill-scores were -0.8$\mu g/m^3$, 2.7$\mu g/m^3$, -28%, 71%, and 50%, respectively.

The CMAQ-simulated $PM_{2.5}$-concentrations were evaluated with the $PM_{2.5}$-concentrations measured by the sniffer during all drives of episode 1. This evaluation yielded a mean bias, RMSE, FB, NMB, NME, and FAC2 of 3.0$\mu g/m^3$, 50.8$\mu g/m^3$, -4%, 8.5%, 93%, and 39% respectively. The corresponding skill-scores for episode 2 were 11.5$\mu g/m^3$, 43.0$\mu g/m^3$, 10%, 42%, 118%, and 28%, respectively. The skill-scores determined for individual sniffer drives differed strongly from each other (up to ±40% of

the skill-scores). On average, CMAQ typically performed better on days with high ($>30\mu g/m^3$) than low $PM_{2.5}$-concentrations (detected by the sniffer).

For episode 1, CMAQ overestimated the frequency of $PM_{2.5}$-concentrations $<15\mu g/m^3$, underestimated the frequency of $PM_{2.5}$-concentrations between 15 and $80\mu g/m^3$, and failed to capture $PM_{2.5}$-concentrations $>270\mu g/m^3$ (Figure 4.8). For episode 2, CMAQ underestimated the frequency of $PM_{2.5}$-concentrations $<35\mu g/m^3$, and overestimated the frequency of $PM_{2.5}$-concentrations between 45 and $100\mu g/m^3$ (Figure 4.9). The correlation between simulated and sniffer-observed $PM_{2.5}$-concentrations obtained for any drive was 0.824 at the highest (statistically significant at the 95% confidence level), and the overall correlation was 0.232 (statistical significant) over the two episodes. Some of the discrepancies are due to the fact that the simulated $PM_{2.5}$-concentrations represent volume-average concentrations for 1.3km$\times$1.3km$\times$4m, while the average sniffer observations represent the average along the route within that grid-cell at 3m height at the same hour.

The temporal evolution of simulated $PM_{2.5}$-concentrations correlated relatively well with the temporal evolution of the simulated meteorological quantities. Over the two episodes, the simulated hourly $PM_{2.5}$-concentrations had statistically significant correlations with the simulated hourly 2m temperature (-0.374), 2m dew-point temperature (-0.397), 10m wind-speed (-0.580), relative humidity (-0.409), and sea-level pressure (0.062). The simulated $PM_{2.5}$-concentrations typically increased as the simulated air temperature, relative humidity and wind-speed decreased (Figure 4.9). As discussed above, the surface inversions that WRF broadly simulated in Fairbanks throughout the

simulation episodes led to high $PM_{2.5}$-concentrations over this time, which were also simulated. These simulated conditions agreed with the observed conditions found to be typically associated with the observed high $PM_{2.5}$-concentrations in Fairbanks and discussed in chapter 3 (i.e., Tran and Mölders, 2011).

There exist relationships between errors in simulated $PM_{2.5}$-concentration and errors in simulated meteorological quantities, especially with errors in simulated temperature and wind-speed. As shown in Figure 4.9, small biases in the simulated $PM_{2.5}$-concentrations were typically associated with small biases in simulated temperatures and wind-speeds. These relationships are similar to those found for the simulations with WRF/Chem for winter 2005/2006 and 2008/2009. However, the patterns of errors in simulated meteorological quantities do not well explain the pattern of errors in simulated $PM_{2.5}$-concentrations. This means uncertainty in the emission inventory also contributed to the errors in the simulated $PM_{2.5}$-concentrations in WRF-CMAQ.

The high overestimation of $PM_{2.5}$-concentrations in episode 2 was caused mainly by errors in emissions. The situation is as follows: There was a decrease in the observed $PM_{2.5}$-concentrations during both episodes. The highest, average, and 90th percentile observed 24h-average $PM_{2.5}$-concentrations over all sites and days of episode 1 were $114\mu g/m^3$, $48\mu g/m^3$, and $75\mu g/m^3$. The corresponding values in episode 2 were $80\mu g/m^3$, $25\mu g/m^3$, and $49\mu g/m^3$, respectively. The meteorological observations at the sites in Fairbanks showed that 2m temperature, relative humidity, and wind-speed varied with similar magnitudes in episode 1 and 2. This fact implies that the decrease in observed $PM_{2.5}$-concentrations was mainly due to the decrease in the emissions of $PM_{2.5}$ and its

precursors. The introduction of a voluntary wood-burning device changeout program in Fairbanks in 2010 may have partially helped to reduce the emissions as uncertified wood-burning devices can contribute appreciably to the total $PM_{2.5}$-concentrations in Fairbanks (Tran and Mölders, 2012b; see also chapter 6). As described in the experimental design (cf. chapter 2), the emissions for episode 2 were assumed to increase by 1.5% as compared to the emissions used for episode 1. This assumption was in accordance with Mölders et al. (2011b; 2012). Note that this assumption did not consider the effects of wood-burning device changeouts due to the lack of information, and therefore may have led to higher simulated $PM_{2.5}$-concentrations than observed. The lower performance for episode 2 than 1 may also be an indicator that the 1.5%/year assumption is too high.

4.3 Conclusions

The performance of WRF/Chem and WRF-CMAQ in simulating the meteorological quantities and $PM_{2.5}$-concentrations and its components for the 2005/2006, 2008/2009, 2009/2010, and the 2010/2011 studies had been evaluated with observations from meteorological and aerosol monitoring sites, and other available data.

With respect to the meteorological quantities, the WRF/Chem and WRF-CMAQ simulations used for this dissertation have comparable performance to previous studies for the Arctic and subarctic (see section 4.1). The features of WRF's performance in the Arctic and subarctic that were common to many studies documented in the literature, were also found for the performance of WRF/Chem and WRF-CMAQ in the studies relevant to this thesis. The performance was usually weakest when the model missed the

timing of frontal passages or when there were sudden changes in temperature. However, the first shortcoming may hardly affect the applicability of the interpolation tool for the public air-quality advisory as $PM_{2.5}$-concentrations are typically low during frontal passage (i.e., no likelihood for false alarm). The second shortcoming may lead to errors in the simulated $PM_{2.5}$-concentrations due to the errors in simulated physical and chemical processes (e.g., transport, gas-to-particle conversion) at the time of sudden changes in temperature. However, such events are rare.

WRF-CMAQ and WRF/Chem captured the occurrence of surface inversions well throughout the simulation episodes, but failed to fully capture their strengths. The reason for this behavior may be the land-surface model that typically predicted a warmer surface condition than observed during winter.

With respect to the performance in simulating $PM_{2.5}$-concentrations, the performance skill-scores showed that the CMAQ simulations in episode 1 (2) have better (slightly weaker) performance than WRF/Chem in the 2008/09 simulation. This means that WRF/Chem and WRF-CMAQ simulations of relevance for this dissertation have similar quality. Out of all studies, the WRF/Chem simulations for the 2005/2006 study had the weakest performance overall. However, this may be an artifact of data availability for the $PM_{2.5}$-evaluation.

Typical findings are that the performance of WRF/Chem and WRF-CMAQ in simulating aerosols strongly depends on the quality of the simulated meteorological quantities, especially temperature, wind-speed and inversion strength, as well as on the accuracy of the emissions. The typically simulated meteorological conditions for high

$PM_{2.5}$-concentrations agree well with the observed conditions that are typically associated with high $PM_{2.5}$-concentrations in Fairbanks (Tran and Mölders, 2011).

Note that the same systematic and random errors exist in the reference and in the experiment simulations as they used the same model setups. The investigations on the contributions of emissions from point sources, traffic and uncertified wood-burning devices to the $PM_{2.5}$-concentrations are performed in terms of differences or in relative form of RRFs or percentages. Therefore, despite some of the shortcomings in the WRF/Chem and WRF-CMAQ performance, these simulations are still usable and valuable for investigating the contributions of emissions from the above emission sources to the $PM_{2.5}$-concentrations in Fairbanks. These investigations are needed to develop a public air-quality advisory tool as these emissions are major sources in the unmonitored neighborhoods and may contribute to the $PM_{2.5}$-concentrations. As was demonstrated in the introduction, additional information on emission contributions is needed to interpolate the mobile measurements into space.

WRF/Chem as well as WRF-CMAQ provided similar overall behavior of the $PM_{2.5}$-meteorology relationship as found in the observations for November to February of 1999 to 2009 by Tran and Mölders (2011) (see chapter 3). Thus, the slight discrepancies between simulated and observed $PM_{2.5}$-concentrations may play a minor role for the database of AQuAT as WRF-CMAQ provides a reasonable climatology of the $PM_{2.5}$-meteorology relationship.

Based on the performance skill-scores and performance criteria, the performance of CMAQ in simulating $PM_{2.5}$-concentrations in the nonattainment area in episode 1

(12/27/2009 – 01/12/2010) is within the range of state-of-the-art models. This means the CMAQ-simulated PM$_{2.5}$-concentrations of episode 1 are close to what was observed. Therefore, the CMAQ simulations of episode 1 were chosen to serve as a database for the development of AQuAT as will be discussed in chapter 9.

References

Boylan, J.W., Russell, A.G., 2006. PM and light extinction model performance metrics, goals, and criteria for three-dimensional air quality models. Atmospheric Environment, 40, pp. 4946-4959.

Bromwich, D.H., Hines, K.M., Bai, L.-S., 2009. Development and testing of Polar Weather Research and Forecasting model: 2. Arctic Ocean. Journal of Geophysical Research, 114, p. 22. doi: 10.1029/2008JD010300.

Cassano, J.J., Higgin, M.E., Seefeldt, M.W., 2011. Performance of the Weather Research and Forecasting Model for month-long pan-Arctic simulations. American Meteorological Society, 139, pp. 3469-3488.

Chang, J.C., Hanna, S.R., 2004. Air quality model performance evaluation. Meteorology and Atmospheric Physics, 87, pp. 167-196.

Chen, F., and J. Dudhia, 2001: Coupling an advanced land surface-hydrology model with the Penn State-NCAR MM5 modeling system. Part I: Model implementation and sensitivity. Monthly Weather Review, 129, pp. 569-585.

Chigullapalli, S., Mölders, N., 2008. Sensitivity studies using the Weather Research and Forecasting (WRF) model. REU-report, Fairbanks, p. 15.

Eder, B., Yu, S., 2006. A performance evaluation of the 2004 release of models-3 CMAQ. Atmospheric Environment, 40, pp. 4811-4824.

EPA, 2005. CMAQ model performance evaluation for 2001: Updated March 2005. U.S. Environmental Protection Agency, Research Triangle Park, NC 27711, p. 140.

EPA, 2007. Guidance on the use of models and other analyses for demonstrating attainment of air quality goals for ozone, $PM_{2.5}$, and regional haze. U.S. Environmental Protection Agency, Research Triangle Park, NC, p. 262.

Gaudet, B.J., Stauffer, D.R., 2010. Stable boundary layers representation in meteorological models in extremely cold wintertime conditions. Report to the Environmental Protection Agency, p. 60.

Hines, K.M., Bromwich, D.H., 2008. Development and testing of Polar Weather Research and Forecasting (WRF) model. Part I: Greenland ice sheet meteorology. Monthly Weather Review, 136, pp. 1971-1989.

Hines, K.M., Bromwich, D.H., Bai, L.-S., Barlage, M., Slater, A.G., 2011. Development and testing of Polar WRF. Part III: Arctic land. Journal of Climate, 24, pp. 26-48.

Leelasakultum, K., Mölders, N., 2012. Alaska adapted CMAQ model. Extended abstract to the 11th Annual CMAS Conference, Chapel Hill, NC, October 15-17, 2012, p. 6.

Mölders, N., 2008. Suitability of the Weather Research and Forecasting (WRF) model to predict the June 2005 fire weather for Interior Alaska. Weather and Forecasting, 23, pp. 953-973.

Mölders, N., 2010. Comparison of Canadian Forest Fire Danger Rating System and National Fire Danger Rating System fire indices derived from Weather Research and Forecasting (WRF) model data for the June 2005 Interior Alaska wildfires. Atmospheric Research, 95, pp. 290-306.

Mölders, N., Kramm, G., 2010. A case study on wintertime inversions in Interior Alaska with WRF. Atmospheric Research, 95, pp. 314-332.

Mölders, N., Leelasakultum, K., 2011. Fairbanks North Star Borough $PM_{2.5}$ nonattainment area CMAQ modeling: Final report phase I. Report, p. 62.

Mölders, N., Leelasakultum, K., 2012. Fairbanks North Star Borough $PM_{2.5}$ nonattainment area CMAQ modeling: Final report phase II. Report, p. 66.

Mölders, N., Luijting, H., Sassen, K., 2008. Use of atmospheric radiation measurement program data from Barrow, Alaska, for evaluation and development of snow albedo parameterizations. Meteorology and Atmospheric Physics, 99, pp. 199-219.

Mölders, N., Porter, S.E., Cahill, C.F., Grell, G.A., 2010. Influence of ship emissions on air quality and input of contaminants in southern Alaska National Parks and Wilderness Areas during the 2006 tourist season. Atmospheric Environment, 44, pp. 1400–1413.

Mölders, N., Tran, H.N.Q., Cahill, C.F., Leelasakultum, K., Tran, T.T., 2012. Assessment of WRF/Chem $PM_{2.5}$-forecasts using mobile and fixed location data from the Fairbanks, Alaska winter 2008/09 field campaign. Atmospheric Pollution Research, 3, pp. 180-191.

Mölders, N., Tran, H.N.Q., Leelasakultum, K., 2011a. Investigation of means for $PM_{2.5}$ mitigation through atmospheric modeling: Final report. Report, p. 75.

Mölders, N., Tran, H.N.Q., Quinn, P., Sassen, K., Shaw, G.E., Kramm, G., 2011b. Assessment of WRF/Chem to simulate sub-Arctic boundary layer characteristics during low solar irradiation using radiosonde, SODAR, and surface data. Atmospheric Pollution Research, 2, pp. 283-299.

PaiMazumder, D., Henderson, D., Mölders, N., 2012. Evaluation of WRF-forecasts over Siberia: Air mass formation, clouds and precipitation. The Open Atmospheric Science Journal, 6, pp. 93-110.

PaiMazumder, D., Mölders, N., 2009. Theoretical assessment of uncertainty in regional averages due to network density and design. Journal of Applied Meteorology and Climate, 48, pp. 1643-1666.

Tran, H.N.Q., Leelasakultum, K., Mölders, N., 2012. A tool for public $PM_{2.5}$-concentration advisory based on mobile measurements. Journal of Environmental Protection *(in press)*, p. 18.

Tran, H.N.Q., Mölders, N., 2011. Investigations on meteorological conditions for elevated $PM_{2.5}$ in Fairbanks, Alaska. Atmospheric Research, 99, pp. 39-49.

Tran, H.N.Q., Mölders, N., 2012a. Numerical investigations on the contribution of point source emissions to the $PM_{2.5}$-concentrations in Fairbanks, Alaska. Atmospheric Pollution Research, 3, pp. 199-210.

Tran, H.N.Q., Mölders, N., 2012b. Wood-burning device changeout: Modeling the impact on $PM_{2.5}$-concentrations in a remote subarctic urban nonattainment area. Advances in Meteorology, 2012, p. 12.

Wilson, A.B., Bromwich, D.H., Hines, K.M., 2011. Evaluation of Polar WRF forecasts on the Arctic System Reanalysis domain: Surface and upper air analysis. Journal of Geophysical Research, 116, p. 18. doi:10.1029/2010JD015013.

Yarker, M.B., PaiMazumder, D., Cahill, C.F., Dehn, J., Prakash, A., Mölders, N., 2010. Theoretical investigations on potential impacts of high-latitude volcanic emissions of heat, aerosols and water vapor and their interactions on clouds and precipitation. The Open Atmospheric Science Journal, 4, pp. 24-44.

Zhang, Y., Dubey, M.K., Olsen, S.C., Zheng, J., Zhang, R., 2009. Comparisons of WRF/Chem simulations in Mexico City with ground-based RAMA measurements during the 2006-MILAGRO. Atmospheric Chemistry and Physics, 9, pp. 3777-3798.

Zhao, Z., Chen, S.-H., Kleeman, M.J., Tyree, M., Cayan, D., 2011. The impact of climate change on air quality-related meteorological conditions in California. Part I: Present time simulation analysis. Journal Climate, 24, pp. 3344-3361.
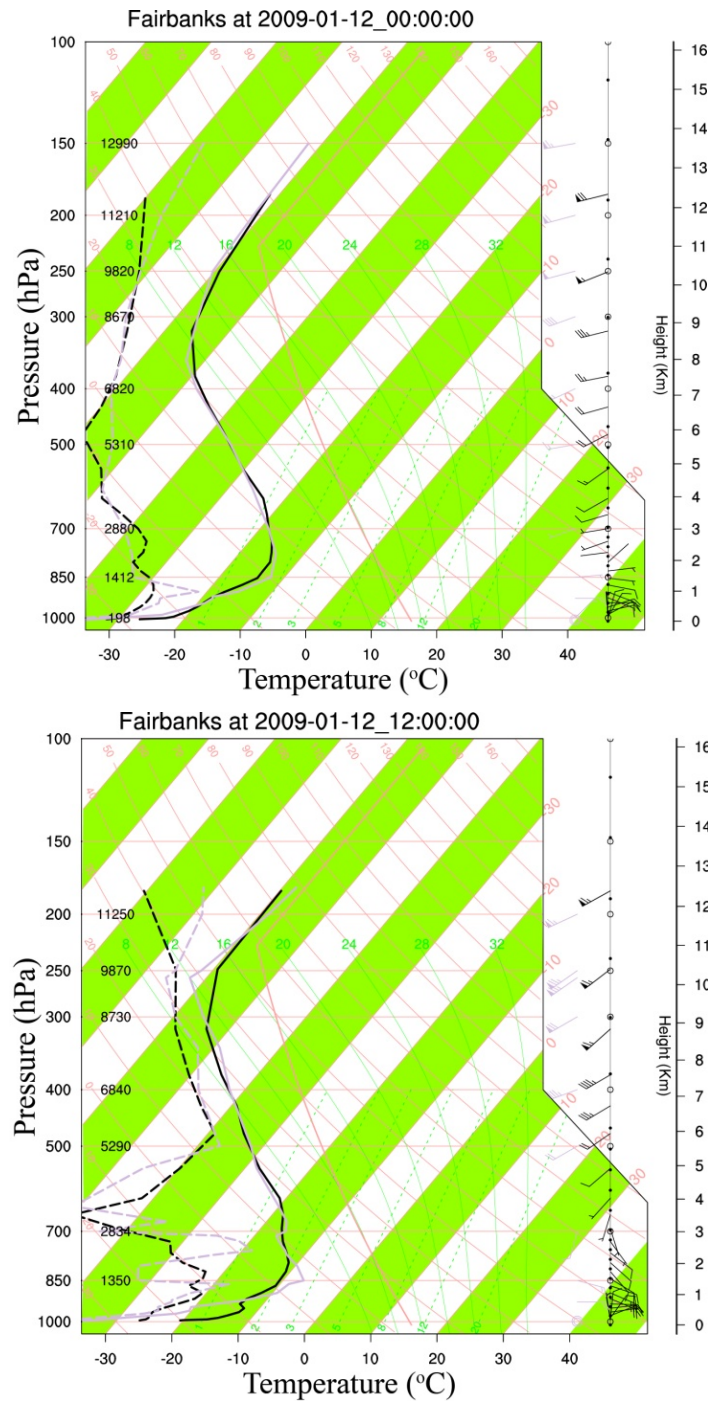
Figure 4.1 Vertical profiles of simulated (black) vs. observed (gray) air temperature (solid line), dew-point temperature (dash line) and wind fields (wind barb) as obtained on 01-12-2009 at 0000UTC and 1200UTC. The comparisons shown here represent typical performance, i.e., neither the best nor the worst.

Figure 4.2 Time-height cross-sections of horizontal wind-speed on 01-24-2009 (top) and 01-27-2009 (bottom) as derived from the SODAR (color) and WRF/Chem (solid lines). Time is UTC.

Figure 4.3 Relative biases of wind-speed and temperature-structure parameter (C_T^2) as determined using all SODAR data available during the 2008/09 simulations. Time is UTC.
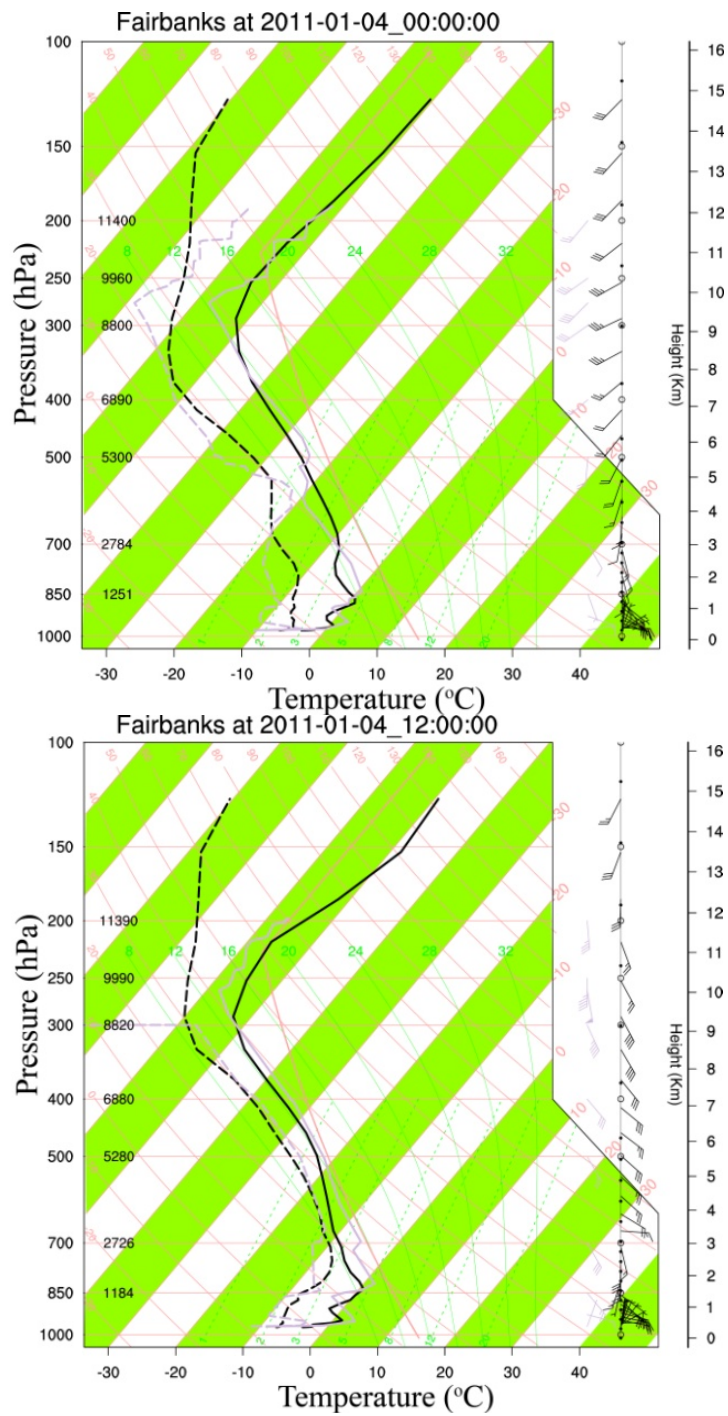
Figure 4.4 Like Figure 4.1, but for 01-04-2011 and 01-13-2011 at (top) 0000UTC and (bottom) 1200UTC. The comparisons shown here represent typical performance, i.e., neither the best nor the worst.
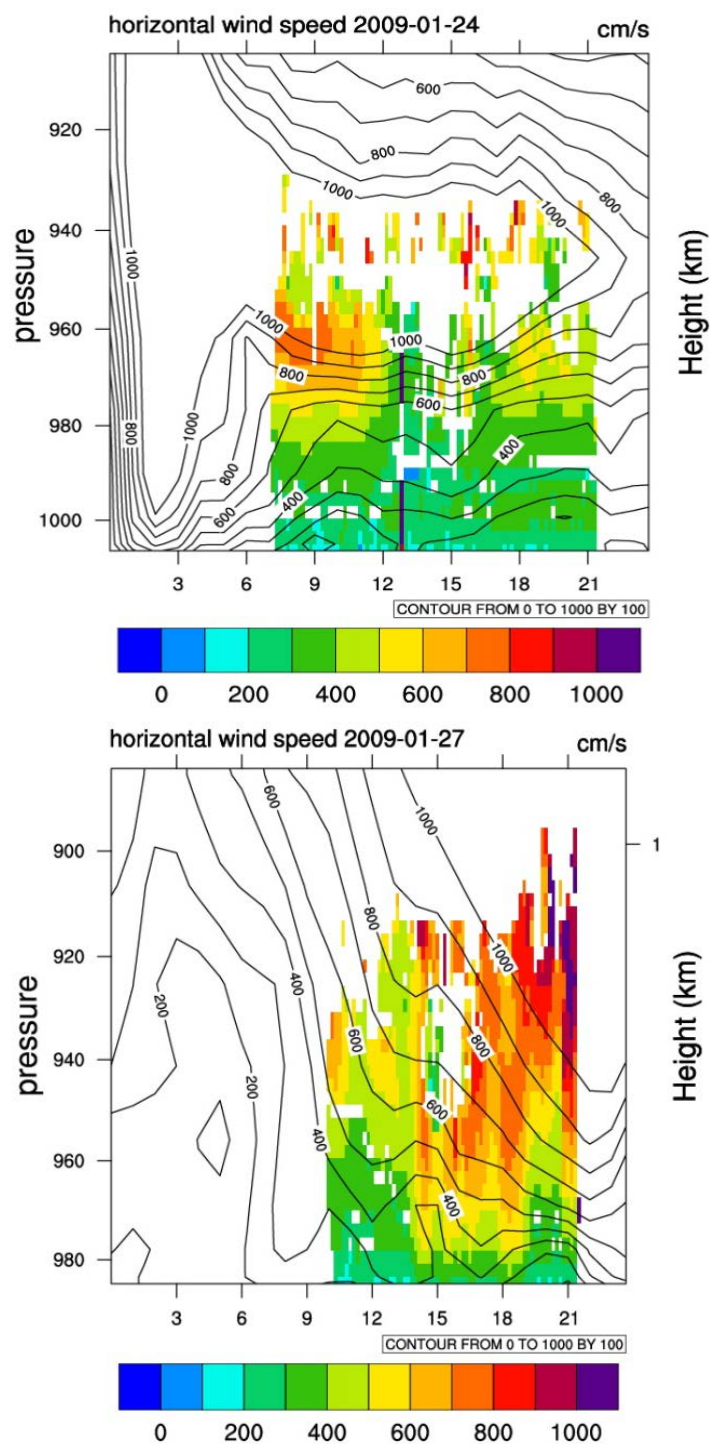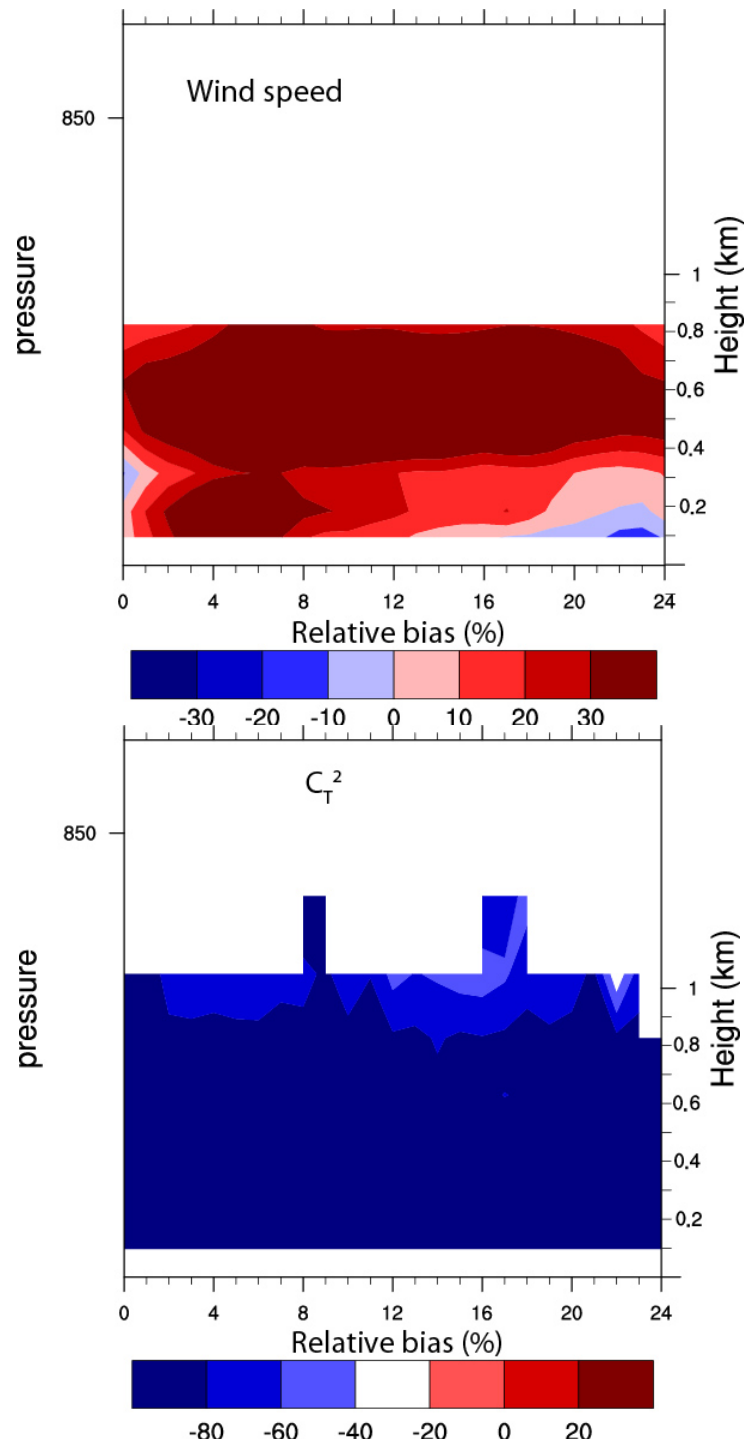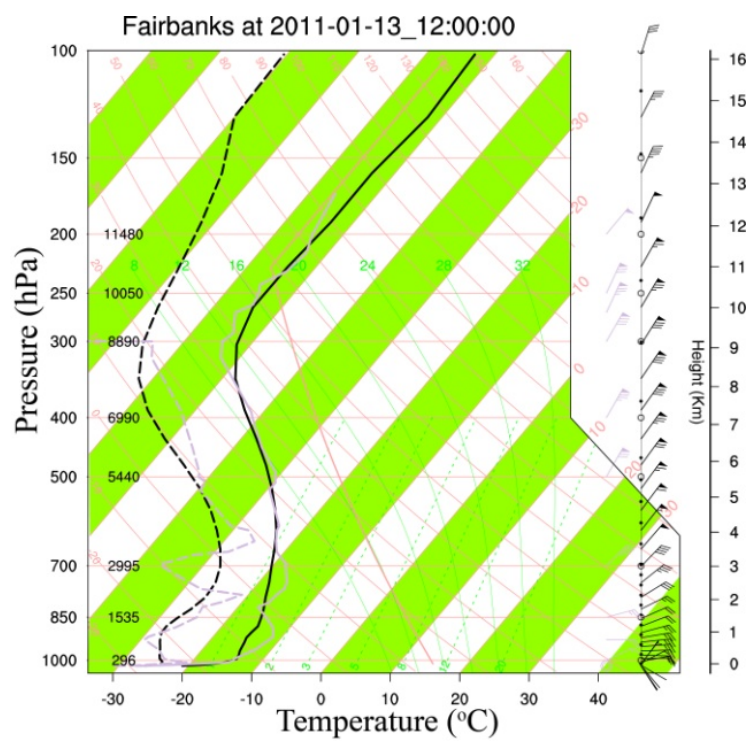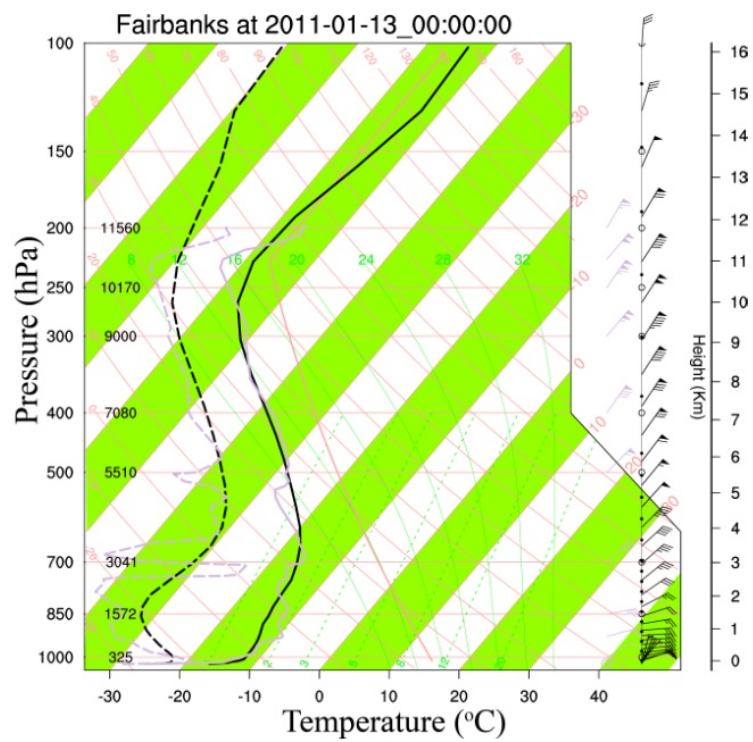
Figure 4.4 (cont.)
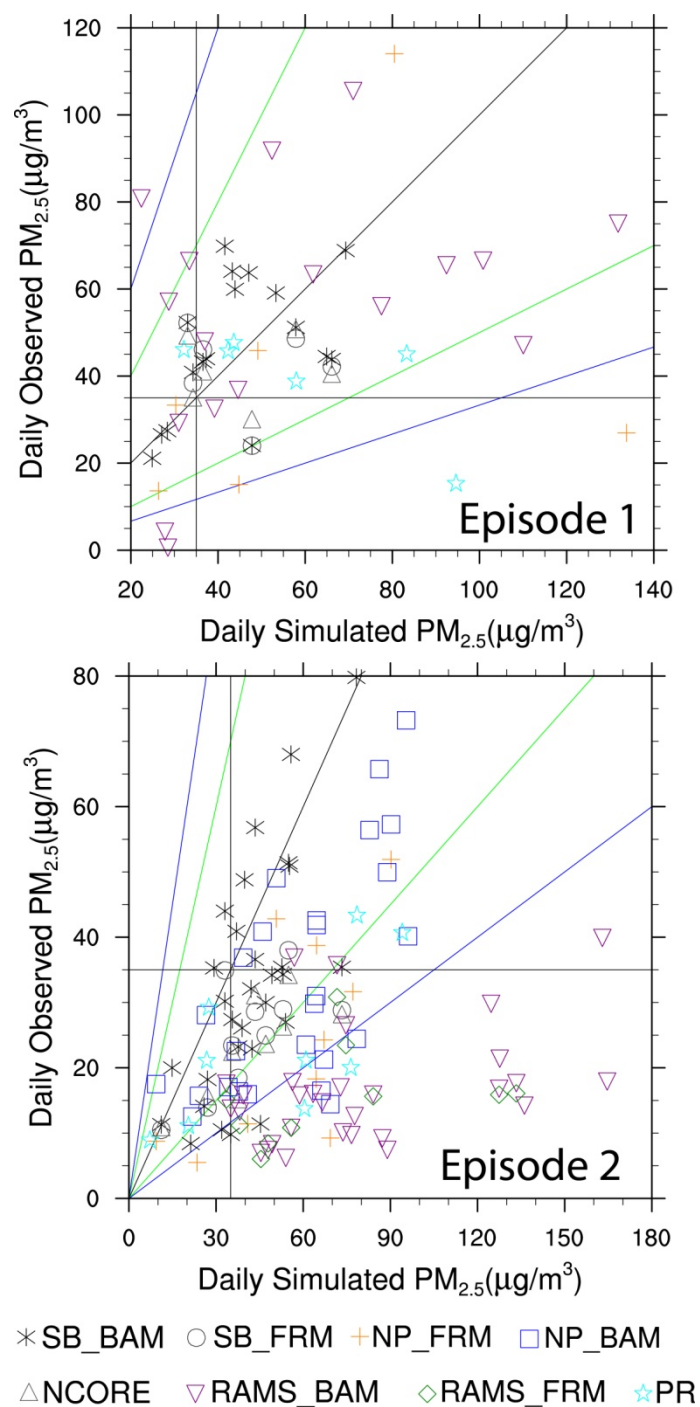
Figure 4.5 Scatter plots of simulated and observed 24h-average PM$_{2.5}$–concentrations at the monitoring sites for which data was available during the two episodes. The black indicates the 1:1-line; the green (blue) line indicates the factor of two (factor of three) agreement between pairs of simulated and observed PM$_{2.5}$-concentrations.
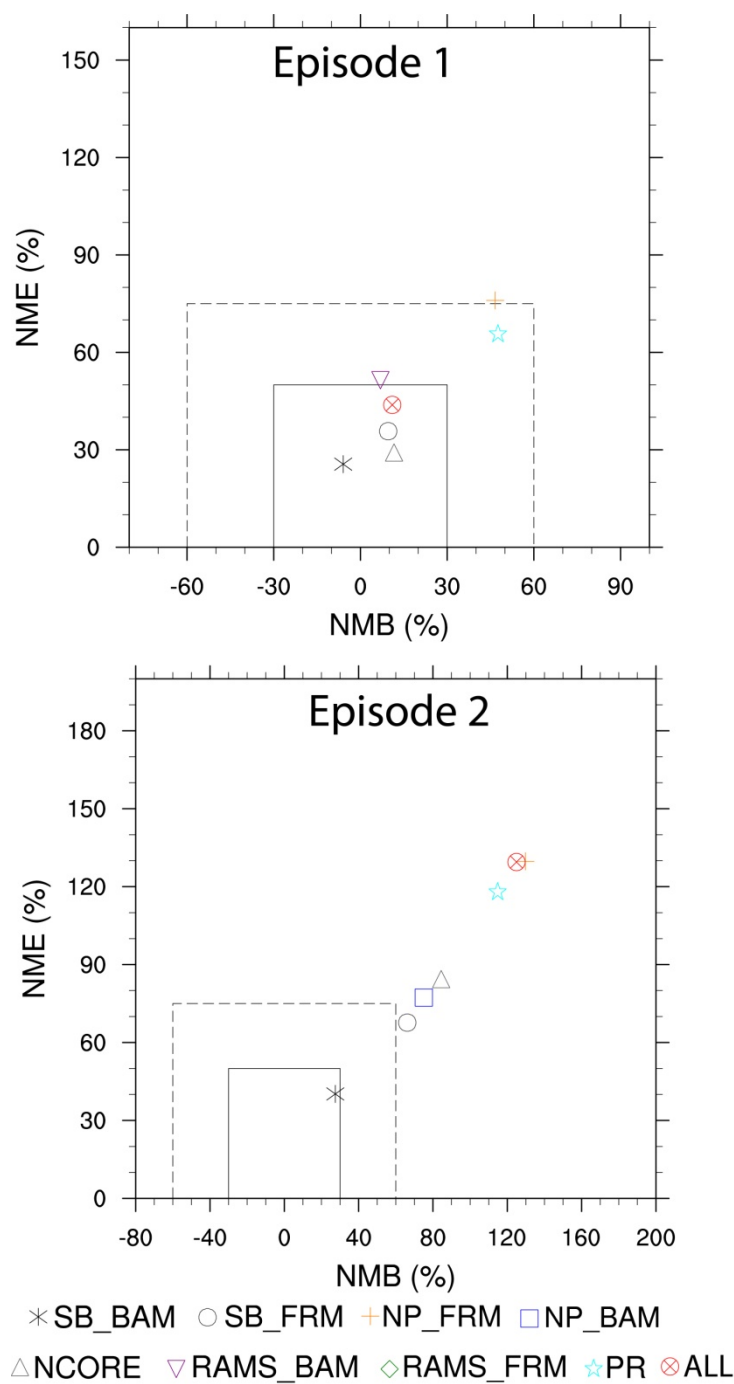
Figure 4.6 Soccer plots of episode-average simulated and observed 24h-average $PM_{2.5}$–concentrations at the monitoring sites for which data was available during the two episodes. The solid and dashed rectangles indicate the performance goal and criteria, respectively, that the model should achieve.
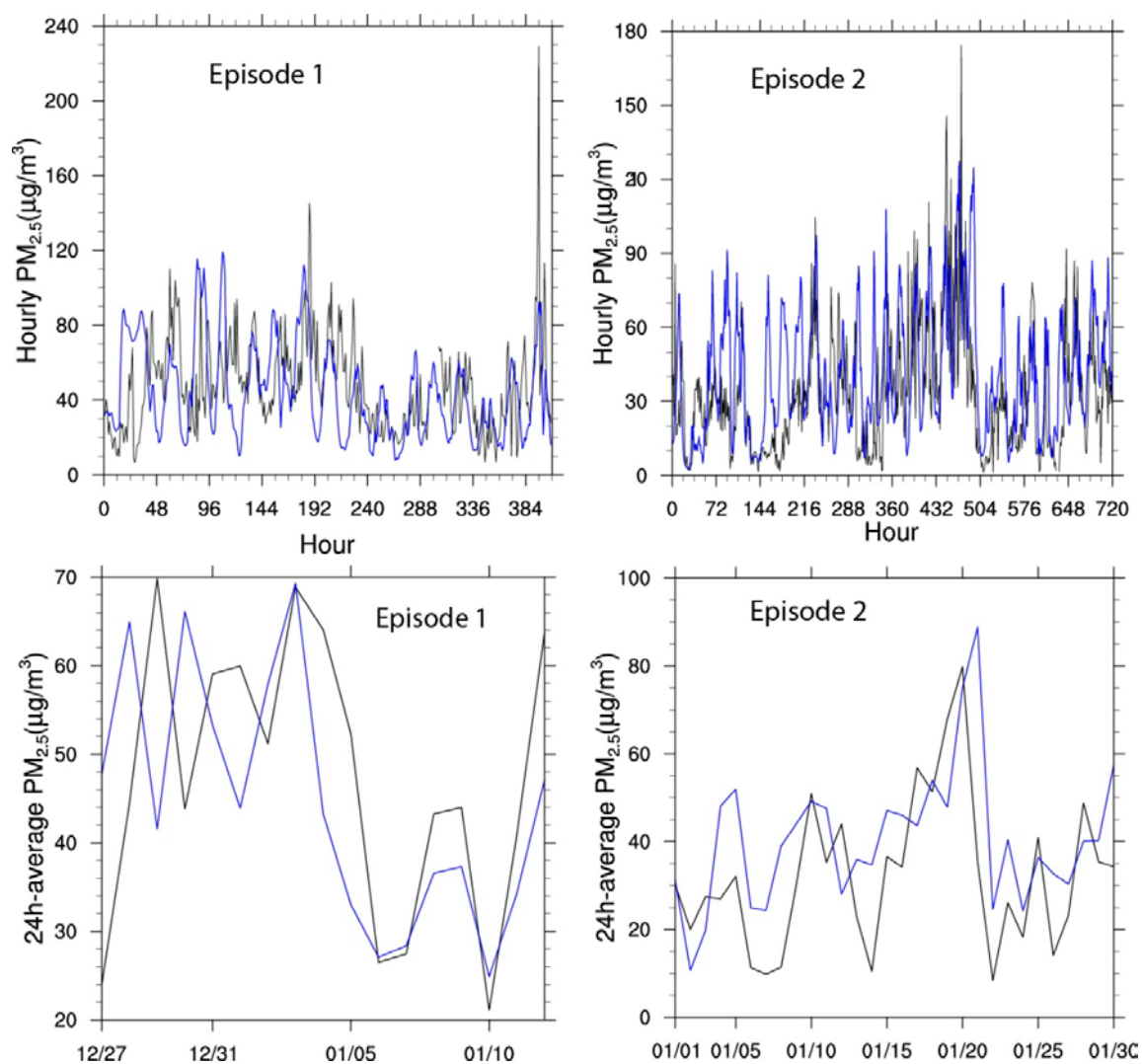
Figure 4.7 Temporal evolution of simulated and observed hourly and 24h-average PM$_{2.5}$-concentrations as obtained at the SB-site for episode 1 and 2. Dashed blue and solid black lines indicate simulated and observed quantities, respectively.
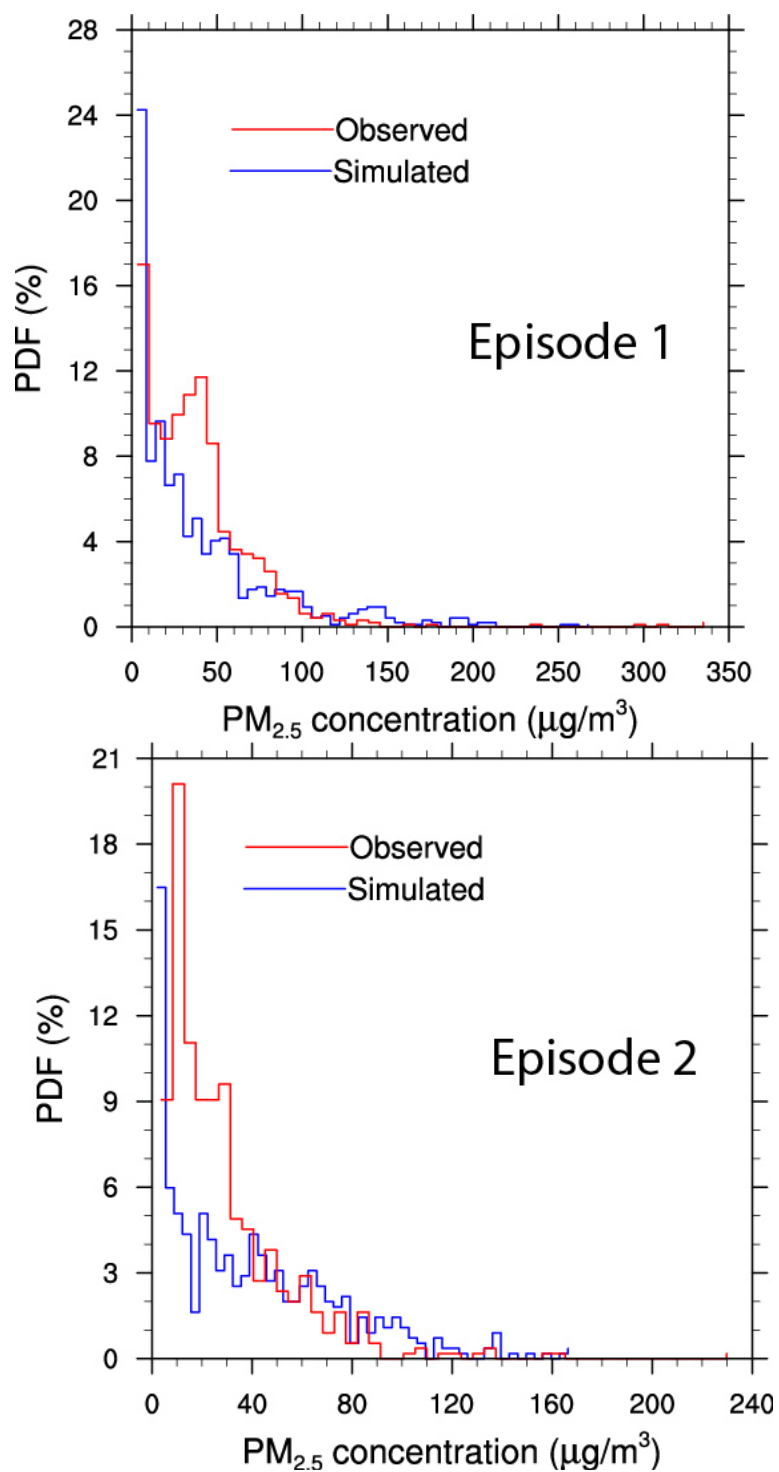
Figure 4.8 Population density distributions of simulated $PM_{2.5}$-concentrations vs. $PM_{2.5}$-concentrations measured by the sniffer for all sniffer drives during episode 1 and 2.
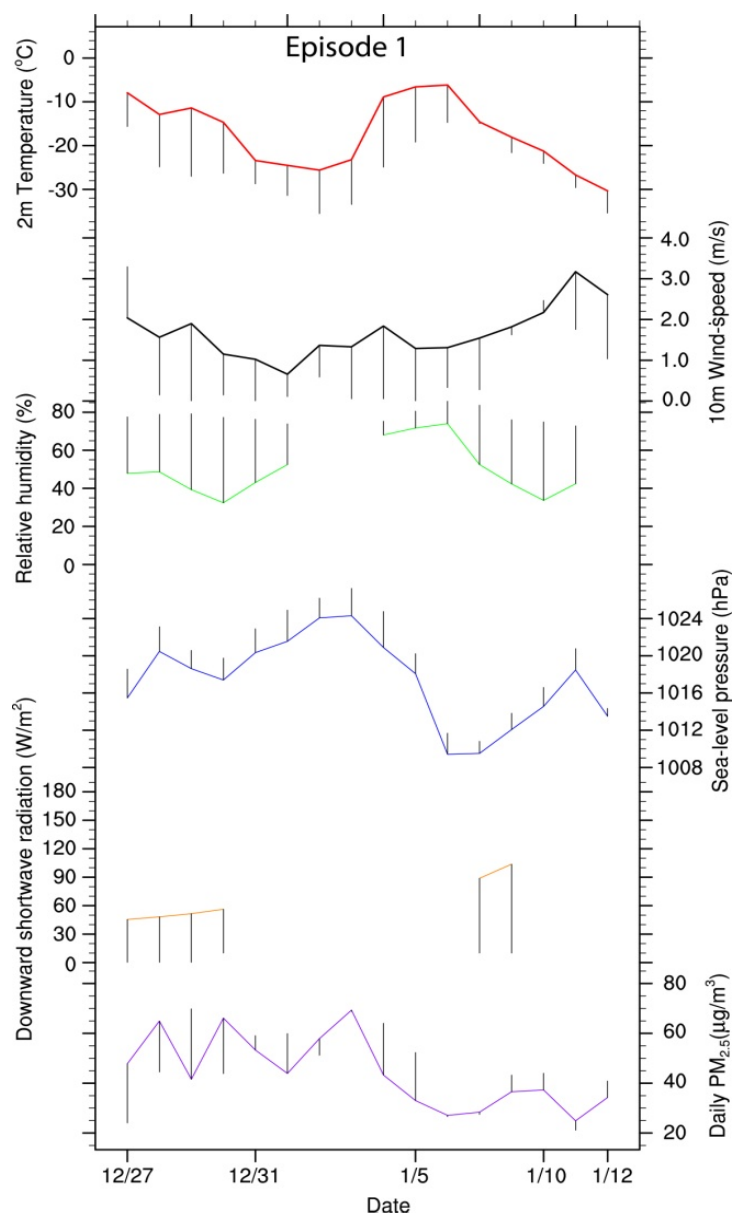
Figure 4.9 Temporal evolution of quantity and error of simulated 24h-average PM$_{2.5}$-concentrations at the SB-site (purple) as function of quantities and errors of the simulated 2m temperature (red), 10m wind-speed (black), relative humidity (green), sea-level pressure (blue), and daily accumulated downward shortwave radiation (orange) at the Fairbanks International Airport site for episode 1 and 2. The solid lines represent the simulated quantities; length of the vertical bars above (below) the solid lines represent the magnitude of negative (positive) biases (simulated minus observed quantities) in each day for the corresponding simulated quantities.
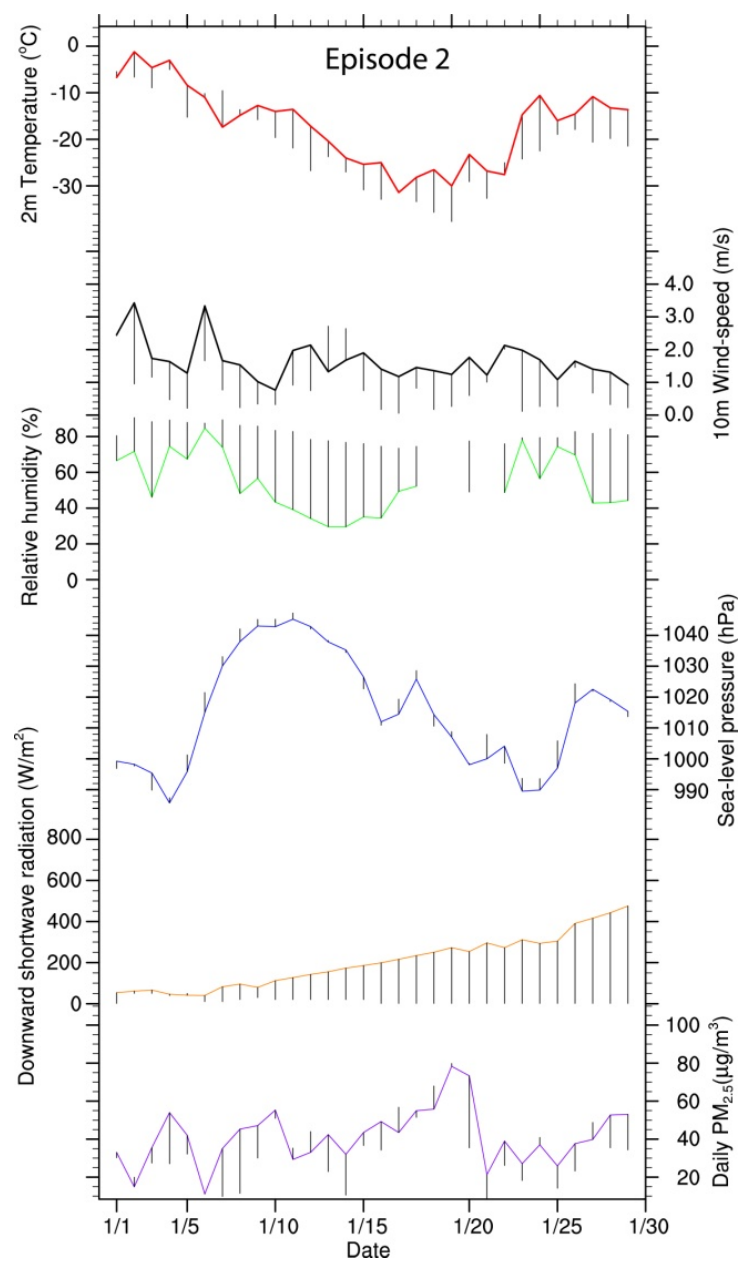
Figure 4.9 (cont.)

Chapter 5   Numerical investigations on the contribution of point-source emissions to the PM$_{2.5}$-concentrations in Fairbanks, Alaska[1]

Abstract

Simulations with and without consideration of emissions from point sources were performed with the Weather Research and Forecasting model with online chemistry (WRF/Chem) to examine the contribution of point-source emissions to the PM$_{2.5}$-concentrations at breathing level in Fairbanks, Alaska during winter. On days and at locations where PM$_{2.5}$-concentrations exceed the National Ambient Air Quality Standard of 35 µg m^{-3}, emissions from point sources account for 4% of the 24h-average PM$_{2.5}$-concentrations on average. The locations of highest concentrations were the same in both simulations. Point-source emissions induced only five additional exceedance days in the nonattainment area. The magnitude of the PM$_{2.5}$-concentrations depended on meteorological conditions (temperature, wind-speed, mixing height) and emissions. The radius of impact of point-source emissions on the PM$_{2.5}$-concentration at breathing level of about 10-12 km downwind results as a combination of low emission heights, low wind-speed and the presence of inversions.

5.1 Introduction

Various studies showed epidemiological relationships between particulate air pollution and mortality and/or morbidity due to cardiovascular and pulmonary diseases, and adverse health effects caused by particulate matter under both short–term and long–term exposure (Dominici et al., 2006; Pope and Dockery, 2006). In response to these findings, the U.S. Environmental Protection Agency has tightened the National Ambient Air Quality Standard (NAAQS) for the 24h–average concentration of particulate matter with diameters of 2.5 μm or less ($PM_{2.5}$) to 35 μg m^{-3} in 2006. Thus, days with $PM_{2.5}$-concentrations exceeding this NAAQS at the official monitoring site in a community are considered as exceedance days.

In Fairbanks, the $PM_{2.5}$-concentrations monitored at the official monitoring site have frequently exceeded the new NAAQS in the cold season, especially from November to February, in the previous years (Tran and Mölders, 2011). Thus, Fairbanks was assigned as a $PM_{2.5}$-nonattainment area. Achieving and remaining in compliance with the new NAAQS requires developing strategies for emission reduction. Such strategies require detailed knowledge about the emission sources, behavior and fate of $PM_{2.5}$. In the atmosphere, $PM_{2.5}$ may stem from direct emission (primary particles) or gas–to–particle conversion (secondary particles). The secondary particles comprise mainly ammonium sulfate and ammonium nitrate from reactions between ammonia and sulfuric and nitric acids.

Numerical modeling is a useful tool to assess the contribution of different emission sources to the pollutants' concentrations. Cheng et al. (2007), for instance,

applied the Mesoscale Model generation 5 (MM5) and the Advanced Regional Prediction System coupled with the Models–3/Community Multiscale Air Quality model to assess the emission source contributions to the PM_{10} concentrations in the Beijing area. They identified emissions from industries, construction sites and road dusts as the major contributors. A study conducted for the Pearl River Delta region, China with the MM5–STEM–2K1 modeling system identified power plants as the major contributors to sulfur dioxide (SO_2) concentrations, and traffic as the main contributor to the NO_x ($NO+NO_2$, nitric oxide and nitrogen dioxide), carbon monoxide (CO) and ozone (O_3) concentrations (Wang et al., 2005). Frost et al. (2006) applied the Weather Research and Forecasting model (Skamarock et al., 2008) with online chemistry (Grell et al., 2005) to investigate the impact of decreased power plant NO_x-emissions on O_3 concentrations. They found that O_3 concentrations generally decreased with the magnitude of the NO_x-emissions and depended on whether the NO_x-emission reduction yielded a plume that was in a high or low NO_x regime. Ying et al. (2009) used WRF/Chem to investigate the sensitivity of O_3 concentrations to the diurnal variations of surface emissions in Mexico City. They found that morning emissions of volatile organic compounds (VOCs) and NO_x both determined daytime O_3 concentrations, and that the O_3 production in Mexico City is VOC–limited. Chapman et al. (2009) performed WRF/Chem simulations to assess the impact of altered emissions from elevated point sources on aerosol radiative forcing and cloud–aerosol interactions. The comparison of their baseline simulation with a simulation in which all stack emissions were set to zero showed that aerosols from point sources reduce the daily mean downward shortwave radiation by 5 W m^{-2}.

Knowledge on air quality in high–latitude cities, especially in Alaska, is scarce (Mölders et al., 2011; Mölders et al., 2012). Fairbanks and its vicinity have four power plants and various other point sources. In Fairbanks during winter, surface–based and low–level inversion layers frequently exist (Mölders and Kramm, 2010; Tran and Mölders, 2011). These inversions may either enhance or reduce the impacts of point-source emissions on the $PM_{2.5}$-concentrations at breathing level depending on whether the point sources emit into, above or below the inversion layer.

The National Emission Inventory of 2005 (NEI2005) shows that in Fairbanks, point-source emissions contributed up to 15% of the total $PM_{2.5}$-emission. If point-source emissions were found to tremendously contribute to the 24h–average $PM_{2.5}$-concentrations in the Fairbanks nonattainment area, controlling these emissions would be an effective tool to reduce the number of exceedance days. Advanced pollution control techniques for point-sources are namely easier to implement and manage than controlling area emissions (e.g., residential heating, traffic).

The goal of this study is to examine the contribution of point-source emissions on the 24h–average $PM_{2.5}$-concentrations at breathing level in the Fairbanks nonattainment area. In doing so, we performed and analyzed WRF/Chem simulations with and without inclusion of point-source emissions.

5.2 Experimental Design

5.2.1 Simulations

We used the WRF/Chem with the modifications for Alaska and the physical and chemical schemes described and evaluated in Mölders et al. (2011). The WRF Single–Moment six–class cloud–microphysics scheme (Hong and Lim, 2006) served to simulate cloud and precipitation formation. This scheme considers mixed–phase processes and the coexistence of super–cooled water and ice. Cumulus convection was treated using the 3D–version of the cumulus–ensemble approach available in WRF (Skamarock et al., 2008). This scheme is a further development of Grell and Dévényi (2002) parameterization. Heat and moisture exchange at the land–atmosphere interface was treated with a modified version of the Rapid Update Cycle Land–Surface Model (Smirnova et al., 2000). Turbulent processes in the atmospheric boundary layer and surface layer were calculated in accord with Janjić (2002). Atmospheric radiative transfer was determined by the Rapid Radiative Transfer Model (Mlawer et al., 1997) for long–wave radiation and by the Goddard scheme (Chou and Suarez, 1994) for shortwave radiation. Gas–phase chemistry was represented by Stockwell et al. (1990) chemical mechanism which includes 21 inorganic and 42 organic species, and considers 156 chemical reactions. Dry deposition of trace gases was treated following Wesely (1989) with the modification by Mölders et al. (2011). The Secondary Organic Aerosol Model (Schell et al., 2001) and Modal Aerosol Dynamics Model for Europe (Ackermann et al., 1998) served to describe aerosol chemistry and physics including inorganic and

secondary organic aerosols, wet and dry removal of aerosols. Direct and indirect feedbacks of aerosols to radiation schemes were considered (Barnard et al., 2010).

The domain of interest for the analysis encompasses the Fairbanks nonattainment area and its adjacent land with 80×70 grid-cells and a 4 km increment (Figure 5.1). There are 28 stretched vertical layers from the surface to 100 hPa. The first layer is 8 m thick and referred to as breathing level, hereafter. The 1°×1° and 6h–resolution global final analyses data obtained from the National Centers for Environmental Prediction was downscaled to provide the meteorological initial and boundary conditions. The meteorology was initialized every five days. The initial conditions for the chemical fields stemmed from a simulation started with Alaska typical background concentrations 14 days prior to November 1, 2005.

Pleim (2011) showed that advection can strongly impact the pollutants' concentrations. Numerical studies (Tran et al., 2011) as well as observational studies with backwards trajectory modeling (Cahill, 2003; Mölders et al., 2012) showed that in Alaska, advection of pollutants marginally affects the background concentrations. In March, when advection is the largest it elevates the $PM_{2.5}$-concentrations at Denali Park from less than 0.5 μg m^{-3} to about 2 μg m^{-3}. Furthermore, the next closed city to the Fairbanks nonattainment area (Anchorage) is 578 km away on the other side of the Alaska Range of which the highest peak is 6193 m (Mt. McKinley). Therefore, and as the focus of this study is on the impact of point sources in the vicinity of Fairbanks on the $PM_{2.5}$-concentrations at breathing level in the nonattainment area, we assumed Alaska–typical background concentrations (e.g., acetylene, CH_3CHO, CH_3OOH, CO, ethane,

HCHO, HNO_3, H_2O_2, isoprene, NO_x, O_3, propene, propane, SO_2) as lateral boundary conditions.

Anthropogenic emissions from the NEI2005 for Alaska were allocated into space dependent on point-source facility coordinates, land use, road network, and population density data, and into time (month, day of the week, hour) according to source profiles' specific local activities. Plume rise calculations were based on Peckham et al. (2009) which considered stack height, exit velocity, exit temperature, ambient temperature and wind-speed. The assumed split for emitted $PM_{2.5}$ was 46% organic carbon (OC), 20% sulfate (SO_4), 5% nitrate (NO_3), 9% elemental carbon (EC) and 20% other fine primary $PM_{2.5}$ aerosols. Biogenic emissions were calculated online according to Simpson et al. (1995).

WRF/Chem simulations were analyzed for November 1, 2005 0000 Alaska Standard Time (AST) to March 1, 2006 0000 AST with (REF) and without (NPE) inclusion of emissions from point sources.

5.2.2 Analysis

The number, frequency and locations of grid-cells with $PM_{2.5}$-exceedances in REF and NPE were compared to assess the contributions of point sources to exceedances. We considered a grid-cell as experiencing an exceedance when its 24h-average $PM_{2.5}$-concentration was greater or equal to 35 μg m^{-3}. We counted a day as an exceedance day when it had an exceedance at least at one grid-cell in the nonattainment area.

In the following, the 24h–average $PM_{2.5}$-concentrations refer to AST. We tested the hypothesis that point-source emissions do not govern the 24h–average $PM_{2.5}$-concentrations at breathing level at the 95% confidence level according to a t–test. In addition, a false–ensemble analysis was applied to further examine whether the point-source emissions affect the $PM_{2.5}$-concentrations at breathing level. Moreover, we examined the various correlations for their significance. In the following, the word significant is only used when data passed the t–test at the 95% level of confidence.

The contributions of point-source emissions to the 24h–average and hourly $PM_{2.5}$-concentrations were assessed by the concentration differences (REF–NPE) called 24h–differences and 1h–differences hereafter, respectively. We assessed the effects of the meteorological conditions (wind-speed – v, temperature – T, mixing height – h_{mix}, sea-level pressure, relative humidity, downward shortwave radiation), point-source and non–point source emissions on the 24h–average $PM_{2.5}$-concentrations and 24h–differences at breathing level by their cross–correlations. We used a linear regression analysis to evaluate the importance of the meteorological conditions and emissions. We started this analysis with the "predictant" (simulated $PM_{2.5}$-concentrations) and all "predictors" (point-source emissions, non–point source emissions, simulated T, v, h_{mix}, relative humidity, sea-level pressure, downward shortwave radiation) of interest as variables. We repeated the analysis by alternatively removing one of the "predictors" from the analysis and evaluated the coefficient of determination (R^2). The largest decrease of R^2 in response to the removal of a "predictor" identifies that "predictor" as the one with highest impact on the $PM_{2.5}$-concentrations.

We investigated the impact radius of the point sources by analyzing the 24h–differences along the cross–sections through the downwind of each point source, and by analyzing the correlation between the point-source emissions at the emission level and the 1h–difference at each model layer below the emission level. Since wind-direction determines the pollutants' transport direction and the locations, the pollutants' impact, we only considered the 1h–differences in grid-cells located downwind of the grid-cell that holds the point source. We considered 16 wind-direction sectors of 22.5° each. We excluded hours with strong wind-direction shears (>90°) at any level of interest from the analysis. Such wind-direction shears occurred in less than 5% of the total hours. For each level and sector in steps of 4 km, the 1h–differences were interpolated and averaged over the area covered by that sector. These values were used to calculate the correlation with the point-source emissions for November to February. Distances with continuously significant correlation coefficients were considered as being impacted by the respective point source. The locations closest to the point source of interest with the highest significant correlation coefficient were considered as those that experience the highest impact from the point-source emissions. Note that other interpolation methods led to similar results.

We examined the correlation behavior of each point source under consideration of potential impacts by other point sources. Once correlation becomes non–significant and then significant again and/or increases in the downwind of point sources that are downwind of the point source of interest, we attributed this change to the impact of the

downwind point source(s) rather than the point source examined originally. Note that the diurnal activity allocation functions were the same for all point sources.

5.3 Results

5.3.1 Evaluation

Mölders et al. (2011) evaluated the reference simulation by data from Doppler sound detection and ranging, twice–daily radiosondes, 33 surface meteorological and four aerosol sites. They found average biases over November to February and all meteorological sites of 1.6 K, 1.8 K, 1.85 m s^{-1}, –5°, and 1.2 hPa for temperature, dew–point temperature, wind-speed, wind-direction, and sea-level pressure, respectively. The Doppler sound detection and ranging data indicated under/over estimation of wind-speed in the upper (lower) atmospheric boundary layer and good performance in capturing the presence of low level jets.

Mölders et al. (2011) evaluated WRF/Chem's performance in simulating PM$_{2.5}$ by data from the State Office Building site in downtown Fairbanks and a remote site in Denali Park. WRF/Chem simulated PM$_{2.5}$ at the urban site better than at the remote site. It captured the temporal evolution of 24h–average PM$_{2.5}$ at the Fairbanks site broadly. Here the overall bias and correlation of hourly (24h–average) observed and simulated PM$_{2.5}$ were 4.9 (4.0) μg m^{-3} and 0.31 (0.59; all statistical significant), respectively. Over November to February, 41% (50%) of the simulated and observed PM$_{2.5}$ (SO$_4$ aerosol) concentrations agreed within a factor of two and the fractional bias was less than 30% on average over the two sites. Note that no other PM$_{2.5}$ data was available for our episode.

Obviously, some bias exists in the $PM_{2.5}$-concentrations (Mölders et al., 2011). Investigations on the sensitivity of $PM_{2.5}$-concentrations to biases in temperature showed marginal impact of temperature errors on simulated $PM_{2.5}$-concentrations except for temperatures close to the temperature threshold for particle formation (Mölders et al., 2012). Since REF and NPE used the same model setup, and the radiation aerosol feedback hardly impacted the meteorological quantities most of the time, biases in $PM_{2.5}$-concentrations due to errors in simulated meteorological quantities can be assumed to be similar in REF and NPE. Bias due to errors in biogenic emissions would be similar too as both simulations calculated biogenic emissions inline depending on the meteorological conditions. Both simulations also used the same emissions for the non–point source sector. Thus, we can assume that REF and NPE were affected the same by errors from these sources. This means that biases in $PM_{2.5}$-concentrations due to errors in simulated meteorological conditions, biogenic and area emissions cancel each other out when differences are examined. Point-source emissions are the best regulated, controlled and verified emissions, for which we can assume that biases in $PM_{2.5}$-concentrations due to errors in point-source emissions are marginal.

5.3.2 Point-source emissions

In the domain of interest, 27 stacks emit into the levels between the second (8–16 m) and the seventh model layer (343–478 m). Among these, some stacks belong to the same facility or stacks from different facilities exist in the same grid-cell. In WRF/Chem, like other photochemical models, all stacks located within the same grid-cell are lumped,

but emit into the layers into which the individual stacks would emit. Due to the lumping, only the joint impacts of point sources within a grid column can be investigated. These columns are denoted PS1 to PS9, hereafter (Figure 5.1). Three point source holding columns (PS4, PS5, and PS6) are located in the nonattainment area. PS6 has the highest $PM_{2.5}$-emission rate (3 g m^{-2} h^{-1}), followed by PS7 (1.3 g m^{-2} h^{-1}). Within the nonattainment area, PS4 has the second highest, but 19 times lower $PM_{2.5}$-emissions than PS6. PS4 has the highest emissions of SO_2 (0.6 g m^{-2} h^{-1}) and NO_x (0.5 g m^{-2} h^{-1}), which are important precursors for $PM_{2.5}$ formation via gas–to–particle conversion, followed by PS6 with 0.24 g m^{-2} h^{-1} SO_2 and 0.18 g m^{-2} h^{-1} NO_x-emissions.

On average over November to February and the domain, the $PM_{2.5}$, SO_2, NO_x and VOC-emissions from point sources made up 15%, 42%, 42% and 0.6% of the total emissions in the domain, respectively. Within the nonattainment area, point-source emissions made up 15%, 36%, 35% and 0.4% of the total $PM_{2.5}$, SO_2, NO_x and VOC-emissions, respectively. During November to February only non–point sources emitted ammonia and their emission rate was low (0.17 kg km^{-2} h^{-1}).

5.3.3 General features

The phase and amplitude of the diurnal cycle of simulated $PM_{2.5}$-concentrations varied strongly among days. In general, the $PM_{2.5}$-concentrations showed a distinct peak around 0300 AST and a stronger, broader peak around 1300 AST. In general, high 24h–average $PM_{2.5}$-concentrations occurred when $PM_{2.5}$-emissions were relatively strong (>0.2 g m^{-2} h^{-1}) and concurrently the wind was calm (<0.5 m s^{-1}), air temperatures were

low (below –20°C) and mixing heights were shallow (<20 m). In the nonattainment area, calm wind occurred 20% of the time and concentrations >35 µg m^{-3} occurred on 46% of the calm wind events. Out of the 24h–average PM$_{2.5}$-concentrations >35 µg m^{-3}, 62% (81%) occurred when air temperatures (mixing heights) were low (shallow). Shallow mixing heights (low temperatures) existed 33% (40%) of the time in November to February. Such shallow mixing heights typically occurred when WRF/Chem simulated surface–based inversions and calm wind over the nonattainment area.

At breathing level and between 100 and 200 m above ground, three and four distinct circulation patterns, respectively, existed that frequently coincided with exceedance days. In the nonattainment area, exceedances occurred on days with calm winds from various directions when the air remained in town (Figure 5.2a). Exceedances also occurred under calm wind conditions when the Fairbanks' air drained toward southwest or air moved into Fairbanks from the southeast (Figure 5.2b). In the latter case, polluted air advected from the community of North Pole (22 km southeast of Fairbanks in the nonattainment area) may contribute to the exceedances. Simulated exceedances were often associated with the following airflows between 100 and 200 m above ground: (1) air moved slowly above town down the Tanana Valley to the southwest, (2) air slowly moved over Fairbanks from the southeast and down the valley to the southwest (Figure 5.2c), (3) air moved southeast up the valley, or (4) air drained to both sides of Fairbanks (Figure 5.2d). For November to February, WRF/Chem simulated 12 exceedances when air masses that passed over Fairbanks and took up pollutants (Figure 5.2e), moved back into Fairbanks thereby advecting aged polluted air (Figure 5.2f). The simulations showed

that winds from north or northeast with v >2.5 m s^{-1} typically advected clean air into Fairbanks that diluted the pollutants' concentrations efficiently and/or moved the polluted air out of town to the west or southwest.

5.3.4 Contribution of point-source emissions

In November to February, the highest 24h–average PM$_{2.5}$-concentrations in REF and NPE anywhere in the domain differed 1 µg m^{-3} on average and barely exceeded 3 µg m^{-3} locally (Figure 5.3). On 65 out of the 120 days, the highest 24h–average PM$_{2.5}$-concentration in REF occurred in the grid-cell holding the official monitoring site. On 38 and 17 days, highest 24h–average PM$_{2.5}$-concentrations occurred in the grid-cell adjacent to the south and west of the monitoring site, respectively. In NPE, the highest 24h–average PM$_{2.5}$-concentrations occurred at the same locations and times as in REF except on 7 days. On these 7 days, however, they occurred still within the three grid-cells mentioned above.

The 98th, 90th, 75th, 50th, and 25th percentile of the 24h–average PM$_{2.5}$-concentrations in REF (NPE) were 35.7 (33.9), 24.0 (22.5), 17.1 (15.9), 10.8 (10.3), and 7.0 (6.8) µg m^{-3}, respectively. When and where the ten highest and ten lowest 24h–average PM$_{2.5}$-concentrations occurred in the nonattainment area during November to February hardly differed between REF and NPE. These findings suggest that point sources marginally affected the spatial distribution of 24h–average PM$_{2.5}$-concentrations in the nonattainment area on polluted (25 µg m^{-3} $\leq$ PM$_{2.5}$ < 35 µg m^{-3}) and hardly affected them on clean (PM$_{2.5}$ <25 µg m^{-3}) days.

Topography and wind-direction influence the distribution of the mean 24h–difference and its significance. During November to February, winds from east and northeast dominated. Small but statistically significant 24h–differences occurred over a relatively large area including the nonattainment area and its downwind (Figure 5.4). Almost all notable 24h–differences existed for grid-cells holding point sources and their adjacent grid-cells. On average over the domain, the nonattainment area and at the grid-cell holding the official monitoring site, the 24h–differences were 0.04, 0.8 and 1.2 μg m^{-3}, respectively which corresponds to 3.8, 1.2 and 3.9% reduction, respectively. In the nonattainment area, the highest 24h–difference was 18 μg m^{-3} and occurred in the grid-cell holding PS6 on January 27 2006 (Figure 5.3), while the highest 24h–difference averaged over the nonattainment area was 4.5 μg m^{-3} on November 13, 2005. In 47% of the time, the highest 24h–differences occurred at PS6 with 7 μg m^{-3} on average, and 5% of the time at other grid-cells in the nonattainment area with 2.3 μg m^{-3} on average. During 48% of the time, most of the highest 24h–differences occurred in the grid-cells holding PS1, PS2, PS3 and PS8 with about 2.5 μg m^{-3} on average. Generally, the highest 24h–difference occurred outside the nonattainment area on clean days when the 24h–average PM$_{2.5}$-concentrations in the nonattainment area were less than 25 μg m^{-3} and vice versa. The highest and second highest 24h–differences frequently occurred at PS6 and its adjacent grid-cells indicating the importance of PS6 for the 24h–average PM$_{2.5}$-concentrations in the nonattainment area.

Despite the t–test indicated statistically significant concentration differences, a possibility remains that the difference is not due to contributions of point sources, but

rather due to some variable random effects between the two simulations (e.g., truncation errors, model sensitiveness). This possibility is most likely for small (<1 μg m^{-3}) differences (Werth and Avissar, 2002) like they occurred in this study. To further assess whether the differences are due to the contribution of point sources, we adopted a false–ensemble analysis method that was developed and applied successfully in the analysis of climate–model scenarios (Werth and Avissar, 2002). This method bases on the concept that two simulations with no difference in the mean emissions and small random effects differ hardly in their mean concentrations.

For each month, we calculated the difference of the 24h–average PM$_{2.5}$-concentrations REF–NPE called the "true" difference hereafter. We created a set of "false REF" and "false NPE" ensembles by randomly replacing results of simulation days of REF (NPE) with the results of the corresponding simulation days of NPE (REF). The replacement was completed when the number of NPE (REF) simulation days made up 50% of the total days of the "false REF" ("false NPE") ensemble. Since the emission rates differ among days, the generated false ensembles negligibly and non–significant differ in their monthly total emission depending on for which days the data were exchanged. In principle, n!/[(n/2)!]×2 false ensembles can be generated from n simulation days in the described way, i.e. in our case 1019 false ensembles for one month. We generated 450 false ensembles for each month to obtain a sufficiently large statistical basis. For each set of "false REF" and "false NPE" ensembles, the difference of the 24h–average PM$_{2.5}$-concentration was calculated. Finally, we ranked the true over the 450 "false" concentration differences. This procedure was applied for each grid-cell.

The results of the false–ensemble analysis indicated that for most grid-cells the true differences fall within the top 5% of all differences although the distribution of these grid-cells differs among months (Figure 5.5). At grid-cells inside the nonattainment area, the true concentration differences consistently fell in the top 5% throughout November to February except at 1, 5 and 1 grid-cells in December, January and February, respectively. Thus, the false–ensemble analysis supports that the point sources contributed to the $PM_{2.5}$-concentrations at breathing level, although the contribution was small on average.

During November to February, the NAAQS was exceeded on 10 (7), 6 (5), 22 (21) and 1(1) days in REF (NPE) in November, December, January and February, respectively. The five exceedance days avoided in NPE had only slightly lower 24h–average $PM_{2.5}$-concentrations (up to 5 µg m^{-3}) than REF. Out of the 104 (80) exceedances that were simulated anywhere in the nonattainment area at any time during November to February by REF (NPE), 37 (34), 29 (20) and 20 (18) exceedances occurred at the grid-cell holding the monitoring site, and in the grid-cells adjacent to its west and south, respectively (Figure 5.6). In REF, 3 and 5 exceedances occurred for the grid-cell holding PS6 and the grid-cells adjacent to it, respectively, and none of them occurred at these locations in NPE. The fractional difference of 24h–average $PM_{2.5}$-concentrations [(REF–NPE)/REF] indicated that on exceedances days, point sources contributed up to 42% to the total 24h–average $PM_{2.5}$-concentrations in the grid-cell holding PS6 and up to 22% in the grid-cells adjacent to it. At other locations, the fractional differences indicated that point sources accounted for 4% of 24h–average $PM_{2.5}$-concentrations on average and barely exceeded 10% on exceedance days. These findings mean that except for PS6 and

its adjacent grid-cells, non–point source emissions led already to high $PM_{2.5}$-concentrations and the point sources just added the small amount needed to exceed the NAAQS.

The speciation of $PM_{2.5}$ was almost identical in REF and NPE. For example, at the grid-cell holding the monitoring site, the overall $PM_{2.5}$ speciation was 20.4, 2.2, 2.6, 9.0, 45.8, 19.9% SO_4, NO_3, NH4, EC, OC and other fine particles, respectively, in REF, while it was 20.5, 2.1, 2.6, 9, 45.9 and 19.9% in NPE. Similar minor changes in $PM_{2.5}$ speciation were also found for the grid-cell holding PS6. Recall that the emitted $PM_{2.5}$ split was 20, 5, 9, 46 and 20% for SO_4, NO_3, EC, OC and other fine particles, respectively. These values imply that secondary aerosol formation was low during November to February. This fact contributed to the small impact of point-source emissions on the $PM_{2.5}$-concentrations at breathing level despite point sources made up 35% of the total SO_2 and NO_x-emissions.

At breathing level the 24h–average $PM_{2.5}$-concentrations averaged over the nonattainment area obtained by REF correlated significantly with v, T, h_{mix} and downward shortwave radiation (–0.689, –0.537, –0.671, –0.220), but non–significantly with relative humidity and sea-level pressure. The 24h–average $PM_{2.5}$-concentrations in the nonattainment area correlated stronger and significantly with the non–point source emissions (0.331) than with the point-source emissions (0.231). The linear regression analysis showed that non–point source emissions were the most important factors governing the 24h–average $PM_{2.5}$-concentrations, followed by T, v, h_{mix}, point-source emissions and downward shortwave radiation. These findings also support that non–point

source emissions mainly contributed to the 24h–average $PM_{2.5}$-concentrations in the nonattainment area.

At the grid-cell holding PS6, the 24h–average $PM_{2.5}$-concentrations obtained by REF showed similar correlation with the emissions from non–point sources (0.281) and point sources (0.275). At PS6, the correlations of the 24h–average $PM_{2.5}$-concentrations with T, v or h_{mix} were –0.608, –0.628 and –0.592, respectively. The linear regression analysis showed that at PS6, temperature was the most important factor, followed by non–point source emissions, point-source emissions, and wind. Mixing height was least important for the 24h–average $PM_{2.5}$-concentrations. However, h_{mix} strongly correlated with v (0.874) and T (0.507). At PS4, the 24h–average $PM_{2.5}$-concentrations correlated with the non–point source emissions (0.337) but not with the point-source emissions. The linear regression analysis indicated that at PS4, wind followed by non–point source emissions and temperature were the most important factors for the 24h–average $PM_{2.5}$-concentrations. Similar behavior like for PS4 was found for PS1, PS2, PS3 and PS5 that all are outside, but not far from the nonattainment area. At PS7, PS8 and PS9, the 24h–average $PM_{2.5}$-concentrations correlated significantly neither with the point source nor with the non–point source emissions. Instead, wind-speed, temperature, mixing height and sea-level pressure mainly governed the 24h–average $PM_{2.5}$-concentrations. These point sources are located far from the nonattainment area (PS8, PS9) or in mountainous terrain (PS7) upwind of the nonattainment area (PS7, PS8). In their vicinity, winds were relatively strong (on average v >6 m s^{-1}) and there were no non–point source emissions or only low point-source emissions (e.g., $PM_{2.5}$ <0.08 g m^{-2} h^{-1} at PS8 and PS9). These

conditions allowed strong dilution and marginal advection of pollutants from the nonattainment area. Therefore, at PS7, PS8 and PS9, the 24h–average $PM_{2.5}$-concentrations were more sensitive to meteorological than to emission conditions. Generally, at grid-cells holding point sources, the 24h–average $PM_{2.5}$-concentrations were typically stronger related to the meteorological conditions and non–point source emissions than to the point-source emissions.

5.3.5 Radius of point-source impacts

The impact radius differs among point sources and depends on emission height, wind-speed and inversion conditions. On average over November to February, the 24h–difference along the cross–sections C1 to C8 (see Figure 5.4 for location) centered over point sources were highest in the grid-cells holding the point sources and at the level into which they emitted the strongest (Figure 5.7). At breathing level, a general feature was that point sources contributed most to the $PM_{2.5}$-concentrations in the grid-cell they are located.

Point sources exist at various places. Hence, point sources in their downwind induced interfering effects with the impact of the point source of interest (e.g., C3, C4, C7, C8). For example, in C5 that is centered on PS7, the second maximum located 20 km downwind of PS7 at about 150 m above ground was caused by emissions from PS6. The $PM_{2.5}$-concentration contributed by the point source of interest was highest right in the grid column it emitted into at the emission level. For regulatory questions, however, the concentration at breathing level is decisive. Therefore, we were interested in the impact

of the point-source emissions on the concentrations at breathing level. Thus, in the following the term "highest impact" refers to the location that has the highest concentration at the breathing level.

Emissions from PS6 (cross–sections C1 and C2 in Figures 5.4 and 5.7) had the strongest impact on the $PM_{2.5}$-concentrations in the grid-cell where PS6 is located. This impact quickly decreased in its downwind. Cross–sections C7 and C8 document a similar behavior for PS2 like for PS6 (Figure 5.7). As shown in C5 and C6, at PS7, the polluted air was strongly diluted before reaching the breathing level because in the mountainous terrain of PS7, the wind was relative strong (on average v $>$6 m s^{-1}). Consequently, PS7 rarely contributed to the breathing level $PM_{2.5}$-concentration in the nonattainment area.

At a point source of interest, due to overlapping effects of all emitting levels, correlation patterns of 1h–differences with point-source emissions at each emitting level were quite similar. Therefore, the impact of individual emission levels on the 1h–differences cannot be clearly distinguished. Generally, the correlation patterns of the 1h–differences with the point-source emissions (Figure 5.8) agreed with the above findings that point sources contributed most to the $PM_{2.5}$-concentration at breathing in or very close to the grid-cell holding it. Highest correlations occurred for PS6 with similar magnitude for all emission levels (~0.26) indicating strong downward mixing of $PM_{2.5}$ from the emission levels to the breathing level. Based on our point source impact radius definition, we conclude that the impact radius of PS6 was about 12 km, and the highest impacted location is the grid-cells holding PS6.

Lowest correlations between the 1h–differences and point-source emissions occurred at PS7 (Figure 5.8), PS8 (up to 0.052, significant) and PS9 (up to 0.088, significant). At these point sources, correlations at breathing level were lower than at upper levels. This finding indicates that the polluted air when it reached the breathing level had much lower $PM_{2.5}$-concentration than at the emission level. The impact radius of PS7 was about 10 km. The impact radius of PS8 was about 4 km due to its low height of emission levels (8–16 m) and the weak $PM_{2.5}$-emission rate (0.08 g m^{-2} h^{-1}). PS9 had an impact radius >40 km as it emitted into levels up to 219–343 m. PS7, PS8 and PS9 exerted their highest impact at the grid-cell holding the respective point sources.

At PS1, PS4 and PS5, interference effects by other point sources close to the point source of interest (Figure 5.8) made it difficult to determine clearly the impact radius. Typically all point sources had an impact radius of about 10 to 12 km, on average over November to February, but the radius differed with the wind-speed at the emission level. Correlation patterns are quite similar for all point sources. Thus, we exemplarily discuss the behavior for PS6. Over November to February, simulated wind-speeds at PS6 were ≤2 m s^{-1}, between 2 and 5 m s^{-1} and >5 m s^{-1} for 38%, 30% and 32% of the time, respectively.

Correlation patterns obtained for wind-speeds ≤2 m s^{-1} indicated a narrow impact radius (<8 km) and correlations were about 0.28 (significant) at all levels. This behavior indicates that $PM_{2.5}$ was distributed almost uniformly from the emission level to the breathing level under this wind condition (Figure 5.9). For wind-speeds between 2 and 5 m s^{-1}, correlations were higher at the emission level (113–219 m) than at subsequently

lower levels. This fact indicates dilution of the polluted air that led to lower $PM_{2.5}$-concentrations at the breathing level than at the emission level. In this wind-speed range, the radius of impact was 8–10 km. Like for wind-speeds <2 m s^{-1}, the correlation peaks indicated the highest impact of the point-source emissions on the 24h–average $PM_{2.5}$-concentrations at breathing level for the grid-cell holding PS6. For wind-speeds >5 m s^{-1}, the point-source emissions and 24h–average $PM_{2.5}$-concentrations correlated up to 0.452 (significant) at the emission level and marginally at the breathing level (up to 0.125, significant). This finding indicates a strong dilution of the polluted air. The correlation peaked at 4 km downwind.

Temperature inversions influence the dispersion of pollutants. We refer to an emission being below the inversion when the bottom of any inversion aloft is less than 50 m above the highest emission level. We considered an emission as being above an inversion layer when the top of the inversion layer is below the lowest emission level. We refer to an emission as going into an inversion layer when the lowest and highest emission levels fall into the inversion layer. In this study, non–inversion condition refers to conditions when the highest emission level is at least 300 m below the bottom of any inversion aloft. Theoretically, point sources contribute to $PM_{2.5}$-concentration at breathing level at lowest to highest magnitude when the emission level is above, in between and below inversion layers, respectively.

During November to February, WRF/Chem simulated emissions to go into, above, and below the inversion 64%, 18%, and 10% of the time, respectively, and "no inversion conditions" occurred 8% of the time. This means the "between–inversion"

conditions dominated the correlation pattern in November to February (Figures 5.8 and 5.10a). Under "below–inversion" conditions, at breathing level, correlations between 1h–differences and the point-source emissions were higher than under the other conditions, and the impact radius extended 10–12 km (Figure 5.10b). Under "below inversion" condition, upward transport of $PM_{2.5}$ was limited which yielded more concentrated polluted air reaching the breathing level than under all other inversion conditions. When the emission level was above the inversion layer, correlations at breathing level (up to 0.157, significant) were much smaller than under the "between–inversion" (up to 0.295, significant) and "below–inversion" conditions (up to 0.416, significant); the correlation peak shifted to 4–6 km downwind of the point source and the impact radius extended to 14–16 km (Figure 5.10c). Emission into layers above the inversion allowed $PM_{2.5}$ to be transported far downwind and the pollutants had to be mixed down into the inversion to reach the ground. When no inversion existed, mixing strongly diluted the polluted air leading to low and non–significant correlations at breathing level (Figure 5.10d). On such days, no exceedance occurred in the nonattainment area.

5.4 Conclusions

The impact of point-source emissions on the $PM_{2.5}$-concentrations at breathing level in the Fairbanks nonattainment area was investigated for one cold season using WRF/Chem simulations alternatively performed with (REF) and without (NPE) consideration of point-source emissions. The statistical analysis of the simulations

showed that point-source emissions were minor contributors to $PM_{2.5}$-exceedances in the nonattainment area.

Point-source emissions are the best known emissions as they are strongly regulated and verified. Given the small absolute differences in $PM_{2.5}$-concentrations at breathing level found between REF and NPE, we have to conclude that even with higher uncertainty in the other emission sectors than the point source sector, point-source emissions are not the main cause for the exceedances. In the nonattainment area, the daily maximum 24h–average $PM_{2.5}$-concentrations obtained by REF and NPE differed about 1.3 µg m^{-3} on average over November to February, and the highest maximum 24h–average $PM_{2.5}$-concentrations of REF barely exceeded that of NPE by 3 µg m^{-3}. However, during November to February the highest difference in 24h–average $PM_{2.5}$-concentrations averaged over the nonattainment area was 4.5 µg m^{-3} (November 13). The highest difference of 24h–average $PM_{2.5}$-concentrations was 18 µg m^{-3} at PS6 (January 27). This means that, on average, the point-source emissions did not affect where the maxima of $PM_{2.5}$-concentrations occurred in the nonattainment area except around PS6.

The locations where $PM_{2.5}$ exceeded the NAAQS occurred at the same locations in the nonattainment area in both simulations except for those exceedances at PS6 and its adjacent grid-cell that only occurred in REF. Five out of 39 exceedance days predicted by REF were avoided in NPE and the highest REF–NPE 24h–difference on these avoided exceedance days was 5 µg m^{-3}. This value is only slightly higher than the highest 24h–difference averaged over the nonattainment area. Out of all point sources in the nonattainment area, PS6 contributed the highest to the $PM_{2.5}$-concentrations at breathing

level as it had the highest $PM_{2.5}$-emission and contributed to the exceedances in the grid-cell holding it and in its adjacent grid-cells 8 (0) times in REF (NPE).

In general, wind-speed, temperature and mixing height were the main meteorological factors driving the $PM_{2.5}$-concentrations. Temperature strongly affected stability. Thus, these meteorological factors determined whether or not $PM_{2.5}$ was transported out of or accumulated in the nonattainment area. Typically $PM_{2.5}$-concentrations were high under calm wind, low temperature and shallow mixing height situations. All point sources had their highest impact on the $PM_{2.5}$-concentrations at breathing level in the grid-cells they fall into. The impact radius at breathing level was usually 10–12 km, but could reach up to 16 km downwind depending on the height of the emission levels, magnitude of wind-speed and the presence of an inversion above the layer the point source emitted into.

The analysis showed that in the Fairbanks nonattainment area except at PS6 and its adjacent grid-cells, the 24h–average $PM_{2.5}$-concentrations depended mainly on non–point-source emissions and the meteorological conditions, and were least sensitive to point-source emissions. At PS6 and its adjacent grid-cells, however, the 24h–average $PM_{2.5}$-concentrations were sensitive to emissions from both the non–point source and point source sector as well as to meteorological conditions.

Based on the low average reduction (1.3 $\mu g\ m^{-3}$) and the low number of exceedance days avoided (5), one has to conclude that emissions from non–point sources are the main contributors to the $PM_{2.5}$-exceedances in the nonattainment area. The differences between the REF and NPE concentrations (up to 5 $\mu g\ m^{-3}$) on the exceedance

days that were avoided in NPE are small. They suggest that only a slight increase in non–point-source emissions (e.g., from traffic, residential heating) is sufficient to exceed the NAAQS. Thus, tightening the filter requirements for point sources may only exclude some areas from experiencing an exceedance or avoid slight exceedances, if at all.

Acknowledgements

References

Ackermann, I.J., Hass, H., Memmesheimer, M., Ebel, A., Binkowski, F.S., Shankar, U., 1998. Modal aerosol dynamics model for Europe: development and first applications. *Atmospheric Environment* 32, 2981-2999.

Barnard, J.C., Fast, J.D., Paredes-Miranda, G., Arnott, W.P., Laskin, A., 2010. Technical note: evaluation of the WRF-Chem "aerosol chemical to aerosol optical properties" module using data from the MILAGRO campaign. *Atmospheric Chemistry and Physics* 10, 7325-7340.

Cahill, C.F., 2003. Asian aerosol transport to Alaska during ACE-Asia. *Journal of Geophysical Research*, 108, 8 pp. doi:10.1029/2002JD003271.

Chapman, E.G., Gustafson, W.I., Easter, R.C., Barnard, J.C., Ghan, S.J., Pekour, M.S., Fast, J.D., 2009. Coupling aerosol-cloud-radiative processes in the WRF-Chem model: investigating the radiative impact of elevated point sources. *Atmospheric Chemistry and Physics* 9, 945-964.

Cheng, S.Y., Chen, D.S., Li, J.B., Wang, H.Y., Guo, X.R., 2007. The assessment of emission source contributions to air quality by using a coupled MM5-ARPS-CMAQ modeling system: a case study in the Beijing metropolitan region, China. *Environmental Modelling and Software* 22, 1601-1616.

Chou, M.-D., Suarez, M.J., 1994. An efficient thermal infrared radiation parameterization for use in general circulation models. Technical Report, NASA Technical Memorandum 104606, 3, 85 pp.

Dominici, F., Peng, R.D., Bell, M.L., Pham, L., McDermott, A., Zeger, S.L., Samet, J.M., 2006. Fine particulate air pollution and hospital admission for cardiovascular and respiratory diseases. *Journal of the American Medical Association* 295, 1127-1134.

Frost, G.J., McKeen, S.A., Trainer, M., Ryerson, T.B., Neuman, J.A., Roberts, J.M., Swanson, A., Holloway, J.S., Sueper, D.T., Fortin, T., Parrish, D.D., Fehsenfeld, F.C., Flocke, F., Peckham, S.E., Grell, G.A., Kowal, D., Cartwright, J., Auerbach, N., Habermann, T., 2006. Effects of changing power plant NOx emissions on ozone in the eastern United States: proof of concept. *Journal of Geophysical Research* 111, D12306. doi:10.1029/2005JD006354.

Grell, G.A., Peckham, S.E., Schmitz, R., McKeen, S.A., Frost, G., Skamarock, W.C., Eder, B., 2005. Fully coupled "online" chemistry within the WRF model. *Atmospheric Environment* 39, 6957-6975.

Grell, G.A., Dévényi, D., 2002. A generalized approach to parameterizing convection combining ensemble and data assimilation techniques. *Geophysical Research Letters* 29, doi:10.1029/2002GL015311.

Hong, S.-Y., Lim, J.-O.J., 2006. The WRF Single-Moment 6-class microphysics scheme (WSM6). *Journal Korean Meteorological Society* 42, 129-151.

Janjić, Z.I., 2002. Nonsingular implementation of the Mellor-Yamada level 2.5 scheme in the NCEP Meso model. National Centers for Environmental Prediction (NCEP) Office Note #437, 61 pp.

Mlawer, E.J., Taubman, S.J., Brown, P.D., Iacono, M.J., Clough, S.A., 1997. Radiative transfer for inhomogeneous atmospheres: RRTM, a validated correlated-k model for the longwave. *Journal of Geophysical Research* 102, 16663-16682.

Mölders, N., Kramm, G., 2010. A case study on wintertime inversions in Interior Alaska with WRF. *Atmospheric Research* 95, 314-332.

Mölders, N., Tran, H.N.Q., Quinn, P., Sassen, K., Shaw, G.E., Kramm, G., 2011. Assessment of WRF/Chem to simulate sub-Arctic boundary layer characteristics during low solar irradiation using radiosonde, SODAR, and surface data. *Atmospheric Pollution Research* 2, 283-299.

Mölders, N., Tran, H.N.Q., Cahill, C.F., Leelasakultum, K., Tran, T.T., 2012. Assessment of WRF/Chem $PM_{2.5}$ forecasts using mobile and fixed location data from the Fairbanks, Alaska winter 2008/09 field campaign. *Atmospheric Pollution Research* 3, 180-191.

Peckham, S.E., Fast, J.D., Schmitz, R., Grell, G.A., Gustafson, W.I., McKeen, S.A., Ghan, S.J., Zaveri, R., Easter, R.C., Barnard, J., Chapman, E., Salzmann, M., Wiedinmyer, C., Freitas, S.R., 2009. WRF/Chem version 3.1 user's guide. 90 pp.

Pleim, J.E., 2011. Comment on "Simulation of surface ozone pollution in the central Gulf coast region using WRF/Chem model: sensitivity to PBL and land surface physics". *Advances in Meteorology* 2011, Article ID 464753, 3 pp. doi:10.1155/2011/464753.

Pope, C.A., Dockery, D.W., 2006. Health effects of fine particulate air pollution: lines that connect. *Journal of the Air and Waste Management Association* 56, 709-742.

Schell, B., Ackermann, I.J., Hass, H., Binkowski, F.S., Ebel, A., 2001. Modeling the formation of secondary organic aerosol within a comprehensive air quality model system. *Journal of Geophysical Research* 106, 28275-28293.

Simpson, D., Guenther, A., Hewitt, C.N., Steinbrecher, R., 1995. Biogenic emissions in Europe 1. estimates and uncertainties. *Journal of Geophysical Research* 100, 22875-22890.

Skamarock, W.C., Klemp, J.B., Dudhia, J., Gill, D.O., Barker, D.M., Duda, M.G., Huang, X.-Y., Wang, W., Powers, J.G., 2008. A description of the Advanced Research WRF Version 3. NCAR Technical Note, NCAR/TN–475+STR, 125 pp.

Smirnova, T.G., Brown, J.M., Benjamin, S.G., Kim, D., 2000. Parameterization of cold-season processes in the MAPS land-surface scheme. *Journal of Geophysical Research* 105, 4077-4086.

Stockwell, W.R., Middleton, P., Chang, J.S., Tang, X., 1990. The second generation regional acid deposition model chemical mechanism for regional air quality modeling. *Journal of Geophysical Research* 95, 16343-16367.

Tran, H.N.Q., Molders, N., 2011. Investigations on meteorological conditions for elevated $PM_{2.5}$ in Fairbanks, Alaska. *Atmospheric Research* 99, 39-49.

Tran, T.T., Newby, G., Molders, N., 2011. Impacts of emission changes on sulfate aerosols in Alaska. *Atmospheric Environment* 45, 3078-3090.

Wang, X.M., Carmichael, G., Chen, D.L., Tang, Y.H., Wang, T.J., 2005. Impacts of different emission sources on air quality during March 2001 in the Pearl River Delta (PRD) region. *Atmospheric Environment* 39, 5227-5241.

Werth, D., Avissar, R., 2002. The local and global effects of Amazon deforestation. *Journal of Geophysical Research* 107, 8087-8094.

Wesely, M.L., 1989. Parameterization of surface resistances to gaseous dry deposition in regional scale numerical models. *Atmospheric Environment* 23, 1293-1304.

Ying, Z.M., Tie, X.X., Li, G.H., 2009. Sensitivity of ozone concentrations to diurnal variations of surface emissions in Mexico City: a WRF/Chem modeling study. *Atmospheric Environment* 43, 851-859.
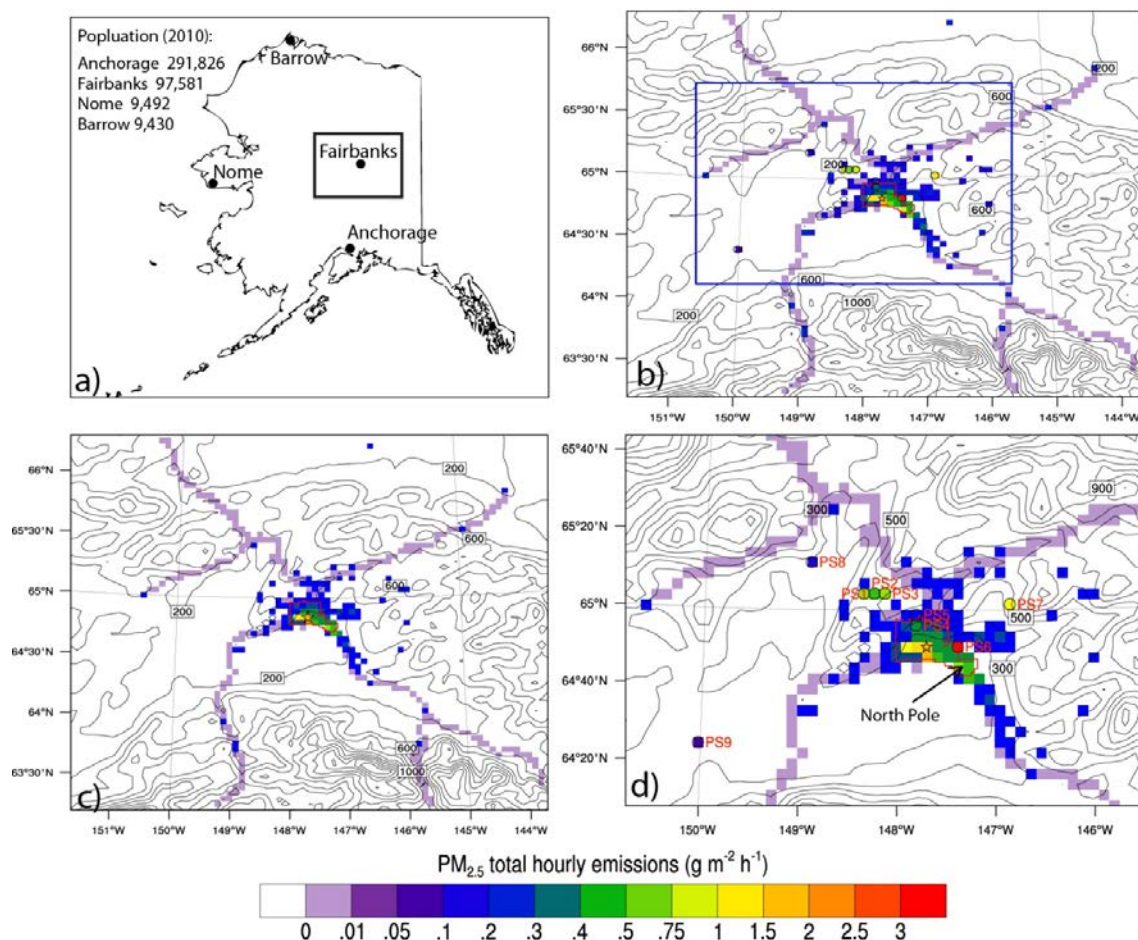
Figure 5.1 (a) Schematic view of the position of the domain of interest and population areas in Alaska, indicated by black rectangular and closed circles, respectively; topography (contours) and hourly emission rates (colors) within the grid-columns averaged over November to February in the domain of interest as used in (b) REF and (c) NPE. The blue box in (b) indicates the position of the (d) zoom-in on REF that illustrates locations of grid-cells with point sources. The star and red polygon indicate the grid–cell holding the official monitoring site at the State Office Building and the outline of the nonattainment area.
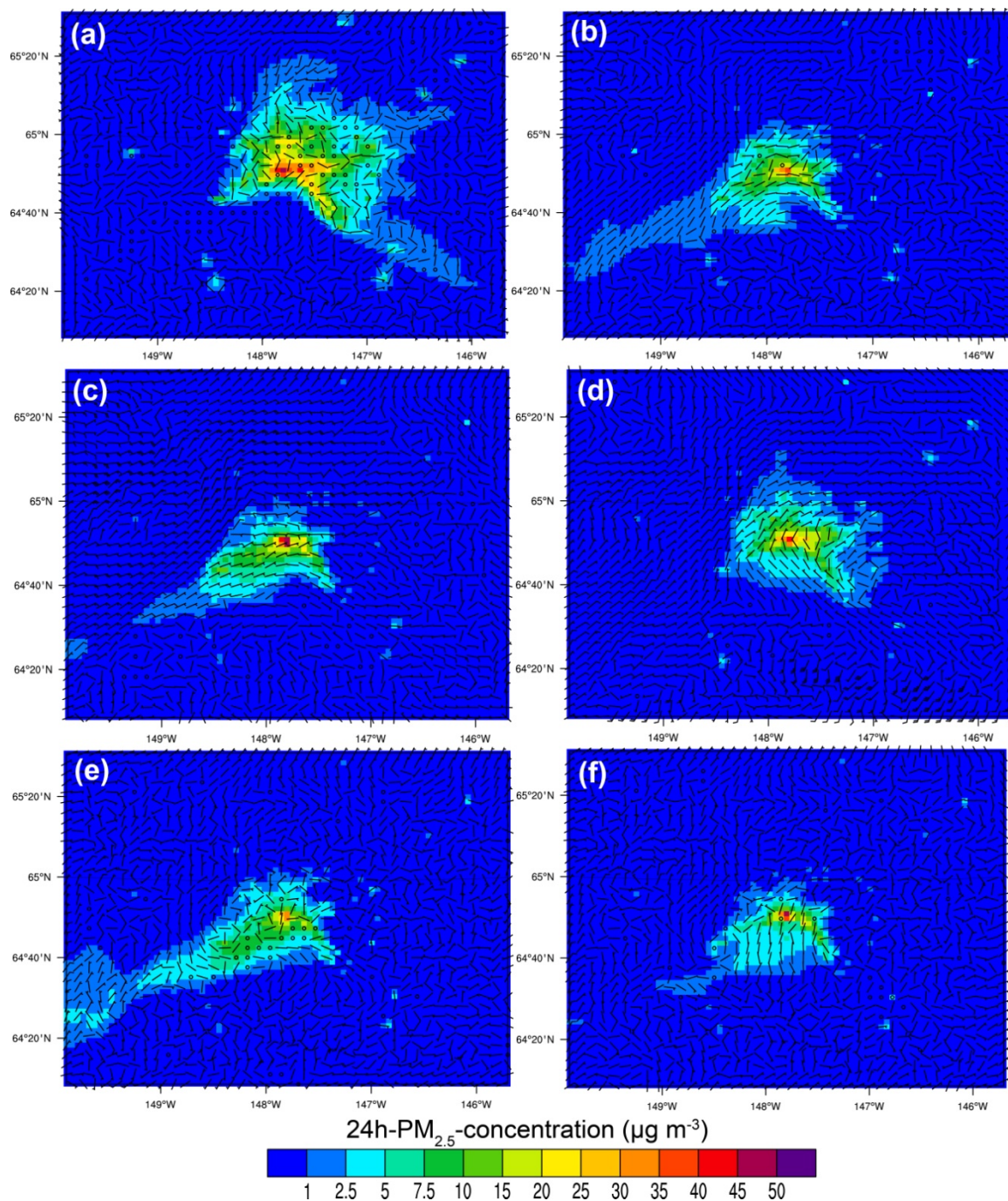
Figure 5.2 Circulation pattern of 10 m-wind (barbs) associated with exceedances at breathing level in the nonattainment area and 24h-average PM$_{2.5}$-concentrations are underlain for (a) November 26, 2005, (b) December 1, 2005, (c) January 11, 2006,(d) January 20, 2006, (e) January 15, 2006, and (f) January 16, 2006.
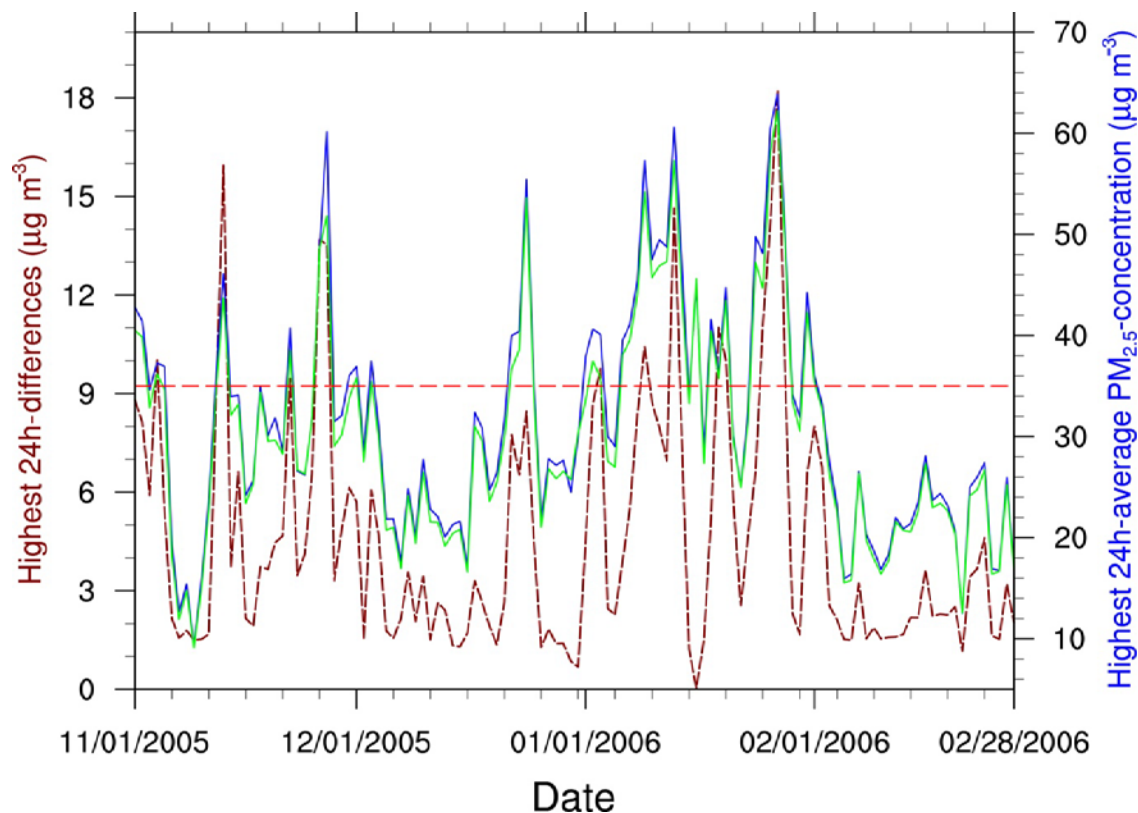
Figure 5.3 Temporal evolution of highest 24h-average PM$_{2.5}$-concentrations within the nonattainment area as obtained by REF (blue) and NPE (green), and highest 24h-differences (brown dashed line). Legends for 24h–average PM$_{2.5}$-concentrations and highest 24h-differences are to be read on the right and left y-axis, respectively. The red dashed straight line indicates the NAAQS. Note that the highest 24h-average PM$_{2.5}$-concentrations in REF and NPE did not necessarily occur in the same grid-cell, and not necessarily occurred at the grid-cell where the 24h–difference (REF-NPE) was highest.
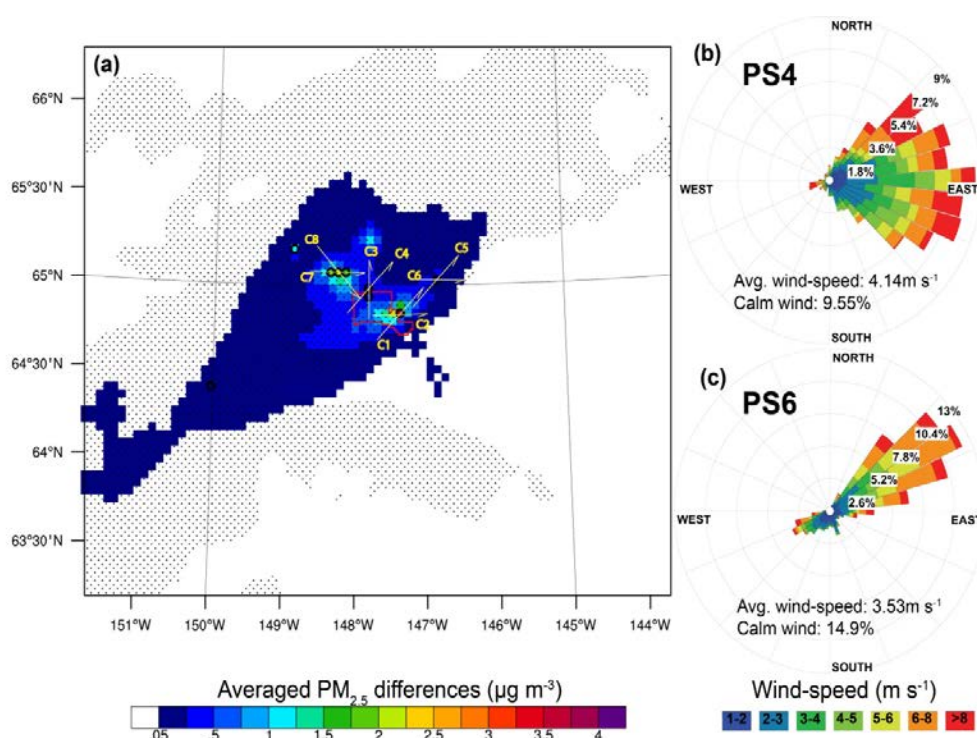
Figure 5.4 (a) PM$_{2.5}$-difference between REF and NPE averaged over November to February. Hatches indicate statistically significant (95% confidence level) differences according to a two tails t-test. The red polygon indicates the nonattainment area. C1 to C8 and arrows indicate the locations of the cross–sections shown in Figure 5.7. Typical wind-roses as obtained by WRF/Chem for the lowest emission level (64-113 m) at (b) PS4 and (c) PS6. Wind–roses at other point-sources look similar. Wind–roses at higher levels show higher wind–speeds (up to 12 m s^{-1}) and wind-direction shifts slightly to the right.
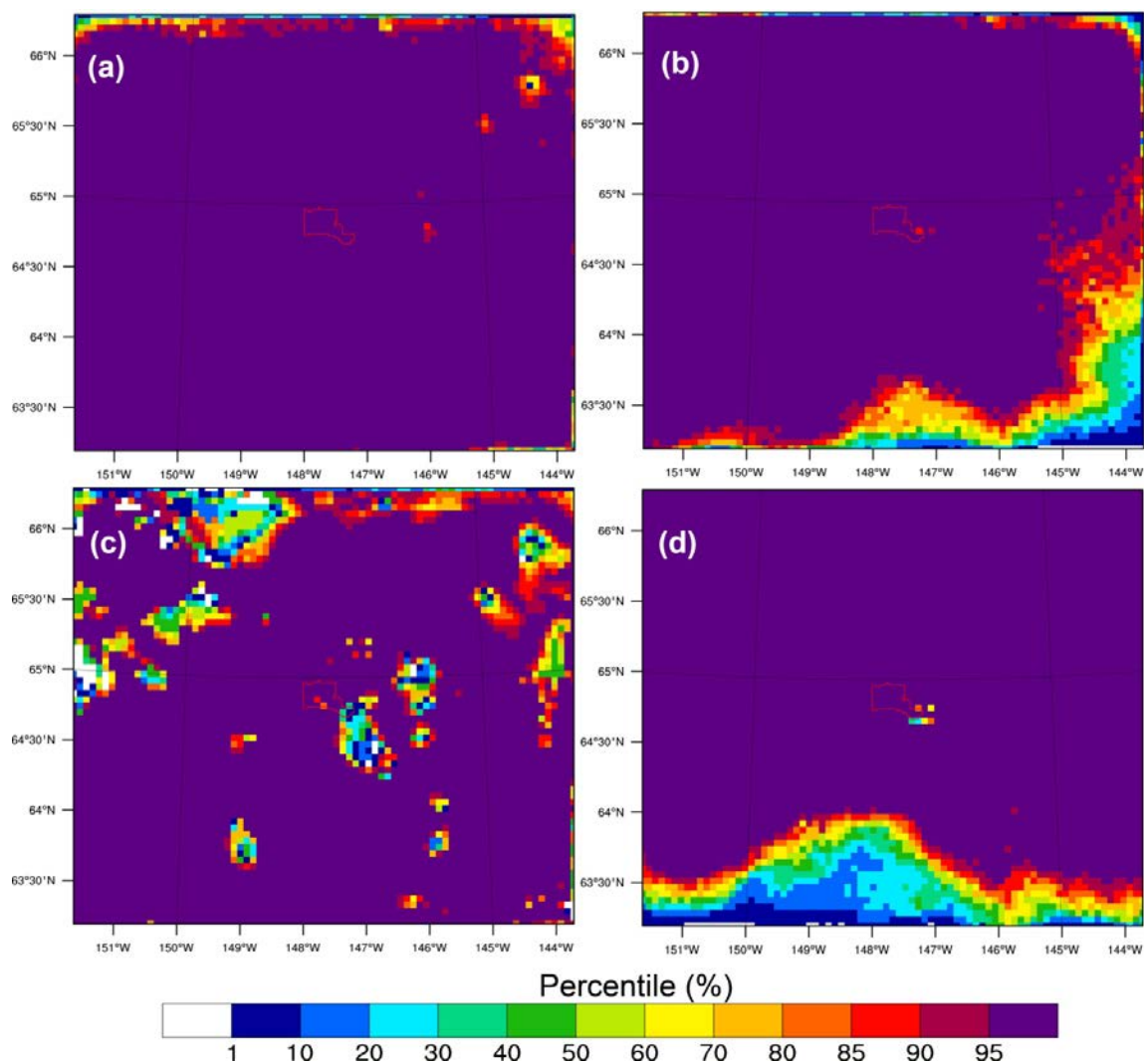
Figure 5.5 Rank of true differences over 450 "false" differences of 24h-average $PM_{2.5}$-concentrations at breathing level for (a) November, (b) December, (c) January, and (d) February. The red polygon indicates the nonattainment area. High percentiles indicate high confidence that the 24h–differences REF-NPE are caused by the point-source emissions.
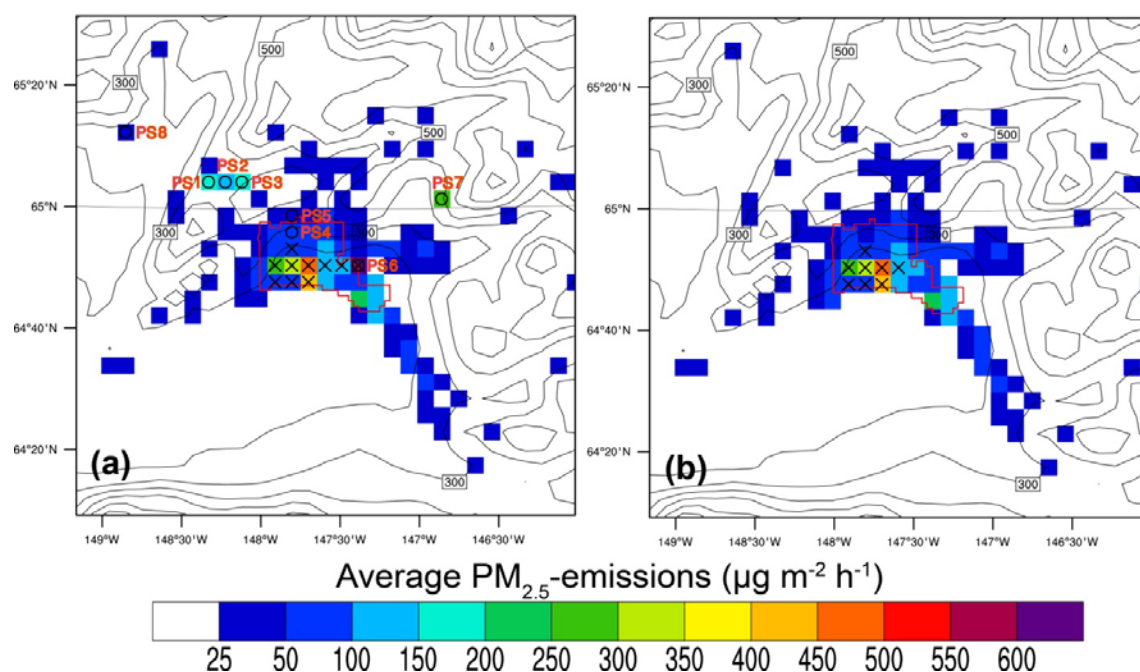
Figure 5.6 Zoom-in on areas with PM$_{2.5}$-concentrations exceeding the NAAQS (crosses) in (a) REF and (b) NPE superimposed on the map of hourly PM$_{2.5}$-emissions averaged over November to February. The red polygon indicates the nonattainment area.
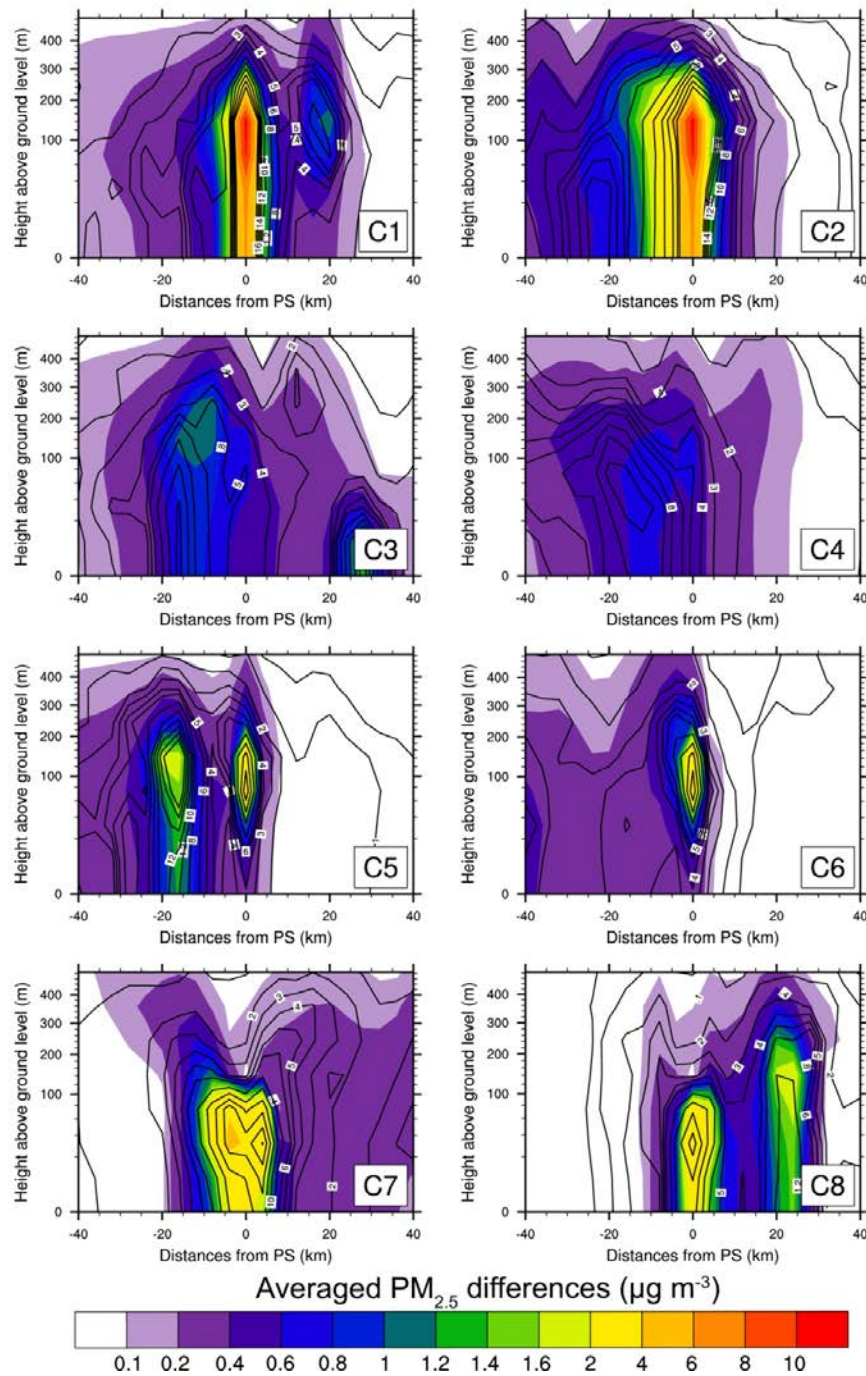
Figure 5.7 Horizontal-vertical cross-sections C1 to C8 of average PM$_{2.5}$-differences (color) and of highest PM$_{2.5}$-differences (REF–NPE) during November to February (contours in steps of 1 μg m^{-3}). For locations of C1 to C8 see Figure 5.4. The point-source investigated is located at x=0.
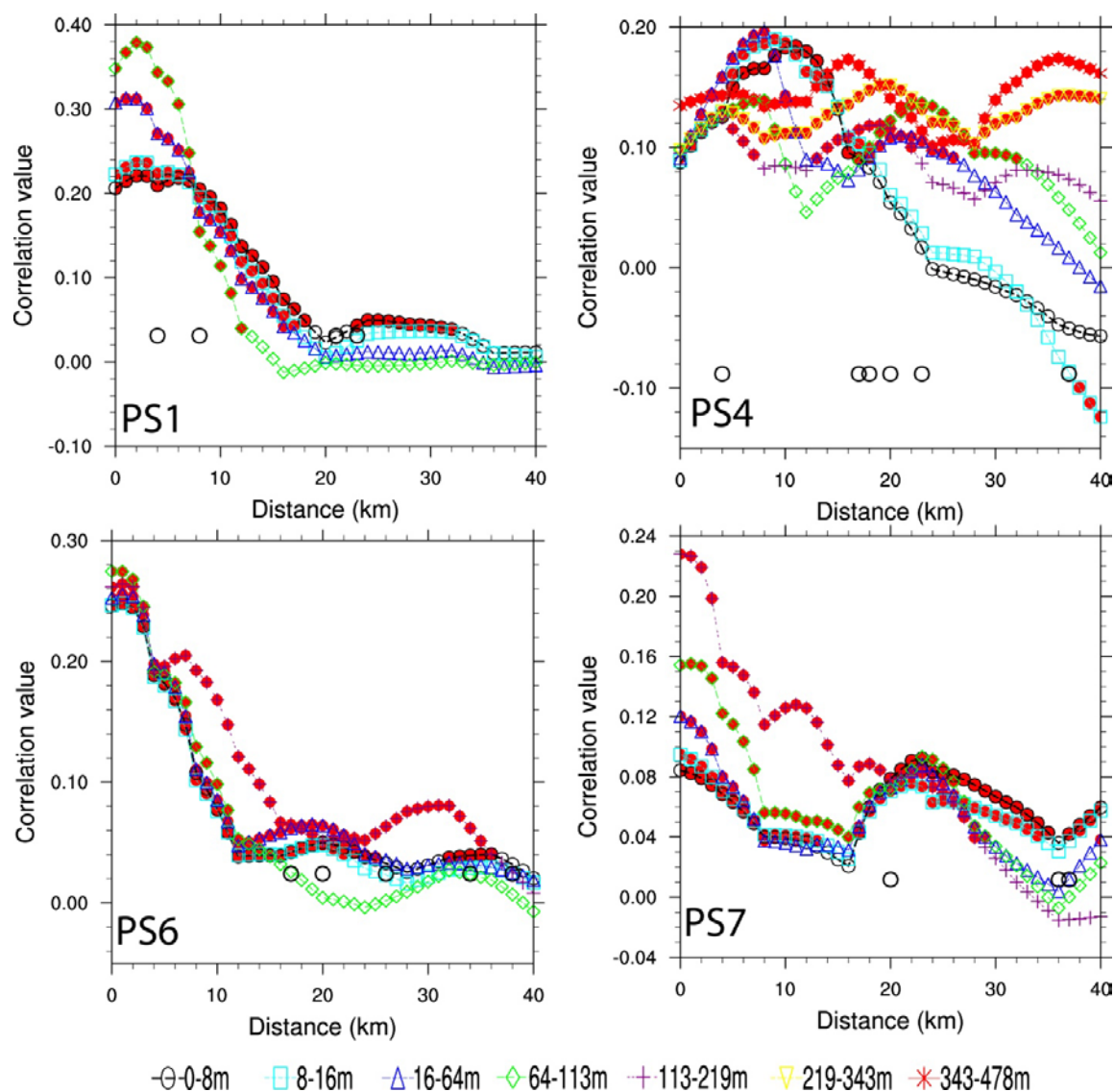
Figure 5.8 Correlations of emission rates with the PM$_{2.5}$-difference (REF–NPE) in downwind grid-cells at subsequently lower levels from the uppermost level that emissions reached due to their buoyancy, to the breathing level (0–8 m) determined for November to February for various point-sources. Open circles indicate the relative position of point–sources around the point source of interest. Closed red circles indicate locations with significant correlations at the 95% confidence level.
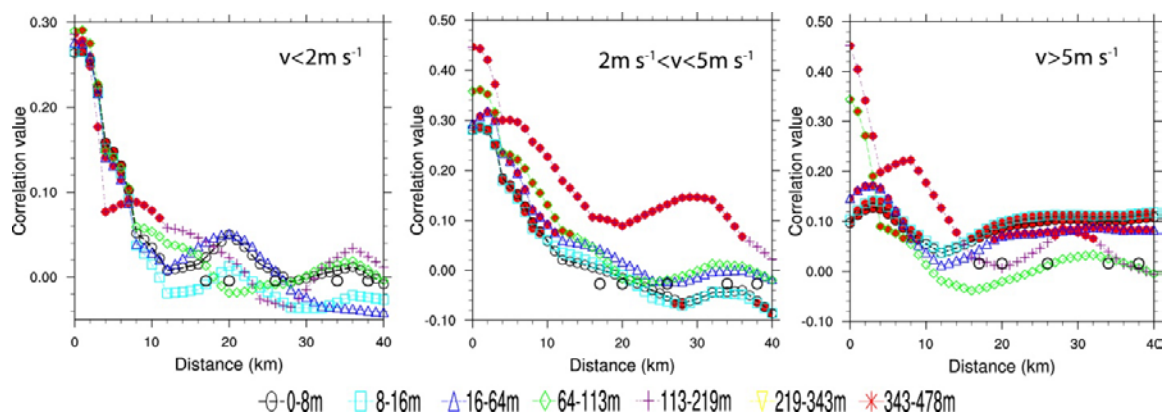
Figure 5.9 Like Figure 5.8, but for the correlations of emission rates at PS6 with the PM$_{2.5}$-difference (REF-NPE) in downwind grid-cells in subsequently lower layers from the uppermost level that emissions reach due to their buoyancy (113-219 m), to the breathing level (0-8 m) as obtained for various wind–speeds. Behavior of other point sources is similar.
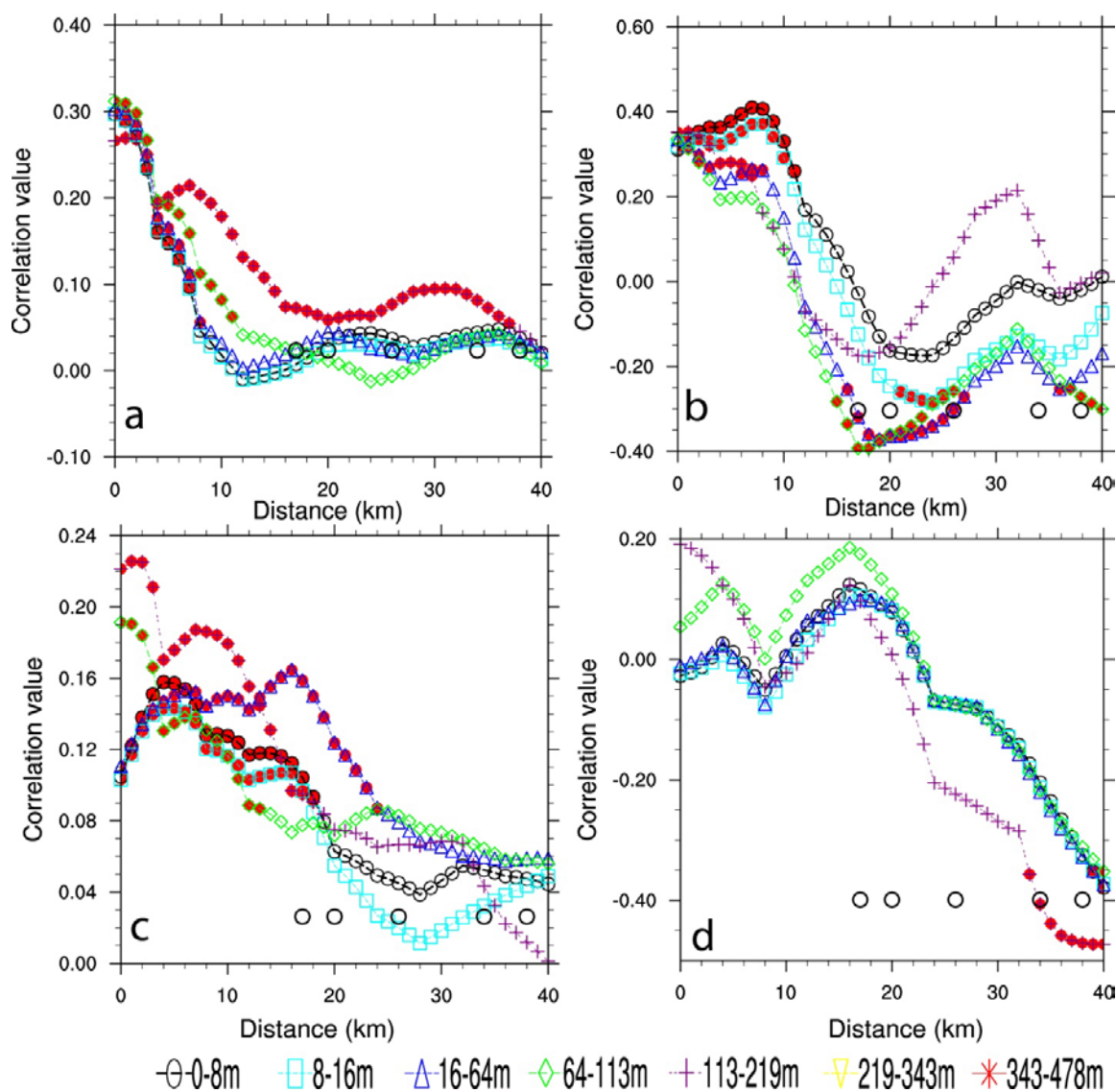
Figure 5.10 Like Figure 5.8, but for PM$_{2.5}$-difference-emission correlations in downwind grid-cells at each level from the uppermost level that the emissions reach due to buoyancy (113-219 m), to the breathing level (0-8 m) for emissions that go (a) between inversions, (b) below the inversion, (c) above the inversion, and (d) for the cases with no–inversions.

Chapter 6 Wood-burning device changeout: Modeling the impact on PM$_{2.5}$-concentrations in a remote subarctic urban nonattainment area[1]

Abstract

The effects of exchanging noncertified with certified wood-burning devices on the 24h-average PM$_{2.5}$-concentrations in the nonattainment area of Fairbanks, Alaska, in a cold season (October to March) were investigated using the Weather Research and Forecasting model inline coupled with a chemistry package. Even changing out only 2930 uncertified woodstoves and 90 outdoor wood boilers reduced the 24 h-average PM$_{2.5}$-concentrations on average by 0.6 μg.m^{-3} (6%) and avoided seven out of 55 simulated exceedance days during this half-a-year. The highest reductions on any exceedance day ranged between 1.7 and 2.8 μg.m^{-3}. The relative response factors obtained were consistently relatively low (∼0.95) for all PM$_{2.5}$-species and all months. Sensitivity studies suggest that the assessment of the benefits of a wood-burning device changeout program in avoiding exceedances heavily relies on the accuracy of the estimates on how many wood-burning devices exist that can be exchanged.

6.1 Introduction

In 2006, the Environmental Protection Agency (EPA) has tightened the 24h National Ambient Air Quality Standards (NAAQS) to 35 μg.m^{-3} for fine particulate matters having diameters equal or less than 2.5 μm (PM$_{2.5}$). During October to March the PM$_{2.5}$ data collected in prior years indicated that PM$_{2.5}$-concentrations exceeded the NAAQS frequently at the official monitoring site in Fairbanks [1] - a remote urban area in the subarctic of Alaska. Therefore, Fairbanks was designated a PM$_{2.5}$-nonattainment area in 2009.

In Fairbanks, wood-burning devices are major contributors to the PM$_{2.5}$-emissions in residential areas [2]. An estimated 9240 wood-burning devices exist in Fairbanks, of which 7980 devices are woodstoves [2]. Due to the increasing price of heating fuel, many Fairbanksan households added wood-burning devices or shifted to a higher percentage of heating with wood as is evident from the three-fold increase of wood-cutting permits from 2007 to 2009 [J. Conner, pers. comm., June 2010].

The emissions from wood-burning devices vary with fuel type, fuel moisture, burning practice and control techniques of the devices [3]. In general, EPA-certified woodstoves emit up to 87% less PM$_{2.5}$ than uncertified ones [3]. EPA [4] estimated 10 million woodstoves are being used in the United States, about 80% of which are uncertified devices. Exchanging uncertified woodstoves with certified ones has been a successful tool to mitigate PM$_{2.5}$-concentrations in many places [5].

The effects of woodstove changeout programs on reducing ambient PM$_{2.5}$-concentrations have been evaluated mainly based on observations. For example, the

$PM_{2.5}$-sampling campaign related to the changeout of 1200 uncertified woodstoves in Libby, Montana showed that 24h-average $PM_{2.5}$-concentrations decreased by 20% during the changeout period [6]. Indoor $PM_{2.5}$-concentration measured in 16 homes prior and after the woodstove changeout in a Rocky Mountain valley community [7] indicated reduction of average and maximum $PM_{2.5}$-concentrations of 71% and 76%, respectively. A similar study performed in 15 homes in British Columbia, Canada found no consistent relationship between the indoor $PM_{2.5}$-reductions and the woodstove changeout [8].

Of the 8610 inserts and woodstoves in Fairbanks, about 2930 devices are uncertified ones [2]. An assessment of the benefits of a wood-burning device changeout for any high latitude urban community based on observational studies in mid-latitudes is difficult. Fairbanks' subarctic meteorological conditions differ strongly from those in the mid-latitude places where wood-burning device changeout programs have been applied successfully to mitigate air pollution. In Fairbanks, the often stagnant air and strong radiative cooling during the long nights lead to low temperatures and strong inversions. Inversions exist on 78 - 97 days between October and March and often last for more than ten consecutive days. The 1971-2000 monthly mean temperatures in October, November, December, January, February and March were -9, -18, -22, -23, -18 and -14°C, respectively. Such extremely low temperatures result in high heating demands. The calm winds (0.5 - 2.5 m.s^{-1} on monthly average between October and March) and inversions mean low mixing of the polluted air with the unpolluted environment.

Whereas the observational approach applied in mid-latitudes requires an extensive measurement campaign over the changeout program lifetime, numerical modeling can

provide a quick and low-cost assessment on the benefits of a wood-burning device changeout program. Furthermore, modeling permits assessment of the potential benefits of a changeout program prior to its implementation/completion and hence permits implementation of additional measures in case the changeout program alone may not be sufficient enough to achieve compliance.

To this aspect, the Weather Research and Forecasting model inline coupled with a chemistry model commonly known as WRF/Chem [9, 10] has been widely used to investigate pollution sensitivity to changes in emissions. For example, WRF/Chem served to investigate the effects of changing emission of nitrogen oxides (NO_x) from power-plants on ozone concentrations in the eastern United States [11]. The simulations elucidated complex relationships between ozone concentrations and NO_x-emission strength, the proximity of other NO_x sources, the availability of volatile organic carbon (VOC), and sunlight. WRF/Chem simulations to study the impacts of urban expansion on the formation of secondary organic aerosol over the Pearl River Delta, China showed that urban expansion can alter the meteorological conditions and therefore induce increases of secondary organic aerosol between 3 and 9% [12]. WRF/Chem investigations showed that the emission changes between 1990 and 2000 in the North Pacific region caused the increasing trends of sulfate aerosols observed at coastal Alaska sites [13]. These simulations also showed that at coastal sites in southern Alaska, sulfate aerosol was not governed by the local emission changes but by the increased ship-emissions and Canadian emissions.

Among many efforts in seeking effective pollution controls to comply with the NAAQS, Fairbanks started conducting a "woodstove replacement" program. Given that Fairbanks' 2008 design value is 44.7 µg.m^{-3}, any emission-control strategy requires a relative response factor (RRF) lower than 0.78 to reach compliance with the NAAQS. In this study, we used WRF/Chem with its modifications for Alaska [14, 15] to assess the benefits of exchanging uncertified with certified wood-burning devices on the PM$_{2.5}$-concentrations at breathing level in the Fairbanks nonattainment area.

6.2 Experimental design

6.2.1 Simulations

Simulations were performed for October 1, 2008 0000 UTC to April 2, 2009 0000 UTC with the Alaska modified WRF/Chem in forecast mode. The physical and chemicals schemes selected for the simulations are listed in Table 6.1 and were described in detail in [15].

The model domain encompasses most of Interior Alaska centered over the Fairbanks nonattainment with 4km horizontal grid-increment from the surface to 100hPa with 28 stretched vertical layers (Figure 6.1). The top of the first layer (breathing level) is at 8m height. The initial conditions for the meteorological fields and meteorological lateral boundary conditions were downscaled from the $1^{o} \times 1^{o}$, 6h-resolution National Centers for Environmental Prediction global final analyses. The chemical fields were initialized with vertical profiles of Alaska-typical background concentrations. Since Fairbanks is the only major emission source and urban area within 578 km radius, and

observational and modeling studies showed hardly any advection of pollutants [13, 15],

Alaska background concentrations served as lateral boundary conditions.

Table 6.1 Parameterizations used in this study

Process	Scheme and reference
Cloud microphysics	Six water-class cloud microphysical scheme [16]
Subgrid-scale convection	Further developed 3D-version of the Grell-Dévényi cumulus-ensemble scheme [17]
Radiation	Goddard shortwave radiation scheme [18], Radiative Transfer Model for long-wave radiation [19], radiative feedback from aerosols [20]
Atmospheric boundary layer and sublayer processes	[21]
Land-surface processes	Modified Rapid Update Cycle land-surface model [22]
Gas-phase chemistry	[23]
Photolysis frequencies	[24]
Aerosol physics, chemistry and dynamics	Modal Aerosol Dynamics Model for Europe [25] and Secondary ORGanic Aerosol Model [26]
Dry deposition	[27] with the modifications by [14]
Biogenic emissions	Calculated inline depending on meteorological conditions [28]

We performed simulations without (REF) and with "woodstove replacement" (WSR). In WSR, the numbers of wood-burning devices to be changed out were based on [2]. These authors estimated there are in total 9240 wood-burning devices of which 2930 and 90 are uncertified woodstoves and outdoor wood-boilers, respectively. Since an

earlier study [29] estimated that there exist 13829 wood-burning devices of which 5042 and 1500 are uncertified woodstoves and outdoor wood boilers, respectively, we performed a sensitivity simulation (WSS1) assuming a changeout based on these numbers. A second sensitivity simulation (WSS2) was based on unpublished data by Carlson and collaborators [pers. comm., November 2009] that marginally differed in the numbers of total wood-burning devices (9241) and uncertified woodstoves (2934) from the numbers published in [2] and used in WSR, but did not consider pellet stoves (0 vs. 370 devices). The sensitivity studies were run for 14 days to assess the sensitivity to the number of wood-burning devices (WSS1) and type of devices (WSS2).

6.2.2 Emission inventories

We developed the annual anthropogenic emission inventory based on the National Emission Inventory (NEI) of 2008 available by October 2010. As no point-source emissions were available at that time, we used point-source emission data from facility operators (if provided) and assumed a 1.5%/y increase from the previous NEI otherwise. For some industrial/commercial/institutional sectors that were not available in the NEI2008, we assumed they remained as in the NEI2005 as there was just marginal change in these sectors over 2005-2008. Emission estimates for residential wood combustion were obtained from [29]. The annual emissions for 2009 were assessed with a 1.5% increase from the 2008 base year.

We considered changes in emission of $PM_{2.5}$, particulate matters having diameters equal or less than 10µm (PM_{10}), sulfur dioxides (SO_2), carbon monoxide (CO), carbon

dioxides (CO_2), ammonia (NH_3), methane (CH_4) and VOC per wood-burning device exchanged. We calculated the emission of the ith species from wood-burning devices in WSR as follows:

$$E_{WSR,i} = E_{REF,i} + N_{exch}E_{cert,i} - \sum_j N_j E_{j,i} \tag{6.1}$$

where $N_{exch} = \sum N_j$ and $E_{cert,i}$ are the number of certified wood-burning devices installed and their emission rates for the ith species; N_j and E_j are the numbers of noncertified wood-burning devices of type j and their emission rates for the ith species per device j; $E_{REF,i}$ and $E_{WSR,i}$ are the total emission rates of the ith species from wood-burning devices in REF and WSR, respectively. The emission rates from wood-burning devices for all species were derived from [29] and [30]. Analogously, we calculated the emissions for the assumed changeout of WSS1 and WSS2 with the corresponding numbers N_{exch} and N_j for each sensitivity study. The emissions from all other sectors than wood-burning remained the same in WSR, WSS1, and WSS2 as they were in REF.

This annual emission data was allocated in space and time based on source specific activity data (land-use, population density, traffic counts, point-source coordinates, hour, day-of-the-week, month, etc.) (e.g., Figure 6.2). In addition, temperature was considered for emissions from traffic, residential and commercial heating and power generation leading to higher (lower) emissions for daily mean temperatures below (above) the monthly mean temperature [15].

6.2.3 Analysis methods

We analyzed the simulations over an area of 80×70 grid-points (Figure 6.1) from October 1 0000 Alaska Standard Time (AST) to April 1 0000 AST (which is UTC+8h) as the 24h-average is to be evaluated with respect to AST. We determined the differences of $PM_{2.5}$ and its components in REF in comparison with WSR, WSS1 and WSS2. The $PM_{2.5}$-concentration differences (REF-WSR, REF-WSS1, REF-WSS2) were tested for their significance at the 95% confidence level by using a t-test with the null hypothesis that $PM_{2.5}$-concentrations in REF and in each of WSR, WSS1 and WSS2 do not differ.

We evaluated the benefit of the wood-burning device changeout by examining how many "exceedances" and "exceedance days" were avoided. In doing so, we considered 24h-average $PM_{2.5}$-concentrations at any grid-cell greater than the NAAQS on any day as an "exceedance", and any day that had at least one "exceedance" anywhere as an "exceedance day".

We calculated the relative response factors in response to the emission changes YYY by dividing the concentrations in YYY by those of REF (YYY/REF) where YYY stands for WSR, WSS1, and WSS2, respectively. The RRFs were calculated for total $PM_{2.5}$ and its major components namely sulfates (SO_4), nitrates (NO_3), ammonium (NH_4), organic carbon (OC), elemental carbon (EC) and other primary inorganic particulate matter (others). The RRFs were calculated for all grid-cells in the nonattainment area including the grid-cell that holds the official monitoring site to assess the effects of the wood-burning device changeout over the nonattainment area.

6.3 Results

6.3.1 Model performance

The evaluation of the baseline simulation (REF) [15] can be summarized as follows. WRF/Chem overestimated temperatures measured at 3, 11 and 22 m at the meteorological tower in downtown Fairbanks by 0.6 K, 0.7 K and 1.1 K, respectively. It overestimated wind-speeds measured at 11 m (12 m) by 1.15 m.s^{-1} (2.39 m.s^{-1}), and overestimated relative humidity by 16%. It well captured the temporal evolution of the meteorological quantities observed at the 23 meteorological surface stations in the domain. In the domain, the overall biases of temperature, dew-point temperature, relative humidity, sea-level pressure, wind-speed and direction over October to March were 1.3 K, 2.1 K, 5%, -1.9 hPa, 1.55 m.s^{-1} and 4°, respectively. WRF/Chem slightly overestimated the 24h-average PM$_{2.5}$-concentration on polluted days (PM$_{2.5}$-concentration > 35 µg.m^{-3}) but failed to capture the extremes to their full extend. The occurrence frequency was acceptably captured for PM$_{2.5}$-concentrations between 15 and 50 µg.m^{-3}. WRF/Chem simulated 52 exceedances at the grid-cell holding the monitoring site where only 26 exceedances were observed.

The failure to capture the PM$_{2.5}$-maxima (minima) to their full extend on extremely polluted (clean) days does not affect the number of simulated exceedance-days and exceedances. During these events, PM$_{2.5}$-concentrations namely were much higher (lower) than the 35 µg.m^{-3} threshold for exceedances. Thus, we can use the REF and WSR-simulations to assess the impact of a wood-burning device changeout on the PM$_{2.5}$-concentration in the nonattainment area.

6.3.2 Emission reduction

On annual average, $PM_{2.5}$-emissions from residential heating devices made up about 21% of the total $PM_{2.5}$-emissions from all source categories. Wood-burning devices contributed 66.6, 1.4, 14.7, 59.9, 96.5 and 95.8% of the emitted $PM_{2.5}$, SO_2, NO_x, NH_3, VOC and CO from residential heating.

On average over the nonattainment area, $PM_{2.5}$-emissions in October, November, December, January, February and March were 941.7, 632.9, 632.5, 799.8, 680.5 and 661.0 $gkm^{-2}h^{-1}$, respectively. Temperatures were appreciably below the 1971-2000 30-year average in October, and above in November, December, January and February. Consequently, $PM_{2.5}$-emissions were higher in October and lower in November, December and January than on average.

Over October to March, WSR reduced the total $PM_{2.5}$-emissions by 3.7% compared to REF. The monthly average $PM_{2.5}$-emission reductions were 4.0, 3.2, 2.7, 3.0, 3.9 and 5.6% in October, November, December, January, February and March, respectively. The magnitude of emission reductions differed among pollutants. On average over the nonattainment area, SO_2-emission reductions were 19.5, 8.16, 9.1, 11.7, 11.0 and 15.8% in October to March, respectively. The respective NO_x (VOC)-emission reductions were 16.0 (20.3), 5.5 (8.1), 6.8 (6.6), 8.9 (10.7), 7.3 (11.0) and 11.4 (11.2)%, respectively.

6.3.3 Reference simulation

The diurnal courses of $PM_{2.5}$-concentrations were similar in REF and WSR, i.e. changes in emissions from wood-burning do not affect the general diurnal course of $PM_{2.5}$-concentration. The diurnal course of $PM_{2.5}$-concentration rather reflects the temporal variation of the emissions from all sources. The diurnal course of hourly $PM_{2.5}$-concentrations on days having 24h-average $PM_{2.5}$-concentrations less than 25 $\mu g.m^{-3}$ showed a peak at 1000 AST followed by a slightly stronger peak at 1900 AST. On days having 24h-average $PM_{2.5}$-concentration greater than 25 $\mu g.m^{-3}$, the second peak often dominated the first one and had its maximum between 1500-1700 AST. Typically, the hourly $PM_{2.5}$-concentrations sharply increased after 600 AST and quickly decreased after reaching the second peak. During October to March, nighttime (2200-0600 AST) hourly $PM_{2.5}$-concentrations were typically lower and fluctuated less ($\mu= 15.7$ $\mu g.m^{-3}$, $\sigma=9.9$ $\mu g.m^{-3}$) than during the remaining hours of the day ($\mu=37.2$ $\mu g.m^{-3}$, $\sigma=22.0$ $\mu g.m^{-3}$).

Over the nonattainment area, REF monthly-average $PM_{2.5}$-concentrations were 12.9, 11.0, 9.2, 11.0, 9.8 and 5.7 $\mu g.m^{-3}$ in October, November, December, January, February, and March, respectively. In the nonattainment area, $PM_{2.5}$-concentrations were governed by the emission strength and meteorological conditions. At the grid-cell holding the monitoring site, the correlations of 24h-average $PM_{2.5}$-concentration with 2m air-temperature (T), 10m wind-speed (v), atmospheric boundary layer height (ABL height), downward shortwave radiation, relative humidity, and sea-level pressure were -0.404, -0.626, -0.613, -0.298, 0.043, and -0.001, respectively (all significant at the 95% confidence level). Here, the 24h-average $PM_{2.5}$-concentrations were strongly driven by

emission strength (R=0.668, significant). The average compositions of the 24h-average PM$_{2.5}$-concentration in all grid-cells in the nonattainment area were 21.3-25.0%, 0.6-0.8, <0.1, 8.9-9.3, 45.4-47.7, 19.8-20.7% SO$_4$, NO$_3$, NH$_4$, EC, OC and OTHERS, respectively. This finding indicates no notable differences in local PM$_{2.5}$-composition within in the nonattainment area.

The on average over the nonattainment area high PM$_{2.5}$-emissions (188.3 g.km^{-2}h^{-1}) and relative low wind-speeds (1.9 m.s^{-1}) in October led to the highest monthly average PM$_{2.5}$-concentrations of October to March. On monthly average, wind-speed and ABL height were lowest (0.9 m.s^{-1} and 122.7 m at the grid-cell holding the monitoring site, respectively) in November which explains the high monthly average PM$_{2.5}$-concentrations despite of the on monthly average second lowest PM$_{2.5}$-emissions of October to March. In March, the on average relatively high wind-speed and ABL-height (2.6 m.s^{-1} and 567.2 m at the grid-cell of the monitoring site) provided good dilution and transported polluted air out of the nonattainment area which yielded low PM$_{2.5}$-concentraton over the nonattainment area.

In REF, all maximum 24h-average PM$_{2.5}$-concentrations obtained on any day during October to March occurred in the nonattainment area. Of the 182 days, the highest 24h-average PM$_{2.5}$-concentrations occurred at the grid-cell holding the monitoring site, and/or the grid-cells adjacent to it to the south and west (these three grid-cells are called site-group hereafter) on 86, 64 and 32 days, respectively. This fact is due to relative strong PM$_{2.5}$-emissions in these grid-cells in comparison with other grid-cells in the

nonattainment area. The site-group's $PM_{2.5}$-emissions made up 34.3% of the total emissions in the nonattainment area that encompasses 31 grid-cells.

In REF, 55 exceedance days and 131 exceedances were simulated during October to March, of which 36 exceedance days and 52 exceedances occurred at the grid-cell of the monitoring site. The number of exceedance days (exceedances) in October, November, January, February and March were 20 (57), 10 (13), 5 (13), 15 (37), 5 (11) and 0 (0), respectively. All exceedances typically occurred in the site-group. The highest and lowest 24h-average $PM_{2.5}$-concentrations on any exceedance day were 72.2 and 35.1 $\mu g.m^{-3}$ and occurred on October 27, 2008 and January 4, 2009, respectively.

Exceedances typically occurred when at least any two of the following conditions co-existed: strong emission rate (>3600 $g.km^{-2}h^{-1}$), low wind-speed (v <1 $m.s^{-1}$), low temperature ($<-20^{o}C$) and low ABL-height (<20 m). These four critical conditions occurred on 23.1, 15.4, 20.3 and 20.3% of the 182 days. Days with high exceedances (>60 $\mu g.m^{-3}$) occurred when all four above mentioned critical conditions occurred concurrently. No exceedances occurred on days with wind-speeds greater than 2 $m.s^{-1}$ and ABL-heights greater than 100 m. On days with wind-speeds greater than 1 $m.s^{-1}$ and ABL heights greater than 100 m anywhere in the nonattainment area but not at the site-group, exceedances were simulated at the grid-cell of the monitoring site and/or its adjacent grid-cells while the 24h-average $PM_{2.5}$-concentrations at the other grid-cells in the nonattainment area remained low (<15 $\mu g.m^{3}$). Large concentration gradients always existed between the grid-cells of the site-group and the other grid-cells in the nonattainment area.

On days with calm wind (<0.5 m.s^{-1}), high 24h-average PM$_{2.5}$-concentrations and often exceedances occurred in the nonattainment area and its surrounding area (Figure 6.3a). During October to March, no exceedance occurred when the prevalent northeast wind or the occasional northwest wind advected clean and relatively warm air into the nonattainment area and flushed the polluted air toward the southwest or southeast (Figure 6.3b). Exceedances typically occurred when (1) in the nonattainment area, weak northeast winds were not able to remove the cold and stable air mass (Figure 6.3c); (2) in the nonattainment area, wind came from different directions and hindered the transport of polluted air out of the nonattainment area (Figure 6.3d); (3) northeast or southwest winds transported polluted air out of the nonattainment area that then was advected back into the nonattainment area as aged polluted air (Figure 6.3e); and (4) southeast winds advected polluted air from the community of North Pole (2226 inhabitants, located in the nonattainment area 22 km southeast of downtown Fairbanks) towards the grid-cell of the monitoring site and slowly drained toward the southwest.

6.3.4 Wood burning device changeout

On all except eight days, the highest 24h-average PM$_{2.5}$-concentrations occurred at the same grid-cells in WSR and REF. On those eight days, the 24h-average PM$_{2.5}$-concentration maxima in WSR, however, still occurred within the site-group like in REF. The slight shifts in position of the local maxima were due to marginal (in the order of measurement accuracy) changes in meteorological conditions due to indirect and direct feedback between the aerosol concentrations and radiation.

In WSR, the monthly-average $PM_{2.5}$-concentrations in the nonattainment area were 12.2, 10.3, 8.6, 10.3, 9.2 and 5.3 $\mu g.m^{-3}$ in October, November, December, January, February, and March, respectively. The values led to monthly-average $PM_{2.5}$-differences (REF-WSR) of 0.7, 0.7, 0.6, 0.7, 0.6 and 0.3 $\mu g.m^{-3}$ for October to March, respectively. The $PM_{2.5}$-differences were higher in months with on average relatively higher than relatively lower $PM_{2.5}$-concentrations.

The highest 24h-average $PM_{2.5}$-differences obtained anywhere in the domain was 5.7 $\mu g.m^{-3}$ (October 27 2008). The highest (2.1 $\mu g.m^{-3}$) and the second highest (2.0 $\mu g.m^{-3}$) 24h-averaged $PM_{2.5}$-differences over the nonattainment area were obtained for October 27 2008 and January 1 2009, respectively. On average over the nonattainment area and October to March, the $PM_{2.5}$-difference was 0.6 $\mu g.m^{-3}$. This value equals to 8% (6%) of the highest (average) $PM_{2.5}$-concentration reductions over the nonattainment area.

In the nonattainment area over October to March, about 45% and 33% of the 24h-average $PM_{2.5}$-differences fell between 0.5-1 $\mu g.m^{-3}$ and 0-0.5 $\mu g.m^{-3}$, respectively. However, for the nonattainment area the frequency distribution of the 24h-average $PM_{2.5}$-differences varied strongly among months (Figure 6.4). High 24h-$PM_{2.5}$-differences (>3 $\mu g.m^{-3}$) only occurred 3, 2.4 and 1.2% of the time in October, January and February, respectively. In November, December and March, more than 75% of the 24h-average $PM_{2.5}$-differences ranged between 0 and 1 $\mu g.m^{-3}$. In October, more than 40% of the 24h-average $PM_{2.5}$-differences in the nonattainment area exceeded 1 $\mu g.m^{-3}$.

On the nine days when the maximum 24h-average $PM_{2.5}$-concentrations exceeded 60 µg.m^{-3}, the average 24h-average $PM_{2.5}$-difference in the nonattainment area was 1.5-2.1 µg.m^{-3} and the maximum 24h-average $PM_{2.5}$-difference in the nonattainment area was 3.4-5.7 µg.m^{-3}. On these days, 60-87% (16-32%) of all grid-cells in the nonattainment area experienced 24h-average $PM_{2.5}$-differences greater than 1 µg.m^{-3} (2 µg.m^{-3}). On the 46 days when the maximum 24h-average $PM_{2.5}$-concentrations ranged between 35 µg.m^{-3} and 60 µg.m^{-3}, the average 24h-average $PM_{2.5}$-differences were 0.7-1.5 µg.m^{-3} and the maximum 24h-average $PM_{2.5}$-differences were 1.9-4.0 µg.m^{-3}. About 52% of the 24h-average $PM_{2.5}$-differences were less than 1.0 µg.m^{-3} and 8% of all grid-cells in the nonattainment area had 24h-average $PM_{2.5}$-differences greater than 2 µg.m^{-3}. On days with maximum 24h-average $PM_{2.5}$-concentration lower than 35 µg.m^{-3}, the 24h-average $PM_{2.5}$-differences were about 0.5 µg.m^{-3} on average, and 77% of them were less than 1.0 µg.m^{-3}. On these days, only 1% of the 24h-average $PM_{2.5}$-differences exceeded 2 µg.m^{-3} and typically occurred in the site-group.

On 111 out of the 182 days, the maximum 24h-average $PM_{2.5}$-difference occurred within the site-group. The maximum 24h-average $PM_{2.5}$-differences typically occurred in the site-group on days with calm winds (v <0.5 m.s^{-1}) or on days with winds (v >2 m.s^{-1}) and uniform wind-direction over the nonattainment area. When the maximum difference occurred at another place in the nonattainment area, winds ranged between 0.7 and 1.2 m.s^{-1} from various directions and advected pollutants from relatively strong polluted areas within the nonattainment area.

In the nonattainment area at grid-cells with strong $PM_{2.5}$-emissions (>1400 g.km^{-2}h^{-1}), the 24h-average $PM_{2.5}$-differences strongly depended on the $PM_{2.5}$-emission reduction (R= 0.617 to 0.894, significant). At grid-cells with low $PM_{2.5}$-emissions ($\leq$1400 g.km^{-2}h^{-1}), the 24h-average $PM_{2.5}$-difference was less sensitive to the $PM_{2.5}$-emission reduction (R=0.161 to 0.556) than at those with high emission rates. Instead, the meteorological conditions gained importance for the magnitude of the concentration reduction.

$PM_{2.5}$-speciation in REF hardly differed from that in WSR (<0.1%). The low changes in the partitioning among SO_4, NO_3 and other $PM_{2.5}$-species was partly due to the low emission reductions, the low availability of NH_3 and low shortwave radiation in Fairbanks during October to March.

In WSR, 1 (8), 3 (5), 2 (3), 1 (8), 0 (0) and 0 (0) exceedance days (exceedances) were avoided in October, November, December, January, February and March, respectively, as compared to REF. Out of them eight exceedances were avoided at the grid-cell holding the monitoring site. On all exceedance days except February 8 2009, the locations of exceedances were identical in WSR and REF. On February 8 2009, more grid-cells experienced exceedances in WSR than REF (three vs. two grid-cells) due to the close to 35 μg.m^{-3} concentrations and slight changes in meteorological conditions due to radiation-aerosol feedbacks.

At exceedance locations, about 18.3, 9.9, 42.0, 22.1, 10.7 and 6.1% of the 24h-average $PM_{2.5}$-differences varied between <2, 2-3, 3-4, 4-5 and >5 μg.m^{-3}, and the maximum 24h-average $PM_{2.5}$-differences obtained on any exceedance day was 5.7 μg.m^{-3}

(October 27 2008). The maximum 24h-average $PM_{2.5}$-differences on any avoided exceedance days were between 1.7 and 2.8 μg.m^{-3}. This finding means the changeout of wood-burning devices avoided exceedance days only on days with 24h-average $PM_{2.5}$-concentrations slightly above 35 μg.m^{-3}.

At the grid-cell of the monitoring site, the RRFs of 24h-average $PM_{2.5}$-concentrations were 0.951, 0.950, 0.952, 0.956, 0.941 and 0.940 in October, November, December, January, February and March, respectively. At this grid-cell, the daily RRFs of 24h-average $PM_{2.5}$-concentration were 0.938, 0.949 and 0.965 at the 50th, 75th, and 90th percentile, respectively. These findings suggest that the RRFs of total $PM_{2.5}$-concentrations at the grid-cell of the monitoring site were relatively consistent throughout October to March. The overall RRFs for NO_3 were 0.835, 0.893, 0.913, 0.868, 1.035 and 0.873 in October to March, and 0.866, 0.897 and 0.960 at the 50th, 75th and 90th percentile, respectively. The RRF of NO_3 greater than 1 may be an artifact related to the very low NO_3-concentrations (<1 μg.m^{-3}). At low concentrations, the RRF becomes highly sensitive to even small concentration changes. The RRFs of NH_4 were relative consistent (~1) throughout October to March.

Similar RRFs as obtained for the grid-cell of the monitoring site were also obtained for the other grid-cells of the site-group. At the other grid-cells in the nonattainment area, the RRFs of all $PM_{2.5}$-species were slightly decreased (increased) as compared to that of the grid-cell with the monitoring site when those grid-cells were located in the upwind (downwind) of the site-group. For all species, the RRFs obtained at these other grid-cells in the nonattainment area varied about ±0.1 of the RRFs obtained at

the grid-cell of the monitoring site. The grid-cells with the lowest RRFs, i.e. lowest reduction were typically located along the boundary of the nonattainment area and in the upwind of grid-cells with high pollution. The grid-cells along the boundary of the nonattainment area namely experienced frequently clean air advection from outside the nonattainment area. Therefore, the emission reductions related to the changeout of wood-burning devices hardly affected them. The grid-cells with the highest RRFs typically occurred inside the nonattainment area and had low 24h-average $PM_{2.5}$-concentrations (<4 µg.m^{-3}) because the RRF tends to be more sensitive to low than to high $PM_{2.5}$-concentrations.

The benefits of the changeout of wood-burning devices on the 24h-average $PM_{2.5}$-concentrations drastically decreased outside and downwind of the nonattainment area. At radii of 4 km, 8 km, 12 km and 16 km downwind of the nonattainment area, the 24h-average $PM_{2.5}$-differences were about 27.5, 13.1, 7.3 and 4.6% of the 24h-average $PM_{2.5}$-differences obtained on average over the nonattainment area. A t-test showed that the 24h-average $PM_{2.5}$-differences were significant nowhere in the domain except within the nonattainment area and some adjacent grid-cells (Figure 6.5).

6.3.5 Sensitivity studies

WSS1 represents a large emission reduction (Figure 6.2) due to the high number of wood-burning devices being changed out. On average over the nonattainment area and the 14 days, the total $PM_{2.5}$-emission was 39.8% less inWSS1 than in REF for the same

time.WSS2 examined the impact of pellet-stove replacement. Over the 14-day period, WSR and WSS2 yielded total $PM_{2.5}$-emission reductions of 5.6% and 6.6%, respectively.

The maximum 24h-average $PM_{2.5}$-concentrations obtained in REF, WSR, WSS1, and WSS2 on any day of the 14d sensitivity study were 51.1, 47.6, 26.9, and 47.5 $\mu g.m^{-3}$ on October 14, 2008. The 24 h-average $PM_{2.5}$-differences of REF-WSS1 were appreciably higher than those of REF-WSR or REF-WSS2 because the emission reduction was the highest in WSS1 (Figures 6.2 and 6.6). The maximum 24h-average $PM_{2.5}$-differences obtained on any day in WSS1 was 24.9 $\mu g.m^{-3}$. On the contrary, the maximum 24h-average $PM_{2.5}$-difference obtained on any of the 14 days in WSS2 was 3.6 $\mu g.m^{-3}$, which was only marginally higher than that obtained in WSR (3.5 $\mu g.m^{-3}$) for the same timeframe. About 16.7, 25.3, 18.2, 8.8, 13.1, 13.4, and 5.5% of the 24h-average $PM_{2.5}$-differences REF-WSS1 fall within <1, 1-2, 2-3, 3-4, 4–6, 6–10, and >10 $\mu g.m^{-3}$, respectively. During the same 14d period, about 77.0 (80.2), 18.4 (17.1), 3.5 (2.3), 1.2 (0.5), and 0 (0)% of 24 h-average $PM_{2.5}$-differences of REF-WSS1 (REF-WSR) fell between <1, 1-2, 2-3, 3-4, and >4 $\mu g.m^{-3}$, respectively.

The average RRFs of the 24h-average $PM_{2.5}$-concentrations obtained at the grid-cell of the monitoring site for WSS1, WSS2, and WSR were 0.543, 0.913, and 0.930, respectively, for the 14d episode. The RRFs of NH_4 were about 1 in all sensitivity simulations. The RRFs of NO_3 were 0.471, 0.815, and 0.818 in WSS1, WSS2 and WSR, respectively, while those of SO_4, OC, EC, and others were similar to those for $PM_{2.5}$.

The spatial variations of RRFs were within ±0.1 of the RRF at the grid-cell of the monitoring site for any species at any grid-cell in the nonattainment area for both WSS2

and WSR. On the contrary, in WSS1, the spatial variations of RRFs reached from no difference to 0.4 greater RRF values than the RRF-value at the grid-cell of the monitoring site. On six and five out of the 14 days of the sensitivity study, the highest response, that is, highest reduction in the nonattainment area, occurred at the grid-cell of the monitoring site and other grid-cells of the site group. The highest response (RRF = 0.821) occurred at the grid-cell of the monitoring site on one day in WSS2. However, on no day the strongest response occurred at the grid-cell of the monitoring site in WSR.

The high number of wood-burning devices changed out in WSS1 led to avoidance of all 4 (6) exceedance days (exceedances) that occurred in REF during the same time. No exceedances were avoided in both WSS2 and WSR during these 14 days. The highest (lowest) 24h-average $PM_{2.5}$-difference obtained at any exceedance location in WSS1 was 24.9 (16.8) $\mu g.m^{-3}$. The locations of exceedances were the same in REF, WSS2, and WSR and all occurred in the nonattainment area.

6.4 Conclusions

The effects of exchanging noncertified wood-burning devices with certified woodstoves on reducing the 24h-average $PM_{2.5}$-concentrations at breathing level in the Fairbanks nonattainment area were investigated for October 1, 2008 to March 31, 2009 using results from WRF/Chem simulations. The results indicated that the assumed wood-burning device changeouts helped to reduce the 24h-average $PM_{2.5}$-concentrations at breathing level in the nonattainment area. However, the reduction effectiveness depends on the number of wood-burning devices changed out and what kinds of devices are

changed out. The wood-burning device changeout scenario based on data reported by [2] yielded only a 3.7% $PM_{2.5}$-emission reduction from the reference scenario, and consequently a low decrease of 24h-average $PM_{2.5}$-concentrations. On average over the nonattainment area and October to March, the 24h-average $PM_{2.5}$-differences (REF-WSR) were 0.6 $\mu g.m^{-3}$ which equals to a 6% $PM_{2.5}$-concentration reduction. About 79% of the 24h-average $PM_{2.5}$-differences were less than 1 $\mu g.m^{-3}$. This means given a design value of 44.7 $\mu g.m^{-3}$ the assumed changeout does not lead to compliance and may only reduce the number of exceedances on days with concentrations slightly higher than the NAAQS.

The magnitude of the 24h-average $PM_{2.5}$-differences REF-WSR differed strongly among days and locations. High 24h-average $PM_{2.5}$-differences (>3 $\mu g.m^{-3}$) often occurred in October, January and February. Wind-speed and wind-direction were the key factors that governed the distribution of the maximum 24h-average $PM_{2.5}$-difference. The magnitude of the 24h-average $PM_{2.5}$-difference depended more on the $PM_{2.5}$-emission reduction at grid-cells having relative strong than relative low $PM_{2.5}$-emissions. The maximum 24h-average $PM_{2.5}$-differences typically occurred in the grid-cells of the site-group on days having calm wind (v <0.5 $m.s^{-1}$) or wind-speeds exceeding $2m.s^{-1}$. Under other wind conditions, the maximum 24h-average $PM_{2.5}$-differences typically occurred at grid-cells in the downwind of the site-group. Based on these findings one has to conclude that mitigation is spatially heterogeneous and local emission conditions together with the meteorological conditions strongly govern the magnitude of mitigation.

The wood-burning device changeout assumed in WSR only effectively helped to avoid 7 out of 55 exceedance days that occurred in REF. Moreover, this avoidance occurred only on days with 24h-average $PM_{2.5}$-concentration slightly above 35 $\mu g.m^{-3}$. The RRFs of $PM_{2.5}$-concentration and its major components typically varied between 0.950-0.965 and were relatively consistent throughout October to March. The lowest RRFs, i.e. highest reduction, were not obtained at the grid-cell of the monitoring site but at other grid-cells in the nonattainment area. These findings support the above conclusion that the assumed changeout is not sufficient to achieve compliance. Thus, one has to conclude that the changeout of wood-burning devices may improve the air quality locally in large parts of the nonattainment area without becoming obvious at the monitoring site. Based on the relative consistency of RRF one has to conclude that wood-burning changeout provides a relative reliable reduction.

The 14d sensitivity simulations assuming the number of wood-burning devices reported by [29] (WSS1) yielded up to a 39.8% $PM_{2.5}$-emission reduction as compared to the baseline simulation (REF) and a much higher 24h-average $PM_{2.5}$-concentration reduction over the nonattainment area than WSR and WSS2. In total four of the exceedance days that were simulated in REF during these 14 days were avoided in WSS1 and the maximum 24h-average $PM_{2.5}$-difference (REF-WSS1) at any exceedance location was 24.9 $\mu g.m^{-3}$. The relative response factors of $PM_{2.5}$-concentrations obtained at the grid-cell of the monitoring site were as high as 0.543 on average and the highest RRFs were frequently obtained at the grid-cell of the monitoring site and other grid-cells of the site group. The results of the sensitivity study WSS2 only marginally differed from those

of WSR. Based on the 14d sensitivity study WSS1, one has to conclude that if the number of uncertified wood-burning devices assumed in WSS1 could be changed out, the number of exceedances in the nonattainment area could effectively be reduced. On the contrary, changing out wood-burning devices at the comparatively low numbers assumed in WSR and WSS2 seems not to be sufficient to achieve compliance with the NAAQS. Together the results of the sensitivity studies suggest that accurate knowledge of the number of noncertified devices that have to be or can be changed out is of greatest importance to assess the potential benefits of a changeout program on the 24h-average $PM_{2.5}$-concentrations.

Acknowledgements

References

[1]   H. N. Q. Tran and N. Mölders, "Investigations on meteorological conditions for elevated $PM_{2.5}$ in Fairbanks, Alaska", *Atmospheric Research,* vol. 99, no. 1, pp. 39-49, 2011.

[2]   T. R. Carlson, S. H. Yoon, and R. G. Dulla, "Fairbanks home heating survey," Tech. Rep., Sierra Research, Sacramento, Calif, USA, pp. 63, 2010.

[3]   J. E. Houck and D. R. Broderick, "$PM_{2.5}$ emission reduction benefits of replacing conventional uncertified cordwood stoves with certified cordwood stoves or modern pellet stoves," Tech. Rep., Arlington, Va, USA, pp. 26, 2005.

[4]   United State Environmental Protection Agency (EPA), "Agencies-changeout guide"*,* 2011, http://www.epa.gov/burnwise/how-to-guide.html.

[5]   United State Environmental Protection Agency (EPA), "Agencies - case studies"*,* 2011, http://www.epa.gov/burnwise/casestudies.html.

[6]   M. A. Bergauff, T. J. Ward, C. W. Noonan and C. P. Palmer, "The effect of a woodstove changeout on ambient levels of $PM_{2.5}$ and chemical tracers for woodsmoke in Libby, Montana", *Atmospheric Environment,* vol. 43, no.18, pp. 2938-2943, 2009.

[7]   T. Ward and C. Noonan, "Results of a residential indoor $PM_{2.5}$ sampling program before and after a woodstove changeout", *Indoor Air,* vol. 18, no. 5, pp. 408-415, 2008.

[8]   R. W. Allen, S. Leckie, G. Millar and M. Brauer, "The impact of wood stove technology upgrades on indoor residential air quality", *Atmospheric Environment,* vol. 43, no. 37, pp. 5908-5915, 2009.

[9]   G. A. Grell, S. E. Peckham, R. Schmitz, S. A. McKeen, G. Frost, W. C. Skamarock and B. Eder, "Fully coupled "online" chemistry within the WRF model", *Atmospheric Environment,* vol. 39, no. 37, pp. 6957-6975, 2005.

[10]   S. E. Peckham, J. D. Fast, R. Schmitz et al., "WRF/Chem version 3.1 user's guide", pp. 78, 2009.

[11]   G. J. Frost, S. A. McKeen, M. Trainer et al., "Effects of changing power plant NO emissions on ozone in the eastern United States: Proof of concept", *Journal of Geophysical Research,* vol. 111, no. D12, Article ID D12306, 2006. doi:112300.112029/12005JD006354.

[12] X. Wang, Z. Wu and G. Liang, "WRF/CHEM modeling of impacts of weather conditions modified by urban expansion on secondary organic aerosol formation over Pearl River Delta", *Particuology,* vol. 7, no. 5, pp. 384-391, 2009.

[13] T. T. Tran, G. Newby and N. Mölders, "Impacts of emission changes on sulfate aerosols in Alaska", *Atmospheric Environment,* vol. 45, no. 18, pp. 3078-3090, 2011.

[14] N. Mölders, H. N. Q. Tran, P. Quinn, K. Sassen, G. Shaw and G. Kramm, "Assessment of WRF/Chem to simulate sub–Arctic boundary layer characteristics during low solar irradiation using radiosonde, SODAR, and surface data", *Atmospheric Pollution Research,* vol. 2, no. 3, pp. 283-299, 2011.

[15] N. Mölders, H. N. Q. Tran, C. F. Cahill, K. Leelasakultum and T. T. Tran, "Assessment of WRF/Chem $PM_{2.5}$-forecasts using mobile and fixed location data from the Fairbanks, Alaska winter 2008/09 field campaign", *Atmospheric Pollution Research,* vol. 3, no. 2, pp. 180-191, 2012.

[16] S. Y. Hong and J.O. J. Lim, "The WRF single-moment 6-class microphysics scheme (WSM6)," *Journal of The Korean Meteorological Society*, vol. 42, no. 1, pp.129-151, 2006.

[17] G. A. Grell and D. Dévényi, "A generalized approach to parameterizing convection combining ensemble and data assimilation techniques," *Geophysical Research Letters*, vol. 29, no. 14, 2002. doi:10.1029/2002GL015311.

[18] M. D. Chou and M. J. Suarez, "An efficient thermal infrared radiation parameterization for use in general circulation models", NASA Center for Aerospace Information, pp. 85, 1994.

[19] E. J. Mlawer, S. J. Taubman, P. D. Brown, M. J. Iacono, and S. A. Clough, "Radiative transfer for inhomogeneous atmospheres: RRTM, a validated correlated-k model for the longwave," *Journal of Geophysical Research*, vol. 102, no. D14, pp. 16663-16682, 1997.

[20] J. C. Barnard, J. D. Fast, G. Paredes-Miranda, W. P. Arnott, and A. Laskin, "Technical Note: Evaluation of the WRF-Chem 'aerosol chemical to aerosol optical properties' module using data from the MILAGRO campaign", *Atmospheric Chemistry and Physics*, vol. 10, no. 15, pp. 7325-7340, 2010.

[21] Z. I. Janjić, "The step-mountain eta coordinate model: further developments of the convection, viscous sublayer, and turbulence closure schemes," *Monthly Weather Review*, vol. 122, no. 5, pp. 927-945, 1994.

[22] T. G. Smirnova, J. M. Brown, S. G. Benjamin, and D. Kim, "Parameterization of cold-season processes in the MAPS land-surface scheme," *Journal of Geophysical Research*, vol. 105, no. D3, pp. 4077-4086, 2000.

[23] W. R. Stockwell, P. Middleton, J. S. Chang, and X. Y. Tang, "The second generation Regional Acid Deposition Model chemical mechanism for regional air-quality modeling," *Journal of Geophysical Research*, vol. 95, no. 10, pp. 16343-16367, 1990.

[24] S. Madronich, "Photodissociation in the atmosphere .1. Actinic flux and the effects of ground reflections and clouds," *Journal of Geophysical Research*, vol. 92, no. D8, pp. 9740-9752, 1987.

[25] I. J. Ackermann, H. Hass, M. Memmesheimer, A. Ebel, F. S. Binkowski, and U. Shankar, "Modal Aerosol Dynamics model for Europe: Development and first applications," *Atmospheric Environment*, vol. 32, no. 17, pp. 2981-2999, 1998.

[26] B. Schell, I. J. Ackermann, H. Hass, F. S. Binkowski, and A. Ebel, "Modeling the formation of secondary organic aerosol within a comprehensive air quality model system," *Journal of Geophysical Research*, vol. 106, no. D22, pp. 28275-28293, 2001.

[27] M. L. Wesely, "Parameterization of surface resistances to gaseous dry deposition in regional-scale numerical-models," *Atmospheric Environment*, vol. 23, no. 6, pp. 1293-1304, 1989.

[28] D. Simpson, A. Guenther, C. N. Hewitt, and R. Steinbrecher, "Biogenic emissions in Europe 1. Estimates and uncertainties", *Journal of Geophysical Research*, vol. 100, no. D11, pp. 22875-22890, 1995.

[29] J. Davies, D. Misiuk, R. Colgan, and N. Wiltse, "Reducing $PM_{2.5}$ emissions from residential heating sources in the Fairbanks North Star Borough: emission estimates, policy options, and recommendations," Tech. Rep., Fairbanks, Alaska, USA, pp. 56, 2009.

[30] United State Environmental Protection Agency (EPA), "AP 42, Fifth Edition, Vol. I - Chapter 1: External combustion sources", 2011, http://www.epa.gov/ttn/chief/ap42/ch01/index.html, 2011.
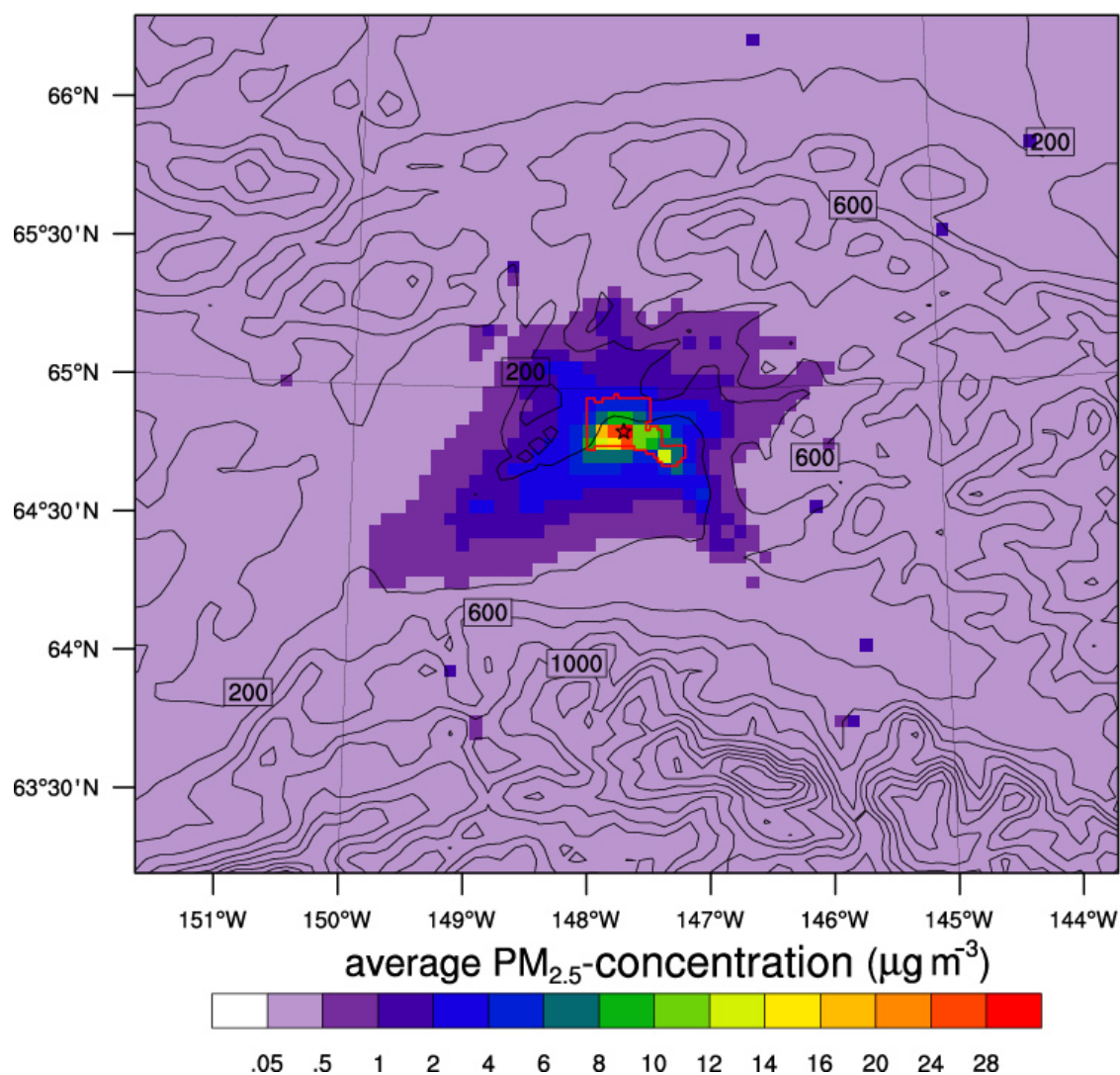
Figure 6.1 Average PM$_{2.5}$-concentrations in the domain of interest in October to March as obtained in REF with terrain contours overlain. The star and red polygon indicate the grid cell holding the official monitoring site and the outline of the nonattainment area.
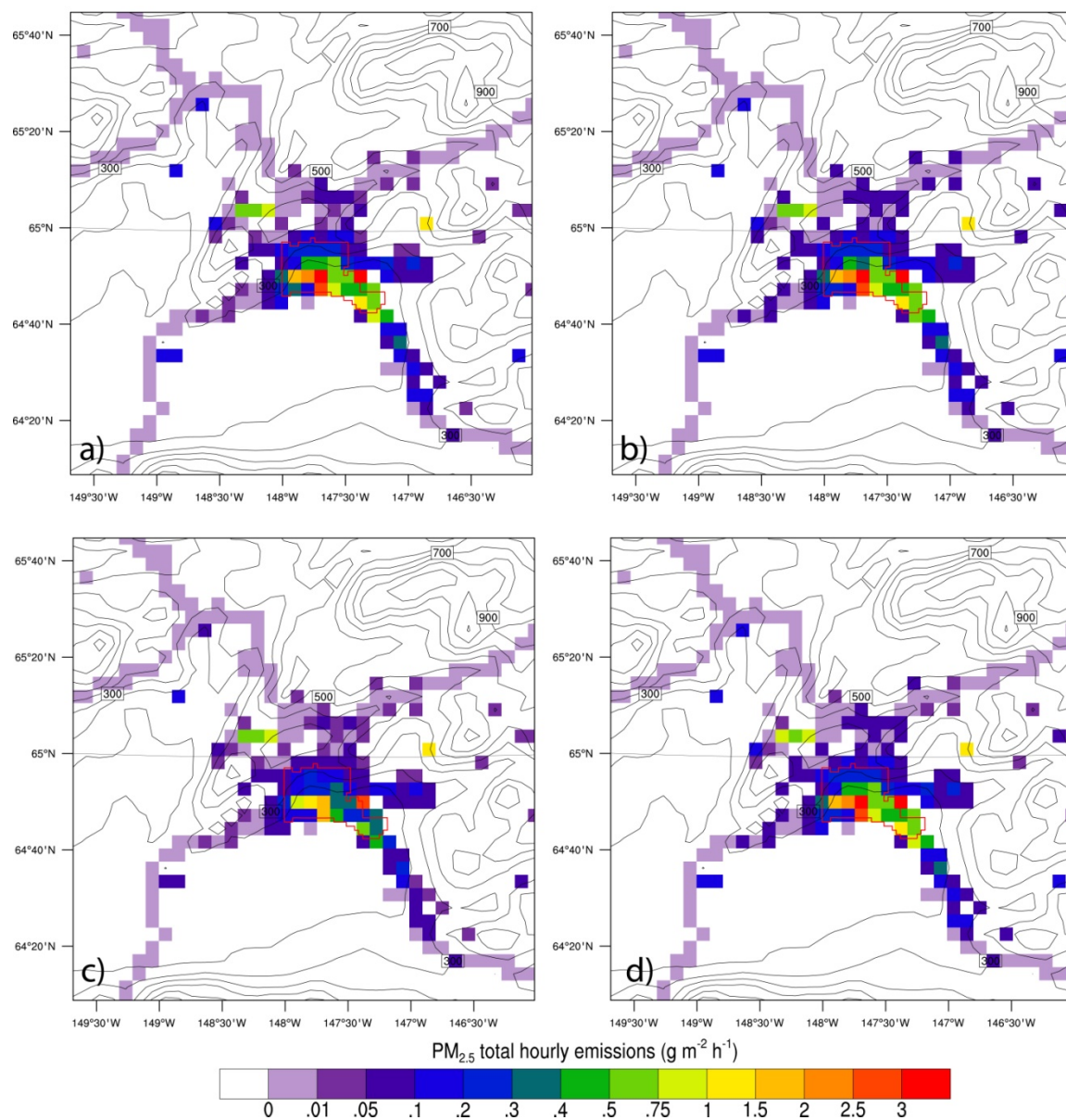
Figure 6.2 Zoom-in on PM$_{2.5}$-emissions in (a) REF, (b) WSR, (c) WSS1, and (d) WSS2 on average over October to March for REF and WSR and October 01–14, 2008, for WSS1 and WSS2.
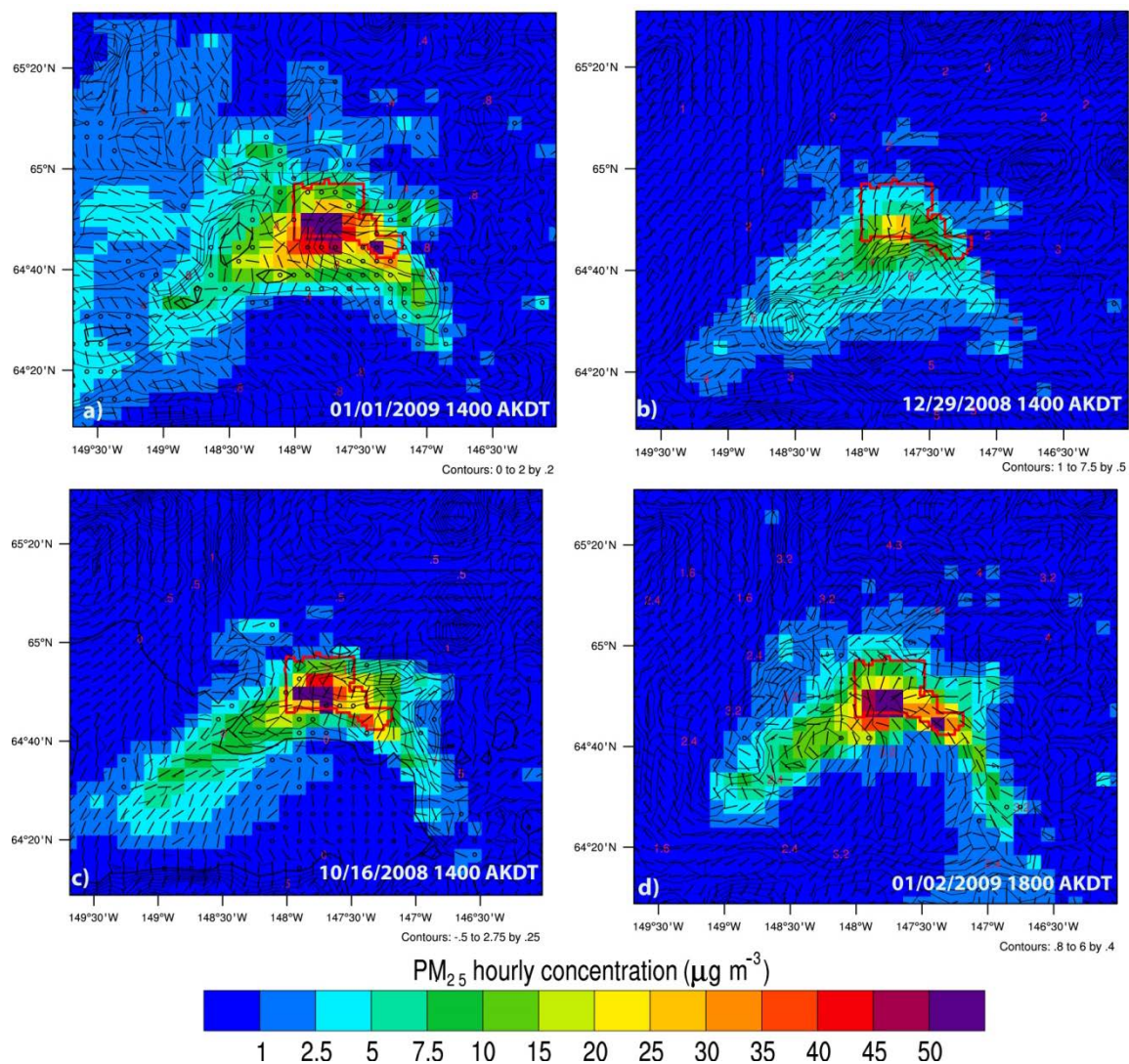
Figure 6.3 Zoom-in on typical wind circulatio patterns at breathing level associated with high and low PM$_{2.5}$-concentrations in the nonattainment area in October to March. The contour lines represent the potential temperature gradient ($\Delta\theta/\Delta z$) (K.100 m^{-1}) between the surface and 150m above the ground; the red polygon indicates the nonattainment area. The community of North Pole is located in the lower right region of the nonattainment area.
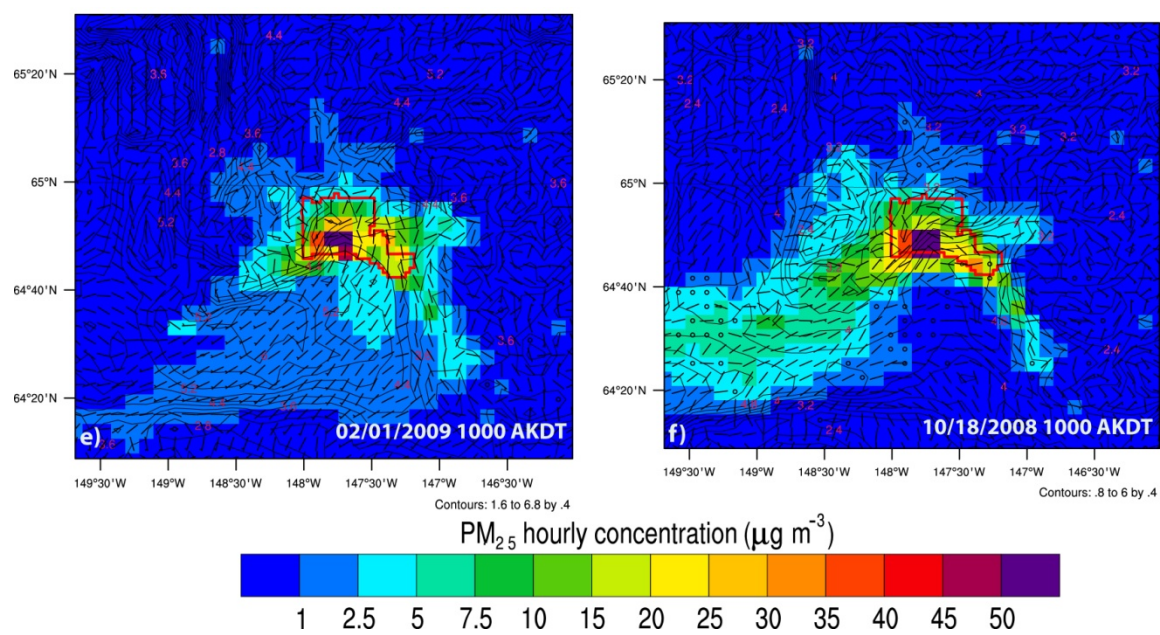
Figure 6.3 (cont.)
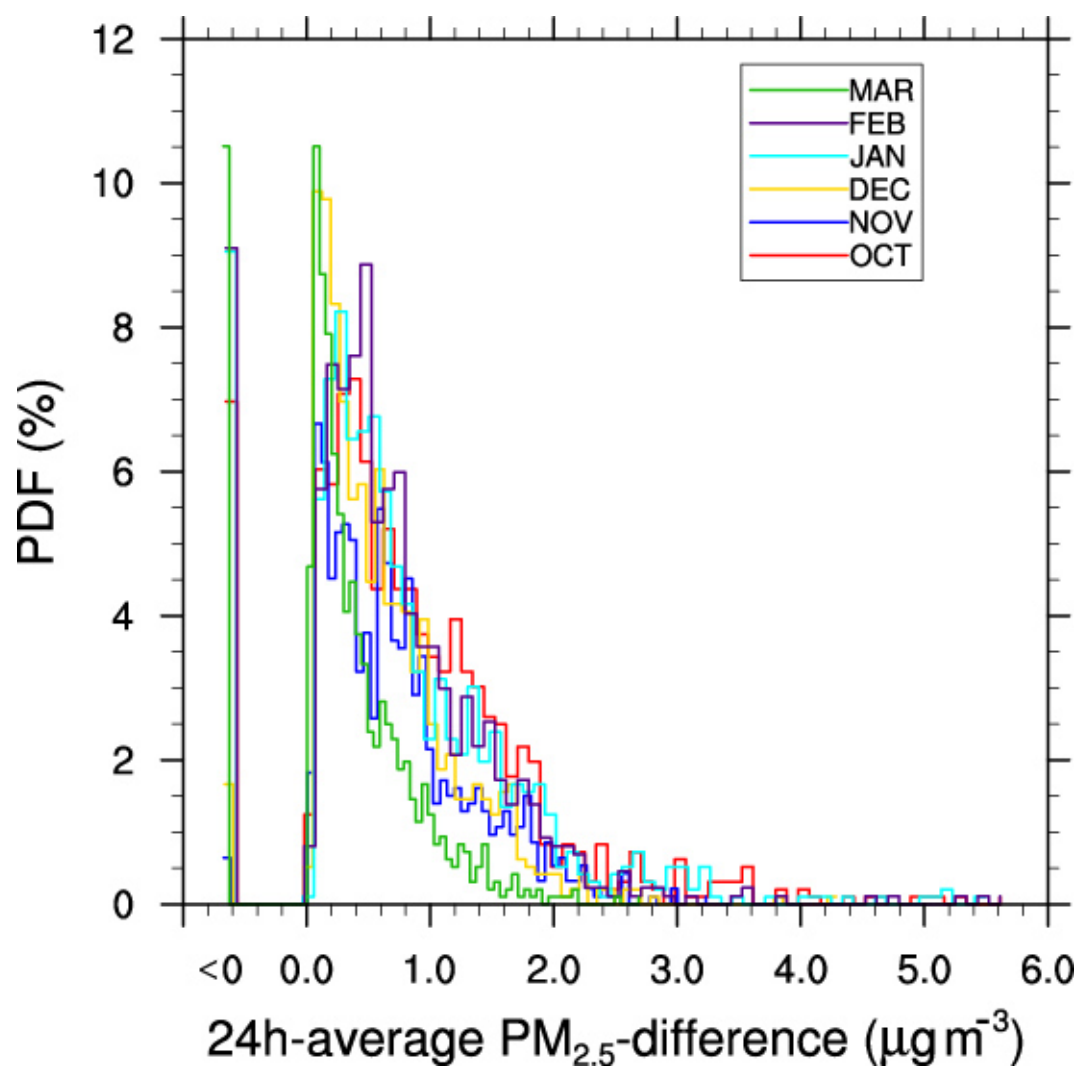
Figure 6.4 Population distribution of 24h-average PM$_{2.5}$-difference in the nonattainment area as obtained for WSR in each month. The occurrences of all 24h-average PM$_{2.5}$-differences <0.0 μg.m^{-3} were summed up and their distribution is shown on the left most of the x-axis.
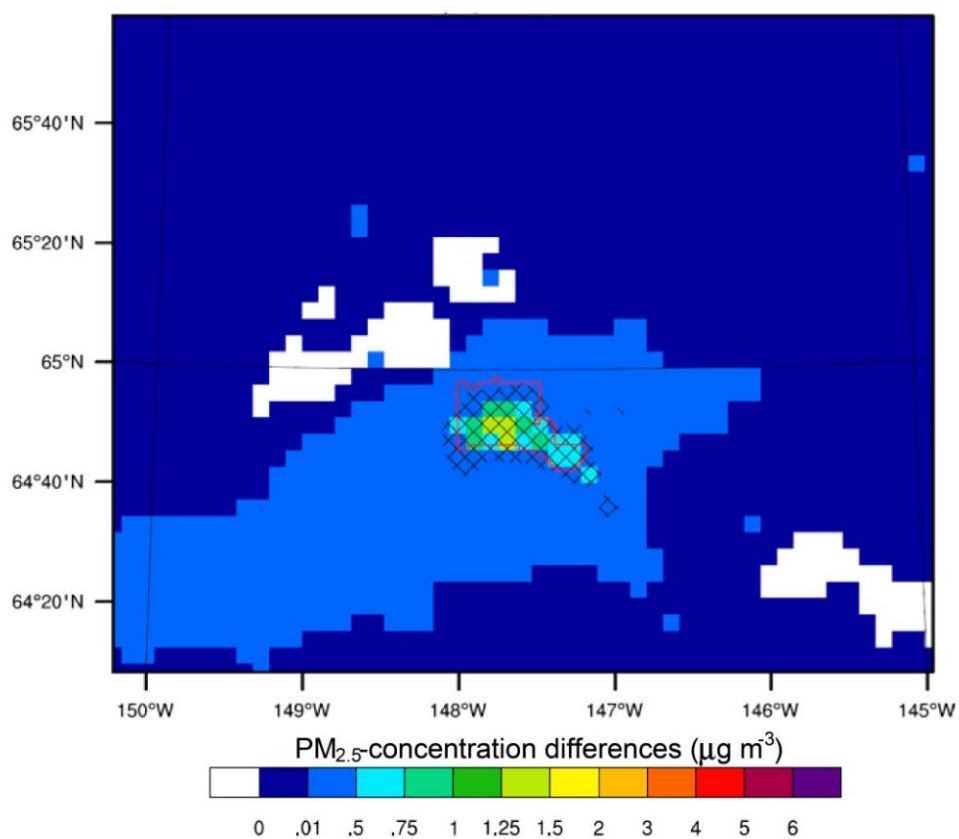
Figure 6.5 Zoom-in on the average differences of PM$_{2.5}$-concentrations between REF and WSR for October to March. Hashed shading indicates grid cells with significant differences at the 95% or higher level of confidence.
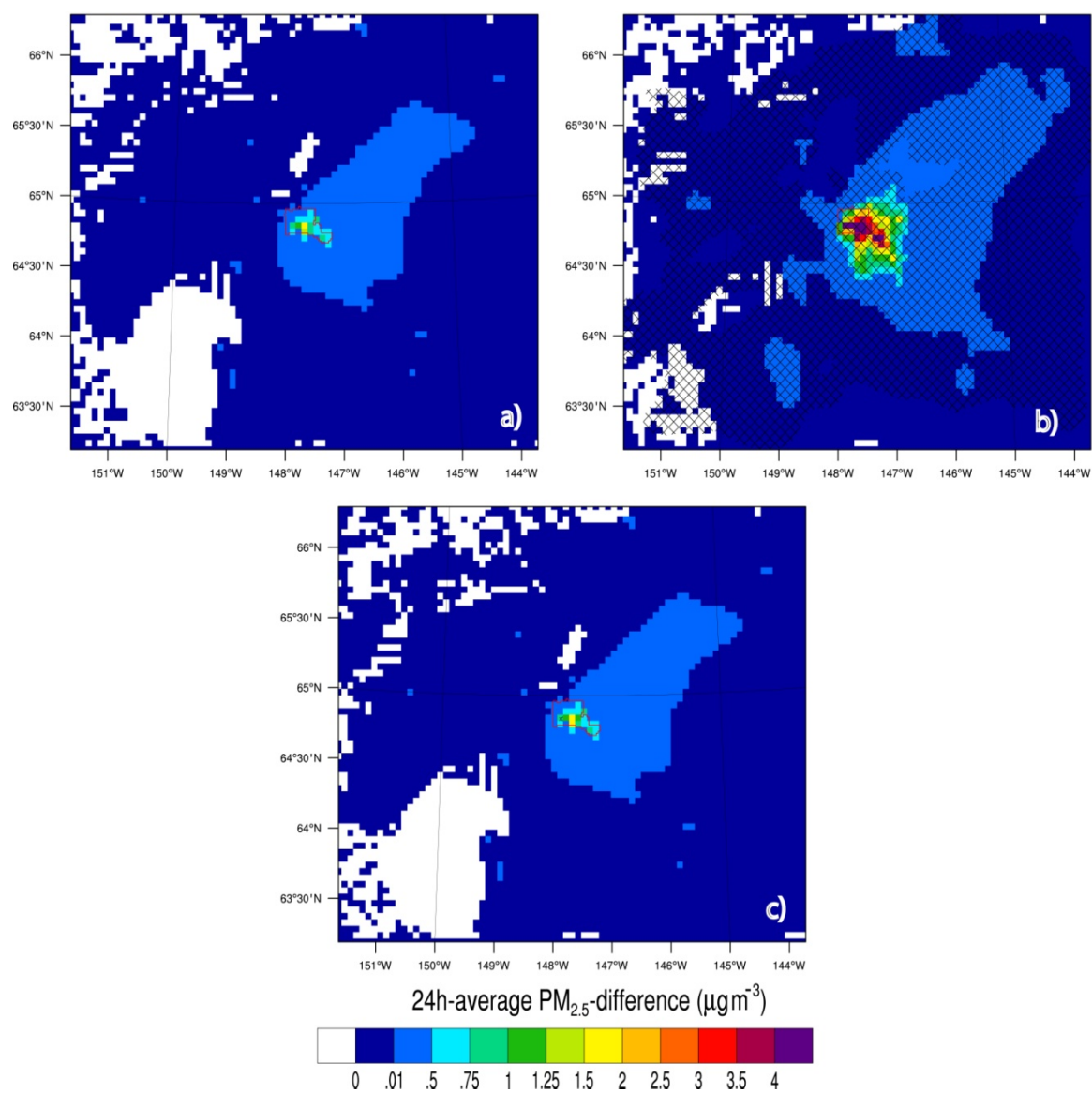
Figure 6.6 Like Figure 6.5, but for 24h-average $PM_{2.5}$-differences (a) REF-WSR, (b) REF-WSS1, and (c) REF-WSS2 from October 1 to October 14 2008 AST.

Chapter 7 Contribution of uncertified wood-burning devices on the Fairbanks PM$_{2.5}$-nonattainment area

As pointed out in chapter 1, the change in the emission inventory due to the introduction of the wood-burning device changeouts since fall 2010 may have affected the emissions, and hence the simulations for the database for the interpolation. Therefore, it is important to investigate the influences of the wood-burning device changeouts in particular, and of the emissions from uncertified wood-burning devices in general on the PM$_{2.5}$-concentrations in Fairbanks.

The potential influences of the wood-burning device changeouts on the PM$_{2.5}$-concentration have been elucidated in Tran and Mölders (2012; chapter 6). Subsequent to chapter 6, in this chapter, additional sensitivity studies were conducted in order to assess the contribution of uncertified wood-burning devices in general to the PM$_{2.5}$-concentrations rather than the impact of wood-burning device changeouts on the PM$_{2.5}$-concentrations. These sensitivity studies were performed to be able to compare the contributions of emissions from uncertified wood-burning devices to the PM$_{2.5}$-concentrations with those from point sources (chapter 5) and traffic (chapter 8). These studies seemed interesting as emissions from wood-burning devices go into the same level as those from traffic, while those from point-sources go into various layers above the ground, but not into the first level. Section 7.1 presents the results of these studies; section 7.2 presents additional conclusions to those presented in Tran and Mölders (2012; chapter 6).

7.1 Contribution of uncertified wood-burning devices to the PM$_{2.5}$-concentrations

The WSS3 and WSS4 sensitivity studies were performed within the scope of this dissertation to investigate the contribution of the emissions from uncertified wood-burning devices to the PM$_{2.5}$-concentrations in the Fairbanks nonattainment area. The assumed emission inventories applied in WSS3 and WSS4 were presented in section 2.3.3.

The results showed that the contributions of the emissions from uncertified wood-burning devices to the total PM$_{2.5}$-emissions in the nonattainment area are 14% and 56% on average in WSS3 and WSS4, respectively (Figure 7.1). The difference in the number of uncertified wood-burning devices assumed in WSS3 and WSS4, as discussed in section 2.3.3, explains the above contribution values. The emission contributions of the uncertified wood-burning devices substantially differed in space, and their patterns are similar in WSS3 and WSS4 (Figure 7.1). For example in WSS3, the PM$_{2.5}$-emissions from the uncertified wood-burning devices typically made up 10% to 45% of the total emissions in densely populated areas (e.g., Fairbanks (FB), North Pole (NP)) and 2% to 9% in sparsely populated areas (e.g., Hill (HL); see Figure 1.1 for locations).

Accordingly, WSS1 represents a large emission reduction (Figure 7.1) due to the high number of wood-burning devices assumed to be changed out. On average over the nonattainment area and the 14 days, the total PM$_{2.5}$-emission was 39.8% less in WSS1 than in REF for the same time. Over the 14-day period, WSR and WSS2 yielded total PM$_{2.5}$-emission reductions of 5.6% and 6.6%, respectively.

The maximum 24h-average $PM_{2.5}$-concentrations obtained in REF, WSR, WSS1, WSS2, WSS3 and WSS4 on any day of the 14d sensitivity study were 51.1, 47.6, 26.9, 47.5, 46.2 and 23.5 $\mu g.m^{-3}$, respectively. The 24h-average $PM_{2.5}$-differences REF-WSS1 were appreciably higher than those of REF-WSR or REF-WSS2 because the emission reduction was highest in WSS1 (Figures 7.1, 7.2a-7.2c). Analogously, the 24h-average $PM_{2.5}$-differences REF-WSS4 were appreciably greater than those of REF-WSS3 (Figure 7.2d-e). On average over the nonattainment and over the 14d-episode, excluding the uncertified wood-burning devices in WSS3 and WSS4 reduced the 24h-average $PM_{2.5}$-concentrations by 1.3 $\mu g.m^{-3}$ and 4.1 $\mu g.m^{-3}$, respectively. These values equal to reductions of $PM_{2.5}$-concentrations of 13% and 43% in WSS3 and WSS4, respectively. Exchanging the uncertified wood-burning devices with the certified ones in WSR, WSS1 and WSS2 yielded reductions of 24h-average $PM_{2.5}$-concentrations of 0.6, 0.7 and 3.7 $\mu g.m^{-3}$ on average, respectively.

The above findings indicate a great sensitivity of the magnitude of $PM_{2.5}$-concentration reductions to the type and the number of the exchanged uncertified wood-burning devices. Note that Davies et al. (2009) and Carlson et al. (2010) estimated that there exist 1500 and 90 outdoor wood boilers and they accounted for 23% and 3% of the total uncertified wood-burning devices in Fairbanks, respectively. According to Davies et al. (2009), to produce the same amount of heat, the outdoor wood boilers emit about seven times higher amounts of $PM_{2.5}$ than the uncertified woodstoves. As a result, WSS1 experiences higher $PM_{2.5}$-reductions per uncertified wood-burning device exchanged than WSR.

The maximum 24h-average $PM_{2.5}$-differences obtained on any day in WSS1 was 24.9 $\mu g.m^{-3}$. On the contrary, the maximum 24h-average $PM_{2.5}$-differences obtained on any of the 14 days in WSS2 was 3.6 $\mu g.m^{-3}$, which was only marginally higher than that obtained in WSR (3.5 $\mu g.m^{-3}$) for the same timeframe. About 16.7, 25.3, 18.2, 8.8, 13.1, 13.4 and 5.5% of the 24h-average $PM_{2.5}$-differences REF-WSS1 fall within <1, 1-2, 2-3, 3-4, 4-6, 6-10 and >10 $\mu g.m^{-3}$, respectively. During the same 14d period, about 77.0 (80.2), 18.4 (17.1), 3.5 (2.3), 1.2 (0.5) and 0 (0)% of 24h-average $PM_{2.5}$-differences REF-WSS1 (REF-WSR) fell between <1, 1-2, 2-3, 3-4 and >4 $\mu g.m^{-3}$, respectively. This means that according to the WSS1 scenario, information on the wood-burning device changeouts should be included in the AQuAT database as this changeout program importantly impacts the $PM_{2.5}$-concentrations. On the contrary, according to the WSR and WSS2 scenarios, the impacts of the changeout program on the $PM_{2.5}$-concentrations are marginal, and the current CMAQ simulations for episode 1 can be used as a database for the AQuAT. As shown in Figure 7.2, the REF-WSS1 and REF-WSS4 differences are greater and are statistically significant over a larger area than for REF-WSR, REF-WSS2 and REF-WSS3. In WSS1 and WSS4, the $PM_{2.5}$-differences were not only noticeable at the locations where the uncertified wood-burning devices contributed most (e.g., FB, NP) but also downwind of the nonattainment area. On the contrary, the $PM_{2.5}$-differences were marginal and not statistically significant in WSR, WSS, and were only statistically significant inside the nonattainment area in WSS3 (cf. Figures 7.1, 7.2). This result agrees with the above finding that the impact of the wood-burning device changeouts is

unimportant according to the WSR and WSS2 scenarios and the current CMAQ simulations for episode 1 can be used as a database for the AQuAT.

The average RRFs of the 24h-average $PM_{2.5}$-concentrations obtained at the grid-cell of the official monitoring (SB) site for WSR, WSS1, WSS2, WSS3 and WSS4 were 0.930, 0.543, 0.913, 0.849 and 0.538, respectively for the 14d episode. The spatial variation of RRFs was within ±0.1 of the RRF at the grid-cell of the SB site at any grid-cell in the nonattainment area for WSS2, WSR and WSS3. On the contrary, in WSS1 and WSS4, the spatial variation of RRFs reached from no difference to 0.4 greater RRF-values than the RRF-value at the grid-cell of the SB site. On six out of the 14 days of the sensitivity study, the highest response, i.e., the highest reduction in the nonattainment area, occurred at the grid-cell of the SB site; on five out of the 14 days, it occurred at other grid-cells of the site-group. The highest response (RRF = 0.821) occurred at the grid-cell of the SB site on one day (October 2, 2008) in WSS2. However, the strongest response occurred on no day at the grid-cell of the SB site in WSR. These findings indicate that the impact of the uncertified wood-burning devices on the $PM_{2.5}$-concentrations is high, and nonlinearly distributed in space. This finding strengthens the need of a spatially differentiated $PM_{2.5}$ air-quality advisory.

These findings also necessitate the use of air-quality simulations as a database for AQuAT to include information on the contributions to the $PM_{2.5}$-concentrations by the uncertified wood-burning devices, which strongly differ in space and time.

7.2 Conclusions

In addition to the sensitivity studies described in chapter 6, the 14d sensitivity simulations described in this chapter showed that the contributions of the emissions from uncertified wood-burning devices to the 24h-average $PM_{2.5}$-concentrations in the Fairbanks nonattainment area based on data reported by Davies et al. (2009) (WSS4) were much higher than those based on data reported by Carlson et al. (2010) (WSS3). On average over the nonattainment and over 14d episode, the uncertified wood-burning devices contributed 13% to the $PM_{2.5}$-concentrations in WSS3 on average, compared to the 43% contribution by the uncertified wood-burning devices in WSS4. The wood-burning device changeout program has more impact on the $PM_{2.5}$-concentrations in WSS1 than in WSR. The replacement of uncertified wood-burning devices in WSR reduced the $PM_{2.5}$-concentrations in the nonattainment by 6% on average, compared to the 38% reduction obtained in WSS1.

The results of all sensitivity studies showed that the contribution of the uncertified wood-burning devices differed in space and time. The contributions were greatest in densely populated areas (e.g., FB, NP) and were marginal in sparsely populated areas (e.g., HL).

Together with the findings on the contributions of point-sources emissions in chapter 5, the findings on the contributions of the emissions from uncertified wood-burning devices to the $PM_{2.5}$-concentrations support the suitability of air-quality simulations as a database for AQuAT. Only with such a database, AQuAT can capture the heterogeneity in space and time of the nonlinear relationships between the emissions

(as well as other physical and chemical processes) and the distribution of $PM_{2.5}$-concentrations in the nonattainment area.

Furthermore, contributions of the emissions from uncertified wood-burning devices to the $PM_{2.5}$-concentrations and the influences of wood-burning device changeouts on the $PM_{2.5}$-concentrations differed drastically with the number of wood-burning devices assumed in the sensitivity studies. These findings show the sensitivity of the changeout program's impact on the $PM_{2.5}$-concentrations to the type of wood-burning devices exchanged. It illustrates the impact on the simulated $PM_{2.5}$-concentrations of the uncertainty in the emission inventory that related to the limited knowledge of the number of wood-burning devices and wood burning behavior in Fairbanks.

Note that the $PM_{2.5}$-observations include information on the emission change due to the wood-burning device changeouts (or any future emission-control measure). This information is therefore also included in AQuAT. This means if in the future, observed $PM_{2.5}$-concentrations decrease due to an introduction of an emission-control measure, the AQuAT-interpolated $PM_{2.5}$-concentrations may also decrease accordingly. However, given the fact that the nonlinear impacts of emission sources on $PM_{2.5}$-concentrations cannot be captured by the observations, the AQuAT-interpolated $PM_{2.5}$-concentrations would expose large uncertainty if the AQuAT database does not include information on the emission changes in response to the introduced emission-control measure, especially if the impacts of such an emission-control measure on the $PM_{2.5}$-concentrations are large (for instance, as in WSS1). Therefore, an updated emission inventory that includes

information on the emission changes, whenever such changes occur, is needed for AQuAT to ensure its accuracy.

Until such an emission inventory becomes available, the air-quality simulations used in this dissertation are considered adequate as a database for AQuAT given the current uncertainty in the data on wood-burning device changeouts, wood-burning behavior, and the number of wood-burning devices in general.

References

Carlson, T.R., Yoon, S.H., Dulla, R.G., 2010. Fairbanks home heating survey. Sacramento, CA, p. 63.

Davies, J., Misiuk, D., Colgan, R., Wiltse, N., 2009. Reducing $PM_{2.5}$ emissions from residential heating sources in the Fairbanks North Star Borough: Emission estimates, policy options, and recommendations. Cold Climate Housing Research Center, Fairbanks, AK, p. 56.

Tran, H.N.Q., Mölders, N., 2012. Wood-burning device changeout: Modeling the impact on $PM_{2.5}$-concentrations in a remote subarctic urban nonattainment area. Advances in Meteorology 2012, p. 12. doi: 10.1155/2012/853405.
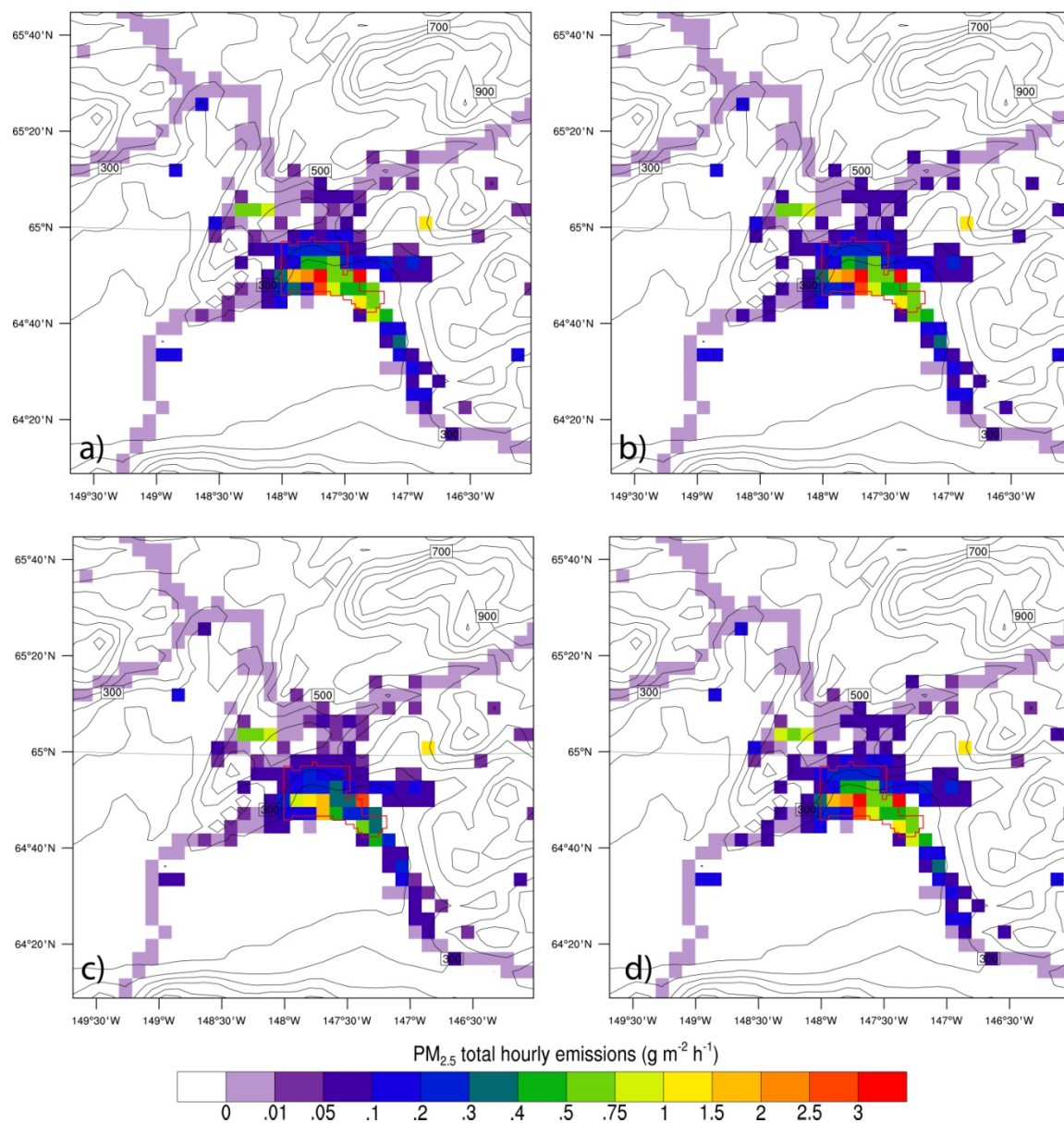
Figure 7.1 A close-up view of PM$_{2.5}$-emissions in (a) REF, (b) WSR, (c) WSS1, (d) WSS2, (e) WSS3 and (f) WSS4 on average over October 01–14, 2008 AST.
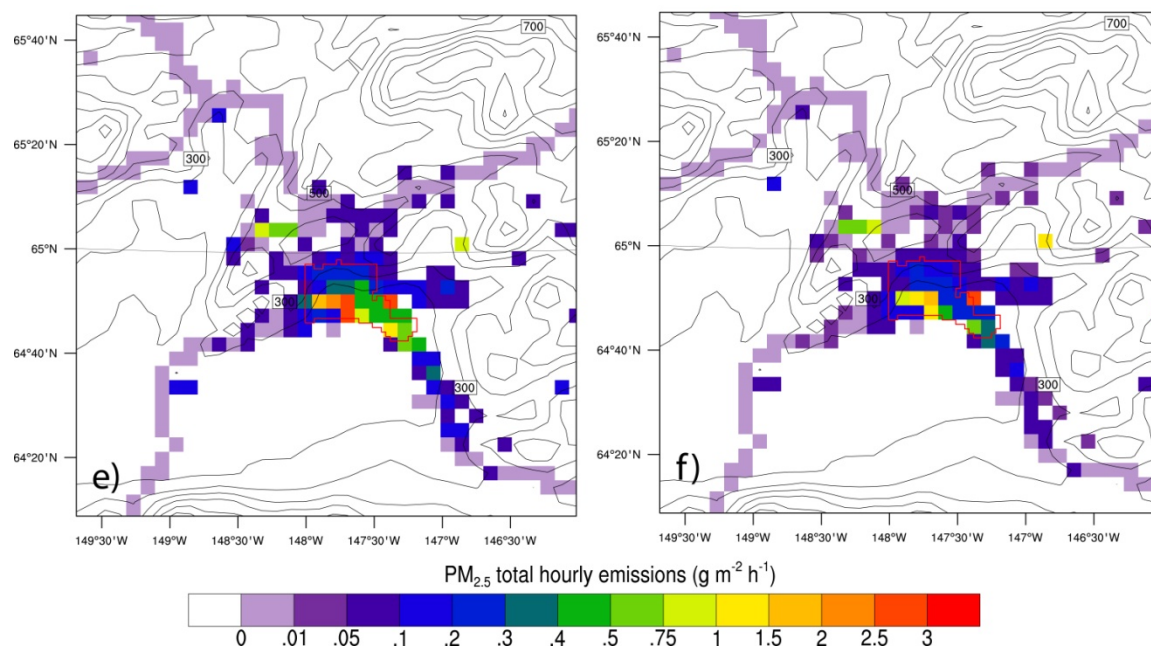
Figure 7.1 (cont.)
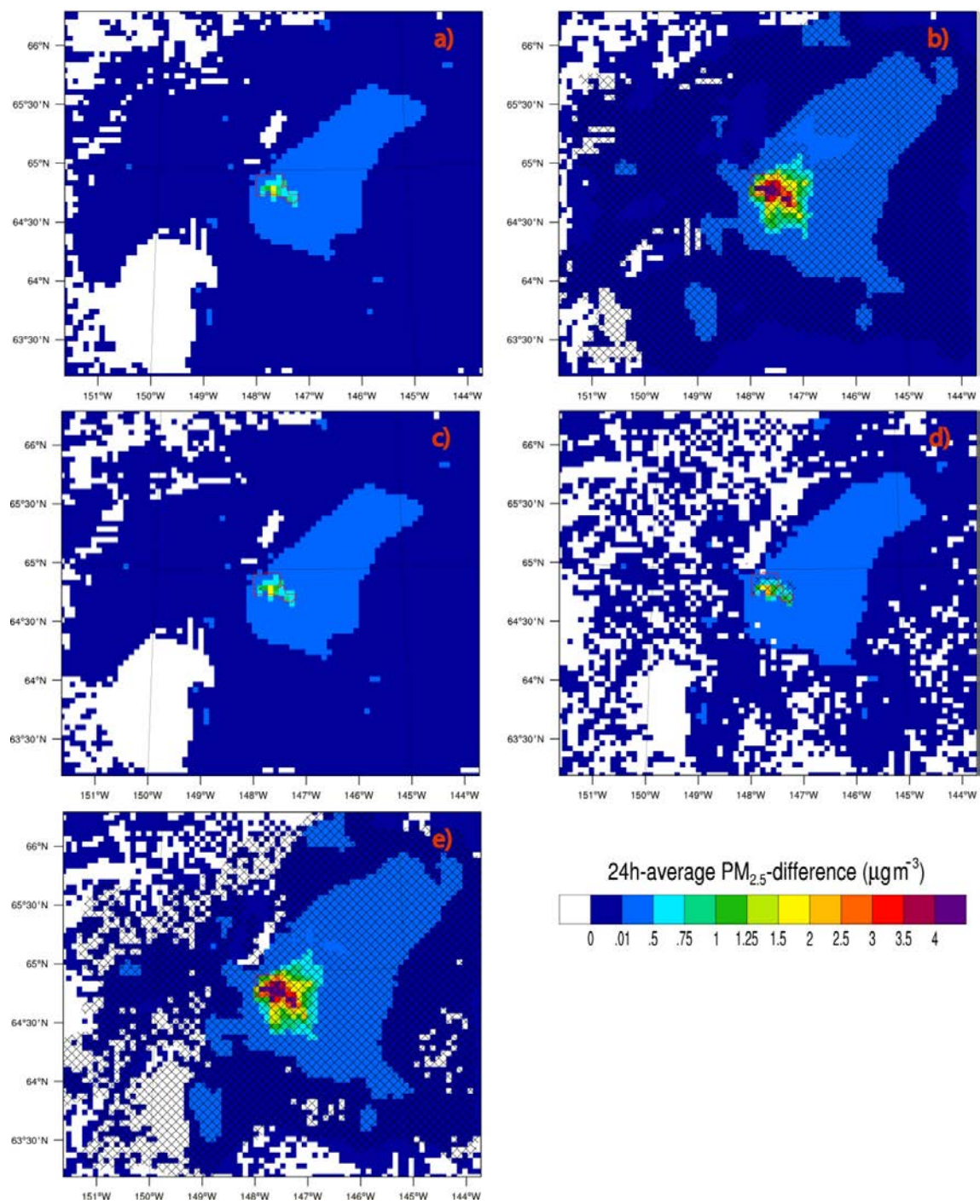
Figure 7.2 A close-up view of the 24h-average PM$_{2.5}$-differences between (a) REF-WSR, (b) REF-WSS1, (c) REF-WSS2, (d) REF-WSS3, (e) REF-WSS4 from October 1 to October 14, 2008 AST.

Chapter 8   Contribution of traffic emissions on the Fairbanks PM$_{2.5}$-nonattainment area

Traffic is considered one of the major contributors to the PM$_{2.5}$-concentrations in many communities (e.g., Querol et al., 2004; Rodríguez et al., 2004). Johnson et al. (2009) estimated that about 30% of the PM$_{2.5}$-concentrations measured in downtown Fairbanks in winter were contributed to by traffic.

As the sniffer travels along the roads collecting data, the mobile measurements include the background PM$_{2.5}$-concentrations combined with those concentrations that could originate either from traffic emissions alone or from the combination of traffic, point-source and area-source emissions. However, as shown by Reponen et al. (2003), beyond 400m from the roads, the contributions of traffic emissions to the aerosol concentrations may vanish.

These facts mean that the mobile measurements could be substantially different from the PM$_{2.5}$-concentrations in the neighborhoods. In such situations, the use of traditional methods (e.g., kriging) to interpolate the mobile measurements into the unmonitored neighborhoods would expose large uncertainty (see Figures 1.2, 1.3). Here, the use of air-quality simulations as a database for an interpolation tool can help to capture the heterogeneity of the contributions of traffic emissions to the PM$_{2.5}$-concentrations.

Therefore, understanding the contributions of traffic emissions to the PM$_{2.5}$-concentrations in Fairbanks is important to assess the information that air-quality simulation data holds on the impact of traffic. For this purpose, simulations with high

horizontal resolution (0.444km×0.444km or better) would provide the best results as it is close to the scale of traffic emissions (Mölders, 2010). However, the emission inventory with the highest resolution that was available for Fairbanks had a 1.3km×1.3km increment, and was therefore used for this study.

In this chapter, simulations using the WRF-CMAQ with (REF) and without (NTE) traffic emissions were performed and their results were compared to investigate the contributions of traffic emissions to the $PM_{2.5}$-concentrations in Fairbanks.

8.1 Reference simulation

Over the nonattainment area, the $PM_{2.5}$-concentrations in the reference simulations were relatively high and were 24µg/m^3 and 23µg/m^3 on average in episode 1 and episode 2, respectively. The distribution of the $PM_{2.5}$-concentrations varied strongly among regions (e.g., Figure 8.1). The $PM_{2.5}$-concentrations were typically high in densely populated areas (e.g., Fairbanks (FB), Badger Road (BG), North Pole (NP)) and they were low in sparsely populated areas (e.g., the hills (HL)) (see Figure 1.1 for locations). In episode 1 (2), the 24h-average $PM_{2.5}$-concentrations were 84 (73), 26 (25), 26 (24), and 6 (8) µg/m^3 on average over FB, NP, BG and in the HL, respectively. The highest 24h-average $PM_{2.5}$-concentrations simulated in the above areas were 249 (213), 148 (129), 190 (168), and 77 (69) µg/m^3 in episode 1 (2). These findings imply that the spatial distribution of $PM_{2.5}$-concentrations was relatively consistent in the two episodes.

The sulfate (SO_4), nitrate (NO_3), ammonium (NH_4), elemental organic carbon (EC), organic carbon (OC) aerosols, and other fine particles made up 10%, 9%, 6%, 5%,

41% and 29%, respectively, of the total $PM_{2.5}$-mass on average over the nonattainment area. However, the partitioning of the $PM_{2.5}$-concentrations substantially differed among locations. At the grid-cells where the 24h-average $PM_{2.5}$-concentrations were typically > $35\mu g/m^3$ (e.g., FB, NP), the corresponding partitionings were 3%, 7%, 3%, 5%, 45% and 32%, respectively. Comparison of the above partitioning of the $PM_{2.5}$-concentrations at polluted grid-cells ($PM_{2.5} > 35\mu g/m^3$) and the partitioning of $PM_{2.5}$-emissions (see section 8.2) suggest that gas-to-particle conversion played a minor role in the simulated $PM_{2.5}$-concentrations. This result agrees with the findings of Mölders and Leelasakultum (2012) that emissions, horizontal transport, and vertical transport are the major processes that determine the distribution of the simulated aerosols in Fairbanks on most winter days. At the grid-cells where the 24h-average $PM_{2.5}$-concentrations were low (<$5\mu g/m^3$, e.g., HL), the CMAQ simulated partitioning of $PM_{2.5}$ into SO_4, NO_3, NH_4, EC, OC and other fine particles was 20%, 10%, 9%, 4%, 30% and 27%, respectively. These grid-cells have no or very low (<10g/h) anthropogenic emissions. Furthermore, their $PM_{2.5}$-concentrations were the combined contributions from advection of polluted air from grid-cells inside the nonattainment area with low SO_4 partitioning (< 3% of total $PM_{2.5}$), and from advection of clean air from outside the nonattainment area where the $PM_{2.5}$-concentrations were close to background concentrations. These background concentrations are dominated by SO_4 and OC (46% and 35%, respectively, of the total $PM_{2.5}$) as these background concentrations were set to the values suggested by Mölders and Leelasakultum (2011). This combined effect explains the high fraction of SO_4 aerosol at grid-cells in the nonattainment area where 24h-average $PM_{2.5}$-concentrations were low.

The simulated $PM_{2.5}$-concentrations are sensitive to meteorological conditions. They typically increased as the simulated air temperature, relative humidity and wind-speed decreased (Figure 3.10). At the SB-site, the simulated 24h-average $PM_{2.5}$-concentration were high ($>50\mu g/m^3$) when the simulated air temperature, wind-speed and relative humidity were below -20^oC, 2m/s and 60%, respectively. Furthermore, surface inversions existed every day over the Fairbanks nonattainment area in both episodes and contributed to these high $PM_{2.5}$-concentrations. The simulated behavior agrees well with the observed features reported by Tran and Mölders (2011). This means that the WRF-CMAQ simulations captured the generally observed $PM_{2.5}$-meteorology relationship. This finding supports the argument to use air-quality simulations as a database for AQuAT.

The simulated wind pattern was similar in episode 1 and episode 2 and played a major role in the distribution of the $PM_{2.5}$-concentrations. Northeasterly winds dominated on most days in episode 1 and episode 2 and advected polluted air towards the southwest. In the nonattainment area, the simulated hourly $PM_{2.5}$-concentrations were typically low ($<30\mu g/m^3$ almost everywhere) when northeasterly or southwesterly winds greater than 3m/s passed over the nonattainment area (Figure 8.1a). Hourly $PM_{2.5}$-concentrations $>40\mu g/m^3$ were simulated everywhere over the FB, NP, BG and part of the HL areas when there were calm (v <0.5m/s) or weak winds ($0.5<v<1$m/s) over the nonattainment area, or when winds came from different directions hindering the transport of polluted air out of the nonattainment area (e.g., Figure 8.1b). The simulated wind patterns indicated that the emissions in the NP area hardly contributed to the $PM_{2.5}$-concentrations in the FB

area during both episodes. On the contrary, the simulated hourly $PM_{2.5}$-concentrations in the BG and NP areas were frequently affected by polluted air advected from the FB area when there were winds from the northeast or northwest over the FB area that slowly drained toward the southeast (e.g., Figure 8.1c). The occasionally southerly or southwesterly winds also advected polluted air from the FB area toward the HL area and caused high $PM_{2.5}$-concentrations ($>35\mu g/m^3$) at some grid-cells in the HL area (e.g., Figure 8.1d).

The above findings mean that the effects of wind-speed and wind-direction should be included in the development of AQuAT. However, it may be sufficient to consider them indirectly as the database already included the underlying effects of wind-speed and wind-direction on the distribution of the $PM_{2.5}$-concentrations.

At grid-cells in the FB, NP and BG areas, correlations between the emission strength and the 24h-average $PM_{2.5}$-concentrations were low (R <0.2, but statistically significant). On the contrary, relatively strong correlations (R >0.4, statistically significant) between the emission strength and the 24h-averaged $PM_{2.5}$-concentrations were found for grid-cells in the HL area. Furthermore, at a grid-cell, the 24h-average $PM_{2.5}$-concentrations typically correlated stronger with the emission strength of its neighboring grid-cells than with the emission strength of itself. These findings mean that the distribution of the 24h-average $PM_{2.5}$-concentrations was more sensitive to the meteorological conditions, which drive the dispersion of $PM_{2.5}$-concentrations, than to the emission strength. It was also more sensitive to the meteorological conditions in the grid-cells in polluted areas (i.e., FB, NP, BG) than in the clean area (i.e., HL).

8.2 Traffic emissions

Over both episodes, traffic contributed 7% to the total $PM_{2.5}$-emissions on average over the domain and it was the largest contributor to the $PM_{2.5}$-emissions outside the nonattainment area (Figure 8.2). In the nonattainment area, traffic emissions contributed 10g/h to the total $PM_{2.5}$-emissions rate of 509g/h, on average, which was equivalent to 3% and varied with source activities. Traffic emissions contributed about 2.6, 3.7, 2.4, and 1% to the total $PM_{2.5}$-emissions on average over the FB, BG, NP and the HL areas, respectively (Figure 8.2). In the nonattainment area, traffic emissions made up about 50%, <1%, 22%, 17% of the total emissions of carbon monoxide (CO, 221 mole/h), sulfur dioxide (SO_2, 20 mole/h), nitrogen oxide compounds (NO_x, 4 mole/h), and volatile organic compounds (VOC, 46 mole/h), respectively. For both episodes, most (99%) of the ammonia (NH_3) emissions came from traffic but their total emission was very low (0.8 mole/h).

Of the total $PM_{2.5}$-emissions in REF, 51%, 9% and 38% were OC, EC, and other fine particles, respectively. $PM_{2.5}$-emissions in the form of SO_4 and NO_3 were very low (about 1%). The partitioning of the $PM_{2.5}$-emissions in NTE marginally differed from that in the REF (52%, 7%, 39%, ~1% and ~1% for OC, EC, other fine particles, SO_4 and NO_3, respectively).

8.3 Contributions of traffic emissions

The contributions of traffic emissions to the $PM_{2.5}$-concentrations in the Fairbanks nonattainment area marginally differed between episode 1 and 2. In the nonattainment area during episode 1 (2), the highest 24h-average $PM_{2.5}$-concentration simulated on any day was 274.4 (213.5) µg/m^3 and 257.1 (193.5) µg/m^3 in REF and NTE, respectively. On average over the nonattainment area for episode 1, the 24h-average $PM_{2.5}$-concentrations were 24.0 and 21.5µg/m^3 in REF and NTE, respectively. The corresponding values for episode 2 were 23.1 and 21.0µg/m^3, respectively. This means traffic contributed about 10% to the 24h-average $PM_{2.5}$-concentrations, on average over both episodes and over the nonattainment area.

The highest 24h-average $PM_{2.5}$-differences (REF-NTE) obtained on any day in episode 1 and 2 were 24.0 and 20.0µg/m^3, respectively, which were obtained at grid-cells in the FB area. At the SB-site, the average and the standard deviation of $PM_{2.5}$-differences obtained in episode 1 (2) were 5.7µg/m^3 and 2.9µg/m^3 (5.0µg/m^3 and 2.7µg/m^3), respectively. The highest 24h-average $PM_{2.5}$-differences obtained at any day at this site during episode 1 and 2 were 13.8µg/m^3 and 11.4µg/m^3, respectively. These findings imply that the mobile $PM_{2.5}$-measurements can be higher than the $PM_{2.5}$-concentrations in the neighborhood. It supports the suitability of air-quality simulations as a database for AQuAT to minimize the impact of traffic emission effects on the interpolation of the mobile measurements.

The amount of $PM_{2.5}$-differences obtained in the FB, NP, BG and HL areas were 3.6, 2.8, 3.3 and 0.3µg/m^3, respectively. The corresponding values for episode 2 were 3.1,

2.4, 2.5, 0.2µg/m^3. These values equal to traffic contributions of 10-12% to the PM$_{2.5}$-concentrations in the FB, NP, BG areas, and of only 3% to the PM$_{2.5}$-concentrations in the HL area, on average over the two episodes. Given that traffic emissions only contributed about 1% to the total PM$_{2.5}$-emissions in the HL area, the PM$_{2.5}$-concentrations in this area seem to be heavily governed by the traffic contributions in other areas of the nonattainment area as advection of the polluted areas to HL area occurred frequently as discussed in section 8.1. These findings illustrate the nonlinear impact of the traffic emissions on PM$_{2.5}$-concentrations. Furthermore, they imply that the mobile PM$_{2.5}$-measurements could significantly differ from the PM$_{2.5}$-concentrations in the neighborhoods. These findings support the need of air-quality simulations as a database for AQuAT to capture those nonlinear effects.

The magnitude of the PM$_{2.5}$-differences was sensitive to the meteorological conditions, especially wind-speed. On average over the nonattainment area, the magnitude of the PM$_{2.5}$-differences was low (<1µg/m^3) when the simulated wind-speed at the SB-site was greater than 2.5m/s. It was high (>3µg/m^3) when calm or weak wind (v$<$1m/s) dominated over the nonattainment area.

The partitioning of the simulated PM$_{2.5}$-concentrations marginally differed between NTE and REF. In NTE, the SO$_4$, NO$_3$, NH$_4$, EC, OC and other fine particles are about <0.01, 1.1, 0.41, 0.18, 0.33 and 0.11µg/m^3, on average, lower than in REF. This finding justifies the use of mobile observed PM$_{2.5}$-concentrations for AQuAT to interpolate the PM$_{2.5}$-concentrations in the neighborhoods as there is marginal difference in the partitioning of these concentrations. Among all PM$_{2.5}$-aerosols, NO$_3$ and NH$_4$

aerosols have the greatest contribution to the $PM_{2.5}$-concentrations from traffic when NTE is compared with REF. The reasons for this finding can be explained as followed: as shown by Mölders and Leelasakultum (2012), gas-to-particle conversion is involved in the NO_3 and NH_4-aerosol formation, but hardly involved in the SO_4-aerosol formation; the low temperatures (2m air temperature $< -20^oC$) that occurred on many days in both episodes favor the formation of NO_3 aerosol over that of nitric acid. Since traffic strongly contributed to the NH_3 and NO_x-emissions (see section 8.2), it greatly contributed to the concentrations of NO_3 and NH_4-aerosols (by 41% and 40%, respectively). Nevertheless, since the fractions of NO_3 and NH_4 aerosols of total $PM_{2.5}$ are small, and because most of the simulated $PM_{2.5}$ originated from primary emissions, the contribution of NO_3 and NH_4 aerosols from traffic made up only a small fraction of the total $PM_{2.5}$.

The average RRF to "no traffic" obtained at the SB-site is 0.867 (0.882) in episode 1 (2). The highest RRF obtained at any time at this site is 0.789. The lowest RRFs typically occurred at grid-cells in the HL area (0.969 on average) whereas relatively stronger RRFs were obtained in the FB, NP and BG areas (0.901, 0.874 and 0.878, respectively). The highest RRF for polluted grid-cells (24h-averaged $PM_{2.5}$-concentration $>35\mu g/m^3$) in the nonattainment area was 0.681 (0.747) in episode 1 (2). At these grid-cells, RRFs of ~1 also occurred on several days. This finding illustrates the heterogeneity of the contribution of traffic to the $PM_{2.5}$-concentrations, and supports the need of air-quality simulations as a database for AQuAT to capture this information.

8.4 Conclusions

The WRF-CMAQ simulations had been performed from 12/27/2009 to 01/12/2010 and from 01/01/2011 to 01/30/2011 with and without consideration of traffic emissions to investigate the contribution of traffic to the $PM_{2.5}$-concentrations in Fairbanks during these winter episodes when the observed $PM_{2.5}$-concentrations exceeded the NAAQS. The evaluation of the REF simulations showed that WRF-CMAQ performed relatively well in simulating $PM_{2.5}$-concentrations (see section 4.2.3). Therefore, its results are valuable for investigating the above purpose, and for serving as a database for AQuAT.

Traffic emissions contributed about 3% to the total $PM_{2.5}$-emissions from all sources in the nonattainment area. However, traffic contributed relatively large amounts to the total emissions of $PM_{2.5}$-precursor gases, such as NO_x (22%), NH_4 (99%) and VOC (17%), than all other sources in the nonattainment area. The results showed that contributions of traffic emissions to the $PM_{2.5}$-concentrations substantially differed among locations in the Fairbanks nonattainment area. Traffic emissions contributed about 2.6, 3.7, 2.4, and 1% of the total $PM_{2.5}$-emissions on average over the FB, BG, NP and the HL areas, respectively. This spatial distribution of traffic emissions drives the spatial distribution of the 24h-average $PM_{2.5}$-differences (REF-NTE) accordingly (10-12% of $PM_{2.5}$-concentrations in the FB, NP, BG areas and only 3% in the HL area on average over the two episodes). The obtained RRFs were also strongest in the FB, NP and BG areas (0.874-0.901) and lowest in the HL area (0.969).

Overall, traffic emissions contributed about 10% to the $PM_{2.5}$-concentrations in the Fairbanks nonattainment area. The fact that WRF-CMAQ was found to underestimate the formation of $PM_{2.5}$ via gas-to-particle conversion, as shown in this study and by Mölders and Leelasakultum (2012), may also mean that WRF-CMAQ underestimated the contributions of traffic to the $PM_{2.5}$-concentrations in the nonattainment area.

The findings on the spatial and temporal heterogeneity of the contributions of traffic emissions to the $PM_{2.5}$-concentrations support the need of air-quality simulations as a database for AQuAT to capture this information.

The findings on the contribution (3-12%) of traffic emissions to the $PM_{2.5}$-concentrations in the Fairbanks nonattainment area imply that the mobile $PM_{2.5}$-measurements, which are the response to a mixture of traffic and other sources, can be higher than the $PM_{2.5}$-concentrations in the neighborhood where the contributions from traffic vanish due to the strong dilution of the pollutants from traffic as shown in the previous studies (e.g., Zhu et al., 2002; Reponen et al., 2003). These findings imply that using the traditional interpolation methods to interpolate mobile measurements into unmonitored neighborhoods would expose large uncertainty.

These findings, in conjunction with the findings for the contributions of point-sources and wood-burning devices, support the suitability of air-quality simulations as a database for AQuAT to capture the heterogeneity of the $PM_{2.5}$- emission-concentration relationships and to minimize the impact of traffic emissions on the mobile measurements in the interpolation process.

References

Johnson, R., Marksik, T., Lee, M., Cahill, C.F., 2009. Helping Fairbanks meet new air quality requirements: Developing ambient PM-2.5 management strategies. In Transportation safety, security, and innovation in cold regions vol. 3, no. 1, Alaska Transportation Research Center, p. 1.

Mölders, N., 2010. Assessment of the contribution of traffic emissions to the mobile vehicle measured $PM_{2.5}$ concentrations by means of WRF-CMAQ simulations. Research proposal to the Alaska University Transportation Center, AUTC Project Number: 410003, p. 24.

Mölders, N., Leelasakultum, K., 2011. Fairbanks North Star Borough $PM_{2.5}$ nonattainment area CMAQ modeling: Final report phase I. Report, p. 62.

Mölders, N., Leelasakultum, K., 2012. Fairbanks North Star Borough $PM_{2.5}$ nonattainment area CMAQ modeling: Final report phase II. Report, p. 66.

Querol, X., Alastuey, A., Viana, M.M., Rodriguez, S., Artiñano, B., Salvador, P., Santos, S.G.d., Patier, R.F., Ruiz, C.R., Rosa, J.d.l., Campa, A.S.d.l., Menendez, M., Gil, J.I., 2004. Speciation and origin of PM10 and PM2.5 in Spain. Journal of Aerosol Science, 35, pp. 1151-1172.

Reponen, T., Grinshpun, S.A., Trakumas, S., Martuzevicius, D., Wang, Z.-M., LeMasters, G., Lockey, J.E., Biswas, P., 2003. Concentration gradient patterns of aerosol particles near interstate highways in the Greater Cincinnati airshed. Journal of Environmental Monitoring, 5, pp. 557-562.

Rodríguez, S., Querol, X., Alastuey, A., Viana, M.a.-M., Alarcón, M., Mantilla, E., Ruiz, C.R., 2004. Comparative PM10–PM2.5 source contribution study at rural, urban and industrial sites during PM episodes in Eastern Spain. Science of the Total Environment, 328, pp. 95-113.

Tran, H.N.Q., Mölders, N., 2011. Investigations on meteorological conditions for elevated $PM_{2.5}$ in Fairbanks, Alaska. Atmospheric Research, 99, pp. 39-49.

Zhu, Y., Hinds, W.C., Kim, S., Sioutas, C., 2002. Concentration and size distribution of ultrafine particles near a major highway. Journal of the Air & Waste Management Association, 52, pp. 1032-1042.
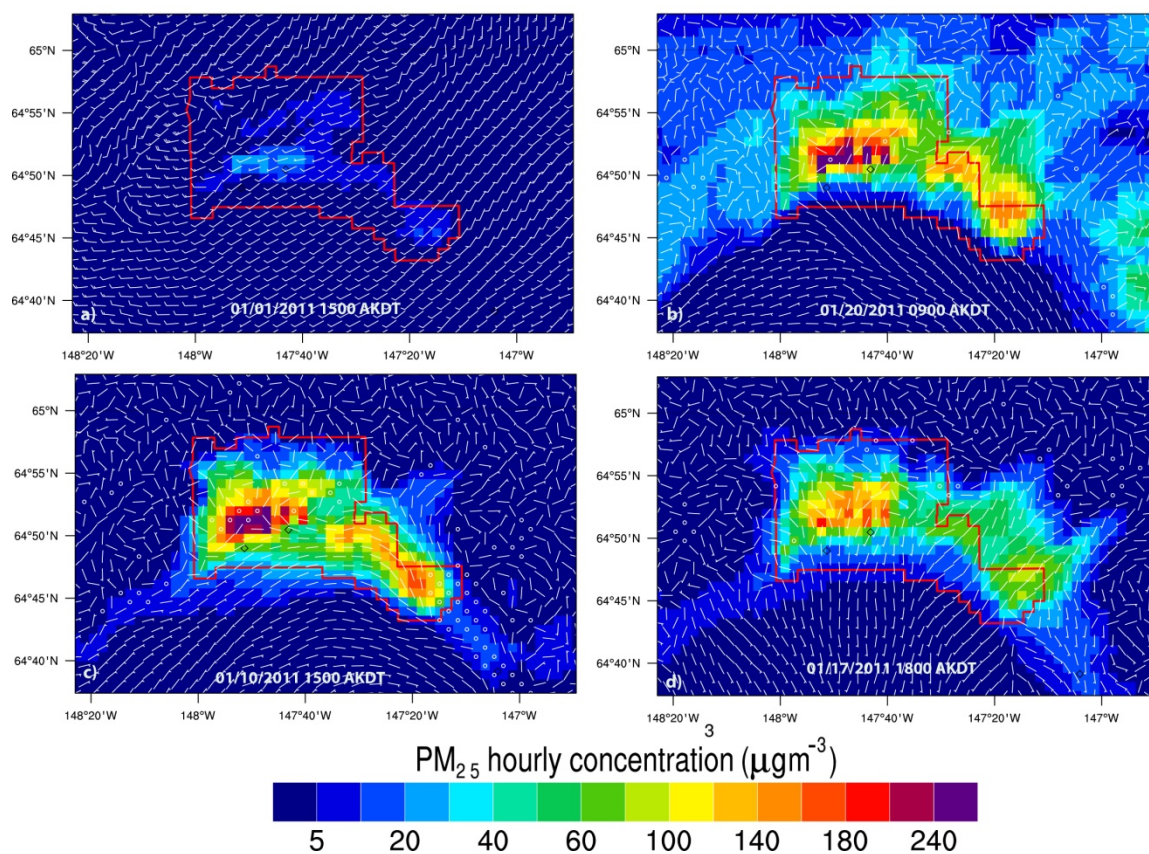
Figure 8.1. A close-up view of typical wind-circulation patterns at breathing level that were associated with (a) low PM$_{2.5}$-concentrations ($<30\mu g/m^3$) and (b, c, d) highly polluted PM$_{2.5}$-concentrations ($>40\mu g/m^3$) in the nonattainment area in episode 1 and episode 2. The red polygon indicates the nonattainment area. See text for discussion.
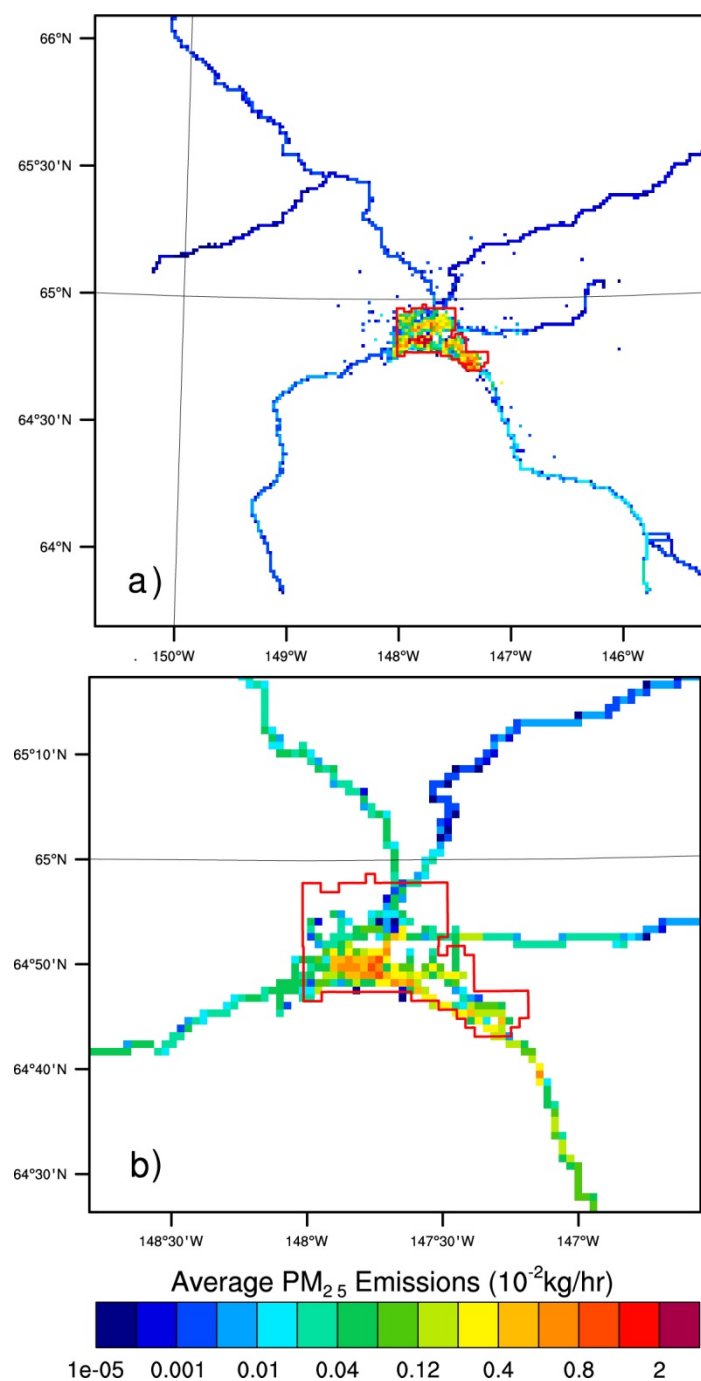
Figure 8.2 (a) Average $PM_{2.5}$-emissions in REF and (b) close-up view of the $PM_{2.5}$-emissions differences (REF-NTE) for episode 2. The red polygon indicates the Fairbanks $PM_{2.5}$-nonattainment area. Similar emission patterns were found for episode 1 (therefore not shown).

Chapter 9   A tool for public PM$_{2.5}$-concentration advisory based on mobile measurements

9.1 Introduction

As demonstrated in chapter 1, the traditional interpolation methods are not able to spatially interpolate the mobile measurements into the unmonitored neighborhood in a reasonable way due to the nonlinear relationships between PM$_{2.5}$-concentrations and meteorology, and between PM$_{2.5}$-concentrations and emissions from various types of sources. Here, an interpolation tool that combines the outputs from air-quality simulations with mobile PM$_{2.5}$-measurements is proposed as air-quality simulations can include such information.

The findings of chapter 4 showed that the air-quality simulations used in this dissertation can reproduce the observed PM$_{2.5}$-meteorology relationship well. The findings of chapters 5, 6, 7 and 8 demonstrated that there exists spatial heterogeneity of the contributions from point sources, wood-burning device changeouts, uncertified wood-burning devices in general, and traffic to the PM$_{2.5}$-concentrations. These findings support the argument for the use of air-quality simulations as a database for AQuAT.

The findings of chapter 6 also showed that the wood-burning device changeouts, introduced in 2010, may or may not appreciably affect the PM$_{2.5}$-concentrations depending on the number of wood-burning devices actually exchanged or existing in total, and on the burning behavior. Consequently, this changeout program could potentially impact the performance of AQuAT as its database was performed with an emission inventory that did not consider this changeout program.

Nevertheless, given the current uncertainty in the data on the wood-burning device changeouts and woodstoves in general, the air-quality simulations used in this dissertation are considered suitable for the AQuAT development.

In this chapter, the AQuAT is presented in section 9.2 which is based on an in print journal article. AQuAT uses simulations performed with the Alaska adapted WRF-CMAQ for Fairbanks for winter 2009/2010 episode (December 27, 2009 to January 12, 2010) as its database. Simulations with WRF-CMAQ for this episode were selected for the database as they had an 1.3km×1.3km horizontal resolution which resolves the spatial scale better than the 4km×4km resolution of the WRF/Chem simulations used in this dissertation. Furthermore, the evaluation showed that the performance of the selected WRF-CMAQ simulations fell in the range of state-of-the-art models (see chapter 4).

The findings of chapter 3 showed that air temperature, wind-speed and inversion strength are the most important factors that drive the observed $PM_{2.5}$-concentrations in Fairbanks. Their roles for the performance of AQuAT were also investigated. However, given the fact that the objective of AQuAT is to provide a public spatially differentiated air-quality advisory, observations of the above meteorological quantities must be accessible when a drive is completed. The observations of the inversion strength do not fulfill this criterion as they are measured at the radiosonde site located in the Fairbanks International Airport in twice per day and are not instantly accessible. Therefore, inversion strength was not considered in the sensitivity study.

9.2 A tool for public PM$_{2.5}$-concentration advisory based on mobile measurements[1]

Abstract

A tool was developed that interpolates mobile measurements of PM$_{2.5}$-concentrations into unmonitored areas of the Fairbanks nonattainment area for public air-quality advisories. The tool uses simulations with the Alaska adapted version of the Weather Research and Forecasting (WRF) and the Models-3 Community Multiscale Air Quality (CMAQ) modeling system as a database. The tool uses the GPS-data of the vehicle's route, and the database to determine linear regression equations for the relationships between the PM$_{2.5}$-concentrations at the locations on the route and those outside the route. Once the interpolation equations are determined, the tool uses the mobile measurements as input into these equations that interpolate the measurements into the unmonitored neighborhoods.

An episode of winter 2009/2010 served as the database for the tool's interpolation algorithm. An independent episode of winter 2010/2011 served to demonstrate and evaluate the performance of the tool. The evaluation showed that the tool well reproduced the spatial distribution of the observed as well as simulated concentrations. It is demonstrated that the tool does not require a database that contains data of the episode for which the interpolation is to be made. Potential challenges in applying this tools and its transferability are discussed critically.

---

[1] Tran, H.N.Q., Leelasakultum, K., Mölders, N., 2012. A tool for public PM$_{2.5}$-concentration advisory based on mobile measurements. Journal of Environmental Protection *(in print)*, p. 18

9.2.1 Introduction

As observations indicated that concentrations of particulate matter with diameter equal or less than 2.5µm ($PM_{2.5}$) exceeded the Environmental Protection Agency 24-hour National Ambient Air Quality standard (NAAQS) of 35µg/m^3 periodically in Fairbanks, Alaska during the past years [1], Fairbanks was assigned a $PM_{2.5}$-nonattainment area. In winter 2008/2009, the Fairbanks North Star Borough started measuring $PM_{2.5}$-concentrations along roads in commercial and residential areas with instrumented vehicles (called sniffer hereafter) (Figure 9.1) to obtain a broad picture of the $PM_{2.5}$-concentration distribution within the nonattainment area and for public air-quality advisories. For public advisory, however, it is desirable to show spatial distributions rather than data along the vehicle routes. Such spatial distributions require intelligent interpolation.

Various studies investigated the accuracy of procedures applied to interpolate concentrations of chemically reactive gases and particles into space. One study [2], for instance, used data of ozone and particulate matter with aerodynamic diameter less than 10µm (PM_{10}) from stationary monitoring sites and left out data from one site to compare the spatial averaging, nearest neighbor, inverse distance weight and the kriging interpolation methods. This cross-validation suggested that all tested interpolation methods performed reasonably well and the kriging method provided the least biases. Application of the universal kriging procedure for spatial interpolation of ozone data from ten monitoring stations to all zip-code areas in Atlanta, Georgia showed that over 1993 to 1995, the ozone distribution highly correlated with the wind fields [3]. This study

also suggested that the Atlanta ozone-nonattainment area would expand from 56% under the 1h ozone-standard to 88% under the 8h ozone-standard of the Atlanta metropolitan statistical area.

While many studies apply these traditional interpolation methods in areas of sufficient data density, these methods may be problematic in areas of sparse data density [4]. The distribution of air pollutants namely is a function of many factors such as atmospheric conditions, land-use, sources (e.g., emissions, chemical reactions) and sinks (e.g., chemical reactions, deposition) [5]. These factors can vary substantially in space and time. Thus, interpolating data from sparse monitoring networks based alone on statistics of observations may provide inadequate results [4]. Therefore, first efforts were made to develop procedures that add other information to provide interpolated values. Fuentes and Raftery [6], for instance, suggested to combine observations from the Clean Air Status and Trends Network with output from an air-quality model in a Bayesian way to obtain a high-resolution sulfur dioxide distribution over the US for model evaluation. Their interpolation approach incorporated information on the emissions and underlying driving physical and chemical processes.

In this study, we present a tool to interpolate mobile measurements of $PM_{2.5}$-concentrations over the Fairbanks nonattainment area. We developed this tool by combining the output from the Weather Research and Forecasting (WRF; [7]) and the Models-3 Community Multiscale Air Quality (CMAQ; [8]) modeling systems in its Alaska adapted version [9] as a database to determine the equations needed to interpolate

the mobile $PM_{2.5}$-concentration observations into unmonitored neighborhoods. The tool is to provide spatial distributions of $PM_{2.5}$-concentrations for public air-quality advice.

9.2.2 Simulations

9.2.2.1 Model setup

The meteorological conditions were simulated by WRF version 3.2 in forecast mode using three nested domains (Figure 9.2; [10]). The outermost domain (domain 1) encompasses Alaska, and parts of Siberia, the North Pacific and Arctic Ocean with 400×300grid-cells of 12km increment. Domain 2 covers Interior Alaska with 201×201grid-cells of 4km increment. The inner most domain (domain 3) encompasses the nonattainment area and western part of the Fairbanks North Star Borough with 201×201grid-cells of 1.3km increment. The simulations were performed concurrently on all three domains in one-way coupled mode. This means the boundary conditions for each child domain stem from its parent domain, but the child domain does not feedback to the simulation of the parent domain. The physical options (Table 9.1) were chosen based on the experience from previous modeling studies over Alaska for winter [10-12].

Table 9.1 Parameterizations used in the WRF simulations

Processes	Scheme and reference
Cloud microphysics	Six water-class cloud microphysical scheme [13]
Subgrid-scale convection	Improved 3D-version of the Grell-Dévényi cumulus-ensemble scheme [14]
Radiation	Goddard shortwave radiation scheme [15], Radiative Transfer Model for long-wave radiation [16], Radiative feedback from aerosols [17]
Atmospheric boundary layer and sublayer processes	Mellor-Yamada-Janjić scheme [18]
Land-surface processes	Modified version of the Rapid Update Cycle land-surface model [19]

The CMAQ-simulations were performed driven by the WRF-simulated meteorology of domain 3. We used CMAQ in its Alaska adapted version [9]. Parameters needed by CMAQ, but not provided by WRF were diagnosed by the Meteorology-Chemistry Interface Processor [20] with the modifications given in [9]. Gas-phase chemistry was treated in CMAQ by the Carbon-Bond mechanism [21]. Aerosol chemistry was calculated by the fifth-generation CMAQ-aerosol model [22]. Aqueous chemistry was treated following the so-called RADM mechanism [23]. The treatment of secondary organic aerosol chemistry and physics was based on the so-called SORGAM [24] with the modifications of the gas-phase chemistry fields and saturation concentrations for aromatics, terpenes, alkanes and cresols as documented by Buyn et al. [20]. Horizontal and vertical advections were calculated using the global mass-conserving scheme [25].

Horizontal diffusion was determined based on diffusion coefficients derived from local wind deformation [8]. Vertical diffusion was calculated using the K-theory approach [9, 26].

We used the modifications tested and implemented for Alaska conditions [9]. The modifications include slightly lower minimum and maximum thresholds for the eddy diffusivity coefficients and a reduction of the minimum mixing height from 50m to 16m as observed in Fairbanks. Dry deposition of aerosols and gases was treated according to the standard procedure in CMAQ [20], but was enlarged for dry deposition on snow and Alaska-specific vegetation [27] and onto the various types of tundra [9].

9.2.2.2 Emission inventory

Anthropogenic emissions stem from the first version of the Fairbanks 2008 emission inventory provided by Sierra Research Inc. [pers. comm., March 2011]. To apply this emission inventory to winter 2009/2010 and winter 2011, we assumed an emission increase of 1.5%/year in accord with other studies [27, 28]. The Sparse Matrix Operator Kernel Emissions Model [29, 30] served to allocate these "updated" emissions onto the CMAQ-domain in time and space based on the information on emission-source activities, land-use and population density within each grid-cell.

Anthropogenic emissions include emissions from point sources, area sources, traffic and non-road traffic. We applied a temperature-adjustment factor to the temporal allocation of the anthropogenic emission. Herein, emissions will be higher (lower) on

days having daily mean temperatures below (above) the 1970-1999 monthly mean temperature [28, 31].

9.2.2.3 Simulations

The meteorological initial and boundary conditions for domain 1 were downscaled from the $1^o \times 1^o$, 6h-resolution National Centers for Environmental Prediction global final analyses. The meteorology was initialized every five days. Alaska typical background concentrations served as initial condition for the chemical fields [9]. Note that various studies [28, 32, 33] showed hardly any advection of $PM_{2.5}$ of notable concentrations ($>2\mu g/m^3$) into Interior Alaska. To spin up the chemical fields we started the simulation three days prior to the period of interest. The chemical fields at the end of a simulation served as the initial conditions for the simulation of the next day.

We performed simulations for two episodes that had mobile measurements and occasional $PM_{2.5}$-concentrations above the NAAQS at the official monitoring site at the State Office Building or other sites. We used episode 1 (December 27, 2009 to January 11, 2010) to build the database needed by the tool that we developed. We used episode 2 (January 1 to 30, 2011) for evaluation of the developed tool. Not every day of these episodes had sniffer measurements. In total, there were 13 and 14 sniffer drives with 49h and 30h of data during episode 1 and 2, respectively.

9.2.2.4 Model evaluation

Meteorological surface observations were available at 14 and 18 sites for episode 1 and 2, respectively, from the Western Regional Climate Center and the National Climate Data Center (Figure 9.2).

PM$_{2.5}$-observations were available at the State Office Building (SB), Peger Road (PR), Pioneer Road (NCORE), in the community of North Pole (NP), and at the Relocatable Air Monitoring System (RAMS) trailer locations (Figure 9.1). Hourly observations of total PM$_{2.5}$-mass measured by Met-One Beta Attenuation Monitors were available at the SB (called SB_BAM hereafter) and the RAMS (RAMS_BAM). Filter based 24h-average PM$_{2.5}$-concentrations using the Federal Reference Method were available at the SB (called SB_FRM hereafter), RAMS (RAMS_FRM), NP, PR and NCORE on a 1-in-3-days basis. The SB and NCORE sites are located in commercial-residential area whereas the PR and NP-sites are located in mixed industrial-residential areas. During episode 1 and 2, the RAMS was located in a residential area. During episode 2, the RAMS was located about 1.5km north of its location during episode 1. Since there had been repeatedly technical problems with the RAMS during episode 2 [J. Conner, pers. comm., June 2009], we excluded the RAMS-observations from the evaluation of episode 2.

We calculated performance skill–scores [34] to evaluate the WRF-performance with respect to simulating meteorological quantities. These skill scores include the mean bias, root–mean–square error (RMSE), standard deviation of error (SDE), and the correlation coefficient (R).

We evaluated the CMAQ-simulated $PM_{2.5}$-concentrations by the fractional bias $(FB = 200\% \times [\sum_{i=1}^{N}(C_{s,i} - C_{o,i})/\sum_{i}^{N}(C_{s,i} + C_{o,i})])$, fractional error $(FE = 200\% \times [\sum_{i=1}^{N}|C_{s,i} - C_{o,i}|/\sum_{i}^{N}(C_{s,i} + C_{o,i})])$, normalized mean bias $(NMB = 100\% \times [\sum_{i=1}^{N}(C_{s,i} - C_{o,i})/\sum_{i=1}^{N}C_{o,i}])$, normalized means error $(NME = 100\% \times [\sum_{i=1}^{N}|C_{s,i} - C_{o,i}|/\sum_{i=1}^{N}C_{o,i}])$, mean fractional bias $(MFB = (200\%/N) \times \sum_{i=1}^{N}[(C_{s,i} - C_{o,i})/(C_{s,i} + C_{o,i})])$, and mean fractional error $(MFE = (200\%/N) \times \sum_{i=1}^{N}[|C_{s,i} - C_{o,i}|/(C_{s,i} + C_{o,i})])$ [e.g., 35, 36]. Here N is the number of pairs of simulated (C_s) and observed (C_o) $PM_{2.5}$-concentrations. In addition, we determined the percentage of pairs of simulated and observed $PM_{2.5}$-concentrations that agreed within a factor of two (FAC2). The correlation-skill score R between simulated and observed quantities was tested for its statistical significant using t–tests at the 95% confidence level.

9.2.3 Tool development

9.2.3.1 Mobile measurements

The mobile measurements encompass GPS-coordinates, $PM_{2.5}$-concentrations and ambient air temperature recorded every 2 seconds while the vehicle traveled at up to 48km/h. We performed a quality assurance/quality control (QA/QC; for details see [28]) on all mobile measurements. This QA/QC discarded all temperature and $PM_{2.5}$-data for which the measured temperature deviated more than the 1971-2000 monthly-mean diurnal temperature range from the mean temperature determined from all temperature-data of the respective drive. This QA/QC ensured to discard data taken when the vehicle pulled out and the sensors were still adjusting to the outside air. The QA/QC-procedure

also discarded all PM$_{2.5}$-concentrations that differed >5µg/m^3 between two consecutive measurements to avoid errors from plumes from buses or trucks that emit at about the sniffer height (~2.44m) and may have hit the sniffer.

We developed the interpolation tool using the output of the CMAQ simulations of the first episode as a "grand truth" as there was no special field campaign that provided high spatial resolution measurements in the nonattainment area. Thus, the spatial resolution of the interpolated mobile measurements is 1.3km, i.e. the same as the CMAQ-simulation. The tool requires a database of PM$_{2.5}$-concentrations simulated by CMAQ or any other air-quality model. In this study, we used PM$_{2.5}$-concentrations simulated by CMAQ in episode 1 as the database. This database is called CMAQ-database hereafter. It has 2592 PM$_{2.5}$-concentrations at each of the 395 grid-cells in the nonattainment area, i.e. 1,023,840 data in total.

As is demonstrated later, the database does not require air-quality model simulations of the episode for which measurements are to be interpolated. The database just needs to cover the range of measurements and ideally should represent similar conditions. The advantage of this concept is that users do not have to run an air-quality model each time when they want to interpolate mobile measurements.

The CMAQ-database serves to establish the linear-regression of the PM$_{2.5}$-concentration at the grid-cell, for which a concentration has to be interpolated, with the PM$_{2.5}$-concentration at the grid-cells traveled by the sniffer. These linear-regression equations – called interpolation equations hereafter - base on simulated data only. Thus,

the tool permits to provide these relationships for any travelled route. This means the tool does not become useless when new roads are constructed or the vehicle is detoured.

The basic operational concept of the tool, data flow and technical steps are schematically viewed in Figure 9.3. Once measurements are taken, the above mentioned QA/QC is performed (see [28] for details). The QA/QC approved $PM_{2.5}$-measurements are projected onto the grid using the GPS-data. Then the tool averages over all QA/QC approved observations that were taken in the same grid-cell and hour. This averaging leads to one value per hour for each grid-cell on the route during that hour. These averaged concentrations are called "observed concentrations" hereafter.

To develop the interpolation equations the tool determines the route based on the GPS data of the drive. In this step of deriving the interpolation equations, the tool uses the CMAQ-database (Figure 9.3). An interpolation equation is determined for each grid-cell i that is not on the route

$$C_{Mi(dtb)} = \sum_{j=1}^{N} a_j \cdot C_{Mj(dtb)} + b \qquad (9.1)$$

Here $C_{Mi(dtb)}$ are the concentrations form the database in the neighborhood at the grid-cell i for which the interpolation is to be done. Furthermore, $C_{Mj(dtb)}$ are the concentrations j=1,…, N in the database at the N grid-cells on the route, and a_j and b are the linear-regression coefficients, respectively. Furthermore, M is the number of data for each grid-cell in the CMAQ-database. Recall that this database was obtained from the CMAQ-simulations on a 1-in-10-minutes basis at each grid-cell. Thus, when using episode 1 as the database M=2592 at each grid-cell. The determination of the interpolation equation (1) leads to the coefficients a_j and b based on least-square linear-regression.

Once the tool has determines the coefficients a_j and b using the database, we have for each grid-cell one equation of the type

$$C_{i(nbh)} = \sum_{j=1}^{N} a_j \cdot C_{j(dtb)} + b \qquad (9.2)$$

At the start of the algorithm development, by using the CMAQ-database the tool considers all the concentrations at all N grid-cells on the route in determining the a_j and b coefficients. In the next step, it determines an adjusted determination coefficient

$$R_{adj}^2 = 1 - \frac{\sum_{m=1}^{M}(C_{mi(dtb)} - C_{mi(nbh)})^2 (M-1)}{\sum_{m=1}^{M}(C_{mi(dtb)} - \overline{C_{i(dtb)}})^2 (M-N-1)} \qquad (9.3)$$

to assess the accuracy of Equation (9.2). In Equation (9.3), $\overline{C_{i(dtb)}}$ is the mean of the M concentrations at i from the database. Note that so far only the GPS-observations are used to determine the route and to derive the coefficients aj and b using the database.

As suggested by Equation (9.3), the closer R_{adj}^2 is to 1, the lower is the interpolation error. The magnitude of R_{adj}^2 increases (decreases) when those concentrations $C_{mj(dtb)}$, m=1,.., M on the route (j=1,…, N) available in the CMAQ-database are excluded (included) in Equation (1) that are unimportant in describing $C_{Mi(nbh)}$. Consequently, not all concentrations available in the CMAQ-database along the route are required to interpolate the concentration at a grid-cell i in the neighborhood outside the route.

Thus, to optimize the accuracy of Equation (9.2), the tool now determines which grid-cells along the route can be excluded from building Equation (9.2). In doing so, the tool calculates the standardized regression coefficient

$$A_j = a_j \frac{\text{standard deviation of } C_{Mj(dtb)}}{\text{standard deviation of } C_{i(nbh)}} \tag{9.4}$$

This coefficient indicates the importance of the concentrations $C_{mi(dtb)}$, m=1,.., M at the grid-cell i on the route in determining the concentrations$C_{Mi(nbh)}$at grid-cell i outside the route. The tool then excludes the concentrations $C_{mj(dtb)}$, m=1,…, M at a grid-cell j on the route for which A_j is lowest. Then it re-determines the a_j and b-coefficients with the concentrations $C_{Mj(dtb)}$, j=1,…, L at the remaining L grid-cells on the route again. In doing so it again uses the concentrations from the CMAQ-database. Note that L is the number of remaining grid-cells on the route deemed important so far. The tool repeats the procedure until the obtained R^2_{adj} reaches a maximum. After this step, the final coefficients a_j and b and final form of Equation (9.2) are established leading to the interpolation procedure

$$C_{i(itp)} = \sum_{j=1}^{L} a_j \cdot C_{j(obs)} + b \tag{9.5}$$

Here $C_{i(itp)}$ is the concentration to be interpolated at grid-cell i, and $C_{j(obs)}$ are the observed concentrations at the L grid-cells on the route.

Now the tool takes the observed concentrations $C_{j(obs)}$, j=1,…, L as the input into the optimized Equation (9.5). Recall that such optimized equations exist for each grid-cell i, for which an interpolation is to be done. Furthermore, L can be as large as N and differs among grid-cells for which the interpolation is to be done. The reason why L is different for different grid-cells is that for each grid-cell i, a different number of grid-cells and different grid-cells on the route may be important for the concentration at i. Thus, for

each grid-cell i by using the optimized Equation (9.5) the tool now interpolates the concentrations $C_{i(itp)}$ at grid-cell i that is in the neighborhood, i.e. outside the route.

In theory, the a_j and b-coefficients can be either positive or negative. Therefore, theoretically, Equation (9.5) could predict $C_{i(itp)} < 0 \mu g/m^3$ if the observed concentration $C_{j(obs)}$ differs strongly from the concentrations in the CMAQ-database $C_{Mj(dtb)}$ at one or more grid-cells of the route. In such case, the tool applies an extra treatment to satisfy the non-negative constrain of $C_{i(itp)}$ (Figure 9.3). The tool applies an analogous procedure as it does when identifying which grid-cells in the CMAQ-database are important to describe the concentration at grid-cell i when optimizing the accuracy of Equation (9.5). However, in the extra treatment, instead of including $C_{i(obs)}$ in all L grid-cells on the route, Equation (9.5) only includes those in the K grid-cells for which the standardized regression coefficients obtained from Equation (9.4) are in descending order $A_1 > A_2 > ... > A_K > ... > A_L$. Here, K is the number of the remaining grid-cells included in Equation (9.5), for which Equation (9.5) interpolates the lowest $C_{i(itp)} > 0 \mu g/m^3$. This means the tool only considers $C_{i(obs)}$, $j = 1, ..., K$ at grid-cells on the route that are most important to interpolate $C_{i(itp)}$.

The tool then assesses the uncertainty of the interpolation. We determined the confidential interval CI, i.e. the uncertainty at the 95% level of confidence for interpolating $C_{i(itp)}$ from $C_{j(obs)}$, j=1,...,L as [37, 38]

$$CI = (\pm) \frac{1.96 \times \sigma_i}{C_{i(itp)}} \sqrt{C'_{L(obs)} \left[C'_{ML(dtb)} C_{ML(dtb)} \right]^{-1} C_{L(obs)}} \times 100 \qquad (9.6)$$

Note that when the above-described extra treatment had to be applied L has to be substituted by K in Equation (9.6). In Equation (9.6), $C'_{L(obs)}$ and $C'_{ML(dtb)}$ are the transposed matrixes of $C_{L(obs)}$ and $C_{ML(dtb)}$ which are expressed as a matrix of the M concentrations at the L grid-cells on the route as:

$$C_{ML(dtb)}= \begin{bmatrix} C_{11} & \dots & C_{1L} \\ \dots & \dots & \dots \\ C_{M1} & \dots & C_{ML} \end{bmatrix}, C_{L(obs)}= [C_1 \quad \dots \quad C_L] \tag{9.7}$$

Furthermore,

$$\sigma_i= \left[\sum_m^M \left(C_{mi(dtb)} - \left(\sum_{j=1}^L a_j \times C_{mj(dtb)} + b \right) \right)^2 / (M-2) \right]^{1/2} \tag{9.8}$$

The uncertainty CI increases as the difference between the observed concentration $C_{L(obs)}$ and the concentration in the CMAQ-database $C_{ML(dtb)}$ increases.

All the above means that there is no unique set of interpolation equations tied for all potential routes in the nonattainment area. Instead, the tool develops self-consistently a set of interpolation equations for each desired route.

Our tool automatically applies the above procedure and determines an optimized interpolation equation set for the grid-cells for which the interpolations are to be done. The design of our tool allows any route within the nonattainment area. Therefore, it provides high flexibility for future mobile measurements and will be still usable after new road construction. Its design also guarantees that the tool can be transferred easily to other regions. The only pre-requisite is that a sufficient large dataset of air-quality model data is established for that region.

9.2.3.2 Sensitivity studies

To assess how large the database has to be, we performed various sensitivity studies with reduced database sizes. These studies showed that a reduction of the database by 30% reduces the interpolation accuracy by 10%.

Wind-patterns and temperatures affect the $PM_{2.5}$-distribution over the nonattainment area [1]. Therefore, we examined whether the accuracy of the tool would increase when the tool considered information on wind-direction, wind-speed or temperature. We developed an interpolation equation like Equation (9.5) for eight wind-direction sectors of 45° width. Analogously, we developed interpolation equations like Equation (9.5) for wind-speeds below 1m/s, between 1 and 2m/s, and above 2m/s, and for temperatures below -20^oC, between -20 and -10^oC, and above -10^oC.

Since the objective of the tool is to provide public spatially differentiated air-quality advice, wind data must be accessible when a drive is completed. The meteorological tower located in downtown Fairbanks is the only site that fulfills this criterion. Temperature data are available directly from the sniffer measurements. Temperature was processed in analogous way as $PM_{2.5}$-concentrations [28] to obtain observed temperature at the resolution of the interpolation grid. These observed temperatures then were included in developing Equation (9.5). The inclusion of any of the meteorological quantities means a reduction of the CMAQ-database to only those concentrations that were determined for the respective meteorological conditions. For instance, there were only 264 concentrations in the CMAQ-database when the simulated wind-direction at the meteorological tower fell between 0 and 22.5^o.

In including wind-direction, we used those concentrations in the database for which the WRF-derived wind-directions fell in the same wind-direction category that was observed at the meteorological tower during the mobile measurements. We evaluated the accuracy of the wind-direction sensitive interpolation algorithm with the CMAQ-simulated $PM_{2.5}$-concentrations of episode 2. Recall that the CMAQ-database based on CMAQ-simulations of episode 1. Consequently, the data used for evaluation and development are independent. We compared the interpolated $PM_{2.5}$-concentration distributions obtained with and without wind-direction-consideration and their accuracy. We repeated the above steps for consideration of wind-speed and for consideration of temperature.

These sensitivity studies showed that the development of Equation (9.5) without considering any meteorological quantities provided best accuracy (see discussion for details). Therefore, the following discussion of the tool evaluation is for the tool without consideration of meteorological quantities in the interpolation procedure.

9.2.3.3 Tool evaluation

We evaluated the interpolation performance by examining the FB, FE, NMB, NME, FAC2 and R using three different methods. We evaluated the interpolated $PM_{2.5}$-concentrations with the $PM_{2.5}$-concentrations observed at the SB_BAM and NP_BAM and RAMS_BAM sites where hourly $PM_{2.5}$-observations were available for episode 1 and 2.

Since the cross-validation method can only be applied to grid-cells that are on the route, we applied a method similar to PaiMazumder and Mölders [4] to further assess the tool's accuracy. In doing so, we considered the CMAQ-simulated $PM_{2.5}$-concentrations of episode 2 as the "grand truth", i.e. we assumed that these concentrations represent the actual situation on any given day during episode 2. We used the GPS-data of routes performed during episode 2, and pulled the $PM_{2.5}$-concentrations simulated for episode 2 at the grid-cells on those routes as "measurements". By using the CMAQ-database and the GPS-observations, the tool developed the interpolation equations along the routes of episode 2. We applied the so determined interpolation equations to interpolate the concentrations from the "measurements" along the routes into the neighborhoods. We then evaluated the interpolated with the "grand truth" $PM_{2.5}$-concentrations.

9.2.4 Results and discussion

9.2.4.1 Evaluation of simulated meteorology

WRF performed relatively similar in predicting the meteorological quantities of episode 1 and 2 (Table 9.2). WRF well captured the temporal evolutions of 2m temperature and 2m dew-point temperature, 10m wind-speed and sea-level pressure. Throughout both episodes, WRF consistently predicted warmer and drier near-surface conditions, and stronger 10m wind-speeds than observed (Figure 9.4, Table 9.2). The overestimation of wind-speed under weak wind conditions (v<1.5m/s) like during our episodes is common to all modern meteorological models [27, 28, 39, 40].

Table 9.2 Performance skill-scores of WRF in predicting 2m temperature (T), 2m relative humidity (RH), 10m wind-speed (v), accumulated downward shortwave radiation (SW), sea-level pressure (SLP), and 2m dew-point temperature (Td) in episode 1 (normal print) and episode 2 (italic). STDEV is the standard deviation.

Quantity	Bias	RMSE	SDE	R	Mean simulated	Mean observed	STDEV simulated	STDEV observations
T (^{o}C)	4.7	7.4	5.7	0.766	-17.5	-22.2	8.2	8.5
	2.1	*5.2*	*4.7*	*0.879*	*-16.9*	*-19.0*	*8.6*	*9.9*
RH (%)	-17	24	16	0.267	56	73	15	12
	-14	*22*	*17*	*0.266*	*59*	*72*	*15*	*13*
v (m/s)	1.4	2.1	1.52	0.667	2.5	1.0	2.0	1.5
	1.4	*2.0*	*1.47*	*0.606*	*2.5*	*1.2*	*1.8*	*1.4*
SW (W/m^2)	-33	242	240	-0.248	78	111	48	224
	46	*279*	*275*	*-0.033*	*203*	*157*	*132*	*237*
SLP (hPa)	-2.18	3.6	2.88	0.845	1017	1019	4.6	5.4
	-1.52	*4.0*	*3.7*	*0.979*	*1015*	*1017*	*18.1*	*18.3*
T_d (^{o}C)	-0.1	8.9	8.9	0.651	-24.6	-24.6	9.3	11.4
	-1.1	*5.2*	*5.1*	*0.873*	*-23.4*	*-22.3*	*9.8*	*10.2*

WRF well captured the temporal evolution and magnitude of sea-level pressure. WRF predicted much drier (27% lower in relative humidity) conditions than observed especially between January 8 and 10, 2011 (Figure 9.4). WRF simulated wind-direction with a mean bias <30°, i.e. this performance falls within the range of other model for this region [27, 28, 41-43]. WRF generally underestimated downward shortwave radiation throughout episode 1 by 33W/m^2, on average In episode 2, WRF underestimated downward shortwave radiation for January 1 to 10 by 63W/m^2 on average, 2011 while it overestimated downward shortwave radiation on the other days by 97W/m^2 on average.

9.2.4.2 Evaluation of simulated PM$_{2.5}$-concentrations

The evaluation with measurements at fixed sites showed that CMAQ performed relatively better in predicting PM$_{2.5}$-concentrations for episode 1 than for episode 2 (Table 9.3). Over all sites and days, the mean bias, RMSE, NMB, NME, and FAC2 of 24h-average PM$_{2.5}$-concentrations for episode 1 are 4.4µg/m^3, 28.8µg/m^3, 9%, 42% and 91%, respectively. The corresponding values for episode 2 are 31.7 µg/m^3, 44.1µg/m^3, 125%, 129% and 49%. Typically, air-quality model simulations that have FB within ±30% and a FAC2 ≥50% are considered as having good performance [35]. Typically, MFB within ±60% and MFE ≤ 75% are recommended as the criteria for a model's performance to be considered as acceptable, and MFB within ±30% and MFE ≤ 50% are the goal that the best state-of-the-art models could reach [36]. For episode 1, 66% and 100% of the pairs of NMB-NME obtained at all stationary sites fell within the EPA [44] recommended performance goals and criteria (Table 9.3). In episode 2, only the pair of

NMB-NME at the SB-site reached the performance goal, while the pairs of NMB-NME at other sites fell outside the performance criteria. Based on the criteria and skill-scores, we conclude that CMAQ's performance was good for episode 1 and acceptable for episode 2.

For both episodes, CMAQ simulated the $PM_{2.5}$-concentrations at the SB-site better than at other sites. Here its performance was better for episode 1 than 2 (Table 9.3, Figure 9.5). The slight temporal offset in simulated meteorology propagated into the simulated 24h-average $PM_{2.5}$-concentrations from December 27 to 31, 2009 (Figure 9.5). The overestimation of $PM_{2.5}$ between January 7 and 9, 2011 was mainly caused by errors in emission allocations rather than by errors in simulated meteorology.

The evaluation of CMAQ-simulated $PM_{2.5}$-concentrations with the $PM_{2.5}$-concentrations measured by the sniffer during all drives of episode 1 yielded a mean bias, RMSE, FB, FE, NMB, NME, MFB, MFE and FAC2 of $3.0\mu g/m^3$, $50.8\mu g/m^3$, -4%, 94%, 8.5%, 93%, -4%, 94% and 39% respectively. The corresponding skill-scores in episode 2 were $11.5\mu g/m^3$, $43.0\mu g/m^3$, 10%, 105%, 42%, 118%, 10%, 105% and 28%. The skill-scores obtained in episode 1 (2) are better (slightly weaker) than those obtained in other studies for this region [28]. Comparison of the skill-scores obtained at the SB of episode 1 (2) with those reported at that site for an episode in January 2008 fall in the same range (are slightly weaker) [9]. The skill-scores determined for individual sniffer drives differed strongly from each other. CMAQ typically performed better on days with high ($>30\mu g/m^3$ on average) than low $PM_{2.5}$-concentrations detected by the sniffer. Highest correlation between simulated and sniffer-observed $PM_{2.5}$-concentrations obtained for

any drive was 0.824 (statistically significant), but typically varied ±0.200 (occasionally statistical significant). Some of the discrepancies are due to the fact that simulated $PM_{2.5}$-concentrations represent volume-average concentrations for 1.3km×1.3km×8m, while the "sniffer observations" represent the average along the route (a line) within that grid-cell at the same hour.

9.2.4.3 Evaluation of the tool

For episode 1, the cross-evaluation of our interpolation tool yielded FB, FE, NMB, NME, MFE, MFB, FAC2 and R over all grid-cells with mobile measurements and all drives of 4%, 42%, 4%, 43%, 8%, 58%, 68%, and 0.728, respectively. The corresponding values for episode 2 were 4%, 40%, 5%, 41%, 2%, 45%, 77% and 0.707 (Figure 9.6).

The skill-scores differ among drives in episode 1 and 2. The relatively strong (>0.7; statistically significant) correlations between the interpolated and observed concentrations for the various routes indicate that the interpolation algorithm captures the spatial distribution of observed $PM_{2.5}$-concentrations along the routes well. Typically, skill-scores were better for days on which the sniffer measured high than low $PM_{2.5}$-concentrations.

Table 9.3 Skill scores of CMAQ in simulating 24h-average $PM_{2.5}$-concentration as obtained at various sites where data were available in two episodes

Site	Mean bias ($\mu g/m^3$)	RMSE ($\mu g/m^3$)	FB (%)	FE (%)	NMB (%)	NME (%)	MFB (%)	MFE (%)	FAC2 (%)	# of observations
Episode 1										
All sites	4.4	28.8	9	40	9	42	7	37	91	56
SB_BAM	-2.8	15.0	-6	26	-6	26	-5	26	100	17
SB_FRM	4.0	16.8	9	34	10	36	8	35	100	6
NP	19.3	47.6	38	62	47	76	43	58	67	6
NCORE	4.8	14.7	11	28	12	29	9	27	100	6
PR	19.0	37.2	38	53	48	66	31	49	83	6
RAMS_BAM	0.8	34.5	1	46	1	46	-5	44	87	15
Episode 2										
All sites	19.3	26.3	50	54	66	72	49	54	67	134
SB_BAM	8.9	15.9	24	35	27	40	30	40	83	30
SB_FRM	16.6	20.6	49	51	66	68	46	47	80	10
NP_FRM	31.5	36.1	79	79	130	130	81	81	40	10
NP_BAM	25.2	30.7	55	57	77	79	54	59	58	26
PR	26.9	35.1	73	75	115	118	59	65	56	9
NCORE	19.5	22.8	59	59	84	84	54	54	67	9

We also performed the cross-validation at grid-cells that the sniffer frequently travelled (≥ 20 times) during episode 1 and 2. At these grid-cells, typical ranges of the performance skill-scores were -33%<FB<29%, 10%<FE<58%, -30%<NMB<10%, 15%<NME<50%, -43%<MFB<33%, 20%<MFE<72%, 54%<FAC2<96% and 0.400<R<0.920 (all correlations are statistically significant), respectively. These scores indicate that the tool even can capture the temporal evolution of the concentrations.

The evaluation of the interpolation tool by data from the SB-site provided overall FB, FE, NMB, NME, MFB, MFE, FAC2 and R of -67%, 78%, -50%, 59%,-69%, -80%, 39% and 0.341 (statistically significant), respectively. The corresponding skill scores obtained at the NP (RAMS) site were 29% (39%), 70% (92%), 33% (48%), 82% (115%), 17% (-5%), 68% (85%), 50% (41%) and 0.215 (-0.120, both correlations statistically insignificant), respectively.

The relatively large discrepancy between the $PM_{2.5}$-concentrations interpolated from the mobile measurements to the fixed sites may be partly explained by the large differences between the $PM_{2.5}$-concentrations observed by the sniffer and at the fixed sites. More than 65% of the times when the measurements on the route were made in a grid-cell with a fixed site, the mobile and fixed site observations differed up to two orders of magnitude (Figure 9.7). This discrepancy can be explained by the fact that the mobile measurements route are made along a line, while the site measurements are point measurements and at higher elevation than the sniffer measurements.

As aforementioned, the equations for the interpolation algorithm were developed using the CMAQ-data of episode 1. We used CMAQ-data for episode 2 as the "grand

truth" for the evaluation of the tool's accuracy to ensure independence of the data used for development and evaluation. Typically, the performance skill scores for the interpolation algorithm over all routes for grid-cells adjacent to the routes were R>0.8, -10%<FB<10%, FE<30%, -20%<NMB<20%, NME<20%, -20%<MFB<20%, MFE<40%, FAC2>75%.

The comparison of interpolated and simulated "grand truth" $PM_{2.5}$-concentrations revealed a sensitivity of the tool's performance to the routes. The performance was weakest when the route only covered a few grid-cells (<10), or just one side of the nonattainment area, for instance, the community of North Pole, or the hills (Figure 9.8). The tool performed best (weakest) for routes that covered the center of nonattainment (the hills). However, since in the hills, $PM_{2.5}$-concentrations are usually below the NAAQS, the relatively weaker performance here than elsewhere will not lead to false alarms, i.e. notifications of unhealthy conditions.

We examined the overall accuracy of the tool over 100 randomly chosen routes for episode 2. In doing so, we randomly picked a day of episode 2 and used the $PM_{2.5}$-concentrations simulated by CMAQ for that day as "grand truth". For that day we also randomly picked a route. We extracted the $PM_{2.5}$-concentrations on this route as measurements from the "grand truth". Then we applied the tool for this route and interpolated the extracted $PM_{2.5}$-concentrations into the neighborhoods. We repeated this procedure 100 times. These 100 interpolated $PM_{2.5}$-concentration datasets were then evaluated with the corresponding "grand truth" CMAQ-simulated $PM_{2.5}$-concentrations. This evaluation led to R>0.720, -20<FB<20, FE<60%, -30%<NMB<30%, NME<50%,

-30%<MFB<30%, MFE<60%, and FAC2>75% for most locations in the nonattainment area on average over all 100 samples (Figure 9.9).

The sensitivity study on the wind-direction dependent interpolation algorithm suggested that consideration of wind-direction does not improve the performance (therefore not shown). The same result was found for the algorithm with consideration of wind-speed. Comparison of the wind observations made at the meteorological tower with those made at Fairbanks International Airport, Eielson Air Force Base and Fort Wainwright suggested that the meteorological tower is not very representative for the wind pattern over the nonattainment area. This finding also agrees with other studies made for Fairbanks [45].

The consideration of a temperature-classification in the interpolation algorithm improved the performance in interpolating $PM_{2.5}$-concentration in the hills. However, it led to decreased performance in downtown Fairbanks and the community of North Pole that are the two hotspot areas for high $PM_{2.5}$-concentrations [28]. As in the hills, $PM_{2.5}$-concentrations are usually below the NAAQS, and the $PM_{2.5}$ hot-spots are of greatest public concerns, the interpolation algorithm without consideration of meteorological quantities seems to be the most suitable for public air-quality advisories on polluted days.

9.2.5 Transferability

The CMAQ-database of the tool developed in this study based on simulations for Fairbanks for one episode in deep winter with calm wind and extremely low temperature conditions. Note that such conditions are typical candidates for exceedances of the

NAAQS at the SB-site [4] and hence suitable for an interpolation algorithm aiming at providing a spatially differentiated air-quality advisories on such days.

Meteorological conditions as well as the emissions of $PM_{2.5}$ and its precursors differ with season and location. Therefore, to apply the tool for a different season, the database of air-quality model simulations has to be enlarged for that season. If the tool is to be transferred to another region, a database has to be created from air-quality model simulations for the respective region and season of interest.

To demonstrate the transferability of the developed tool, we created a $PM_{2.5}$-concentration database from simulations of the WRF with inline chemistry package (WRF/Chem; [7]) in its Alaska adapted version [21] for an episode in May/June 2008 for a domain of 110×110 grid-cells with a 7km increment over Southeast Alaska (Figure 9.10). We used ten days of the episode (May 15 to May 24, 2008) to create a database for the tool. This database includes 240 data at each grid-cell in total 2,851,440 values. Another 15 days (May 25 to June 8, 2008) were used as "grand truth" as there were no mobile measurements for this region. We assumed arbitrary routes of an instrumented ship that travels and measures $PM_{2.5}$-concentrations around the islands in the domain during the 15 "grand truth" days (Figure 9.10). We extracted the $PM_{2.5}$-concentrations along the assumed route from the "grand truth" data as "proxy" data of observations. Like in the evaluation of the interpolation tool, we used the database to build the interpolation equations, and interpolated the "observations". Then the interpolated $PM_{2.5}$-concentrations were evaluated with WRF/Chem-simulated $PM_{2.5}$-concentrations that we assumed as "grand truth" (Figure 9.10). This evaluation showed that the interpolation

procedure captured the spatial distribution and magnitude of the "grand truth" $PM_{2.5}$-concentrations well (Figure 9.10). Except at grid-cells on and near the route, the uncertainties were greater than 30% everywhere, especially at grid-cells where the $PM_{2.5}$-concentration were low ($<1\mu g/m^3$). Over all seven assumed instrumented ship cruises during the 15 "grand truth" days, the tool generally performed well over the domain. The performance skill-scores fell in the following ranges: 0.34<R<1.0, -60%<FB<60%, 5%<FE<180%, -40%<NMB<120%, 5%<NME<180%, -80%<MFB<140%, 5%<MFE<160%, and 20%<FAC2<100% (Figure 9.11).

In some regions of the domain, the performance was relatively weak (Figure 9.11) due to the drastic changes in the meteorological conditions between the days used as the database (May 15 to 24) and the days used as "grand truth" (May 25 to June 8). For instance, there was a change in wind-direction. From May 15 to 24 2008, land-sea-breeze circulations, mainly in west-east direction, dominated. On May 17 and 18, west wind dominated and advected aged polluted air from the ocean deep land inwards. From May 26 to 31, northern winds interfered with the land-sea-breeze circulations. Starting from June 1, the south and southeast winds interfered with and eventually shut down the land-sea-breezes. Because of this change, the spatial distribution of $PM_{2.5}$-concentration in the database did not well represent the conditions of the "grand truth" days, for which the performance of the tool is weaker after the change occurred.

This transferability experiment illustrates the following: The tool can be easily transferred to other regions. Even with a large database, the ability of the tool is limited

when the conditions at the time of the "measurements" differ strongly from the condition from which the interpolation equations were derived.

9.2.6 Conclusions

A tool to interpolate mobile $PM_{2.5}$-measurements into unmonitored neighborhoods is presented. The tool uses simulations of the Alaska adapted CMAQ [9] or any other air-quality model as a database and the GPS-coordinates of the route to determine a set of interpolation equations for the neighborhood of interest, e.g., a nonattainment area. Once the interpolation equations are determined, the tool interpolates the mobile measurements into the unmonitored neighborhoods using the set of interpolation equations. The resulting concentration distributions can be used for spatially differentiated public air-quality advisories.

The tool allows any route within the area for which a database of simulated concentrations exits. The tool is transferable into other regions and seasons assuming a database of air-quality simulations exists or is established for that region and/or season. A great advantage of this tool is that its database just needs to have values in the range of the mobile measured concentration and to represent similar seasonal conditions in the region of interest. The tool does not require a simulation of the episode of the actual mobile measurements. Consequently, the spatial interpolation can be made within minutes after the end of a drive.

The results of cross-validations suggested that the interpolation algorithm performs best for grid-cells close to the route. The evaluation by using a CMAQ-simulation as

"grand-truth" that has not been included in the database and hence for the determination of the interpolation equations showed that the interpolation algorithm captured the spatial distribution of the "grand-truth" $PM_{2.5}$-concentrations well.

The evaluation efforts also showed that the performance of the tool is sensitive to the route. Performance is best for routes with large coverage of the region into which the mobile measurements are to be interpolated.

Sensitivity studies that included wind fields and temperature into the determination of the interpolation equations led to the conclusion that in a complex urban environment under calm wind conditions, a simpler algorithm that only considers $PM_{2.5}$-concentrations is superior for capturing the conditions in hot-spot areas.

Our investigations showed that the tool does not need simulations of the actual day of the mobile measurements to interpolate measurements successfully into unmonitored neighborhoods. This fact is of great advantage for public air-quality advisories as it tremendously reduces the time between the end of the measurements and the time the advisory can be released.

The tool presented here provides the flexibility for all types of routes, i.e. it is not tied to a specific route. Based on the transferability tests to southeast Alaska, one has to conclude that this tool can easily be applied to other regions and seasons. To apply the tool for another season, the database of air-quality model data must be enlarged by results from simulations representative for the season in the region of interest. The tool developed and evaluated in this study was based on 2592 concentrations at each grid-cell

in the CMAQ-database. A reduction of this database by 30% reduces the tool's accuracy by 10%.

Acknowledgements

We thank C.F. Cahill, G. Kramm, W.R. Simpson, G.A. Grell, and T.T. Tran and the anonymous reviewers for fruitful discussions. We thank J. Conner, J. McCormick, and N. Swensgard from the Fairbanks North Star Borough Air Quality Division for access to their $PM_{2.5}$-data and Sierra Research Inc. for providing the emission data. The Arctic Super Computer Center provided computational support. The study was supported partly under the AUTC Project No. 410003 by the Alaska Department of Transportation & Public Facilities and the National Park Service under contract H9910030024.

References

[1] H. N. Q. Tran and N. Mölders, "Investigations on Meteorological Conditions for Elevated $PM_{2.5}$ in Fairbanks, Alaska", *Atmospheric Research,* 99, 2011, pp. 39-49.

[2] D. W. Wong, L. Yuan and S. A. Perlin, "Comparison of Spatial Interpolation Methods for the Estimation of Air Quality Data", *Journal of Exposure Analysis and Environmental Epidemiology,* 14, 2004, pp. 404-415.

[3] J. A. Mulholland, A. J. Butler, J. G. Wilkinson and A. G. Russell, "Temporal and Spatial Distributions of Ozone in Atlanta: Regulatory and Epidemiologic Implications", *Journal of Air & Waste Management Association,* 48, 1998, pp. 418-426.

[4] D. PaiMazumder and N. Mölders, "Theoretical Assessment of Uncertainty in Regional Averages Due to Network Density and Design", *Journal of Applied Meteorology and Climate,* 48, 2009, pp. 1643–1666.

[5] J. F. Clarke, E. S. Edgerton and B. E. Martin, "Dry Deposition Calculations for the Clean Air Status and Trends Network", *Atmospheric Environment,* 31, 1997, pp. 3667-3678.

[6] M. Fuentes and A. E. Raftery, "Model Evaluation and Spatial Interpolation by Bayesian Combination of Observations with Outputs from Numerical Models", *Biometrics,* 61, 2005, pp. 36-45.

[7] S. E. Peckham, J. D. Fast, R. Schmitz, G. A. Grell, W. I. Gustafson, S. A. McKeen, S. J. Ghan, R. Zaveri, R. C. Easter, J. Barnard, E. Chapman, M. Salzmann, C. Wiedinmyer and S. R. Freitas, "WRF/Chemversion 3.1 User's Guide", 2009, http://ruc.noaa.gov/wrf/WG11/Users_guide.pdf.

[8] D. W. Byun and K. L. Schere, "Review of the Governing Equations, Computational Algorithms, and Other Components of the Models-3 Community Multiscale Air Quality (CMAQ) Modeling System", *Applied Mechanics Reviews,* 59, 2006, pp. 51-77.

[9] N. Mölders and K. Leelasakultum, "CMAQ Modeling: Final Report Phase I", *Rep.*, 2011, p. 62.

[10] B. J. Gaudet and D. R. Stauffer, "Stable Boundary Layers Representation in Meteorological Models in Extremely Cold Wintertime Conditions", *Environmental Protection Agency*, 2010, p. 60.

[11] N. Mölders and G. Kramm, "Influence of Wildfire Induced Land-Cover Changes on Clouds and Precipitation in Interior Alaska – a Case Study. ", *Atmospheric Research,* 84, 2007, pp. 142-168.

[12] N. Mölders and G. Kramm, "A Case Study on Wintertime Inversions in Interior Alaska with WRF", *Atmospheric Research,* 95 (2-3), 2010, pp. 314-332.

[13] S.-Y. Hong and J.-O. J. Lim, "The WRF Single-Moment 6-Class Microphysics Scheme (Wsm6)", *Journal Korean Meteorological Society,* 42, 2006, pp. 129-151.

[14] G. A. Grell and D. Dévényi, "A Generalized Approach to Parameterizing Convection Combining Ensemble and Data Assimilation Techniques", *Geophysical Research Letters,* 29 (1693), 2002, p. 4.

[15] M.-D. Chou and M. J. Suarez, "An Efficient Thermal Infrared Radiation Parameterization for Use in General Circulation Models", *NASA - Technical Memorandum,* 104606, 3 (3), 1994, p. 85.

[16] E. J. Mlawer, S. J. Taubman, P. D. Brown, M. J. Iacono and S. A. Clough, "Radiative Transfer for Inhomogeneous Atmospheres: Rrtm, a Validated Correlated-K Model for the Longwave", *Journal of Geophysical Research,* 102(D14), 1997, pp. 16663-16682.

[17] J. Barnard, J. Fast, G. Paredes-Miranda, W. Arnott and A. Laskin, "Technical Note: Evaluation of the WRF-Chem 'Aerosol Chemical to Aerosol Optical Properties' Module Using Data from the Milagro Campaign", *Atmospheric Chemistry and Physics,* 10, 2010, pp. 7325-7340.

[18] Z. I. Janjić, "The Step-Mountain Eta Coordinate Model: Further Developments of the Convection, Viscous Sublayer and Turbulence Closure Schemes", *Monthly Weather Review,* 122, 1994, pp. 927-945.

[19] T. G. Smirnova, J. M. Brown, S. G. Benjamin and D. Kim, "Parameterization of Cold Season Processes in the Maps Land-Surface Scheme", *Journal of Geophysical Research,* 105(D3), 2000, pp. 4077-4086.

[20] D. W. Byun, J. E. Pleim, R. T. Tang and A. Bourgeois, "Science Algorithms of the Epa Models-3 Community Multiscale Air Quality (CMAQ) Modeling System - Chapter 12: Meteorology-Chemistry Interface Processor (Mcip) for CMAQ Modeling System", *Technical Report to U.S. EPA, EPA/600/R-99/030*, 1999, p. 91.

[21] G. Yarwood, S. Rao, M. Yocke and G. Z. Whitten, "Updates to the Carbon Bond Chemical Machanism: CB05", *Final report to the U.S. EPA, RT-04000675, 2005. [Available online at http://www.camx.com]*.

[22] F. S. Binkowski and S. J. Roselle, "Models-3 Community Multiscale Air Quality (CMAQ) Model Aerosol Component, 1, Model Description", *Journal of Geophysical Research,* 108(D6), 4183, 2003, p. 18. doi:10.1029/2001JD001409.

[23] J. S. Chang, R. A. Brost, I. S. A. Isaksen, S. Madronich, P. Middleton, W. R. Stockwell and C. J. Walcek, "A Three-Dimensional Euledan Acid Deposition Model: Physical Concepts and Formulation", *Journal Geophysical Research,* 92, 1987, pp. 14,681-14,700.

[24] B. Schell, I. J. Ackermann, H. Hass, F. S. Binkowski and A. Ebel, "Modeling the Formation of Secondary Organic Aerosol within a Comprehensive Air Quality Model System", *Journal of Geophysical Research,* 106, 2001, pp. 28275–28293.

[25] R. J. Yamartino, "Nonnegative, Conserved Scalar Transport Using Grid-Cell-Centered, Spectrally Constrained Blackman Cubics for Applications on a Variable-Thickness Mesh", *Monthly Weather Review,* 121, 1993, pp. 753-763.

[26] J. E. Pleim and J. S. Chang, "A Non-Local Closure Model for Vertical Mixing in the Convective Boundary Layer", *Atmospheric Environment,* 26A, 1992, pp. 965-981.

[27] N. Mölders, H. N. Q. Tran, P. Quinn, K. Sassen, G. E. Shaw and G. Kramm, "Assessment of WRF/Chem to Simulate Sub–Arctic Boundary Layer Characteristics During Low Solar Irradiation Using Radiosonde, Sodar, and Surface Data", *Atmospheric Pollution Research,* 2, 2011, pp. 283-299.

[28] N. Mölders, H. N. Q. Tran, C. F. Cahill, K. Leelasakultum and T. T. Tran, "Assessment of WRF/Chem $PM_{2.5}$-Forecasts Using Mobile and Fixed Location Data from the Fairbanks, Alaska Winter 2008/09 Field Campaign", *Atmospheric Pollution Research,* 3, 2012, pp. 180-191.

[29] C. J. Coast, Jr., "High-Performance Algorithms in the Sparse Matrix Operator Kernel Emissions (Smoke) Modeling System.", Ninth AMS Joint Conference on Applications of Air Pollution Meteorology with Air & Waste Management Association , 1996, pp. 584-588.

[30] M. R. Houyoux, J. M. Vukovich, C. J. Coats, N. J. M. Wheeler and P. S. Kasibhatla, "Emission Inventory Development and Processing for the Seasonal Model for Regional Air Quality (Smraq) Project", *Journal of Geophysical Research,* 105 (D7), 2000, pp. 9079-9090.

[31] N. Mölders, H. N. Q. Tran and K. Leelasakultum, "Investigation of Means for $PM_{2.5}$ Mitigation through Atmospheric Modeling - Final Report", 2011, p. 75.

[32] C. F. Cahill, "Asian Aerosol Transport to Alaska During Ace-Asia", *Journal of Geophysical Research,* 108 (8664), 2003, p. 8. doi:10.1029/2002JD003271.

[33] T. T. Tran, G. Newby and N. Mölders, "Impacts of Emission Changes on Sulfate Aerosols in Alaska", *Atmospheric Environment,* 45, 2011, pp. 3078-3090.

[34] H. von-Storch and F. W. Zwiers, "Statistical Analysis in Climate Research". Cambridge University Press, Cambridge, UK, 1999, p. 495.

[35] J. C. Chang and S. R. Hanna, "Air Quality Model Performance Evaluation", *Meteorology and Atmospheric Physics,* 87, 2004, pp. 167–196.

[36] J. W. Boylan and A. G. Russell, "PM and Light Extinction Model Performance Metrics, Goals, and Criteria for Three-Dimensional Air Quality Models", *Atmospheric Environment,* 40, 2006, pp. 4946-4959.

[37] J. Devore, "Probability and Statistics for Engineering and the Sciences", 6th Edition, Brooks/Cole, Belmont, CA, 2004, p. 816.

[38] S. Weisberg, "Applied Linear Regression", 3rd Edition, New York: Wiley, 2005, p. 221.

[39] Y. Zhang, M. K. Dubey, S. C. Olsen, J. Zheng and R. Zhang, "Comparisons of WRF/Chem Simulations in Mexico City with Ground-Based Rama Measurements During the 2006-Milagro", *Atmospheric Chemistry and Physics,* 9, 2009, pp. 3777–3798.

[40] Z. Zhao, S.-H. Chen, M. J. Kleeman, M. Tyree and D. Cayan, "The Impact of Climate Change on Air Quality–Related Meteorological Conditions in California. Part I: Present Time Simulation Analysis", *Journal Climate,* 24, 2011, pp. 3344-3361.

[41] N. Mölders, "Suitability of the Weather Research and Forecasting (WRF) Model to Predict the June 2005 Fire Weather for Interior Alaska", *Weather and Forecasting,* 23, 2008, pp. 953-973.

[42] N. Mölders, "Comparison of Canadian Forest Fire Danger Rating System and National Fire Danger Rating System Fire Indices Derived from Weather Research and Forecasting (WRF) Model Data for the June 2005 Interior Alaska Wildfires", *Atmospheric Research,* 95 (2-3), 2010, pp. 290-306.

[43] M. B. Yarker, D. PaiMazumder, C. F. Cahill, J. Dehn, A. Prakash and N. Mölders, "Theoretical Investigations on Potential Impacts of High-Latitude Volcanic Emissions of Heat, Aerosols and Water Vapor and Their Interactions on Clouds and Precipitation", *The Open Atmospheric Science Journal,* 4, 2010, pp. 24-44.

[44] U. S. EPA, "Guidance on the Use of Models and Other Analyses for Demonstrating Attainment of Air Quality Goals for Ozone, $PM_{2.5}$, and Regional Haze", Research Triangle Park, North Carolina, 2007, p. 262.

[45] H. N. Q. Tran and N. Mölders, "Wood-Burning Device Changeout: Modeling the Impact on $PM_{2.5}$-Concentrations in a Remote Subarctic Urban Nonattainment Area", *Advances in Meteorology,* 2012, p. 12. doi:10.1155/2012/853405.
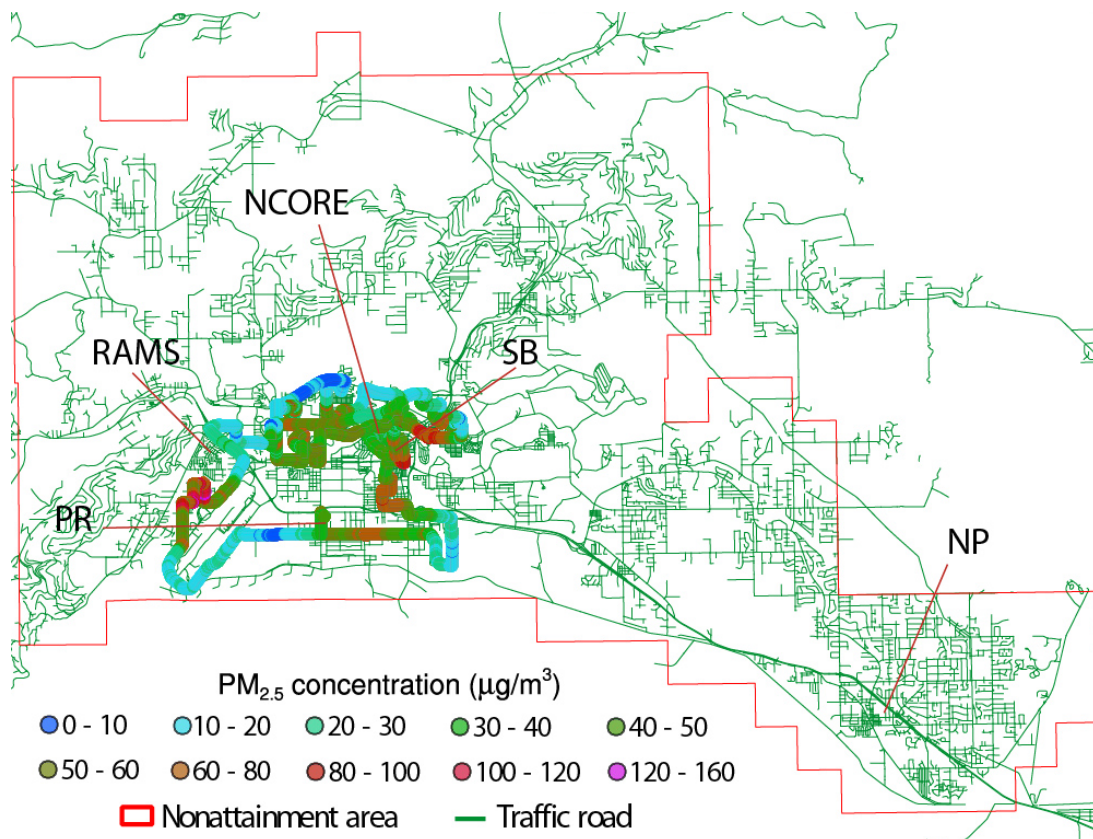
Figure 9.1 PM$_{2.5}$-concentrations as measured in Fairban*ks by the sniffer (lines* of dots) on 01-02-2010 during the drive starting at 1404AST with the street network superimposed. The locations of the SB, RAMS, PR, NP, and NCORE stationary PM$_{2.5}$-observation are indicated.
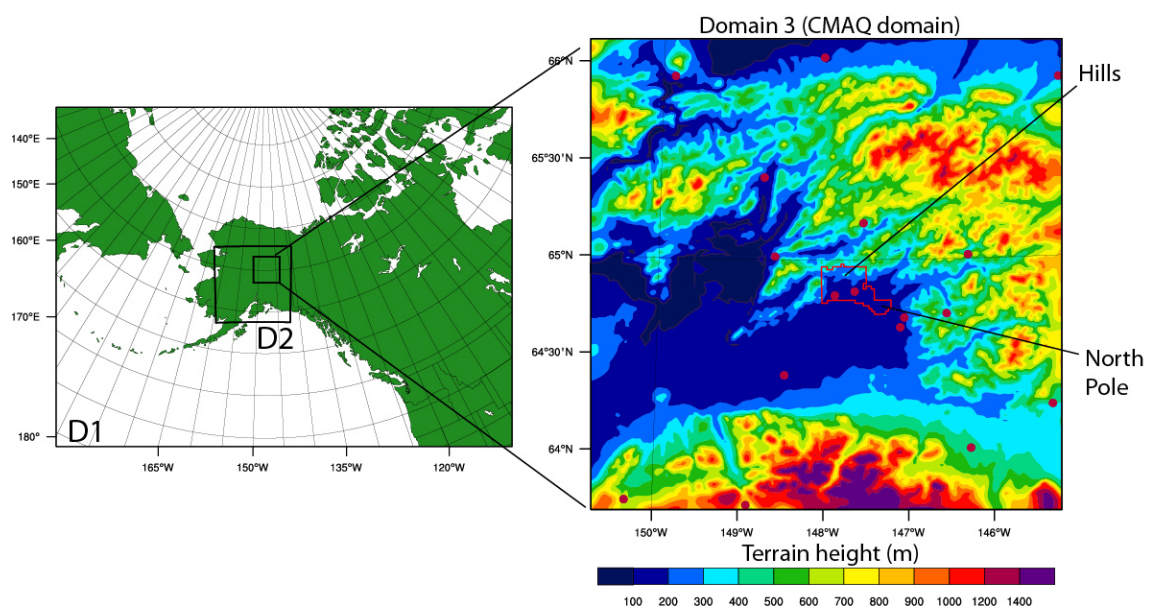
Figure 9.2 Schematic view of the domains used in the WRF (left) and CMAQ simulation domains. On domain 3, terrain height is superimposed (right). Red circles indicate the surface meteorological sites used in the evaluation. The red polygon marks the Fairbanks PM$_{2.5}$-nonattainment area.
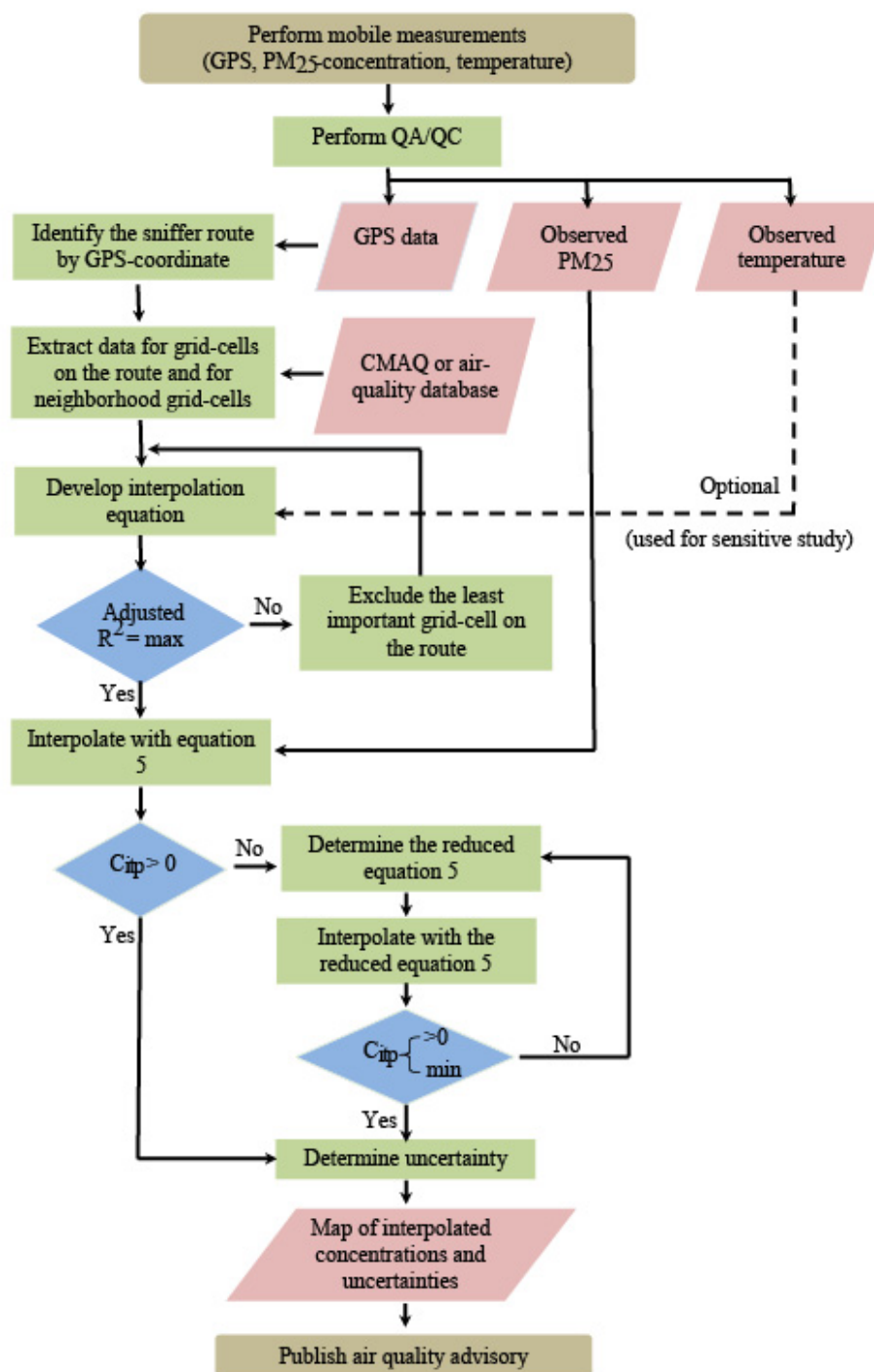
Figure 9.3 Schematic view of the data flow and procedure of the development of the interpolation equations.
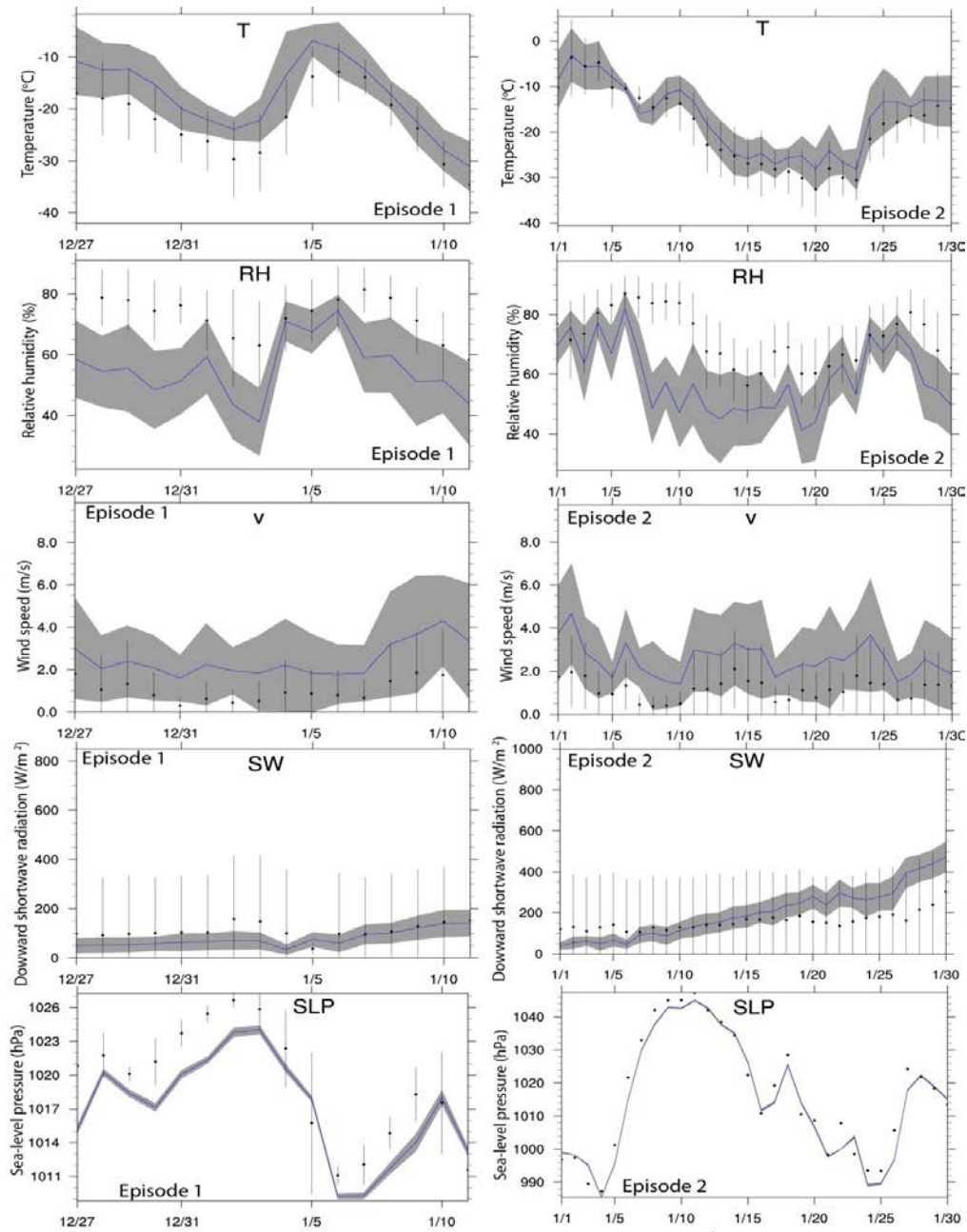
Figure 9.4 Temporal evolution of daily averaged 2m temperatures (T), wind-speed (v), relative humidity (RH), accumulated downward shortwave radiation (SW), and sea-level pressure (SLP) averaged over the 14 and 18 sites for which observations were available during episode 1 and 2, respectively. The solid blue line and closed circles indicate simulated and observed quantities; grey-shading and vertical bars indicate the variance of the simulated and observed quantities, respectively.
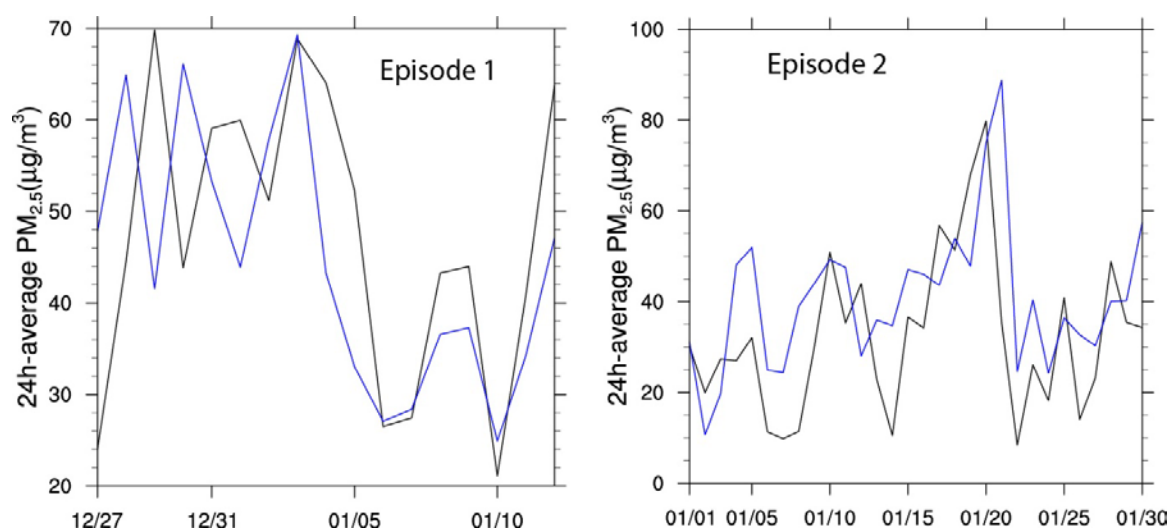
Figure 9.5 Temporal evolution of simulated (blue) and observed (black) 24h-average PM$_{2.5}$-concentrations as obtained at the SB-site for episode 1 and 2, respectively.
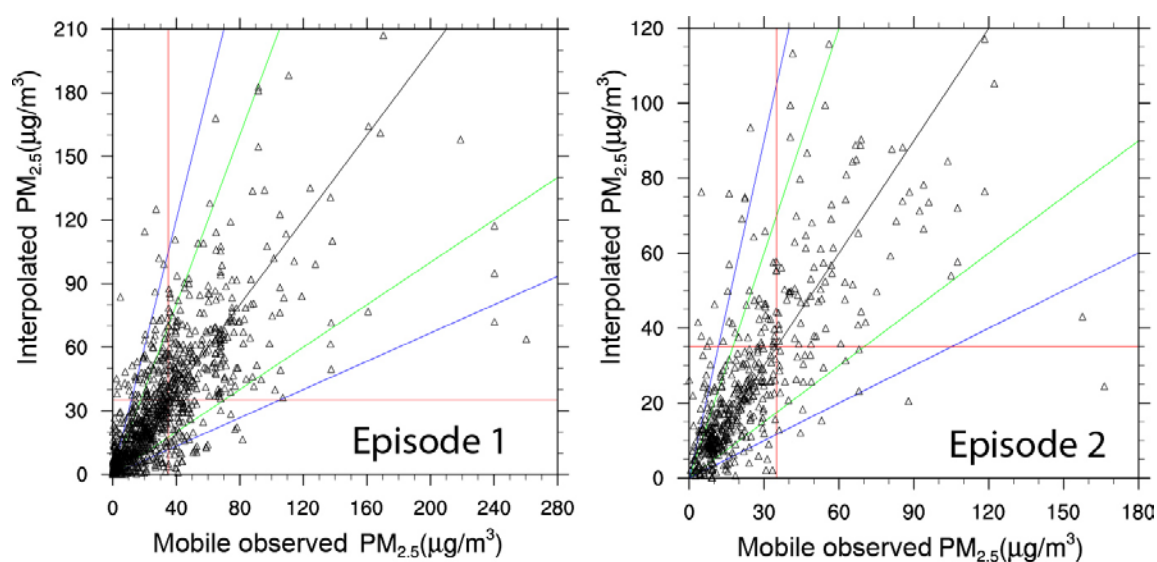
Figure 9.6 Scatter plots of interpolated and mobile observed PM$_{2.5}$–concentrations at grid-cells on all routes of episode 1 and 2. The black, green and blue lines indicate the 1:1-line and a factor of two and three agreement between pairs of simulated and observed values, respectively. The red lines indicate the PM$_{2.5}$-NAAQS of 35µg/m^3.
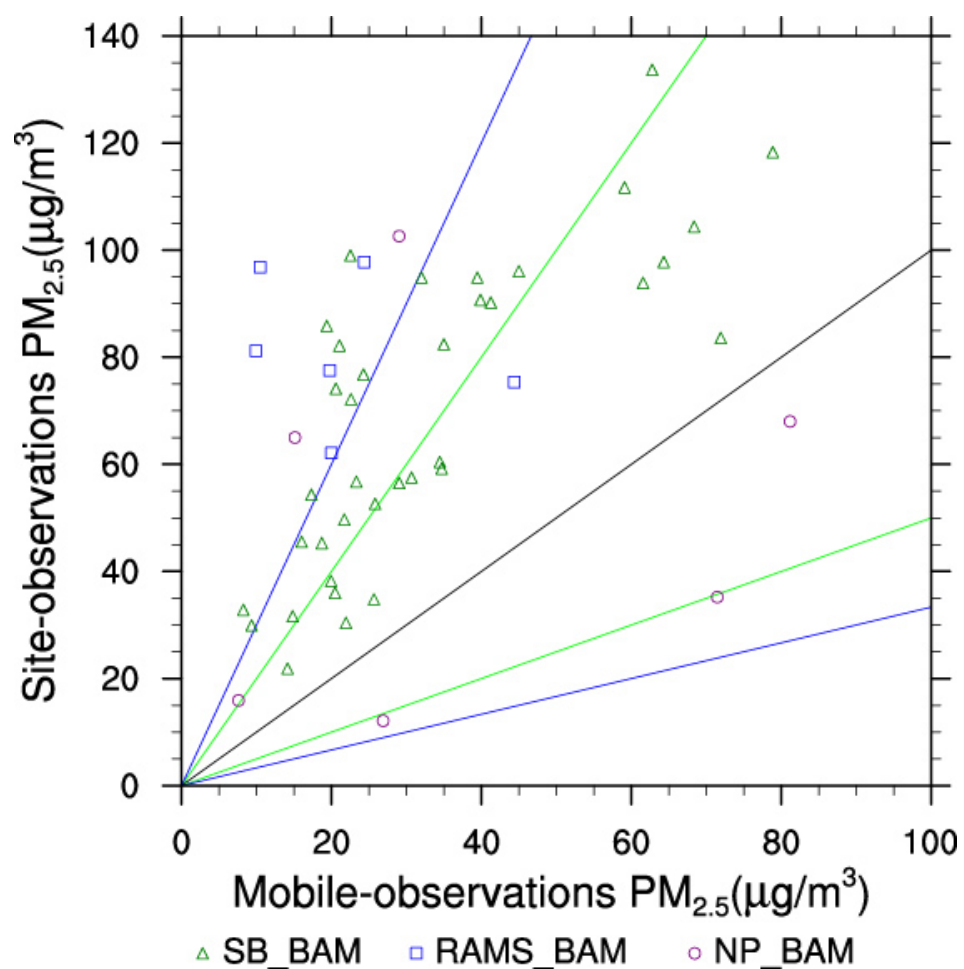
Figure 9.7 Like Figure 9.6, but for site-observations and mobile-observations at times when they were measured at same grid-cell in the route.
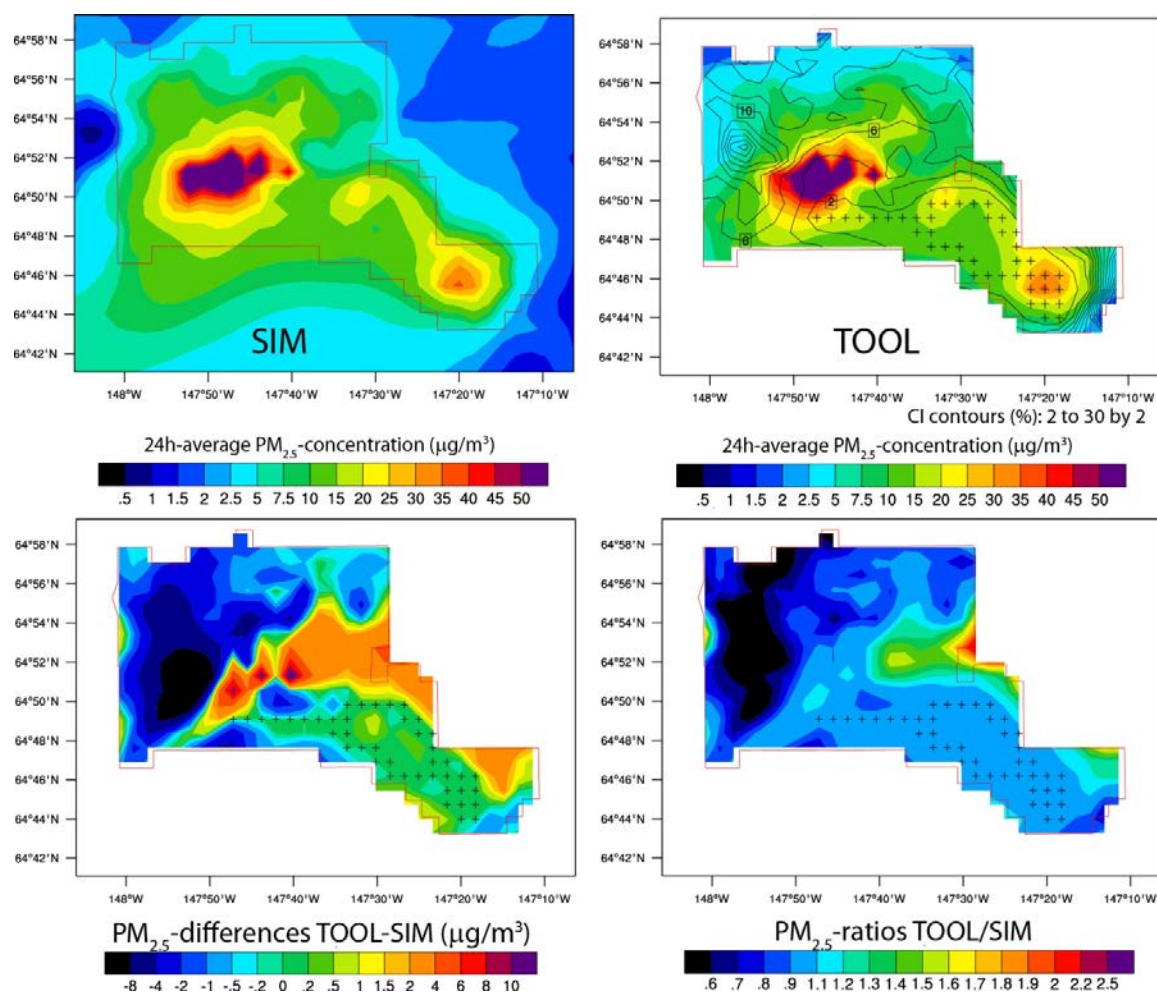
Figure 9.8 Example of interpolated (TOOL) vs. simulated, i.e. "grand truth", (SIM) $PM_{2.5}$-concentrations as obtained with the developed interpolation algorithm using the CMAQ-data pulled at grid-cells on the actual route performed on 01/06/2011 as "proxy" for sniffer observations in the nonattainment area (see text for details). The red polygon indicates the Fairbanks $PM_{2.5}$-nonattainment area. The black cross indicates the grid-cells on the route for this day.
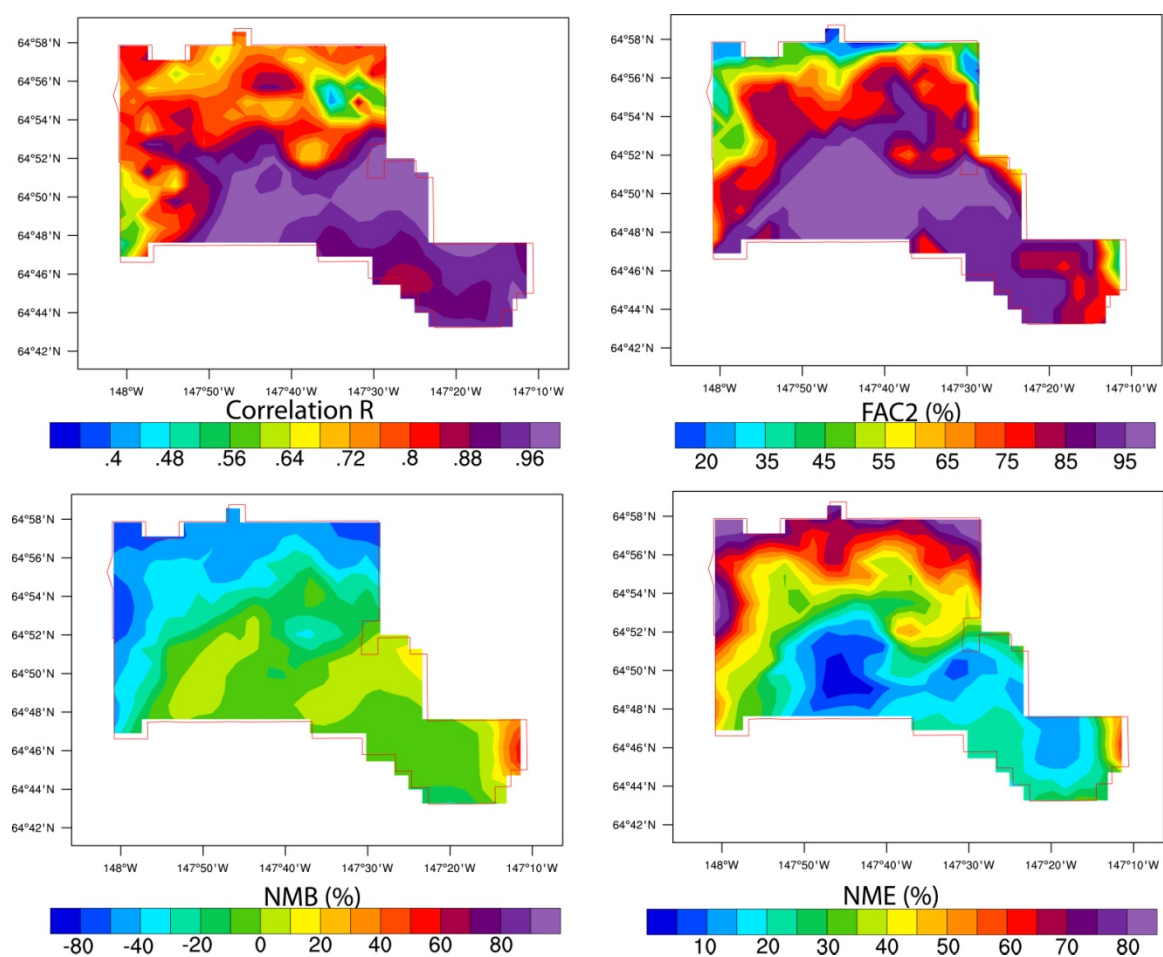
Figure 9.9 Overall performance of the interpolation algorithm as obtained on average over 100 arbitrarily chosen routes.
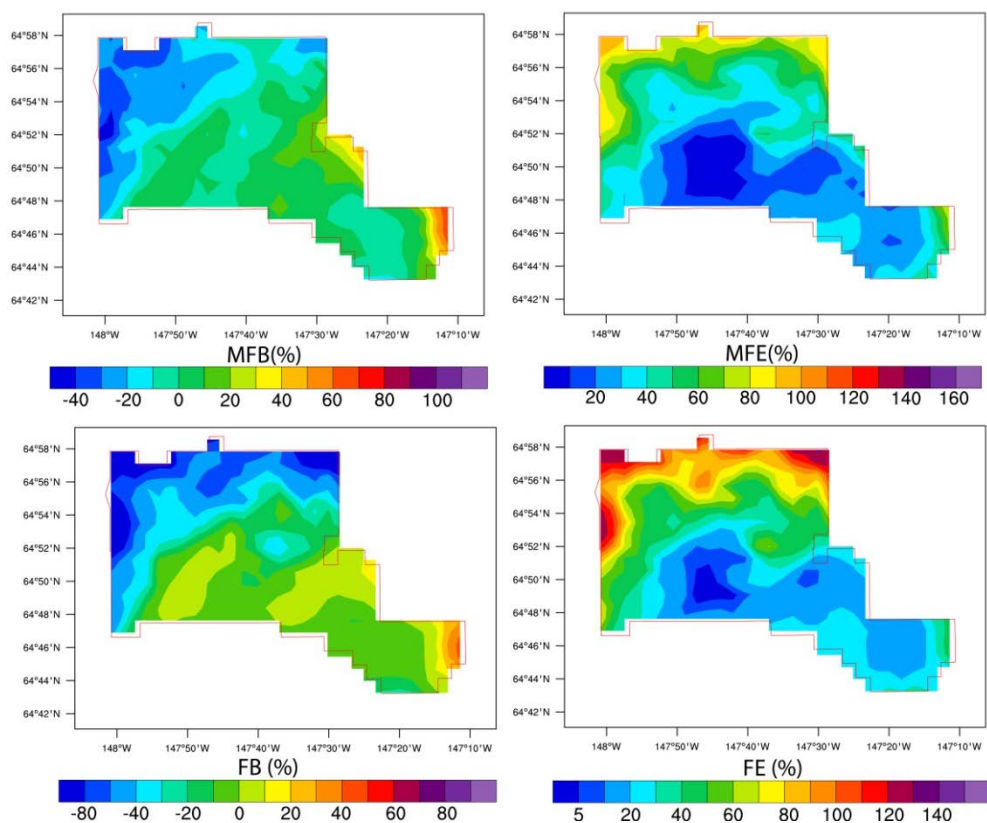
Figure 9.9 (cont.)
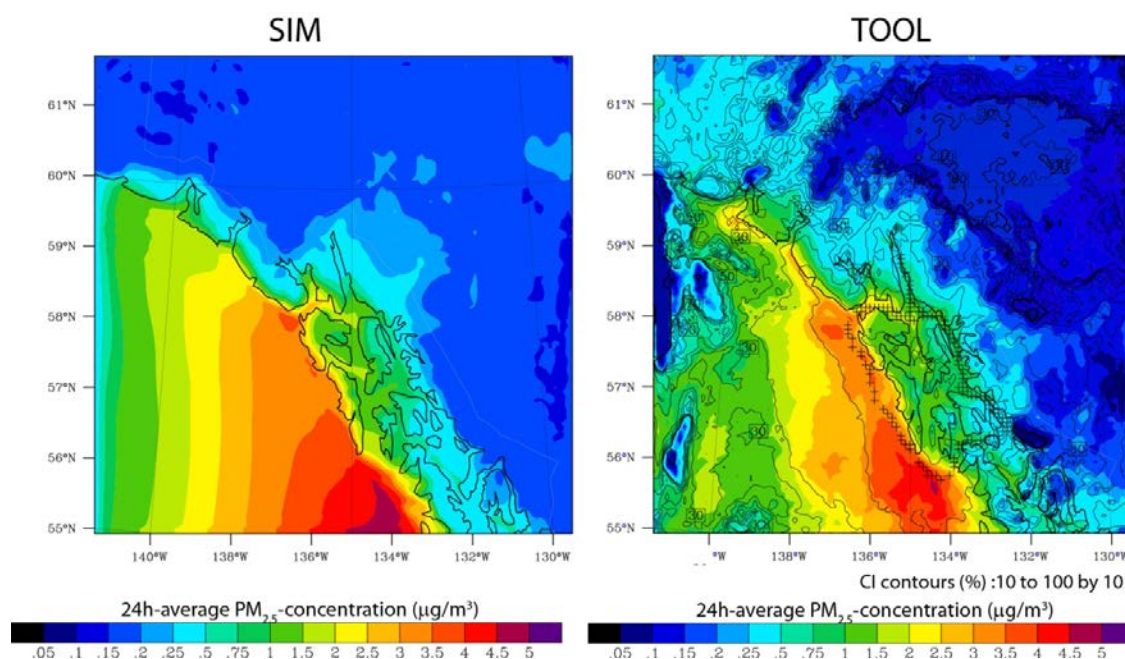
Figure 9.10 Example of interpolated (TOOL) vs. simulated, i.e. "grand truth", (SIM) PM$_{2.5}$-concentrations on May 28, 2008 as obtained with the developed interpolation algorithm using WRF/Chem-data as "proxy" for observation in Southeast Alaska (see text for details). The plus signs indicate the assumed route of an instrumented ship cruising on this day.

Figure 9.11 Overall performance of the interpolation performance as obtained over seven instrumented ship cruises from May 25 to June 8 2008 using WRF/Chem-data as "proxy" for observation in Southeast Alaska (see text for details).

Figure 9.11 (cont.)

Chapter 10 Conclusions and recommendations

10.1 Summary

In Fairbanks, Alaska, a tool that interpolates mobile $PM_{2.5}$-measurements into adjacent unmonitored neighborhoods and thereby 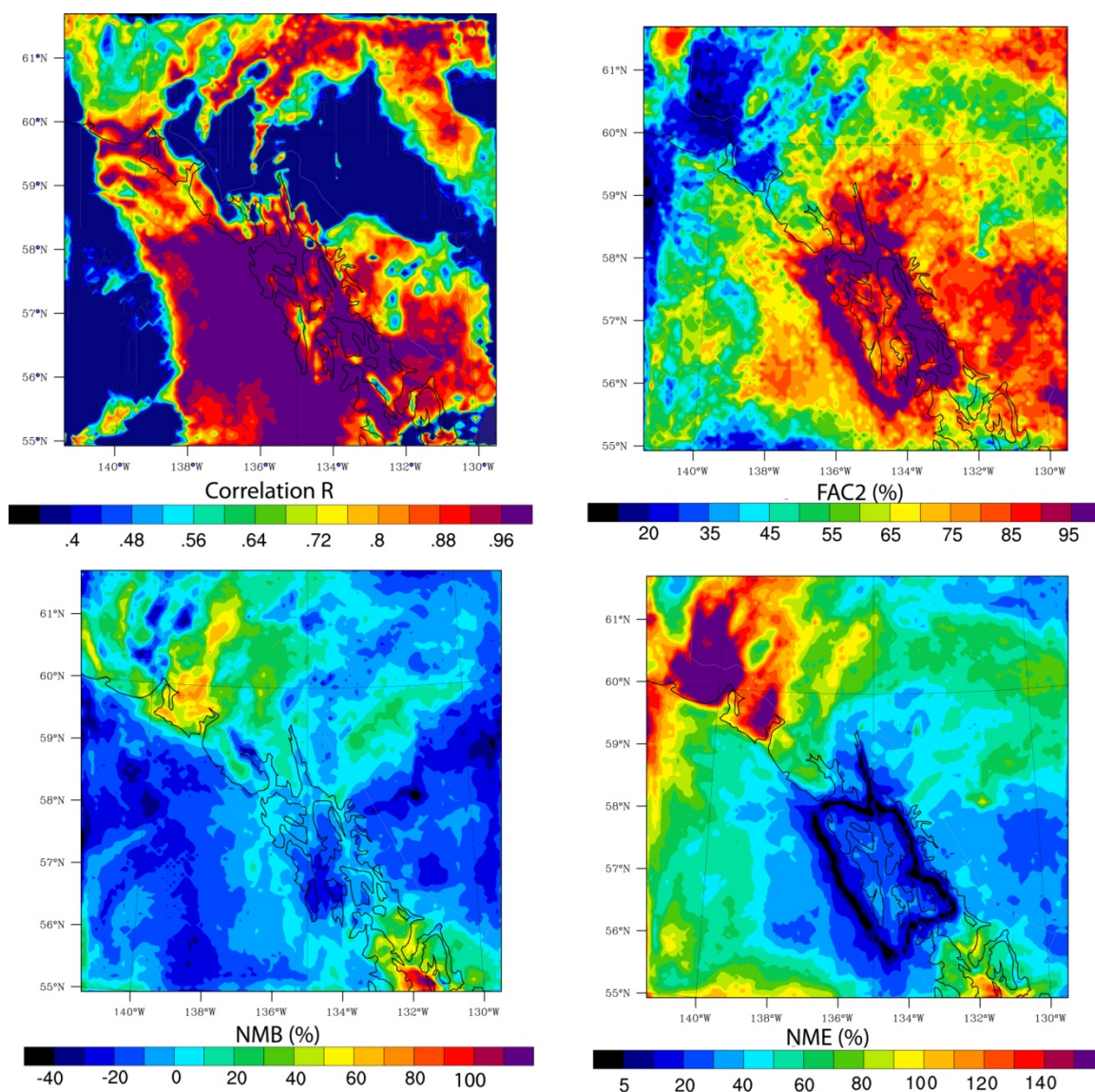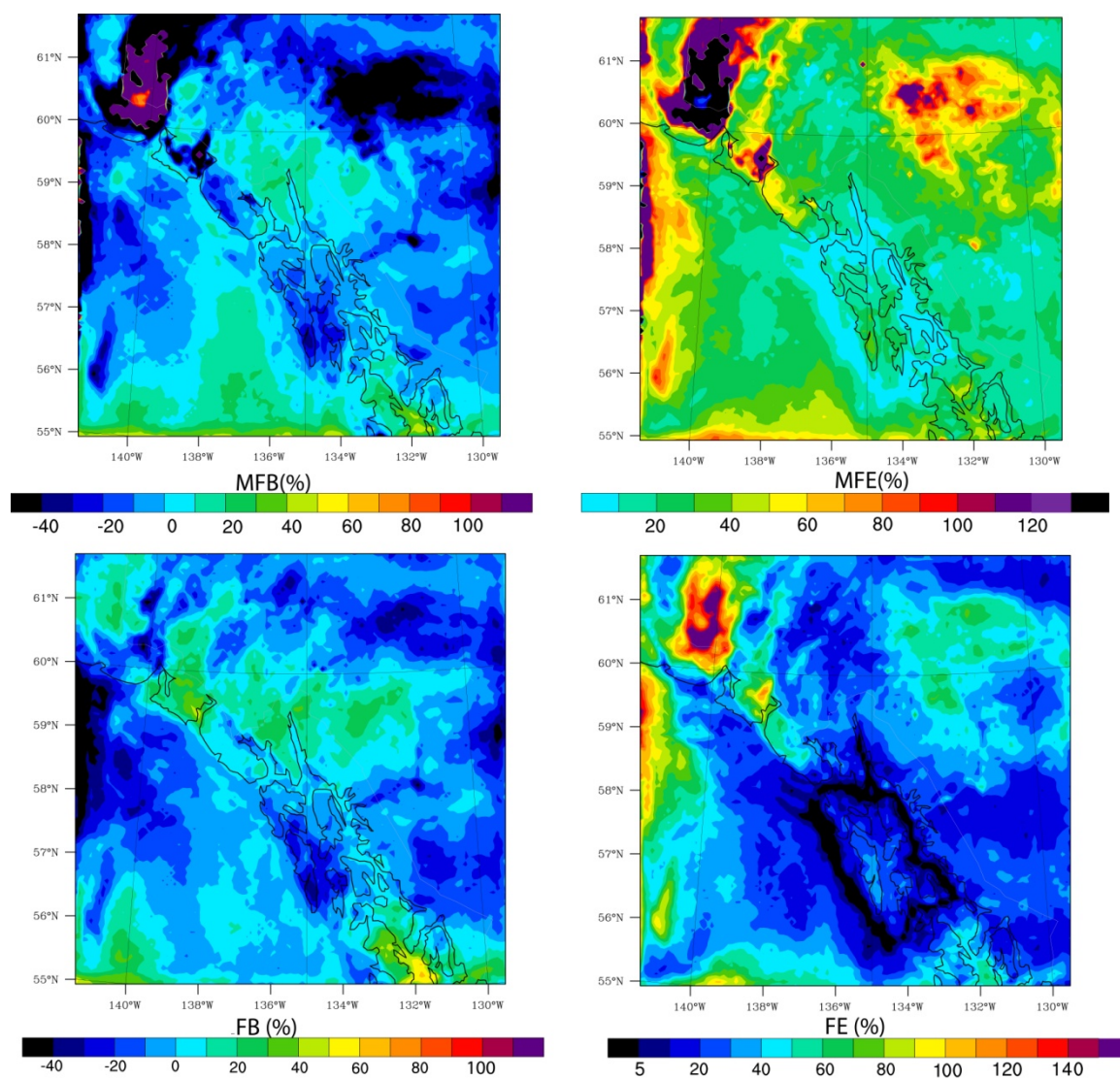provides a spatially differentiated public $PM_{2.5}$ air-quality advisory is highly desired. This public desire arises from the health concerns regarding $PM_{2.5}$ and the fact that the observed $PM_{2.5}$-concentrations frequently exceeded the National Ambient Air Quality Standards in Fairbanks during the past winters (Tran and Mölders, 2011). The current $PM_{2.5}$ air-quality advisory is provided based on the $PM_{2.5}$-measurements at the State Office Building and North Pole official monitoring sites, which are not able to represent the $PM_{2.5}$-concentrations in the entire nonattainment area. The use of traditional methods for interpolating the observed data to unmonitored neighborhoods was unsuccessful. This behavior is due to the lack of information on the underlying physical and chemical processes that drive the $PM_{2.5}$-concentrations.

The above shortcomings can be overcome by using an interpolation tool that combines mobile $PM_{2.5}$-observations with outputs of an existing air-quality model which includes all available information on sources and sinks of $PM_{2.5}$ in areas of interest. Such a $PM_{2.5}$ air-quality advisory tool (AQuAT) has been successfully developed in this thesis. The suitability for using AQuAT to provide a spatially differentiated air-quality advisory has been evaluated through various investigations which are summarized below.

As air-quality simulations were used as a database for AQuAT, the accuracy of these simulations in simulating meteorological and chemical quantities, and their ability in

capturing the observed meteorology-$PM_{2.5}$ relationships are key factors influencing the accuracy of AQuAT.

The relationships between observed meteorological conditions and $PM_{2.5}$-concentrations were investigated using ten years (1999-2009) of observations from the meteorological and radiosonde sites located at the Fairbanks International Airport, and the $PM_{2.5}$ official monitoring site located on the roof of the Fairbanks State Office Building. The results showed that during winter (November through February), high $PM_{2.5}$-concentrations ($> 35\mu g/m^3$) typically occurred under calm winds ($v < 0.5m/s$), extremely low temperatures ($< -20^oC$), low relative humidity ($RH < 75\%$, and $e < 2hPa$), and multiday surface-inversion conditions that trap pollutants in the breathing level and inhibit transport of polluted air out of Fairbanks. Of all the meteorological fields that have been investigated, temperature is the most important factor that determines the magnitude of the $PM_{2.5}$-concentrations. This behavior implies the effects of temperature on the gas-to-particle conversions as low temperature enhances the formation of secondary aerosols (e.g., Leelasakultum et al., 2012). Furthermore, temperature also impacts the emission strength as shown in previous studies (e.g., Hart and de Dear, 2004; Timmer and Lamb, 2007; Weilenmann et al., 2009; Nam et al., 2010) where emission strength increases as temperature decreases.

The above findings suggest that temperature, wind-speed and inversion strength might need to be considered in the development of AQuAT. Given the fact that the objective of AQuAT is to provide the public with spatially differentiated air-quality advice, observations of the above meteorological quantities must be accessible when a

measurement drive is completed. The observation of the inversion strength, which is available at the radiosonde site at the Fairbanks International Airport, does not fulfill this criterion. Therefore it was not considered in the sensitivity study made during the development of AQuAT. Observed wind-speed, wind-direction, and temperature can be obtained instantly from the meteorological tower in Fairbanks and from the mobile observations. Therefore, their observations were included in the sensitivity studies.

The performance of the simulations performed with the Alaska adapted (Mölders et al., 2011) version of the Weather Research and Forecasting model (WRF; Skamarock et al., 2008) inline "coupled" with chemistry packages (WRF/Chem; Grell et al., 2005; Peckham et al., 2009) for Fairbanks in winters 2005/2006 and 2008/2009, and with the Alaska adapted WRF "decoupled" with the Alaska adapted (Mölders and Leelasakultum, 2011) version of the Community Multiscale Air Quality (CMAQ; Byun and Schere, 2006) modeling systems for Fairbanks in winters 2009/2010 and 2010/2011 had been evaluated with observations from meteorological sites and aerosol monitoring sites, and other available data.

The results of the evaluation showed that these simulations well captured the relationships between observed meteorology and $PM_{2.5}$-concentrations found for Fairbanks in winters as discussed above. Simulated $PM_{2.5}$-concentrations typically increased as the simulated temperatures, wind-speeds, and relative humidity decreased. Furthermore, the performance of WRF/Chem and WRF-CMAQ in simulating aerosols strongly depends on the quality of the simulated meteorological quantities, especially temperature, wind-speed and inversion strength, as well as on the accuracy of the

emissions. These findings confirm the sub-hypothesis that *the air-quality models can reproduce the observed features that drive the distribution of the PM$_{2.5}$-concentrations*.

The WRF/Chem and WRF-CMAQ simulations used in this study have relatively good performance in simulating the meteorological quantities. Their performance is comparable with the performance reported in previous studies performed for Arctic and sub-Arctic regions (e.g., Hines and Bromwich, 2008; Mölders, 2008; Mölders and Kramm, 2010; Yarker et al., 2010; Cassano et al., 2011; Hines et al., 2011; PaiMazumder et al., 2012). They also share common performance shortcomings such as overestimation of temperature and wind-speed, and difficulty in capturing the full magnitude of the inversion strength.

Based on the performance skill-scores and their criteria proposed by various authors (Chang and Hanna, 2004; Boylan and Russell, 2006; EPA, 2007), the WRF/Chem and WRF-CMAQ simulations used in this study proved themselves to have good to acceptable performance in simulating PM$_{2.5}$-concentrations. Their performance is comparable with previous studies performed for the contiguous U.S. for winter months (e.g., EPA, 2005; Eder and Yu, 2006). Out of all the simulations, the WRF-CMAQ simulations for Fairbanks in the winter 2009/2010 episode (12/27/2009 – 01/12/2010) had performance in the range of state-of-the-art models. Because of this finding, WRF-CMAQ simulations of the winter 2009/2010 episode were selected as a database for AQuAT for Fairbanks.

The benefit of using air-quality simulations as a database for AQuAT is that this database can include information on the nonlinear impacts of various emission sources on

the PM$_{2.5}$-concentrations in monitored and unmonitored areas. This benefit was illustrated by investigations of the impacts from major sources (including point sources, traffic, and uncertified wood-burning devices) on the PM$_{2.5}$-concentrations in Fairbanks. These investigations were performed by analyzing WRF/Chem simulations for winters 2005/2006 and 2008/2009, and WRF-CMAQ simulations for winters 2009/2010 and 2010/2011. These simulations were performed with all emissions as they were in the emission inventory (i.e., no change), and with the emissions from the source-category of interest excluded or exchanged by the emissions from the replacement source-category. Their results were compared to investigate the contribution of the above individual sources to the PM$_{2.5}$-concentrations.

Emissions from point sources (e.g., power plants) are of interest as a review of the National Emission Inventory (NEI) of 2005 revealed that point-source emissions contributed up to 15% of the total PM$_{2.5}$-emissions in Fairbanks. Furthermore, each point source may impact the PM$_{2.5}$-concentrations differently depending on the stack characteristics (e.g., stack height, exit velocity) and the local meteorological conditions. In general, point-source emissions were found to be a minor contributor to the PM$_{2.5}$-concentrations at breathing level in the nonattainment area. On days and at locations where high PM$_{2.5}$-concentrations ($>35\mu g/m^3$) occurred, emissions from point sources accounted for 4% of the 24h-average PM$_{2.5}$-concentrations at breathing level on average. All point sources had their highest impact on the PM$_{2.5}$-concentration at breathing level in the grid cells containing them. The impact radius at breathing level was usually 10–12 km, but could reach up to 16 km downwind depending on the height of the emission

levels, magnitude of wind-speed and the presence of an inversion above the layer into which the point source emitted. These findings support the suitability of air-quality simulations as a database for AQuAT as with this database, information on the near-field influences of point-source emissions on $PM_{2.5}$-concentrations are included for a reasonable interpolation.

A wood-burning device changeout program began in Fairbanks in fall 2010. This changeout program was supposed to reduce the $PM_{2.5}$-emissions in the Fairbanks nonattainment area. However, the emission inventory for Fairbanks of 2008 (Sierra Research Inc., pers. comm., March 2011) was used for air-quality simulations which served as a database for AQuAT. Note that this emission inventory was the most current inventory available at 1.3km×1.3km grid increment. This means that the current database of AQuAT does not include information on the emission situation in response to the changeout program. The impact of the wood-burning device changeouts on $PM_{2.5}$-concentrations was investigated to assess the uncertainty that AQuAT would expose due to the lack of such information in its database. Furthermore, as emissions from uncertified wood-burning devices make up a large amount of the emissions from all wood-burning devices, the contribution of uncertified wood-burning devices to the $PM_{2.5}$-concentrations was examined as well.

As there was contradictory data on the number of wood-burning devices and no data on burning behavior, various sensitivity studies were performed to investigate the potential influences of wood-burning device changeouts and of uncertified wood-burning devices in general on the $PM_{2.5}$-concentrations.

The impacts of the uncertified wood-burning devices on the $PM_{2.5}$-concentrations at the breathing level in the nonattainment area differed in space and time, and are highly sensitive to the number and type of the uncertified wood-burning devices that were exchanged. The uncertified wood-burning devices in WSS3 contributed 13% on average to the $PM_{2.5}$-concentrations in the nonattainment area, compared to 43% in WSS4. Note that the uncertified wood-burning devices in WSS3 and WSS4 were made based on the assumptions with data reported by Carlson et al. (2010) and Davies et al. (2009), respectively. The uncertified wood-burning device replacements in WSR reduced the $PM_{2.5}$-concentrations at breathing level in the nonattainment area by 6% on average, compared to 38% in WSS1. Here, the uncertified wood-burning device replacements in WSR and WSS1 were made based on the assumptions with data reported by Carlson et al. (2010) and Davies et al. (2009), respectively. The contributions of uncertified wood-burning devices were greatest in densely populated areas and marginal in sparsely populated areas. The spatial variations of relative response factor (RRF) were within ±0.1 of the RRF at the State Office Building (SB) site for any species at any grid-cell in the nonattainment area for WSR. On the contrary, in WSS1, the spatial variations of RRFs reached from no difference to 0.4 greater RRF-values than the RRF-value at the SB-site.

The sensitivity studies on wood-burning devices illustrate the impact of uncertainty in the emission inventory related to the limited knowledge of the number of wood-burning devices and on the burning behavior on the $PM_{2.5}$-concentrations in Fairbanks.

Note that the information on the emission change due to the wood-burning device changeouts is indirectly included in AQuAT by the use of mobile observations. This

means if the future observed $PM_{2.5}$-concentrations decrease due to an introduction of an emission-control measure (such as wood-burning device changeouts), the AQuAT-interpolated $PM_{2.5}$-concentrations may also decrease accordingly. However, given the fact the nonlinear impacts of emission sources on $PM_{2.5}$-concentrations cannot be captured by the observations, the AQuAT-interpolated $PM_{2.5}$-concentrations would expose large uncertainty if the AQuAT database does not include the updated information on the emission situation in response to the introduced emission-control measure, especially if the impacts of such an emission-control measure on the $PM_{2.5}$-concentrations are large (for instance, as in WSS1). Therefore, an updated emission inventory that includes information on the wood-burning device changeouts is needed for the AQuAT database as soon as possible to enhance its accuracy.

Until such an emission inventory becomes available, the CMAQ simulations for winter 2009/2010 are considered adequate as a database for AQuAT given the current uncertainty in the data on the wood-burning device changeouts, wood-burning behavior and the number of wood-burning devices in general.

Previous studies have shown that the contribution of traffic emissions to the $PM_{2.5}$-concentrations may decrease quickly within 400m downwind of an actively used road (e.g., Zhu et al., 2002; Reponen et al., 2003). This fact means that the mobile measurements, which are impacted by the traffic emissions, could be substantially different from the $PM_{2.5}$-concentrations in neighborhoods farther from the roads. Such heterogeneity in space of the distribution of $PM_{2.5}$-concentrations between the roads and their neighborhoods can be captured either by air-quality simulations, or by a dense

monitoring network that is not applicable in Fairbanks. Therefore, an investigation of the contributions of traffic to the $PM_{2.5}$-concentrations was performed to assess the suitability of using air-quality simulations for the AQuAT database in capturing such heterogeneity in space of the distribution of $PM_{2.5}$-concentrations.

Overall, traffic emissions contributed about 10% to the $PM_{2.5}$-concentrations at breathing level in the Fairbanks nonattainment area, and their impacts on the $PM_{2.5}$-concentrations substantially differed in space. On average over the winter 2009/2010 and 2010/2011 episodes, traffic emissions contributed 10-12% to the total $PM_{2.5}$-concentrations in areas with high traffic activity (e.g., Fairbanks (FB), North Pole (NP), Badger Road (BG)) and only 3% in the areas with low traffic activity (e.g., in the hills around Fairbanks (HL)). The obtained RRFs were lowest in the FB, NP and BG areas (0.874-0.901) and highest in the HL area (0.969). Note that the smaller the RRF is, the stronger is the impact of traffic emissions on the $PM_{2.5}$-concentrations. The fact that WRF-CMAQ tends to underestimate the formation of $PM_{2.5}$ via gas-to-particle conversion may imply an underestimation of the contribution from traffic to the $PM_{2.5}$-concentrations in the nonattainment area.

The relatively high contributions from traffic emissions (about 10% on average) to the $PM_{2.5}$-concentrations in the nonattainment area mean that using traditional interpolation methods to interpolate mobile measurements into unmonitored neighborhoods would expose large uncertainty. This behavior occurs due to the strong dilution gradient in the pollutant concentrations between the road and its surrounding neighborhoods (e.g., particle concentrations decreased by 60% at 100m downwind of the

road; Zhu et al., 2002). Therefore, the use of air-quality simulations as a database for AQuAT is necessary as this data can capture the heterogeneity of the contributions from traffic emissions to the $PM_{2.5}$-concentrations.

Considering the contributions from traffic emissions (10%), point sources (4%), uncertified wood-burning devices (13 - 43%), and the wood-burning devices changeouts (6 - 38%) to the $PM_{2.5}$-concentrations in the nonattainment area, and that these contributions varied with time and space, one has to conclude that AQuAT without this information will not be able to provide reasonable $PM_{2.5}$-concentration interpolations into unmonitored neighborhoods. Such information, among others, can only be obtained from air-quality simulations.

All the above findings confirmed the sub-hypothesis that *besides the meteorology, the emissions from various sources influence the distribution of $PM_{2.5}$-concentrations* in the Fairbanks nonattainment area. Consequently, air-quality simulations may provide a good database for AQuAT to include information on the nonlinear effects of emissions from different types of sources on the distribution of $PM_{2.5}$-concentrations.

AQuAT has been developed in the following way: (1) it uses simulations by any air-quality model as a database and the GPS-coordinates of the routes to determine a set of interpolation equations for the neighborhoods of interest, for instance, a nonattainment area. The simulations do not need to be performed for the measurement episode. (2) Once the interpolation equations are determined and optimized, AQuAT interpolates the mobile measurements into the unmonitored neighborhoods using the set of interpolation equations.

The great advantages of AQuAT are that it allows for quick spatial interpolation after the mobile measurements are collected, and allows for any route within an area for which a database of simulated concentrations exists. Therefore, it provides high flexibility for future mobile measurements and will be still usable after new road construction. The resulting concentration distributions can be used for a spatially differentiated public air-quality advisory. The design of AQuAT also guarantees that it can be transferred easily to other regions. The only prerequisite is that a sufficiently large dataset of air-quality model data is established for that region.

The evaluation of AQuAT with the cross-validation using the sniffer observations, measured $PM_{2.5}$-concentrations from fixed monitoring sites, and the "grand-truth" CMAQ simulations for Fairbanks for winter 2010/2011 showed that AQuAT well captures the magnitude and temporal evolution of the sniffer observations, acceptably captures the observations at the fixed sites, and well captures the magnitudes and spatial distribution of the "grand-truth" $PM_{2.5}$-concentrations. These findings confirm the main hypothesis of this dissertation that for Fairbanks public air-quality advisory applications, *the spatial interpolation of $PM_{2.5}$-concentrations can be reasonably performed by AQuAT which combines mobile $PM_{2.5}$-observations with outputs of an air-quality model that includes all available information on sources and sinks of $PM_{2.5}$.*

The transferability of AQuAT has been tested exemplarily for southeast Alaska. The results demonstrated that AQuAT can easily be transferred to and applied in other regions and for other seasons. The performance of AQuAT when applied to southeast Alaska, however, was slightly lower than in the applications for the Fairbanks nonattainment

area. The overall performance skill-scores of AQuAT for southeast Alaska fell in the following ranges: 0.34<R<1.0, -60%<FB<60%, 5%<FE<180%, -40%<NMB<120%, 5%<NME<180%, -80%<MFB<140%, 5%<MFE<160%, and 20%<FAC2<100%, compared to R>0.720, -20<FB<20, FE<60%, -30%<NMB<30%, NME<50%, -30%<MFB<30%, MFE<60%, and FAC2>75% as obtained for application of AQuAT in the Fairbanks nonattainment area. The reason for this slightly weaker performance is that the meteorological conditions represented by the database used by AQuAT and the conditions at the time for which the interpolations were performed differed strongly.

This transferability experiment illustrates the following: (1) AQuAT can be easily transferred to other regions, and (2) the database of AQuAT must well represent the conditions of the measurement day to archive high accuracy in the interpolation.

The sensitivity studies that included wind fields and temperature in the determination of the interpolation equations led to the conclusion that in a complex urban environment under calm wind conditions, such as in Fairbanks during winter, a simpler algorithm that only considers $PM_{2.5}$-concentrations is superior for capturing the conditions in hot-spot areas. However, it has to be examined whether this conclusion might only be valid for Fairbanks and for the examined episode (i.e., deep winter when wind-speed and temperature were typically low and did not significantly change over time).

10.2 Conclusions and recommendations

AQuAT was developed and applied successfully to interpolate the mobile $PM_{2.5}$-measurements into unmonitored neighborhoods. Outputs of AQuAT can be used for

providing a spatially differentiated air-quality advisory to the public. Therefore, AQuAT helps to improve quality of life of the community.

In addition to their importance for AQuAT development, the studies performed in this dissertation provided various insights into the $PM_{2.5}$-conditions in the Fairbanks nonattainment area. They provided understandings of the meteorological conditions that drive elevated $PM_{2.5}$-concentrations in Fairbanks during winter. They also provided insights into the contributions of the emissions from several major sources to the $PM_{2.5}$-concentrations at breathing level.

The efficiency of AQuAT in interpolating $PM_{2.5}$-concentrations in Fairbanks under conditions with stronger winds and/or higher temperatures (e.g., October, March, summer) was beyond the scope of this dissertation, but seems worth addressing in the future. The expansion of the database for such situations would require additional air-quality model simulations.

The evaluation of the CMAQ-modeling package needed for the AQuAT development also provided an additional independent assessment of the Alaska adapted (Mölders and Leelasakultum, 2011) CMAQ. The additional evaluations performed for WRF/Chem also further assessed the performance for the Alaska adapted (Mölders et al., 2011) WRF/Chem. The major challenge in these evaluations is the sparse data availability. There was hardly any data outside of Fairbanks. To fully assess air-quality models for this region, additional observations are urgently needed.

This study has demonstrated that an interpolation tool such as AQuAT can be developed and used for the Fairbanks public air-quality advisory. However, the performance of AQuAT still needs further improvements.

Obviously, the understanding of the contributions of the emissions from several major sources to the $PM_{2.5}$-concentrations, as well as the performance of AQuAT highly depend on the performance of the numerical models used. The evaluation of the models employed in this study, despite having shown good to acceptable performances, indicate uncertainty in the simulated meteorology and chemistry quantities. The uncertainty is typically due to inadequately simulated meteorology and air-quality, discrepancies in the model parameterizations (Fox, 1984), inconsistencies between parameterizations within the model packages (Mölders et al., 1994), as well as uncertainty in the emissions data (Dolwick et al., 2001, Mölders et al., 2012).

The sensitivity studies of chapters 6 and 7 illustrated the impact of uncertainty in the emission inventory related to the knowledge of the number of wood-burning devices and burning behavior on the $PM_{2.5}$-concentrations in Fairbanks. This uncertainty would potentially induce large uncertainty in the AQuAT-interpolated $PM_{2.5}$-concentrations.

The above remaining discrepancies suggest that the air-quality simulations used as a database for AQuAT should be improved with model modifications and an updated emission inventory as soon as they become available. Recently, an updated version of the emission inventory for Fairbanks has been released (Sierra Research Inc., pers. comm., August 2012). In addition, further refinements of the Alaska adapted CMAQ became available (Mölders and Leelasakultum, 2012). It is strongly recommended to update the

database of AQuAT with air-quality simulations performed using this improved Alaska adapted CMAQ and the updated version of the emission inventory. This step should be done before the implementation of AQuAT for the Fairbanks routine air-quality advisory.

The current horizontal resolution of the database of AQuAT is 1.3km×1.3km. This means AQuAT will provide the spatially differentiated public air-quality advisory at this spatial scale. This spatial scale can be improved by using air-quality simulation at higher resolution (e.g., 0.4km×0.4km) for AQuAT database. However, such simulations are only possible if there exists an emission inventory at equal or higher resolution, and the air-quality model is still applicable at that resolution. Furthermore, with every update of the database, the new accuracy of AQuAT should be reassessed.

References

Boylan, J.W., Russell, A.G., 2006. PM and light extinction model performance metrics, goals, and criteria for three-dimensional air quality models. Atmospheric Environment, 40, pp. 4946-4959.

Byun, D.W., Schere, K.L., 2006. Review of the governing equations, computational algorithms, and other components of the Models-3 Community Multiscale Air Quality (CMAQ) Modeling System. Applied Mechanics Reviews, 59, pp. 51-77.

Carlson, T.R., Yoon, S.H., Dulla, R.G., 2010. Fairbanks home heating survey. Sacramento, CA, p. 63.

Cassano, J.J., Higgin, M.E., Seefeldt, M.W., 2011. Performance of the Weather Research and Forecasting Model for month-long pan-Arctic simulations. American Meteorological Society, 139, pp. 3469-3488.

Chang, J.C., Hanna, S.R., 2004. Air quality model performance evaluation. Meteorology and Atmospheric Physics, 87, pp. 167–196.

Davies, J., Misiuk, D., Colgan, R., Wiltse, N., 2009. Reducing $PM_{2.5}$ emissions from residential heating sources in the Fairbanks North Star Borough: Emission estimates, policy options, and recommendations. Cold Climate Housing Research Center, Fairbanks, AK, p. 56.

Dolwick, P.D., Jang, C., Possiel, N., Timin, B., Gipson, G., Godowitch, J., 2001. Summary of results from a series of models-3/CMAQ simulations of ozone in the Western United States. Proceeding of the 94th Annual Air & Waste Management Association Conference and Exhibition, Orlando, FL, June 24-28, Paper #957, p. 18.

Eder, B., Yu, S., 2006. A performance evaluation of the 2004 release of models-3 CMAQ. Atmospheric Environment, 40, pp. 4811-4824.

EPA, 2005. CMAQ model performance evaluation for 2001: Updated March 2005. U.S. Environmental Protection Agency, Research Triangle Park, NC 27711, p. 140.

EPA, 2007. Guidance on the use of models and other analyses for demonstrating attainment of air quality goals for ozone, $PM_{2.5}$, and regional haze. U.S. Environmental Protection Agency, Research Triangle Park, NC, p. 262.

Fox, D.G., 1984. Uncertainty in air quality modeling. Bulletin American Meteorological Society, 65, pp. 27-36.

Grell, G.A., Peckham, S.E., Schmitz, R., McKeen, S.A., Frost, G., Skamarock, W.C., Eder, B., 2005. Fully coupled "online" chemistry within the WRF model. Atmospheric Environment, 39, pp. 6957-6975.

Hart, M., de Dear, R., 2004. Weather sensitivity in household appliance energy end-use. Energy and Buildings, 36, 161-174.

Hines, K.M., Bromwich, D.H., 2008. Development and testing of Polar Weather Research and Forecasting (WRF) model. Part I: Greenland ice sheet meteorology. Monthly Weather Review, 136, pp. 1971-1989.

Hines, K.M., Bromwich, D.H., Bai, L.-S., Barlage, M., Slater, A.G., 2011. Development and testing of Polar WRF. Part III: Arctic land. Journal of Climate, 24, pp. 26-48.

Leelasakultum, K., Mölders, N., Tran, H.N.Q., Grell, G.A., 2012. Potential impacts of the introduction of low-sulfur fuel on $PM_{2.5}$ concentrations at breathing level in a subarctic city. *Advances in Meteorology*, 2012, p.16. doi:10.1155/2012/427078.

Mölders, N., 2008. Suitability of the Weather Research and Forecasting (WRF) model to predict the June 2005 fire weather for Interior Alaska. Weather and Forecasting, 23, pp. 953-973.

Mölders, N., Hass, H., Jakobs, H.J., Laube, M., Ebel, A., 1994. Some effects of different cloud parameterizations in a mesoscale model and a chemistry transport model. Journal of Applied Meteorology, 33, pp. 527-545.

Mölders, N., Kramm, G., 2010. A case study on wintertime inversions in Interior Alaska with WRF. Atmospheric Research, 95, pp. 314-332.

Mölders, N., Leelasakultum, K., 2011. Fairbanks North Star Borough $PM_{2.5}$ non-attainment area CMAQ modeling: Final report phase I. Report, p. 62.

Mölders, N., Leelasakultum, K., 2012. Fairbanks North Star Borough $PM_{2.5}$ non-attainment area CMAQ modeling: Final report phase II. Report, p. 66.

Mölders, N., Tran, H.N.Q., Cahill, C.F., Leelasakultum, K., Tran, T.T., 2012. Assessment of WRF/Chem $PM_{2.5}$-forecasts using mobile and fixed location data from the Fairbanks, Alaska winter 2008/09 field campaign. Atmospheric Pollution Research, 3, pp. 180-191

Mölders, N., Tran, H.N.Q., Quinn, P., Sassen, K., Shaw, G.E., Kramm, G., 2011. Assessment of WRF/Chem to simulate sub–Arctic boundary layer characteristics during low solar irradiation using radiosonde, SODAR, and surface data. Atmospheric Pollution Research, 2, pp. 283-299.

Nam, E., Kishan, S., Baldauf, R.W., Fulper, C.R., Sabisch, M., Warila, J., 2010. Temperature effects on particulate matter emissions from light-duty, gasoline-powered motor vehicles. Environmental Science & Technology, 44, 4672-4677.

PaiMazumder, D., Henderson, D., Mölders, N., 2012. Evaluation of WRF-forecasts over Siberia: Air mass formation, clouds and precipitation. The Open Atmospheric Science Journal, 6, pp. 93-110.

Peckham, S.E., Fast, J.D., Schmitz, R., Grell, G.A., Gustafson, W.I., McKeen, S.A., Ghan, S.J., Zaveri, R., Easter, R.C., Barnard, J., Chapman, E., Salzmann, M., Wiedinmyer, C., Freitas, S.R., 2009. WRF/Chem version 3.1 user's guide. Retrieved from http://ruc.noaa.gov/wrf/WG11/Users_guide.pdf, p. 90.

Reponen, T., Grinshpun, S.A., Trakumas, S., Martuzevicius, D., Wang, Z.-M., LeMasters, G., Lockey, J.E., Biswas, P., 2003. Concentration gradient patterns of aerosol particles near interstate highways in the greater Cincinnati airshed. Journal of Environmental Monitoring, 5, pp. 557-562.

Skamarock, W.C., Klemp, J.B., Dudhia, J., Gill, D.O., Barker, D.M., Duda, M.G., Huang, X.-Y., Wang, W., Powers, J.G., 2008. A description of the Advanced Research WRF version 3. NCAR Technical Note, NCAR/TN-475+STR, p. 125.

Timmer, R.P., Lamb, P.J., 2007. Relations between temperature and residential natural gas consumption in the Central and Eastern United States. American Meteorological Society, 46, pp. 1993–2013.

Tran, H.N.Q., Mölders, N., 2011. Investigations on meteorological conditions for elevated PM$_{2.5}$ in Fairbanks, Alaska. Atmospheric Research, 99, pp. 39-49.

Weilenmann,M., Favez, J.-Y., Alvarez, R., 2009. Cold-start emissions of modern passenger cars at different low ambient temperatures and their evolution over vehicle legislation categories. Atmospheric Environment, 43, pp. 2419–2429.

Yarker, M.B., PaiMazumder, D., Cahill, C.F., Dehn, J., Prakash, A., Mölders, N., 2010. Theoretical investigations on potential impacts of high-latitude volcanic emissions of heat, aerosols and water vapor and their interactions on clouds and precipitation. The Open Atmospheric Science Journal, 4, pp. 24-44.

Zhu, Y., Hinds, W.C., Kim, S., Sioutas, C., 2002. Concentration and size distribution of ultrafine particles near a major highway. Journal of the Air & Waste Management Association, 52, pp. 1032-1042.

Appendix A Contributions to thesis chapters

A.1 Chapter 3

The literature research, analysis, text and figures were prepared by Huy N.Q. Tran. Professor Nicole Mölders helped Huy N.Q. Tran in the physical interpretation and refining of the text and the figures and had the idea for the study.

A.2 Chapter 5

The key topic of this chapter was adapted from Professor Nicole Mölders' grant LGFEEQ. The reference and experimental simulations were performed by Professor Nicole Mölders. The literature research, analysis, text and figures were prepared by Huy N.Q. Tran. Professor Nicole Mölders helped Huy N.Q. Tran in the physical interpretation and refining of the text and the figures.

A.3 Chapter 6

The key topic of this chapter was adapted from Professor Nicole Mölders' grant LGFEEQ. The reference and the experimental simulations were performed by Professor Nicole Mölders. Huy N.Q. Tran prepared the annual emission inventory for these simulations. The literature research, analysis, text and figures were prepared by Huy N.Q. Tran. Professor Nicole Mölders helped Huy N.Q. Tran in the physical interpretation and refining of the text and the figures.

A.4 Chapter 8

The key topic of this chapter was adapted from Professor Nicole Mölders' grant AUTC Project No. 410003 and grant H9910030024. Professor Nicole Mölders and Ketsiri Leelasakultum provided the CMAQ code and simulation setup that they had adapted to the Alaska conditions. Sierra Research Inc. provided the emission inventory. Huy N.Q. Tran performed the WRF, MCIP, SMOKE and CMAQ simulations. The literature research, analysis, text and figures were prepared by Huy N.Q. Tran. Huy N.Q. Tran developed AQuAT under the instruction of Professor Nicole Mölders. Professor Nicole Mölders provided the WRF/Chem simulations for southeast Alaska that were used to demonstrate the transferability of AQuAT. Professor Nicole Mölders also helped Huy N.Q. Tran in the physical interpretation and refining of the text and the figures.